

Progress towards the pyrrolizidine alkaloid xenovenine (**223H**) *via* hydroamination

Submitted in fulfilment of the requirements
for the degree of

Master of Science

By

Lesley Dralle
BSc (Hons) UKZN

January 2016



School of Chemistry and Physics
University of KwaZulu-Natal
Pietermaritzburg
South Africa

Thesis Declaration

The experimental work described in this thesis was carried out in the School of Chemistry and Physics, University of KwaZulu-Natal, Pietermaritzburg, under the supervision of Professor Ross S. Robinson.

These studies represent the original work of the author and have not otherwise been submitted in candidature for any other degree.

Signed: _____ L. Dralle (Candidate)

Signed: _____ Prof. R.S. Robinson (Supervisor)

School of Chemistry and Physics
University of KwaZulu-Natal
Pietermaritzburg
South Africa

Abstract

Many natural products, pharmaceuticals and fine chemicals possess carbon-nitrogen bonds and thus the formation of such bonds is of great importance. Pyrrolizidine, indolizidine, quinolizidine and lehmizidine alkaloid skeletons all contain C–N bonds and are potentially accessible *via* a general synthetic route utilising hydroamination. The synthesis of the biologically active nitrogen containing pyrrolizidine alkaloid xenovenine **4** isolated from *Solenopsis* cryptic thief ants and *Dendrobates* poison dart frogs was attempted. One of the key intermediates, ethyl 2-[(5*R*)-5-methyltetrahydro-2*H*-pyrrol-2-ylidene]acetate **127**, was successfully synthesised in 7 steps from (*S*)-pyroglutamic acid through a lactim ether intermediate. The pivotal ring forming ZnCl_2 catalysed 5-*exo*-dig hydroamination was unfortunately not attempted after the failed *C*-propargylation of ethyl 2-[(5*R*)-5-methyltetrahydro-2*H*-pyrrol-2-ylidene]acetate **127**.

Acknowledgements

I would firstly like to thank my supervisor Prof Ross Robinson for his guidance, support and valuable input throughout the course of my postgraduate studies.

I would like to thank Mr Craig Grimmer for all his assistance with NMR Spectroscopy, Mrs Caryl Janse van Rensburg for HRMS data and Dr Mathew Akerman for X-ray crystallographic data. Thank you to Mr Fayzil Shaik and Dr Avela Majavu for all of their assistance as well as to Mr Shawn Ball, Mr Clarence Mortlock and Mr Paul Forder, and to my colleagues in the Warren lab and other postgraduate students. Thank you to my friends and family for all your support and encouragement. Lastly, I would like to thank the National Research Foundation for their generous funding.

List of Abbreviations

Abbreviation		Abbreviation	
Ac	acetyl	L	ligand
AIBN	azobisisobutyronitrile	LDA	lithium diisopropylamide
aq	aqueous	LHMDS	lithium hexamethyldisilazide
Ar	aryl	Ln	lanthanide
atm	atmosphere	LRMS	low resolution mass spectrometry
9-BBN	9-borabicyclo[3.3.1]nonane	M	metal
b.p.	boiling point	Me	methyl
bmim	1-butyl-3-methylimidazolium	mg	milligram
Boc	<i>n</i> -butyloxycarbonyl	m.p.	melting point
Bu	butyl	Ms	mesyl
cat	catalyst/catalytic	MS	mass spectrometry
Cbz	carboxybenzyl	nAChR	nicotinic acetylcholine receptor
cp	cyclopentadiene	<i>n</i> -BuLi	<i>n</i> -butyl lithium
DBU	1,8-diazabicycloundec-7-ene	NMR	nuclear magnetic resonance
DCE	dichloroethane	OA	oxidative addition
DCM	dichloromethane	Ph	phenyl
DIBAL-H	diisobutylaluminium hydride	ppm	parts per million
DIP-Cl	diisopinocampheylchloroborane	Pr	propyl
DME	dimethoxyethane	pTSA	para toluenesulfonic acid
DMF	dimethylformamide	Py	Pyridine
DNA	deoxyribonucleic acid	RE	reductive elimination
e.e.	enantiomeric excess	RNA	ribonucleic acid
El	electron impact	RT	room temperature
Et	ethyl	TBAF	tetrabutylammonium fluoride
eq	equivalents	TBDPS	Tertiary butyl diphenylsilyl
HOTf	Trifluoromethanesulfonic acid	THF	tetrahydrofuran
hr	hour	TMS	trimethylsilyl
Hz	Hertz	Ts	tosyl
HRMS	high resolution mass spectrometry		
Ind	indenyl		
IR	infrared		
KHMDS	potassium hexamethyldisilazide		

Contents

Thesis Declaration	ii
Abstract	iii
Acknowledgements	iv
List of Abbreviations	v
Chapter 1: Introduction	1
1.1 Alkaloids and their importance	1
1.1.1 Biologically Significant Alkaloids	4
1.1.2 Pyrrolizidine Alkaloids	5
1.1.3 3,5-Disubstituted Pyrrolizidine Alkaloids	7
1.2 Synthesis of 3,5-disubstituted Pyrrolizidines	10
1.2.1 Reductive Cyclisation <i>via</i> Triketones	11
1.2.2 Reductive cyclisation <i>via</i> Nitrodiketones	13
1.2.3 Reductive Cyclisation <i>via</i> Intramolecular Amidomercuration	14
1.2.4 Reductive Cyclisation <i>via</i> Hydroamination	15
1.2.5 Reductive Cyclisation <i>via</i> Allylic Amination	15
1.2.6 Reductive Cyclisation <i>via</i> Coupling of <i>N</i> -acylcarbamates	17
1.2.7 Epoxidation	19
1.2.8 Reverse Cope Elimination	20
1.2.9 Double Nucleophilic Substitution	21
1.3 Hydroamination	22
1.3.1 Base Catalysed Hydroamination	24
1.3.2 Acid Catalysed Hydroamination	26
1.3.3 Metal-complex Catalysed Hydroamination	30
1.3.4 Regioselectivity of Hydroamination	32
1.3.5 Stereoselectivity of Hydroamination	36
1.3.5 Hydroamination in Natural Product Synthesis	38
1.4 Previous Work within the Research Group	40
	vi

1.5	Aims of the Project	44
Chapter 2: Results and Discussion		45
2.1	Focus of the Project	45
2.2	Proposed Synthetic Route	45
2.3	Studies toward 223H	47
2.3.1	Part 1: Synthesis of (5 <i>R</i>)-5-methyltetrahydro-2 <i>H</i> -pyrrol-2-one	47
2.3.2	Part 2: Synthesis of ethyl 2-[(5 <i>R</i>)-5-methyltetrahydro-2 <i>H</i> -pyrrol-2-ylidene]acetate	67
2.3.3	Part 3: Synthesis of 1-bromo-2-nonyne	87
2.4	Catalytic Hydroamination Study	103
2.4.1	Part 4: Synthesis of ethyl (3 <i>R</i>)-5-heptyl-3-methyl-2,3-dihydro-1 <i>H</i> -pyrrolizidine-7-carboxylate	103
2.4	Summary of Synthesis	107
2.5	Future Work	108
2.6	Conclusion	111
Chapter 3: Experimental		112
3.1	General information	112
3.2	Preparative Procedures and Spectrometric Data	113
Chapter 4: References		124
Appendix		132

Chapter 1: Introduction

1.1 Alkaloids and their importance

Alkaloids are naturally occurring nitrogen containing organic compounds and can be acidic, neutral or basic. The name 'alkaloid' is derived from the words 'alkali' and 'είδος' (Greek for type or similarity).¹ The name suggests that such substances are alkaline in character; however this is not necessarily true for all alkaloids; some may be neutral or even slightly acidic.² In the 1800's alkaloids referred to only those substances extracted from plant material. However, alkaloids have been found in both the plant and animal kingdoms. Many are poisonous to mammals.¹

Alkaloids are the most diverse of all the natural products with a large number of differing structure types, biosynthetic pathways and pharmacological activities. Many plants have been used for over 4 000 years as medicines, teas, and poisons. However, it was only early in the 19th century that it was attempted to isolate the active ingredients from these plants. Below follows a brief history of alkaloid isolation, characterization and synthesis.³

1803	The French apothecary Derosine ⁴ isolates a semi pure alkaloid from opium, calls it narcotine
1805	The Hanoverian apothecary Serturmer ⁴ isolates morphine, discovers its basic character
1817-1820	Pelletier and Caventon isolate strychnine, emetine, brucine, piperine, caffeine, quinine, cinchonine and colchicine
1826	Pelletier and Caventon obtain coniine
1826	Morphine first commercially marketed ²
1870	Coniine is the first alkaloid to be characterised by Schiff
1886	Coniine is the first alkaloid to be synthesised
1946	Robinson and co-workers determine the structure of strychnine

By the mid 1940's approximately 800 alkaloids had been isolated. By 1990 this number had increased drastically to about 10 000.⁴ By 2001 there were approximately 26 900 characterised alkaloids from plants alone.²

Initially it was presumed that alkaloids came only from flowering plants (the angiosperms), but in the late 1970's and early 1980's a number of alkaloids were discovered from animals, insects, marine organisms and microorganisms as well as lower plants.³ There has been an increased drive in the search for alkaloid derived plant drugs with anti-tumour, anti-aging and anti-viral activities in the 21st century.⁴

With such enormous variety it is difficult to classify all types of alkaloids. There are two very broad divisions:-

- I. Non-heterocyclic alkaloids encompassing protoalkaloids or biological amines, and
- II. Heterocyclic alkaloids with 14 sub-groups based on ring structure.⁴

Even with such enormous variety, there are only a few biosynthetic building blocks, with most naturally occurring alkaloids being derived from amino acids (ornithine, lysine, nicotinic acid, phenylalanine, tyrosine, tryptophan, anthranilic acid and histidine). Others include polyterpene units, polypeptide units and purine bases.^{2, 5} In some cases the alkaloids are derived *via* amination of other substrates, for example acetate and malonate. In such cases the nitrogen is introduced into the structure at a much later stage. It has been mentioned that alkaloids are nitrogen containing compounds¹ and it can be in the form of a primary, secondary or tertiary amine.

Before the development of modern medicine, drugs were of an entirely natural origin. Such drugs were obtained from many sources including plants, animals and inorganic materials. The largest and most widely utilised sources for such remedies were herbs. However, with the advancement of chemical techniques, the active ingredients of such herbs could be extracted and analysed. Structural characterisation followed allowing for the synthesis of such compounds in the laboratory, either by modification of the active ingredients or by total synthesis of structural analogues. Many of these active ingredients are now known to be alkaloids. Such activity often depends on how the amine function is transformed by protonation at physiological pH.⁵

The structure may be a complex heterocycle such as atropine, morphine and strychnine or simpler structures such as coniine and dolichotheline or even a simple open chain as found in certain spider toxins such as δ -philanthotoxin (Figure 1).¹

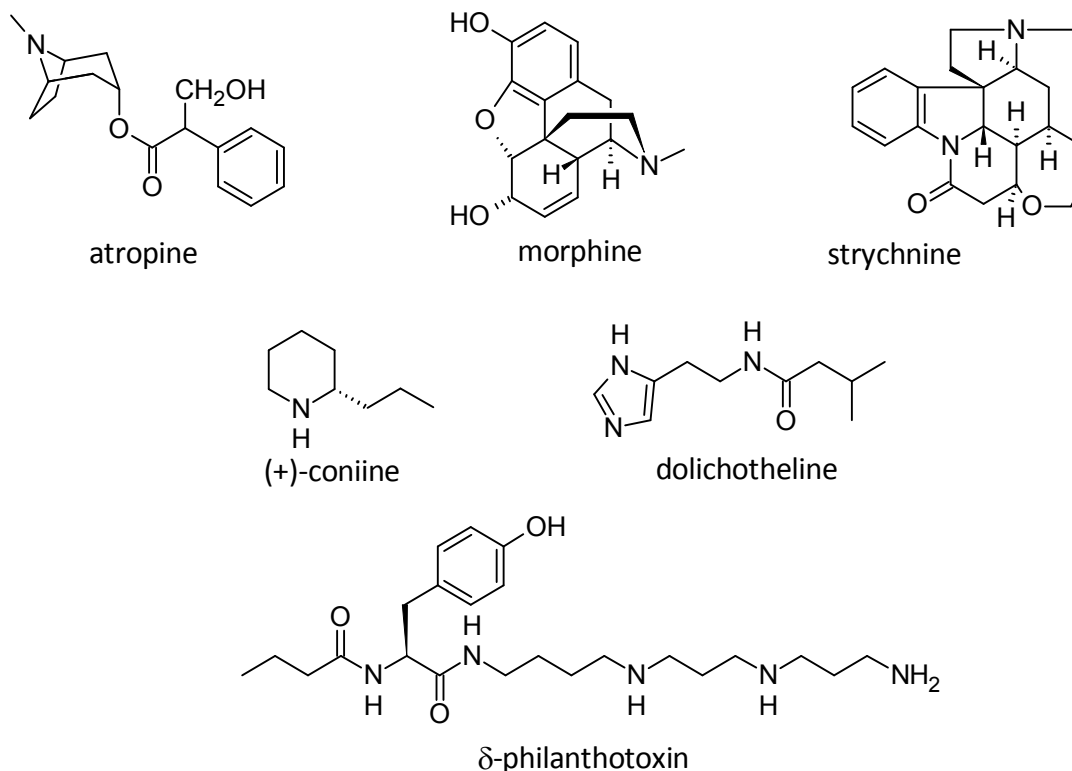


Figure 1

With such a large number of alkaloids originating from many different plant, fungal and animal species, it is difficult to determine why exactly organisms produce alkaloids. Amongst some of the known reasons for plant alkaloids are as:-

- antifungal agents,
- protection against UV irradiation,
- insecticides, herbicides and fungicides, and
- feeding deterrents.¹

Animals utilise alkaloids for a number of reasons, such as for use as pheromones or poisons. Spiders use alkaloids as poisons to immobilize and kill their prey whilst many amphibian species use alkaloids solely for defensive purposes.¹ Over 350 alkaloids have been detected from the skins of amphibians of the *Mantellidae* family alone. They usually contain pyrrolizidine, indolizidine, or quinolizidine alkaloids and are acquired by diet from mites, ants, beetles and millipedes.⁶ Extracts from amphibian skins from the *Dendrobatidae* family have been used to make poison darts by the people in the Colombian coastal provinces of Buenaventura and Chocó. Batrachotoxin is one example of a toxin used to make poison darts. The amphibians of the *Dendrobates* family are believed to obtain the alkaloid xenovenine from the poison glands of the fire ants of the *Solenopsis* family.¹

1.1.1 Biologically Significant Alkaloids

Alkaloids have been used in medicine as analgesic potentiators (cocaine), anti-cholinergics (atropine, scopolamine), anti-hypertensives (protopoveratrine A), anti-malarials (quinine) and anti-tumour agents (vinblastine) and as diuretics (theobromine) to name a few. Alkaloids generally act upon the nervous system of humans (as opposed to the endocrine system). Information is carried electrically in the neurons, and chemically across synapses. Neurotransmitters are those chemicals responsible for the transfer of information across the synapses. Acetylcholine is one such neurotransmitter, and some pyrrolizidines have been found to interact with acetylcholine receptors.⁷

Tropane alkaloids (Figure 2) are a well known class of alkaloids which exhibit physiological activity. For example, (-)-hyoscyamine and (-)-hyoscine are two of the most important alkaloids in medicine. They are found in *Atropa belladonna* (deadly nightshade), *Datura stramonium* (thornapple) and *Hyoscyamus niger* (henbane) amongst others. It is the alkaloids that confer the toxicity to these plants. Both (-)-hyoscyamine and (-)-hyoscine have agonist properties and have been used as anti-spasmodics on the gastrointestinal tract and as anti-secretory agents to control saliva secretion during surgical procedures. Hyoscine has been used to treat motion sickness.⁵

Atropine has found application as an antidote for cholinesterase inhibitors such as organophosphate insecticides. Benztropine has been used in the treatment of Parkinson's disease.⁵

Another important tropane alkaloid is cocaine which has led to the development of a number of synthetic anaesthetic drugs, for example, procaine, benzocaine, amethocaine, and lidocaine. Lidocaine is now used in the treatment of ventricular arrhythmias.⁵

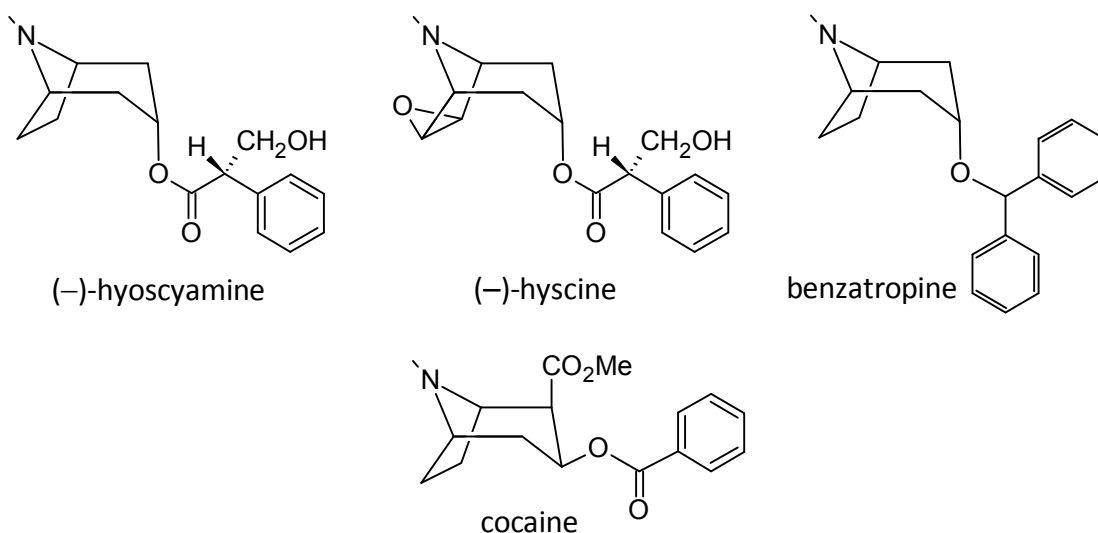


Figure 2

Pyrrolizidines and indolizidines with alkyl chains α to the nitrogen tend to be biologically active. For example, monomorine **I** is a trail pheromone of the Pharaoh ant *Monomorium*, **223AB** has been isolated from the *Solenopsis Diplophoptrum* Worker ant and from amphibians, and (-)-xenovenine has been found in the venom of ants belonging to the genus *Solenopsis* and the species *Monomorium* (Figure 3).⁸

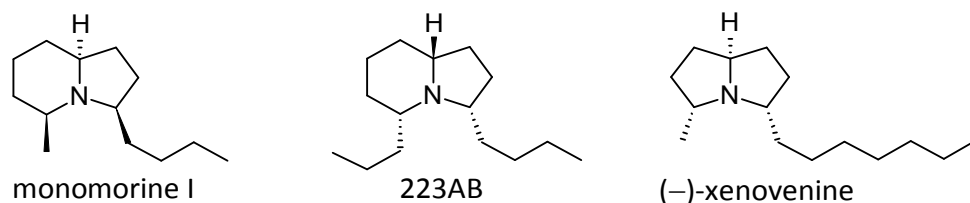


Figure 3

1.1.2 Pyrrolizidine Alkaloids

Pyrrolizidine alkaloids, also known as Senecio alkaloids, contain a necine base as the main skeleton. Necine bases are bicyclic 1-azabicyclo[3.3.0]octane ring structures⁹ as depicted in Figure 4. They are found in a wide range of plant species throughout the world¹⁰ with many being cytotoxic.¹¹ These alkaloids are generally poisonous to mammals and birds and have been responsible for many livestock and human deaths.^{1,12}

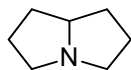


Figure 4

Pyrrolizidines are derived from the amino acid ornithine and are widely distributed in both the plant and animal kingdoms. They are, however, characteristic of certain genera of *Boraginaceae*, *Compositae/Asteraceae* (*Senecio*) and *Luguminosae/Fabaceae*.⁵ Figure 5 depicts 1,7-disubstituted alkaloids with fairly complex structures. They all contain the pyrrolizidine skeleton (also referred to as a necine base) and a necic acid upper portion.

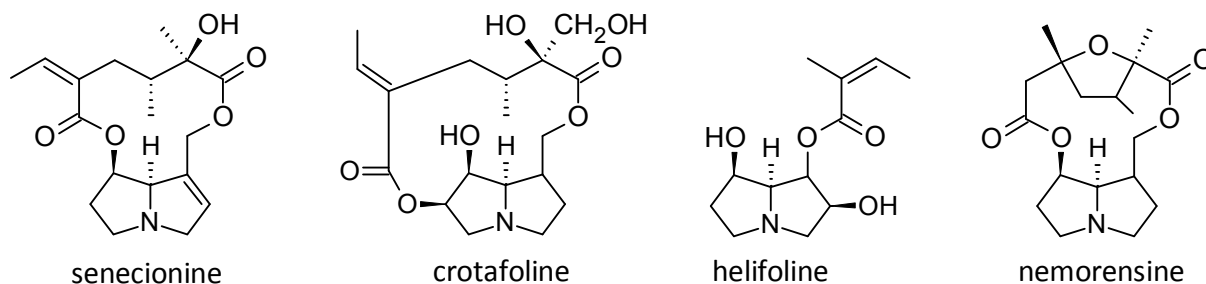


Figure 5

There are a number of biologically active pyrrolizidine alkaloids.⁹ They are among the most hepatotoxic of all the natural products.¹³⁻¹⁴ Those with hydroxyl groups tend to be the most biologically active,¹⁵ for example as glycoprotein-processing glycoside inhibitors, glycosyltransferases¹⁶ and as potential chemotherapeutic agents.¹⁵ Some pyrrolizidines are non-competitive blockers of nicotinic acetylcholine receptors.⁷ The most toxic are pyrrolizidines with cyclic dilactones with unsaturation at the 1,2-position.¹⁴

Pyrrolizidines that are toxic tend to have similar structural features. These include:-

- I. An unsaturated ring at the 1,2-position, and
- II. An ester moiety within the side chain (see Figure 5).¹⁷

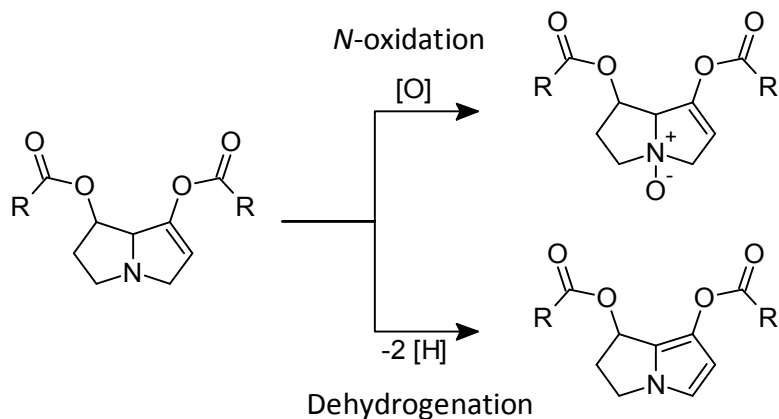
They are generally hepatotoxic,⁵ but it is believed that it is the metabolites that confer the toxicity on these alkaloids, and not necessarily the alkaloids themselves and as such are pro-toxins.¹⁷ Evidence supporting this theory is that the sites of injection of such toxins are undamaged, some organisms go completely unharmed, and the liver is the main organ damaged.¹² Plants also tend to store such alkaloids in their non-toxic form, that is, as *N*-oxides. This makes for easier transport and storage within the plant. The *N*-oxides are then converted in the gut of herbivores into tertiary amines by mild reduction.^{5, 18} In animals cytochrome P₄₅₀ generates the toxic pyrrolic intermediates which then bind to proteins.^{14, 17} Studies of laboratory animals show the major routes of metabolism are:-

- I. Ester hydrolysis,
- II. Conversion to *N*-oxides, and
- III. Dehydrogenation.

Route I and II are considered to be detoxification pathways whereas route III affords cytotoxic pyrrolic derivatives.¹²

Both *N*-oxides and the pyrrolic derivatives are metabolites of enzymic oxidation in animals.¹² The product of dehydrogenation (Scheme 1), the pyrrolic ester, acts as an electrophile which bonds covalent with nucleophiles such as proteins, DNA and RNA, leading to acute liver or lung toxicity, or genotoxicity.^{13-14, 17}

Pyrrolizidines have been used medicinally in the treatment of traumatic injury, pain and inflammation.¹⁴ Pyrrolizidines with alkyl chains α to the nitrogen are responsible for control and protective function against other living organisms.⁸



Scheme 1

1.1.3 3,5-Disubstituted Pyrrolizidine Alkaloids

Much of the early literature concerning pyrrolizidine alkaloids covers only the necine and necic acid type alkaloids (Figure 5). Not until the mid 1970's to early 1980's that 3,5-disubstituted pyrrolizidines began to make an appearance. This may be attributed to the fact that most plant based pyrrolizidines tend to be polyhydroxylated, whilst those found in ants, moths and poison frogs tend to be of the 3,5-disubstituted variety.¹⁹

Xenovenine (**223H**) is a 3,5-disubstituted pyrrolizidine alkaloid, *cis*-3-heptyl-5-methyl-1*H*-pyrrolizidine, first extracted in 1980 from the Cryptic Thief ant *Solenopsis xenovenenum*.²⁰⁻²¹ The IUPAC name is *cis*-2-heptyl-8-methyl-1-azabicyclo[3.3.0]octane. It was later isolated from the skins of bufonid toads *Melanophryniscus stelzneri* and frogs *Dendrobates auratus* and named *cis*-**223H**.²²

The bicyclic ring structure can be either *cis*-fused or *trans*-fused. This refers to the relative orientation of the 8-*H* proton relative to the nitrogen lone pair as can be seen in Figure 6. Most pyrrolizidine alkaloids in nature are *cis*-fused as there is less strain. Thus the bridgehead proton and the nitrogen lone pair are on the same side of the ring.

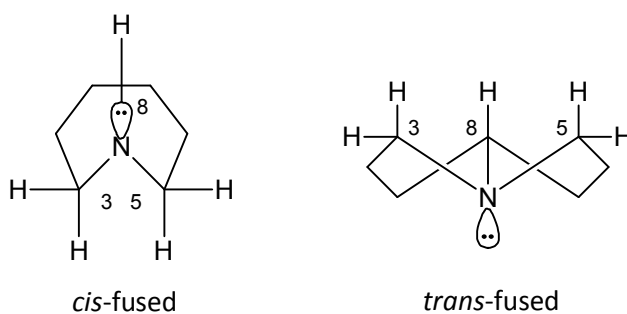


Figure 6

In some cases *endo*, *exo* notation is used to distinguish the relative stereochemistry of the substituents and in others *zusammen* (*Z*) and *entgegen* (*E*) are used instead.

A substituent that is *endo* (or *syn*) is said to be nearest the longest bridge in the bicyclic system. A substituent that is *exo* (or *anti*) is said to be furthest from the longest bridge in the bicyclic system. Thus it can be seen in Figure 7 that when the R group is pointed downwards it is *endo* to the downward ring system. When the R group is in the horizontal position it is said to be *exo* as it is furthest away from the downward ring system.²³ It is important to note that both the *endo* and the *exo* isomer are *cis* with respect to the 8-*H* proton and the nitrogen lone pair.

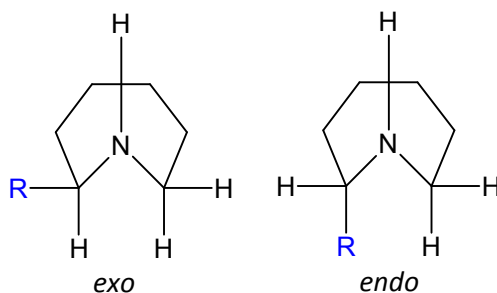


Figure 7

Zusammen and *entgegen* notation in pyrrolizidines refers to the orientation of the 5-*H* and 8-*H* protons relative to the 3-*H* proton as is illustrated in Figure 8. However, systematic names are seldom used when naming pyrrolizidine alkaloids. A naming system based on the nominal mass of such alkaloids has instead been developed. The mass is followed by a letter(s) to distinguish between alkaloids of the same mass. The number and letter(s) are in boldface. Thus xenovenine is represented as **223H**.

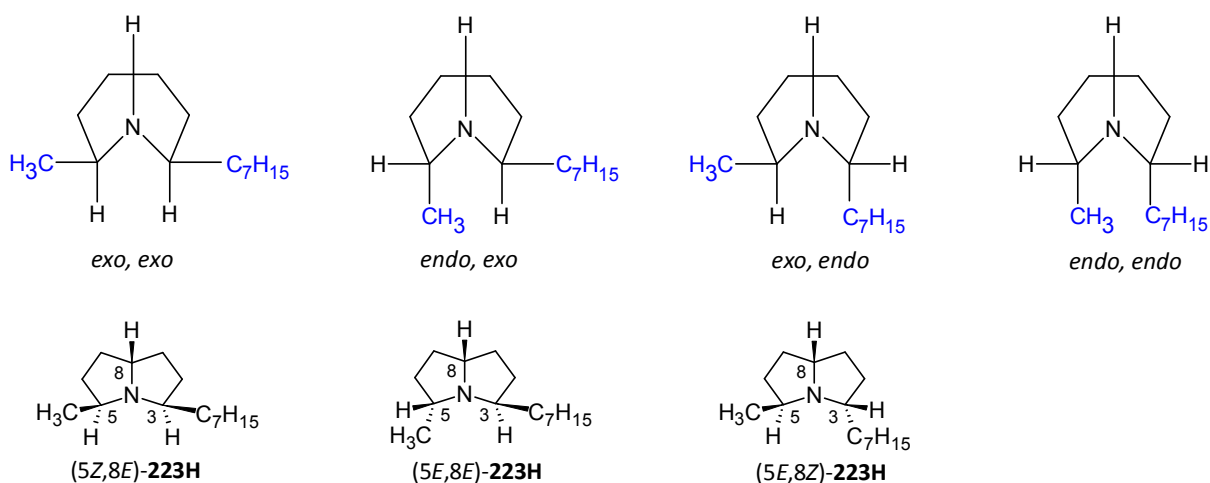


Figure 8

Both ants and frogs appear to use this alkaloid for defensive purposes. The frogs do not produce **223H** themselves but rather acquire it from ants through their diet.²⁰ Some ants may use **223H** as a fungicide.¹ It may be possible that the ants too acquire these alkaloids from plants.²⁴

Liu *et. al.*²² and Daly *et. al.*²⁵ have reported that xenovenine from ants and frog skins have the same absolute configuration of 3*R*, 5*S*, 8*S*. However, it was reported by Toyooka *et. al.*²⁶ that the natural enantiomer in frog skins has an absolute configuration 3*R*, 5*S*, 8*S*, while Uchiyama *et. al.*²⁷ reported the natural enantiomer from the Thief ant is 3*S*, 5*R*, 8*S* (Figure 9).

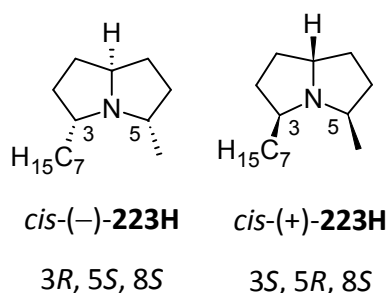


Figure 9

The ants of *Solenopsis* often have potent sting and are therefore referred to as fire ants. Those with necrotizing and hemolyzing venoms usually contain 2-methyl-6-alkylpiperidines.²⁸ Figure 10 shows examples of some other 3,5-disubstituted pyrrolidines.

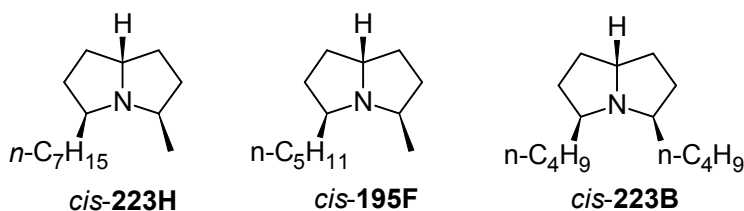


Figure 10

Much of the available information regarding pyrrolizidine toxicity is limited to the plant derived alkaloids. Much less is known about animal derived pyrrolizidine alkaloids but it is, however, known that these alkaloids have displayed neurotoxic activity (more so than their plant derived counterparts).²⁹ In particular, alkaloids from amphibian skins have been found to be noncompetitive blockers of nicotinic acetylcholine receptors.⁷ The affinity of indolizidines substituted at the 5 and 8 position³⁰ led to a study on the affinity of pyrrolizidines and their affinity for such nicotinic acetylcholine receptors (nAChR). The results are shown in Table 1 for the binding interaction of the

alkaloid with sites on carbamylcholine activated nAChR channel complex from the Pacific electric ray (*Torpedo californica*) electric organ.

Table 1: Affinity of alkaloids for nicotinic acetylcholine receptors

Compound	a	6'S-b	6'R-b	c	6'S-d	6'R-d	e	f
Ki, mM	0.05	3.3	8.3	0.83	3.1	3.1	0.42	0.37

The affinity of **a** (**223H'**) was one order larger than the corresponding indolizidines. The hydroxyl moiety in compounds **b** and **d** was expected to lower the affinity due to hydrophobic interactions with the receptor site and thus the absolute stereochemistry had little effect on the affinity.³⁰

Another study completed in 2013 by Stockman and co-workers²⁹ tested the activity of xenovenine with regard to nAChR's. The authors completed an electrophysiology assay on human muscle-type nAChR. Xenovenine was found to inhibit the nicotinic acetylcholine response at high concentrations, with an inhibitory concentration (IC₅₀) of 43.2 μM. However, this IC₅₀ value was found to be relatively low when compared to those of other pyrrolizidines from amphibian skins.

Such studies on the inhibitory activity of pyrrolizidines are significant in finding therapeutic leads for congenital myasthenic syndromes.²⁹ These syndromes affect nerve and muscle cells leading to muscle weakness.³¹

1.2 Synthesis of 3,5-disubstituted Pyrrolizidines

There has been increased interest in the synthesis of 3,5-disubstituted pyrrolizidines over the last 40 years. Initially the syntheses were carried out racemically in order to determine the relative configurations.³² However, focus has shifted to asymmetric synthesis in order to determine the

absolute configuration of the naturally obtained pyrrolizidines.³² Pyrrolizidines substituted at the 2 and 5 positions have shown to be useful intermediates in the synthesis of such pyrrolizidines.^{7, 22, 33-34} There are a number of synthetic routes, the most common of which utilise reductive cyclisations. The number of syntheses will be discussed in more detail, some of which are general routes to 3,5-disubstitued pyrrolizidines and other direct routes to xenovenine. The historically important first synthesis of xenovenine will be discussed as well as the much more recent method utilizing *N*-acylcarbamates. Thus the following listed items will be addressed in more detail.

- Reductive cyclisation *via* triketones²¹
- Reductive cyclisation *via* nitrodiketones³⁵
- Reductive cyclisation *via* intramolecular amidomercuration³³
- Reductive cyclisation *via* hydroamination²⁰
- Reductive cyclisation *via* allylic aminations⁷
- Reductive cyclisation *via* coupling of *N*-acylcarbamates^{22, 34}

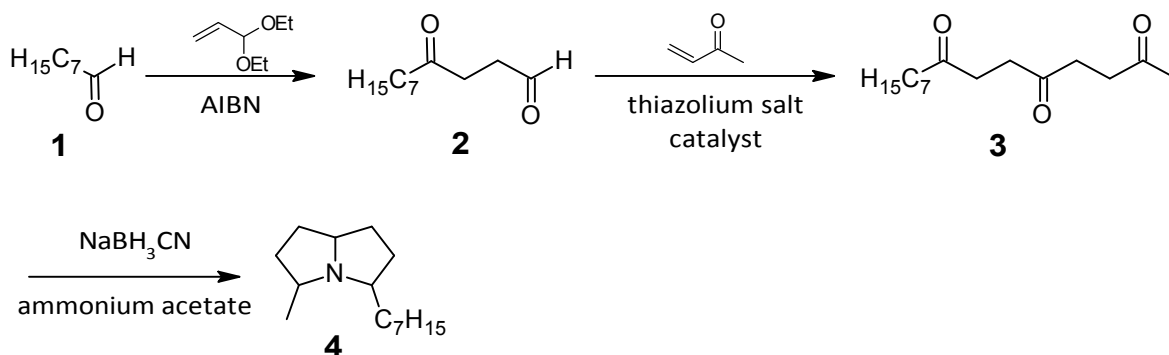
Other methods not utilizing reductive cyclisations include:-

- Epoxidation,³²
- Reverse Cope Elimination,³⁶ and
- Double nucleophilic substitution.³⁷

The first reported synthesis of **223 H** was by Jones and Blum in 1980 *via* triketone cyclisation.

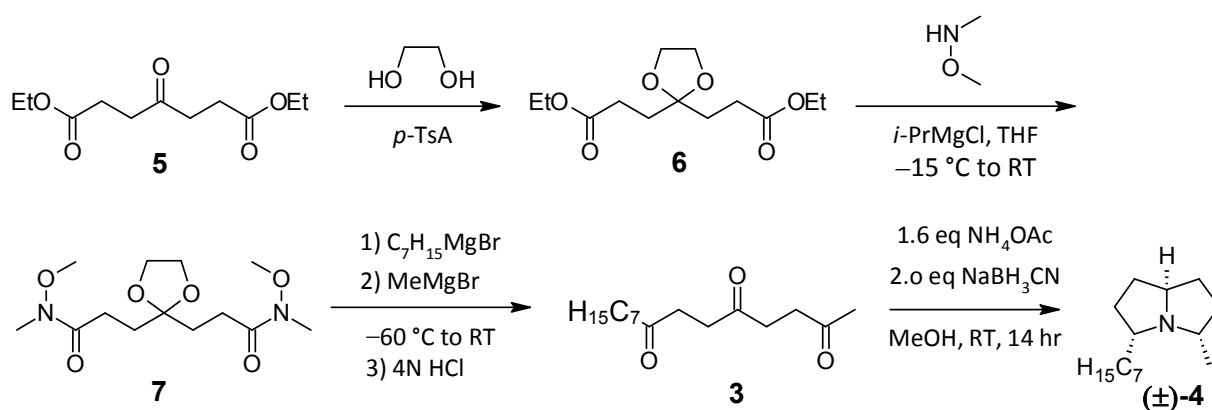
1.2.1 Reductive Cyclisation *via* Triketones

Jones and co-workers²¹ first synthesised xenovenine in racemic form in 1980. Their main aim was to determine the orientation of the bicyclic ring structure as either *cis* or *trans*. Octanal **1** was treated with acrolein diethyl acetal and AIBN (Scheme 2) and then hydrolysed to afford 4-oxoundecanal **2**. This was then reacted with methyl vinyl ketone in triethylamine and a thiazolium salt to give the trione **3**. Reductive amination of the trione with sodium cyanoborohydride and ammonium acetate yielded xenovenine **4** as a mixture of diastereomers with a 20 % yield over 3 steps.



Scheme 2

This method has seldom been utilised by others, in particular because it does not allow for asymmetric synthesis. A similar approach by Stockman and co-workers²⁹ in 2013 afforded (\pm)-**4** as a single diastereomer (Scheme 3). Their two-directional approach began with an acetal protection of diethyl 4-oxopimelate **5** to afford the diester **6**. The diester was next converted to the Weinreb diamide **7**. Sequential Grignard addition to the diamide yielded triketone **3**, which underwent a triple reductive cyclisation to afford (\pm)-**4** as a single diastereomer in a 5 % yield.



Scheme 3

Jones and Blum carried out the synthesis in order to determine the overall carbon nitrogen skeleton of xenovenine. Four isomers (**a-d**) were detected by gas chromatographic analysis (Figure 11). The isomers were separated by preparative gas-liquid chromatography and their mass spectra and NMR spectra compared to xenovenine isolated from Thief ants. The *cis*-fused isomer **b** was the most prevalent and proposed by the authors to be the natural isomer of xenovenine.²¹

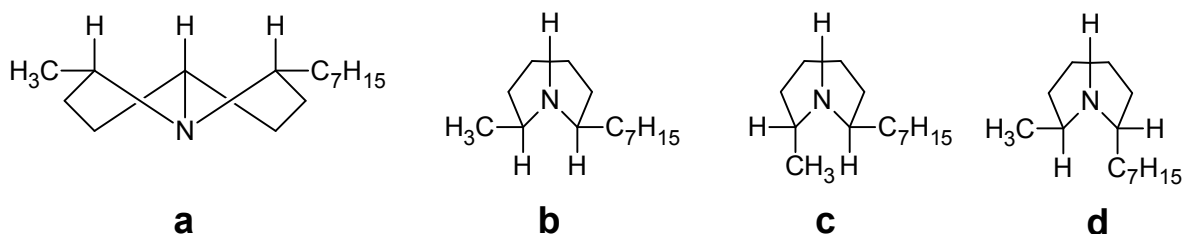
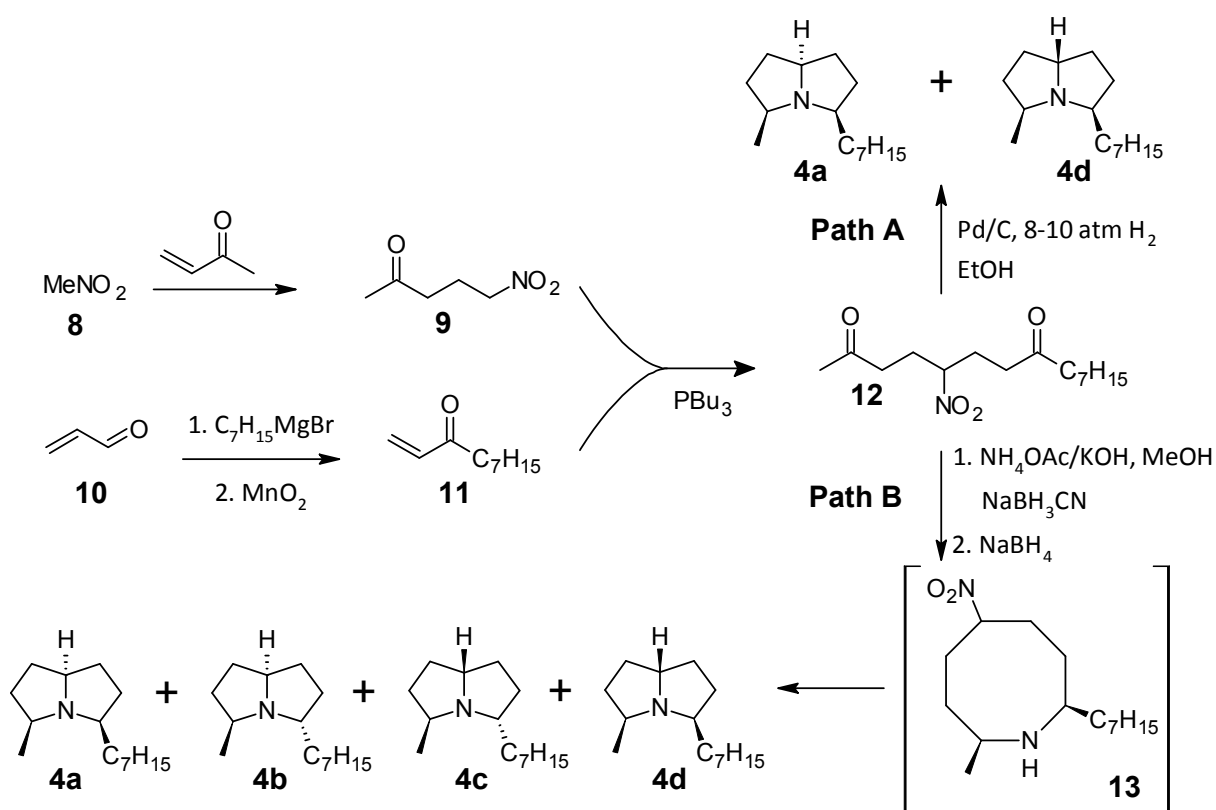


Figure 11

1.2.2 Reductive cyclisation *via* Nitrodiketones

Hesse and co-workers³⁵ have investigated the conversion of nitrodiketones of differing chain lengths for conversion into pyrrolizidines, indolizidines and quinolizidines. Xenovenine was thus synthesised from 5-nitropentadecan-2,8-dione **12**. The nitrodiketone was prepared from nitromethane **8** and methyl vinyl ketone (Scheme 4). The ketone was prepared *via* a Grignard reaction between acrolein **10** and heptyl magnesium bromide.



Scheme 4

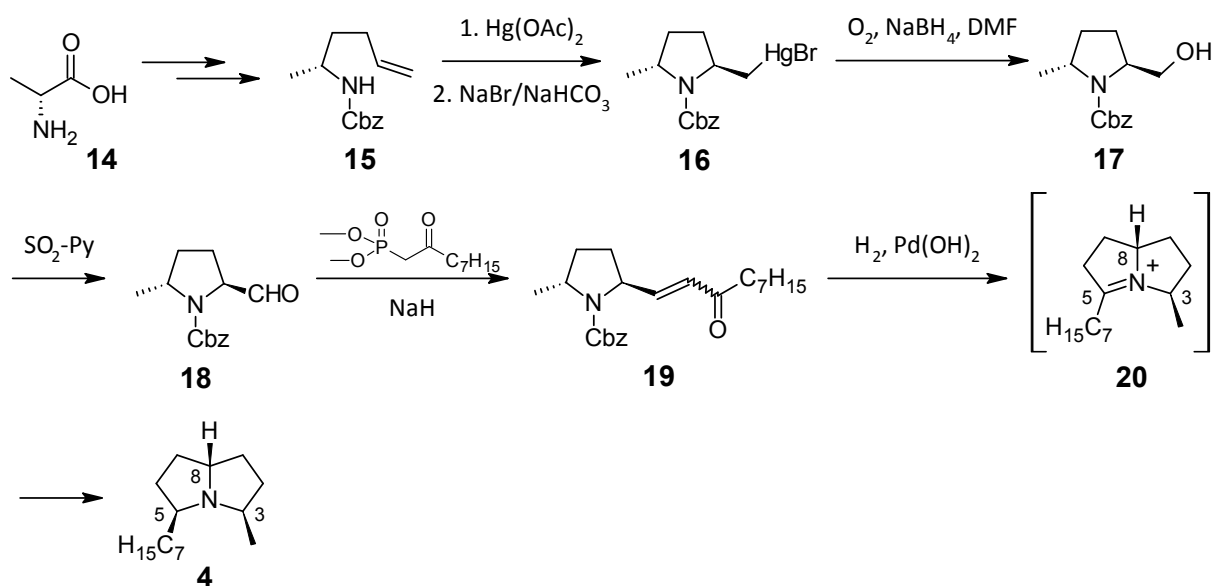
Two different methods of reduction were then investigated. In Path A the reduction was carried out with 8-10 atm H₂ catalysed by Pd/C. This gave the expected *syn* product **4a** in a yield of 65 % as well

as xenovenine **4d** (5% yield). The *syn* product **4a** was then oxidised with $\text{Hg}(\text{OAc})_2/\text{AcOH}$ and then reduced to xenovenine **4d** with NaBH_3CN . The conversion ratio was >60%.³⁵

In Path B the reduction was performed with NaBH_3CN , MeOH, NH_4OAc , KOH and NaBH_4 . These conditions led to the formation of four isomers of xenovenine *via* intermediate **13** with 88% being xenovenine **4d** and 12% the remaining three isomers. ^{15}N labelling indicated the nitrogen source in the reduction was NH_4OAc and from this data the authors proposed three possible intermediates, a triketone, an amino-nitroketone or the eight-membered ring **13** depicted in Scheme 4. From the three intermediates the authors proposed that the eight member ring intermediate accounts for the observed stereoselectivity.³⁵

1.2.3 Reductive Cyclisation *via* Intramolecular Amidomercuration

Takahata and co-workers³³ have synthesised (+)-xenovenine from D-(–)-alanine **14** (Scheme 5). This was converted to (*R*)-*N*-(benzyloxycarbonyl)-1-methyl-4-pentenylamine **15** which then underwent intramolecular amidomercuration. The resulting compound **16** was then oxidatively demercurated to form the *trans* isomer exclusively. Parikh-Doering oxidation of the alcohol **17** afforded the aldehyde **18** which reacted with dimethyl (2-oxononyl)phosphonate *via* the Horner-Wadsworth-Emmons reaction. This yielded the α,β -unsaturated ketone **19** (*E:Z* = 8:1) which was subsequently reduced to (+)-xenovenine **4**. The reduction occurred simultaneously with debenzyloxycarbonylation, annulative imination and reduction of the iminium intermediate **20**.

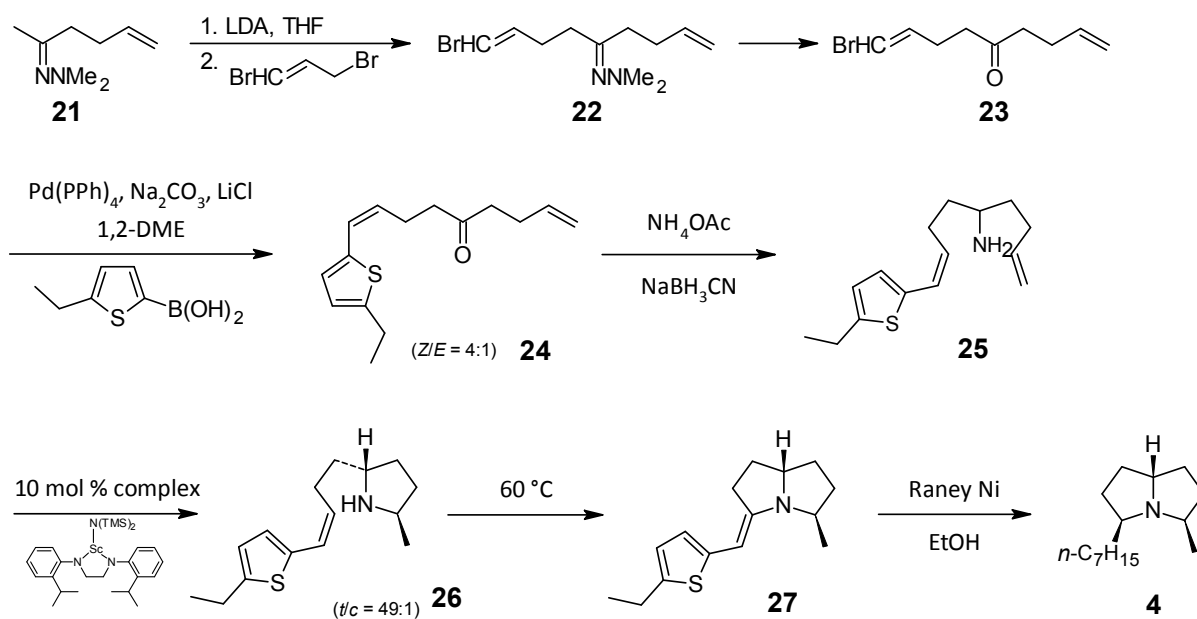


Scheme 5

The e.e. of **19** was determined to be > 98 % by HPLC with a Daicel AS column and (+)-xenovenine was formed as a single product and thus it was assumed that the synthesis was carried out without racemisation in a yield of 19 % from **17**.

1.2.4 Reductive Cyclisation *via* Hydroamination

Livinghouse and Jiang²⁰ have utilised a Sc(III)-catalysed hydroamination in their synthesis of (±)-xenovenine. 1,2-Disubstituted aminoalkenes undergo internal hydroamination very reluctantly and as such a terminal heteroaromatic group was instead employed. Such groups are known to cyclise at much faster rates than the 1,2-disubstituted aminoalkenes. Thus amine **21** was alkylated and hydrolysed to afford ketone **23** (Scheme 6). The ketone was next coupled with 5-ethylthiophene-2-boronic acid. The *Z*-isomer **24** was isolated *via* chromatography on silica. This was followed by reductive amination. The resulting amine **25** was treated with the Sc(III) complex to diastereoselectively generate the 2,5-disubstituted pyrrolidine **26**. An increase in reaction temperature to 60 °C led to a rapid and stereospecific bicyclisation to yield pyrrolizidine **27**. This was followed by reductive desulfurisation to afford (±)-xenovenine **4** in an overall yield of 44 % from **21**.²⁰

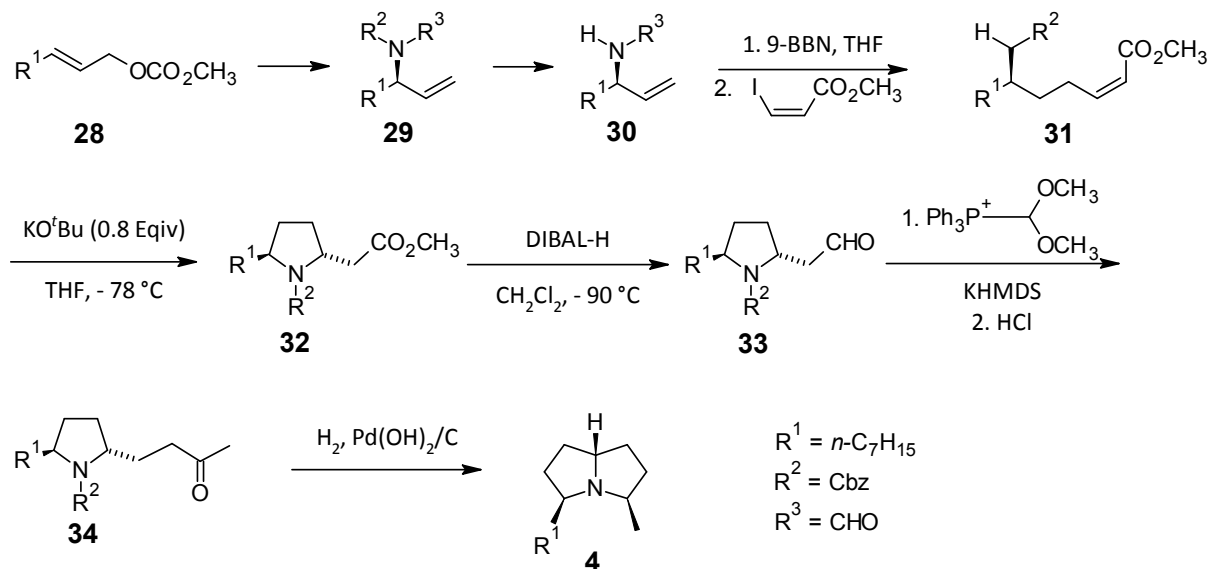


Scheme 6

1.2.5 Reductive Cyclisation *via* Allylic Amination

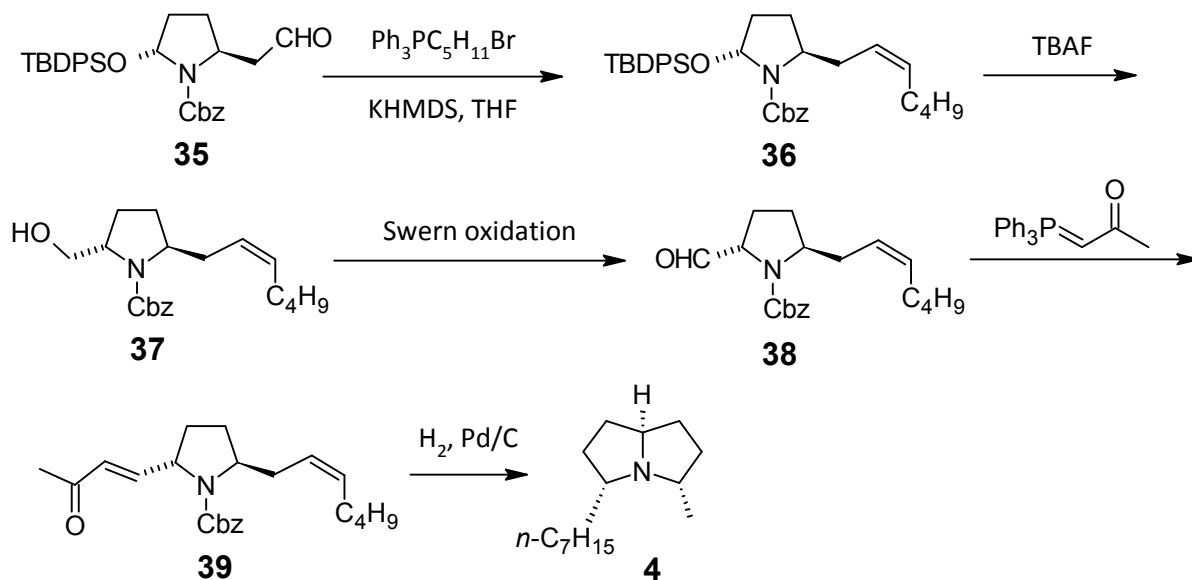
Both (+)-**223H** and (–)-**223H** have been synthesised by Gärtner and co-workers⁷ *via* iridium-catalysed allylic aminations. There are three key steps to the synthesis (Scheme 7).

- 1) Synthesis of a protected allylamine **30**. This is achieved through Ir-catalysed allylic amination with an *N,N*-diacylamine.
- 2) Hydroboration of the allylic double bond followed by Suzuki-Miyaura cross coupling to afford the α,β -unsaturated ester **31**.
- 3) Base promoted intramolecular aza-Michael addition to ring close.



Compound **32** is then transformed into the aldehyde **33**, a key intermediate utilised in many alkaloid syntheses such as Lhommet's synthesis of (-)-**223H** in 1998.³⁸ The Wittig reaction affords ketone **34** which then undergoes Pd(OH)₂/C catalysed reduction with H₂ to yield (+)-xenovenine **4** in a yield of 56% from **32**. The e.e. was determined by GC analysis and was found to be 94.5%. This was identical to the e.e. of the starting materials.⁷

Similarly, (-)-**223H** can be accessed *via* **32** where R¹ is CH₂OTBDPS. This too is treated with DIBAL-H to afford the aldehyde **35**. This is followed by the Wittig olefination to yield the (*Z*)-olefin **36** exclusively (Scheme 8). Deprotection with TBAF afforded the alcohol **37** which then underwent Swern oxidation to **38**. Another Wittig reaction gave (*E*)-**39** which was subsequently reduced with H₂ to afford diastereomerically pure (-)-xenovenine **4** in a 49% yield from **32** with an e.e. of 96%.⁷



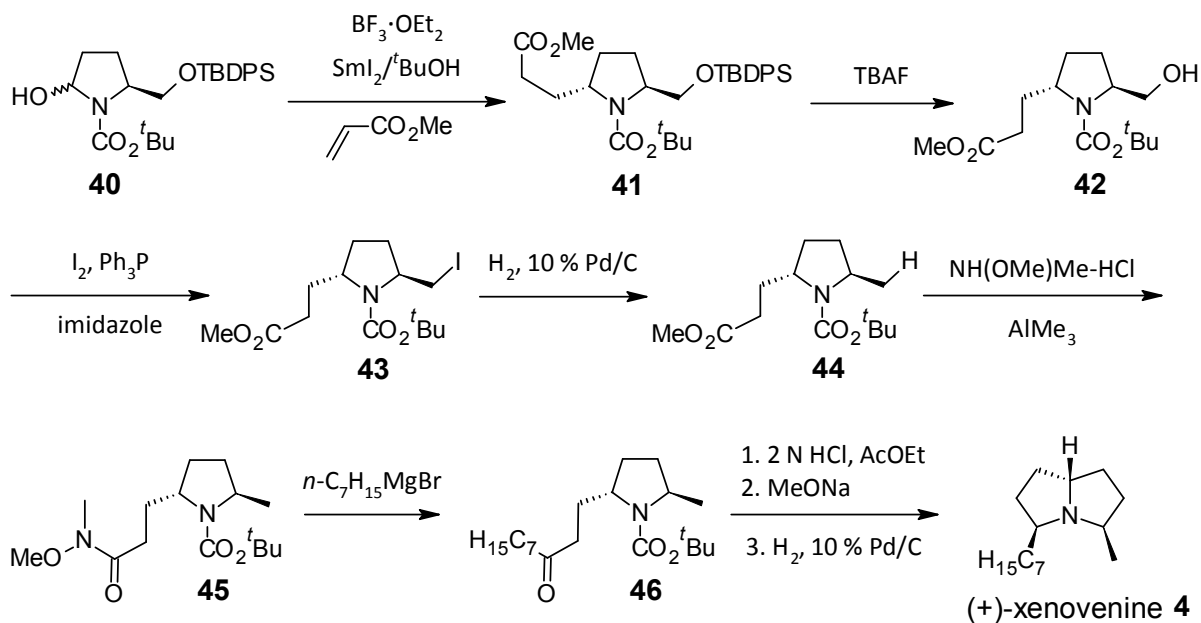
Scheme 8

Both enantiomers were thus synthesised and further inspection proved that there was no significant racemisation in either method.

1.2.6 Reductive Cyclisation *via* Coupling of *N*-acylcarbamates

Xiang and co-workers^{22, 34} have synthesised both the (+)- and (–)-enantiomers of xenovenine *via* a SmI_2 catalysed intermolecular cross coupling of *N*-acylcarbamates and activated alkenes.

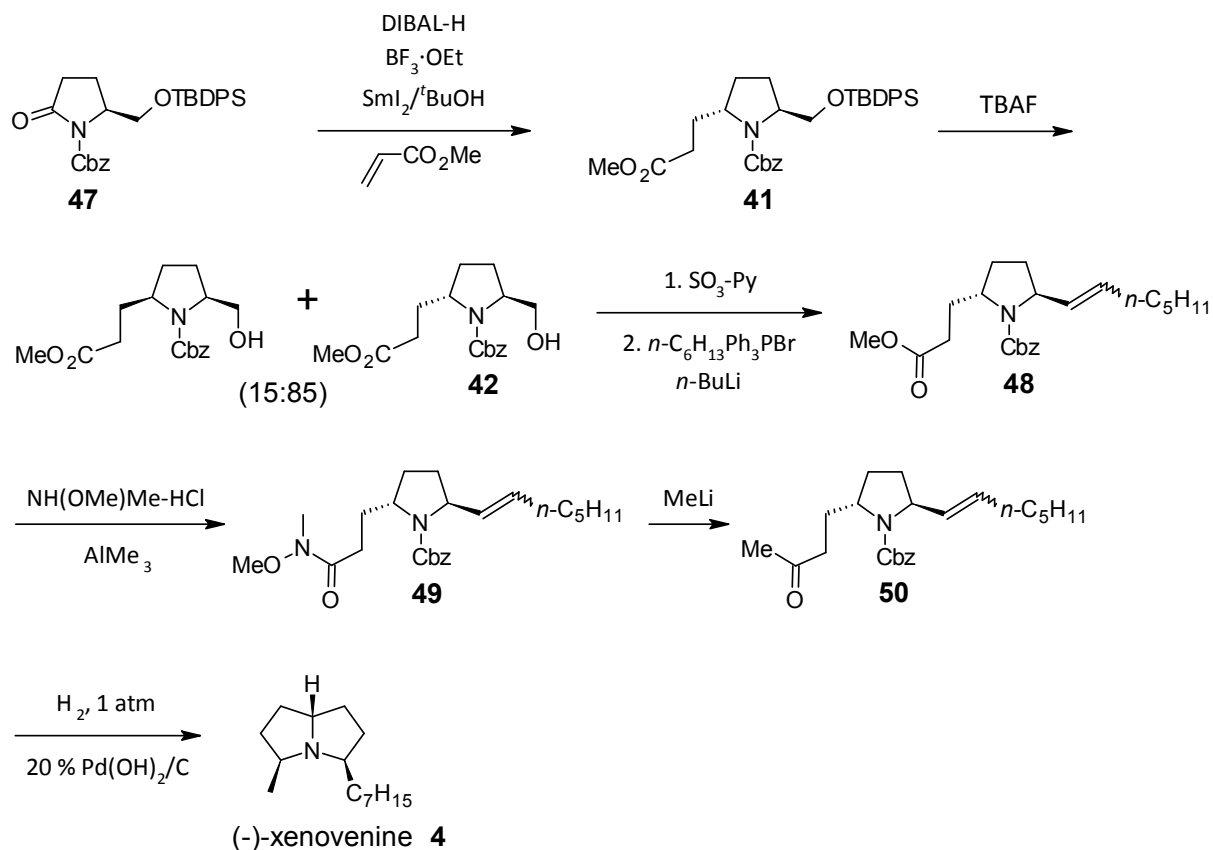
Cross coupling (Scheme 9)³⁴ of the pyroglutamic derived *N*- and *O*-protected alcohol **40** with methyl acrylate afforded *trans*-**41** (91:9). This was treated with TBAF to give the deprotected alcohol **42**, the diastereomers of which were separated by flash chromatography. The major *trans* diastereomer was next treated with I_2 and Ph_3P to give **43** and then reduced with H_2 over 10 % Pd/C to afford **44**. This was then converted to the Weinreb amide **45** followed by the Wittig reaction to give the (2*S*, 5*R*)-pyrrolidine **46**. *N*-deprotection followed by reductive amination afforded (+)-xenovenine **4** (17 % yield from **40**).



Scheme 9

It was found that the *N*- and *O*-protecting groups influenced the diastereoselectivity of the reaction. The sterically hindered TBDPS for *O*-protection was found to favour *trans*-diastereoselectivity. The *N*-carbamoyl *N,O*-acetal was 2,5-*trans* diastereoselective for the pyrrolidine allowing for the conversion to (+)-**223H**.³⁴

Similarly, (–)-**223H** was synthesised from the pyroglutamic acid derived *N*-L-acylcarbamate **47** and methyl acrylate (Scheme 10).²² The resulting diastereomeric mixture was treated with TBAF and the resulting diastereomers **42** separated by chromatography. The major *trans* diastereomers **42** next underwent a Parikh-Doering oxidation followed by the Wittig reaction. The resulting olefin **48** was converted to the Weinreb amide **49** and then to the methyl ketone derivative **50**. This was then reduced to (–)-xenovenine **4** as the only observed diastereomer in a yield of 19 % from **47**.²²

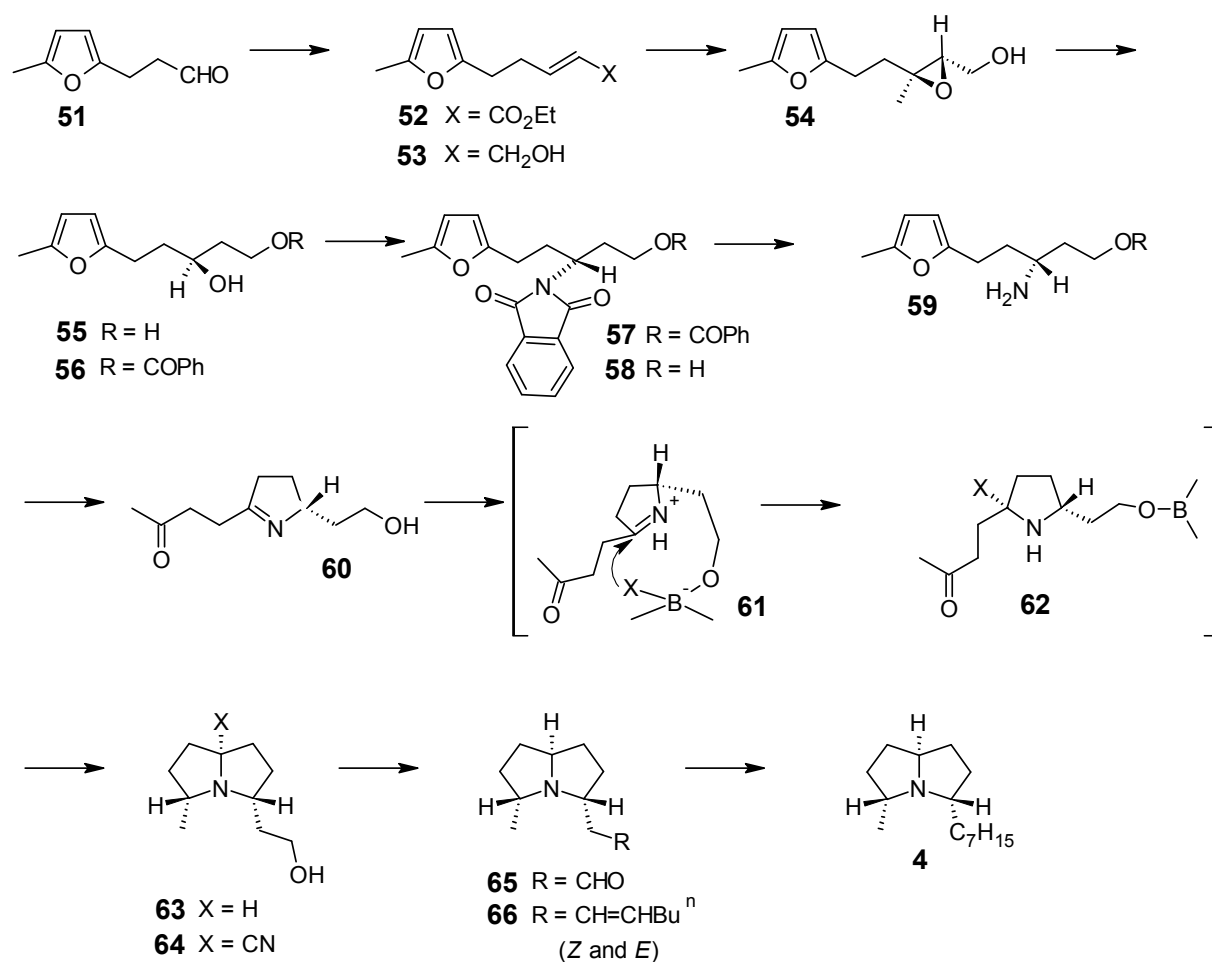


Scheme 10

1.2.7 Epoxidation

An asymmetric synthesis *via* epoxidation was carried out by Takano and co-workers in 1983 (Scheme 11).³² 3-(5-Methyl-2-furyl)propionaldehyde **51** underwent the Horner-Wadsworth-Emmons reaction with triethyl phosphonoacetate to give the unsaturated ester **52**. This was reduced with di-isobutylaluminium hydride to give the alcohol **53**. This was then oxidised with *t*-butyl hydroperoxide and titanium isopropoxide in the presence of (+)-L-tartrate resulting in the formation of the chiral epoxide **54**. This was then regioselectively cleaved with bis-(2-methoxyethoxy)aluminium hydride to afford the 1, 3- diol **55**. Treatment with benzoyl chloride in triethylamine yielded the primary benzoate **56**. The secondary alcohol was next substituted by phthalimide with the configuration being inverted in the process. Debenzoylisation followed to give **58** which was then reacted with hydrazine hydrate to give the amino alcohol **59**. The pyrrolone derivative **60** resulted from treatment with perchloric acid in water in slight molar excess (pH *ca.*1). This was then reduced with sodium cyanoborohydride at pH 4 to give a mixture of pyrrolizidines **63** and **64**, which were then separated by chromatography on Al₂O₃. The nitrile **64** was converted into **63** by treatment with either sodium borohydride or liquid ammonia. The alcohol was next oxidised under Moffatt-Swern conditions to afford the aldehyde **65**. Wittig reaction with

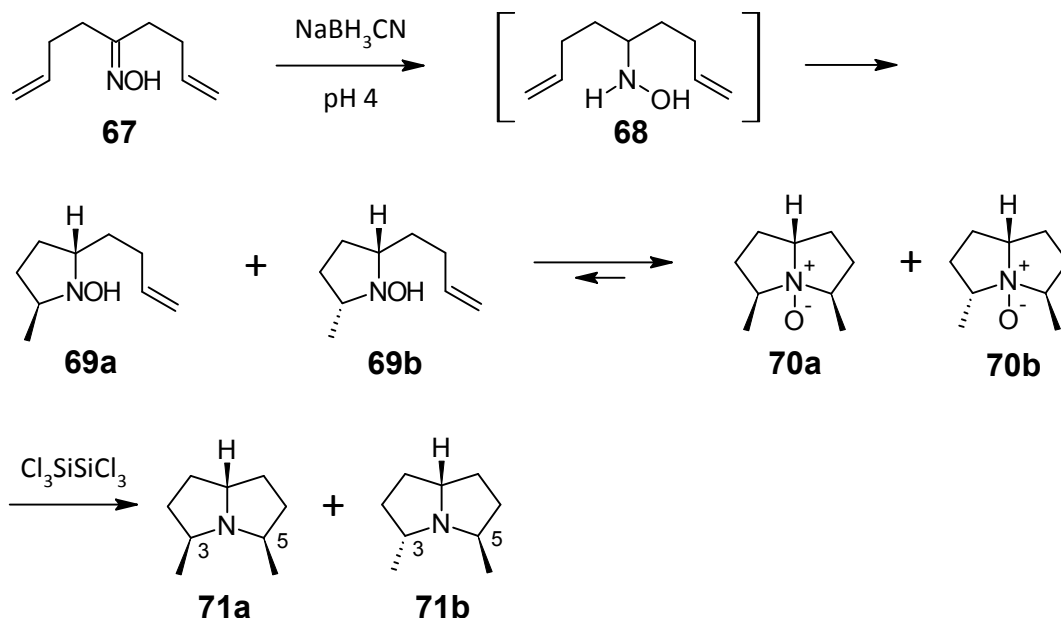
n-pentylidetriphenylphosphorane yielded the olefin **66** as a mixture of *Z* and *E* isomers. Catalytic hydrogenation on platinum afforded xenovenine **4**. The overall yield was reported to be 28 % from **63**.³²



Scheme 11

1.2.8 Reverse Cope Elimination

In general, 3,5-disubstituted pyrrolizidines are accessible by Reverse Cope elimination of oximes. The oxime is obtained from a dienone. Reduction of **67** with NaBH₃CN at pH 4 affords intermediate **68**, which undergoes Reverse Cope elimination to give two *N*-oxide epimers **70a** and **70b** (Scheme 12). The *N*-oxides are reduced with hexachlorodisilane to give the corresponding 3,5-disubstituted pyrrolizidines **71a** and **71b** (55:45 mixture) with an overall yield of 41 %.³⁶

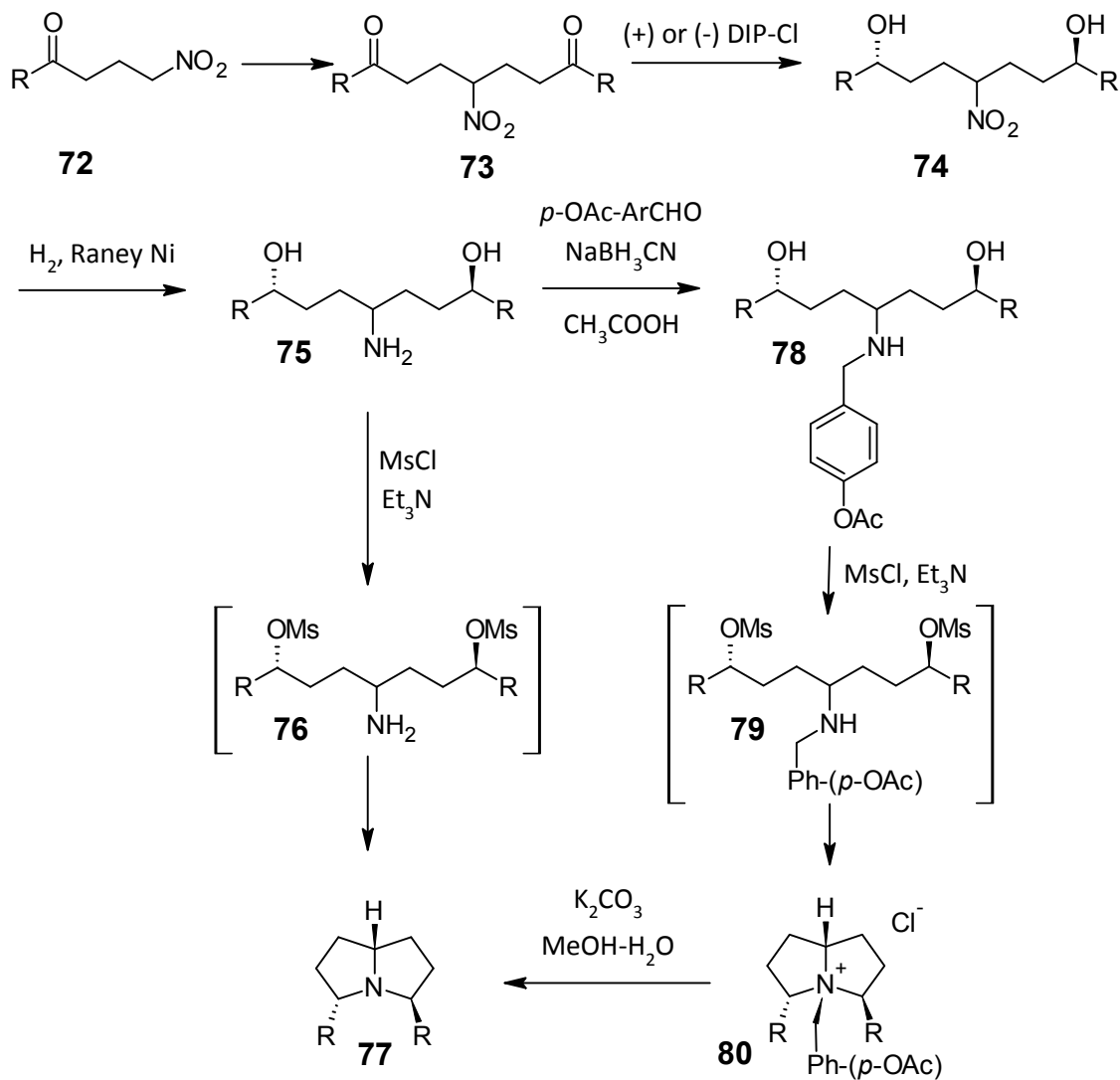


Scheme 12

Thus by altering the dienone various chain lengths at the 3 and 5 positions can be accessed.

1.2.9 Double Nucleophilic Substitution

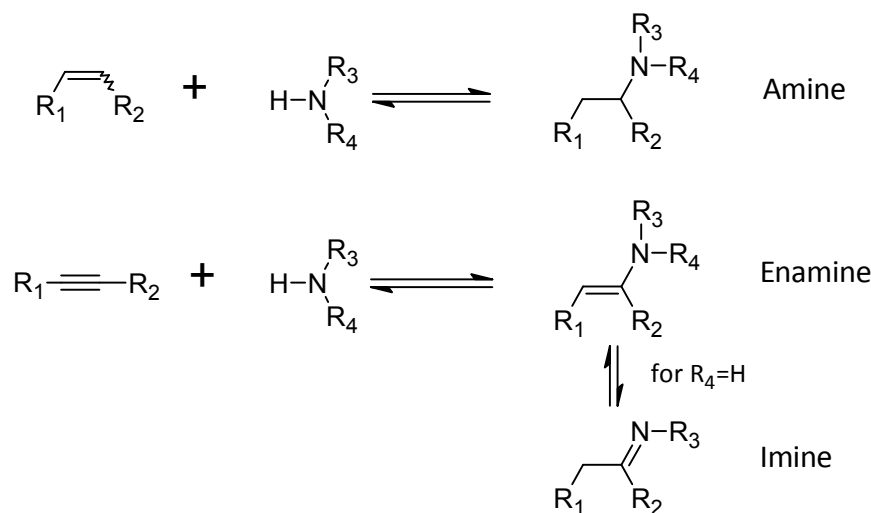
Scarpi and co-workers³⁷ have developed a route to 3,5-diarylpyrrolizidines from γ -nitroketone. Nitrodiketone **73** (R = Ph) was prepared by conjugate addition of nitroketone **72** to phenyl vinylketone in the presence of Amberlyst A21 (Scheme 13). Reduction of **73** with (+)- or (-)- diisopinocampheylchloroborane (DIP-Cl) afforded nitrodiol **74**. The nitro group was reduced over Raney Ni to afford aminodiol **75**. The diol was treated with MsCl but direct conversion to **77** through **76** gave poor results due to *N*-mesylation in the aminodiol. Thus, the aminodiol **75** was instead reacted with *p*-acetyloxybenzaldehyde and reduced with NaBH₃CN to the *N*-*p*-acetyloxybenzyl protected diol **78**. The *N*-*p*-acetyloxybenzyl allowed for smooth double cyclisation as the steric hindrance slowed the *N*-mesylation in comparison to *O*-mesylation. Thus diol **78** was treated with MsCl to give **79** and double nucleophilic substitution gave the pyrrolizidine salt **80**. Hydrolysis of the acetyl with K₂CO₃ in MeOH-H₂O afforded the debenzylated 3,5-diarylpyrrolizidine **77** with yields ranging from 33-46 % depending on the R group.³⁷



Scheme 13

1.3 Hydroamination

Hydroamination is the addition of ammonia or primary or secondary amines to alkenes, alkynes or allenes as shown in Scheme 14.³⁹ More specifically, it is the addition of an N-H bond across carbon-carbon multiple bonds.⁴⁰ The reaction proceeds with 100 % atom economy from readily available and affordable materials.⁴¹ It is the most atom economic process for the formation of amines, enamines and imines.⁴²



Scheme 14

Hydroamination of alkynes affords reactive enamine or imine species depending on the amine utilised. Such reactive intermediaries provide flexibility in synthesis and can be used for a number of different transformations. However, if an amine is the desired product then the enamine or imine must be reduced.⁴²

Hydroaminations can proceed through intermolecular additions or intramolecular cyclisations. In general, intramolecular reactions are more readily achieved than the corresponding intermolecular reactions.⁴³ However, intermolecular hydroaminations were the first to be successful.⁴⁰ Whether the hydroamination proceeds intra- or intermolecularly, unactivated substrates (those without electron withdrawing substituents) do not react spontaneously and catalysts are required. However, some activated substrates do not require catalysts to undergo hydroamination. These are generally Michael acceptor type alkenes.⁴⁴ Alkynes are also much better substrates for hydroaminations than alkenes, both intra- and intermolecularly. This is partially due to steric factors and partially due to the weakness of the alkyne π -bond in comparison to the alkene π -bond (approximately 70 kJmol^{-1} weaker in alkynes than in alkenes).⁴⁵

Hydroamination reactions are thermodynamically favoured; they are exergonic and exothermic under standard conditions. However, the entropy of reaction is negative and thus simply increasing the reaction temperature has no effect on overcoming the high activation barrier⁴¹ as this would shift the equilibrium of the reaction towards the starting materials. The high activation barrier for the direct addition of amines across C–C multiple bonds is in part due to electrostatic repulsion between the lone pair of electrons on nitrogen and the electron rich π -bonds of the alkene/alkyne/allene.⁴² It is for this reason that catalysts are required for hydroamination.⁴¹

Both heterogeneous and homogeneous catalytic systems have been employed for hydroamination reactions. The method of activation for heterogeneously catalysed hydroaminations is difficult to determine, but the activation method and mechanism can be determined for homogeneously catalysed hydroamination reactions.⁴⁴

A number of heterogeneous catalysts have been used for hydroamination reactions. These include zeolites, pillared interlayered clays (PILCs) such as K-10, mesoporous oxides and acid treated sheet silicates. Attention will be focused on homogeneous methods for this discussion.

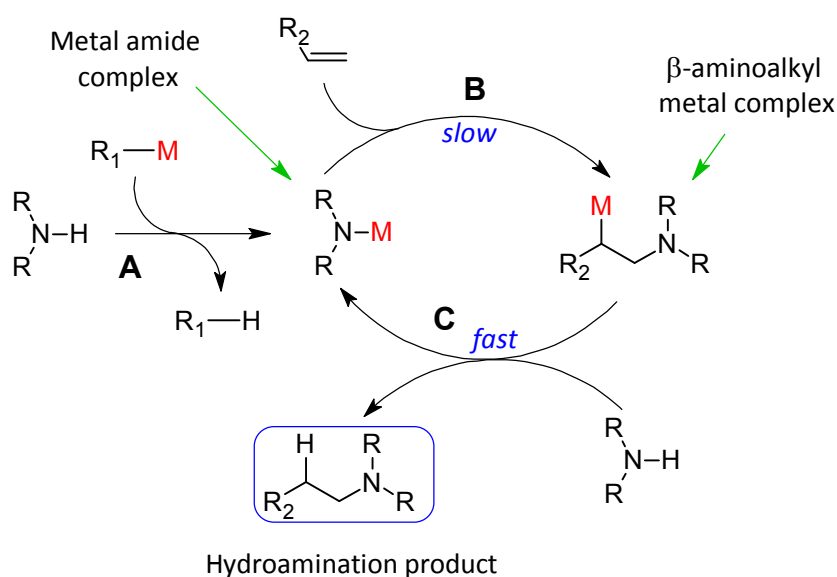
There are three possible homogeneous methods

- I. Base catalysed,
- II. Acid catalysed, and
- III. Metal complex catalysed.

1.3.1 Base Catalysed Hydroamination

Strongly electropositive metals such as alkali metals, alkali earth metals and lanthanides are able to activate amines by deprotonation. This affords a highly nucleophilic alkali-metal amide ion capable of reacting with C–C multiple bonds.⁴⁶

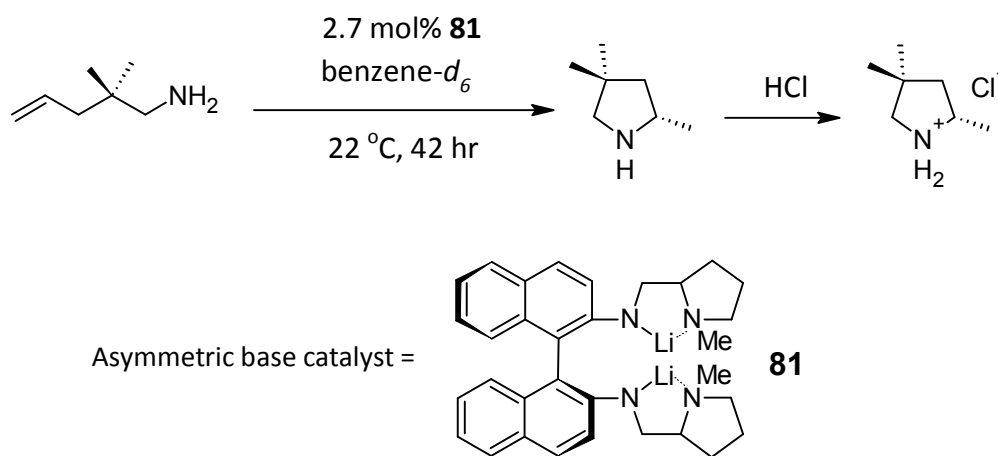
Cornils and Herrmann have proposed an appropriate electropositive metal, M, deprotonates the amine (**A**) to form the metal-amide complex (*i.e.* the activated amine) depicted in Scheme 15. Nucleophilic addition of the alkene follows (**B**) to generate the highly polar β -aminoalkyl metal complex intermediate. Addition of the amine then generates the alkylamine hydroamination product by protonolysis and the metal-amide complex is regenerated in the process (**C**).⁴⁶



Scheme 15

(-)-Menthol has been synthesised industrially *via* base catalysed hydroamination.⁴⁷

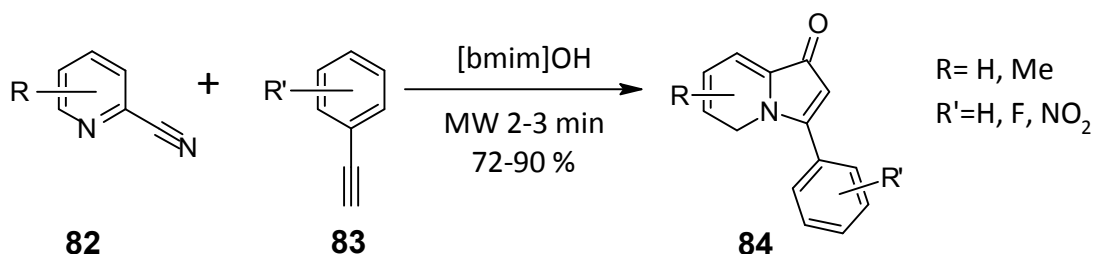
The first base catalysed asymmetric intramolecular hydroamination was carried out by Hultzsch and co-workers in 2006 using a chiral diamidobinaphthyl dilithium salt **81** (Scheme 16).^{43, 47}



Scheme 16

The isolated yield was 86 % and an enantiomeric excess of 64 % (*S*) was achieved.

More recently basic ionic liquids have been utilised for the intermolecular hydroamination of cyanopyridines **82** and alkynylbenzenes **83** under microwave irradiation. 1-Butyl-3-methylimidazolium hydroxide ([bmim]OH) was the ionic liquid used for the hydroamination (Scheme 17).⁴⁸



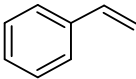
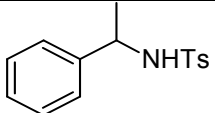
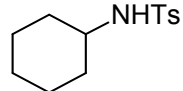
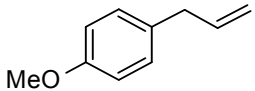
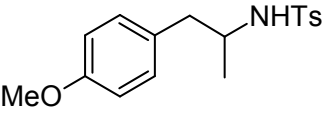
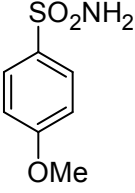
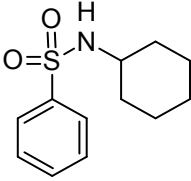
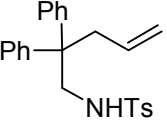
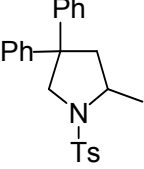
Scheme 17

The reaction was first carried out in ethanol with 20 mol% NaOH and 5 mol% CuI catalyst and refluxed for 5 hours to afford the desired product **84** in a 62 % yield. The same reaction was performed with [bmim]OH at room temperature and stirred for 1 hour to give a yield of 80 %. Microwave irradiation was then utilised to give yields of 72-90 % in 2 to 3 minutes. Increasing the reaction times further did not improve the yields.

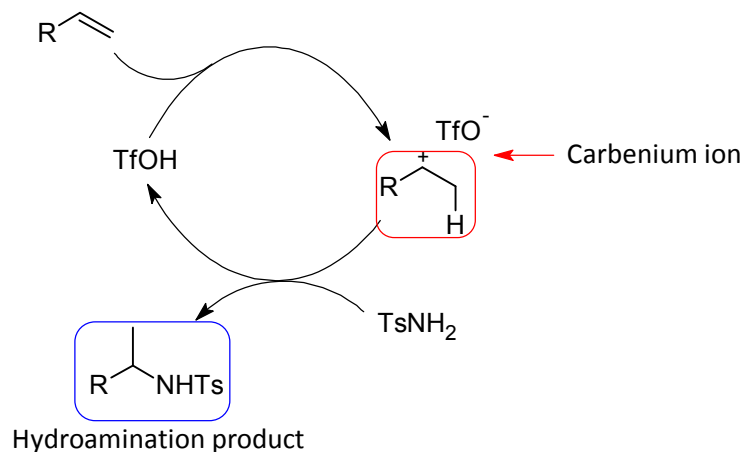
1.3.2 Acid Catalysed Hydroamination

Historically, hydroamination reactions have been either base or metal catalysed. More recently, acid catalysed hydroamination reactions have successfully been carried out. The challenge for acid catalysis in hydroamination is that the amine is more basic than the alkene/alkyne π -system and the formation of amine salts destroys the nucleophilicity thus hampering activation of the π -system. Brønsted acids have found application in hydrophosphorylation, aziridination and hydroamination reactions. Trifluoromethanesulfonic acid, HOTf (triflic acid), at low concentrations has catalysed hydroamination of simple olefins under mild conditions. A variety of protected amines were reacted successfully with olefins and 1,3-dienes as depicted in Table 2. Addition to unactivated olefins required slightly elevated temperatures (60-85 °C) to afford good conversions.⁴⁹

Table 2: HOTf catalysed hydroamination of olefins and amines

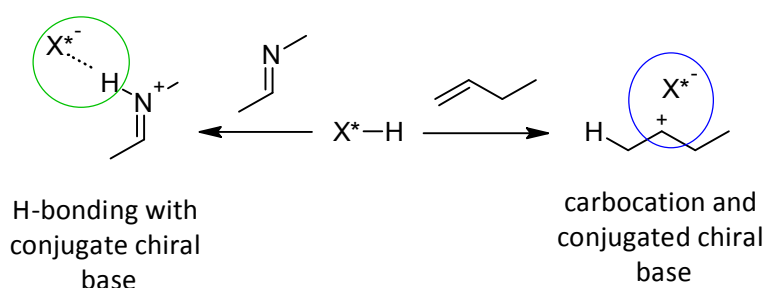
$\text{R}-\text{CH}=\text{CH}_2 + \text{TsNH}_2 \xrightarrow[\text{Toluene}]{\text{HOTf}} \text{R}-\text{CH}_2-\text{CH}_2-\text{NHTs}$				
Amine	Olefin	Temperature/°C	Product	Yield
TsNH ₂		85		70
TsNH ₂		85		85
TsNH ₂		60		88
		85		95
		85		90

The reaction is believed to proceed *via* the generation of a carbenium ion, followed by attack of the amine, resulting in the hydroamination product, whilst regenerating the acid catalyst (Scheme 18).⁴⁹ The formation of the carbenium ion intermediate is essential in order for nucleophilic amines or ammonia to react to give the more substituted amine products.⁴³



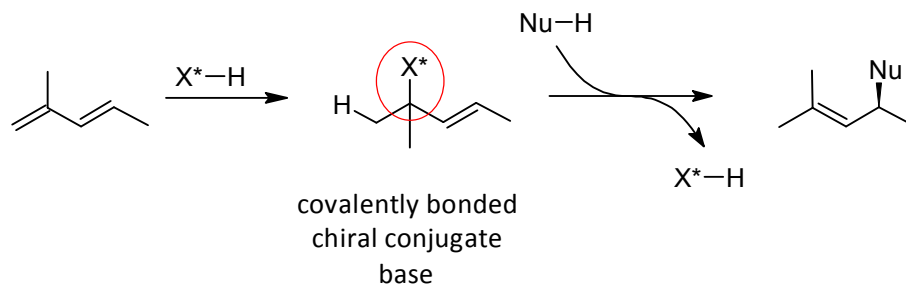
Scheme 18

The first asymmetric acid-catalysed hydroamination was reported by Shapiro and co-workers⁵⁰ in 2011. Two problems had to be overcome in order to carry out a successful asymmetric synthesis shown in Scheme 19. Firstly, the imine formed on addition of the chiral acid, X^*H , is capable of hydrogen bonding with the conjugate base of the chiral Brønsted acid, which then anchors the chiral acid near the reactive electrophile (reaction depicted on the left in Scheme 19). The authors claim this would result in one diastereomeric transition state being favoured due to molecular configuration. Secondly, if the alkene is protonated a carbocation is formed (reaction depicted on the right in Scheme 19). Now electrostatic interactions hold the conjugate base close, but there is an absence of rigidity which is presumed to be responsible for the poor discrimination between the enantiotopic faces of the carbocation.



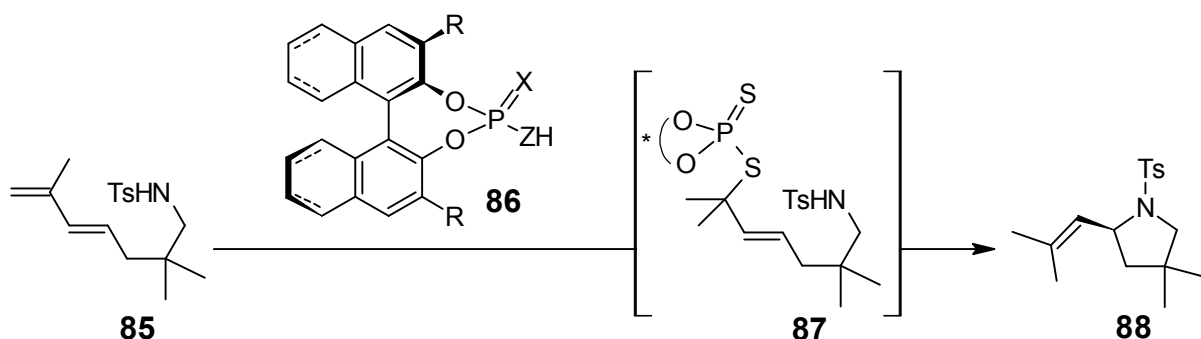
Scheme 19

In order to overcome such problems the authors proposed a Brønsted acid with a nucleophilic conjugate base that is capable of forming a covalent bond with the carbocation must be chosen. The incoming nucleophile could potentially displace the chiral group in a S_N2' reaction as depicted in Scheme 20.⁵⁰



Scheme 20

Such an acid must be strong enough to protonate an alkene and possess a nucleophilic conjugate base. Thus the authors considered dithiophosphoric acids. The sulfur confers greater acidity and nucleophilicity on the acid since sulfur is more polarisable than oxygen.⁵⁰ Scheme 21 shows the reaction catalysed by the acid catalyst.



Scheme 21

Four variations of the catalyst system **86** were tested

- I. X = Z = S, R = 1-naphthyl
- II. X = Z = O, R = 1-naphthyl
- III. X = S, Z = NTf, R = 1-naphthyl
- IV. X = O, Z = NTf, R = 1-naphthyl

The solvent (CDCl₃) and temperature (30 °C) were held constant. Those catalysts where X = O did not catalyse the reaction. Those where X = S did so in high yields but poor enantioselectivities. However, the authors found that the following changes improved the enantioselectivities to above 90 % e.e.

- Bulk of the R group substituent
- A partially hydrogenated catalyst backbone
- Fluorobenzene as a solvent with 4 Å molecular sieves
- A reduction in temperature (15 °C)

Thus the optimised catalyst system is shown in Figure 12.

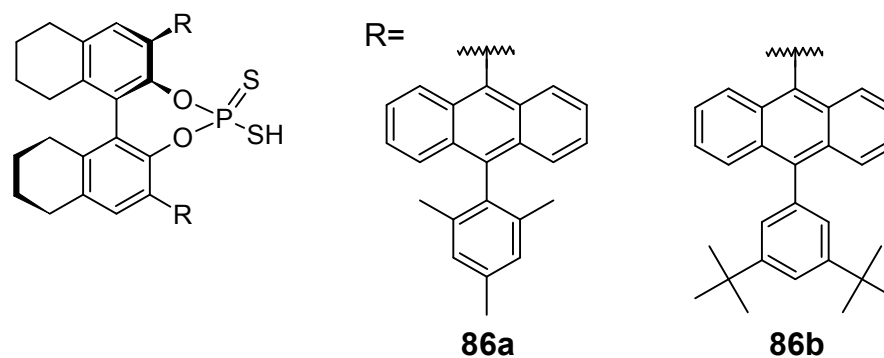


Figure 12

These catalysts were then utilised for a number of enantioselective hydroamination reactions with 1,2- and 1,3-dienes as depicted in Table 3.⁵⁰

Table 3: Enantioselective hydroamination with 1,2- and 1,3-dienes

Diene	Temperature/°C	Product	Yield	e.e. (%)
	23		99	95
	23		91	97
	23		99	95
	40		67	97
	23		70	90

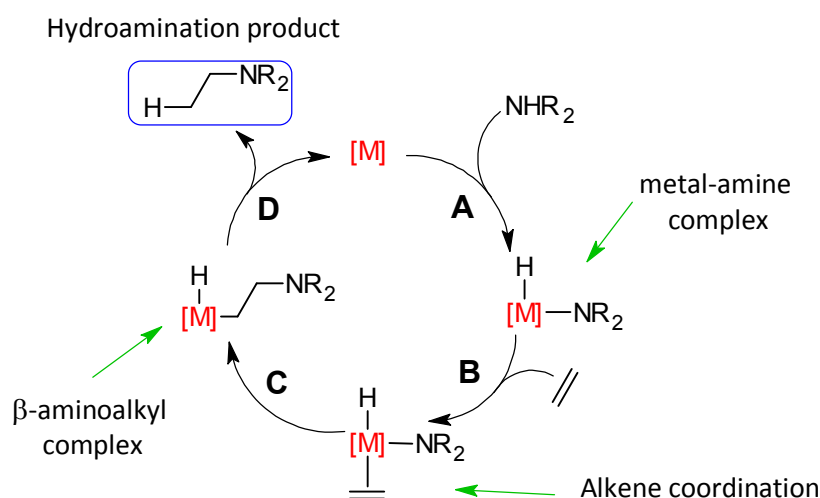
1.3.3 Metal-complex Catalysed Hydroamination

For unactivated C–C multiple bonds to undergo hydroamination either the unsaturated system or the amine must first be activated. The C–C bonds can be activated through coordination to various electrophilic metals. The drawback to this approach is the necessity for stoichiometric amounts of such transition metals. On the other hand, the N–H bond can be activated either by deprotonation or by oxidative addition to electropositive transition metals. This, however, is rarely done.⁴⁰ Amine activation and alkene activation will be discussed below.

Amine activation pathway⁴¹

The amine activation pathway has been successfully utilised but it tends to give modest yields and low selectivities. The catalysts are generally metals of Group 1 and 2, which form nucleophilic species with the amines and then undergo additions to the unsaturated species.⁵¹

In the catalytic cycle reported by Senn and co-workers,⁴¹ oxidative addition (**A**) of the N–H bond to the coordinatively unsaturated low oxidation state transition metal centre M affords the activated metal-amine complex (Scheme 22). The alkene coordinates to the metal-amine complex (**B**). Insertion of the alkene (**C**) into the transition metal-nitrogen bond affords the β -aminoalkyl complex. Reductive elimination (**D**) affords the hydroamination product and regenerates the metal complex.^{41, 46}



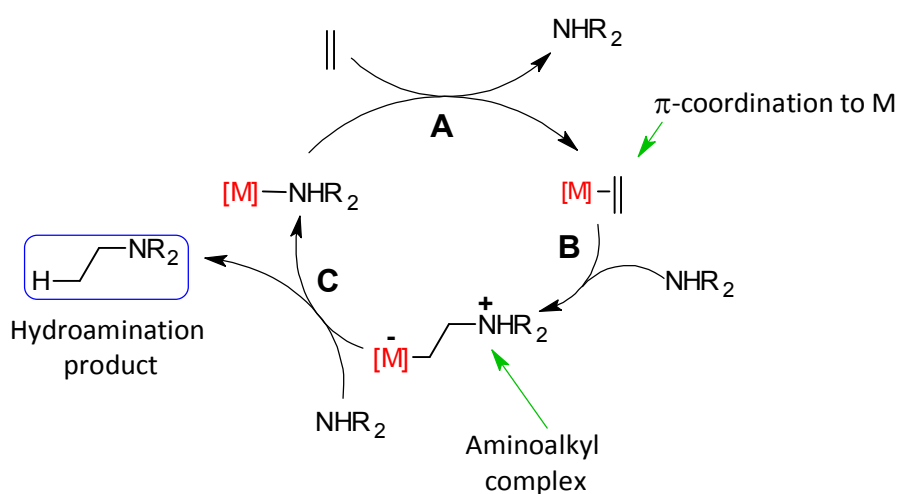
Scheme 22

The first successful catalytic amination of an olefin by N–H activation was reported in 1988 by Casalnuovo and co-workers. Aniline and norbornylene underwent intermolecular hydroamination in the presence of an electron rich iridium complex.⁵²

Alkene activation pathway⁴¹

Alternatively, the alkene may be activated employing transition metal catalysts such as Pd²⁺ or Rh⁺. In this case, the olefin is activated by complexation with the metal and the amine adds *via* nucleophilic attack.⁵¹ The C–C multiple bond is activated by coordination to metal centre M.

Senn and co-workers also reported a catalytic cycle for alkene activation where the alkene coordinates (**A**) to a d-electron rich transition metal (Scheme 23). Nucleophilic addition of the amine (**B**) to the coordinated alkene forms a C–N bond. The metal-carbon bond of the aminoalkyl complex can be cleaved by either direct intramolecular protonolysis or by protonation at the metal centre.⁴¹ Direct protonolysis is kinetically suppressed in coordinatively saturated β -aminoethyl transition metal complexes. It is thus more likely that the transition metal centre be protonated (**C**) *via* a 1,3-hydride shift.⁴⁶ This is followed by reductive elimination to afford the aminoalkyl product and the remaining complex undergoes ligand exchange with a new alkene.⁴¹



Scheme 23

Computational work by Senn and co-workers⁴¹ showed that nucleophilic attack of the amine on the coordinated alkene is thermodynamically favourable for Group 10 metals. However, if Group 9 metals are used it becomes the rate-determining step. For Group 10 metals the rate-determining step is cleavage through protonolysis of the M–(μ -H)–C bridged transition state. The same cleavage is facile for Group 9 metals, where protonolysis affords a hydride intermediate allowing for

reductive elimination. In general, Group 10 complexes are better hydroamination catalysts than Group 9 complexes. Of the Group 10 metals studied, Ni had the lowest rate determining activation barrier in the cleavage step of 108 kJmol^{-1} . The kinetically favourable β -hydride elimination from the ammonioalkyl complex with protonolytic cleavage is thermodynamically disfavoured and can be completely eliminated depending on the substrate choice as well as steric and electronic ligand effects.

Successful intermolecular hydroamination of aniline derivatives and aromatic and aliphatic alkynes has been achieved *via* the alkene activation pathway with $(\text{Ph}_3\text{P})\text{AuCH}_3$ catalysts.^{45, 53}

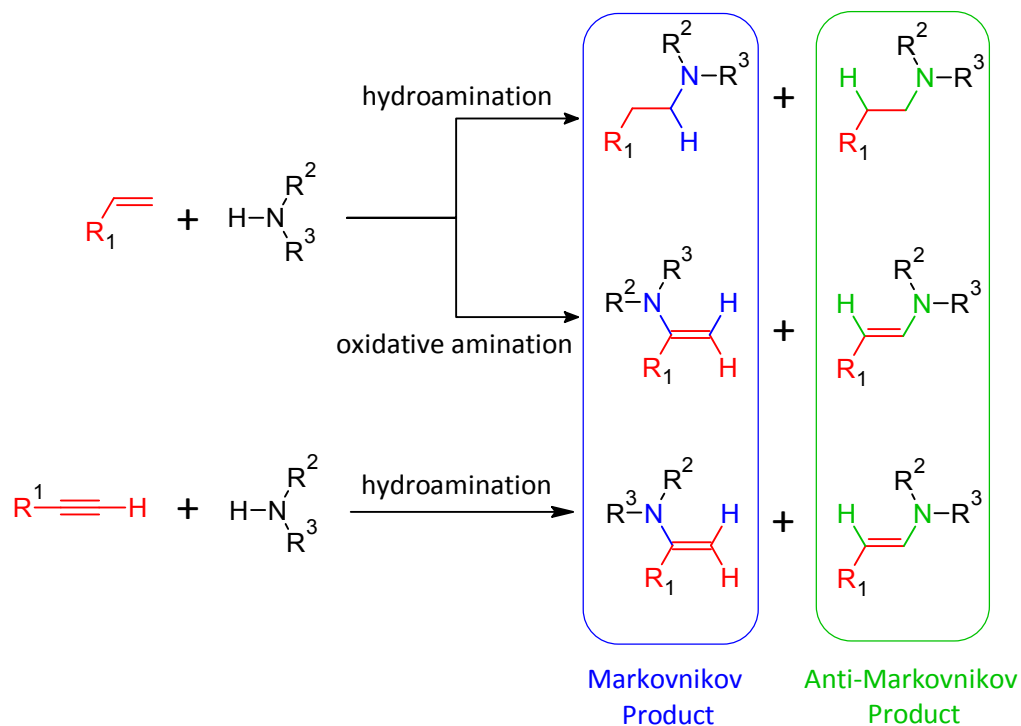
There are, however, limitations involving transition metals as catalysts as they are often associated with short catalytic lifetimes, low turnover frequencies and may have limited reaction scope.⁵¹

More recently organo-lanthanides and actinides have been used to activate both alkenes and amines. The mechanism for such catalyst systems does not follow the more traditional oxidative addition/reductive elimination routes. Bond activation tends to be achieved through concerted four-centred σ -bond metathesis. Organolanthanide complexes catalyse intramolecular hydroaminations of aminoalkenes, aminoalkynes and aminoallenes very well.⁵¹

1.3.4 Regioselectivity of Hydroamination

Hydroamination reactions can proceed in either a Markovnikov or anti-Markovnikov manner. In a Markovnikov addition the nucleophile adds to the more substituted carbon and in an anti-Markovnikov addition the nucleophile adds to the least substituted carbon.

If asymmetric alkenes, alkynes or allenes are used as starting materials for hydroaminations, either Markovnikov or anti-Markovnikov products can be formed (Scheme 24). Thus the reaction must be forced to favour one geometric isomer over the other. However, there is no set rule as to what reaction conditions will yield one specific isomer over the other.⁴⁵



Scheme 24

In general, Markovnikov and anti-Markovnikov selectivities in hydroamination/cyclisation reactions follow Baldwin's rules of ring closure. Baldwin's rules are guidelines describing cyclisation reactions which are either favoured or disfavoured based on stereoelectronic effects.⁵⁴

They are expressed with three terms (see Figure 13). The first term is a numerical number corresponding to the number of atoms present in the forming ring. The second term describes the position of the breaking bond relative to the forming ring (as endocyclic or exocyclic). The third term describes the hybridisation at the ring closure point (as tetrahedral or tet, trigonal or trig, and diagonal or dig).⁵⁵

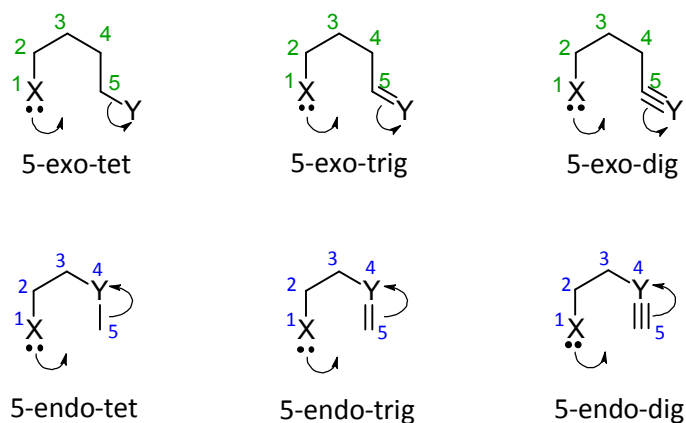


Figure 13

According to the rules published by Baldwin in 1976, all endo-dig cyclisations are favoured.⁵⁴ Tabulated in Table 4 is a summary of the rules, as published by Baldwin in 1976, for alkyne (dig) cyclisations according to ring size.

Table 4: Baldwin's rules for alkyne (dig) cyclisations

	3	4	5	6
Endo	✓	✓	✓	✓
Exo	✗	✗	✓	✓

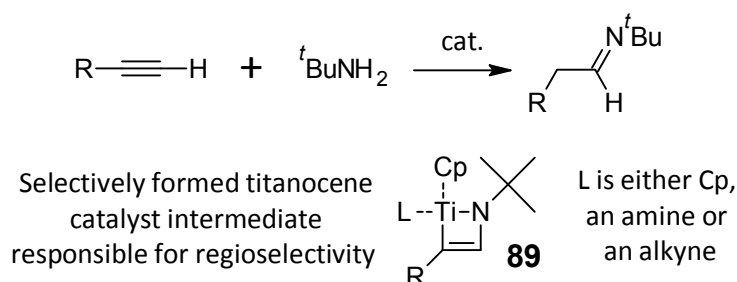
However, a computational study by Alabugin and Gilmore in 2013 has shown that the 4-exo-dig cyclisation (unfavourable according to Baldwin's rules) occurs far more readily than the 5-endo-dig cyclisation (favourable according to Baldwin's rules). They found experimentally that 5-endo-dig products were only obtained in good yields for intramolecular cyclisations. Thus the authors proposed a reverse prediction on favourability with regard to alkyne cyclisations (Table 5).⁵⁶

Table 5: Modified rules for alkyne (dig) cyclisations

	3	4	5	6
Endo	✗	✗	✓	✓
Exo	✓	✓	✓✓	✓✓

Thus the type of cyclisation may influence the regioselectivity of the formed products.

The regioselectivity may also be influenced by the catalyst system used for the reaction. Some titanocene based catalysts ($[\text{Cp}_2\text{Ti}(\eta^2\text{-Me}_3\text{SiC-CSiMe}_3)]$ and $[\text{Cp}_2\text{Ti}(\eta^2\text{-Me}_3\text{SiC-CSiPh})]$) have yielded anti-Markovnikov products exclusively in the hydroamination of terminal aliphatic alkynes.

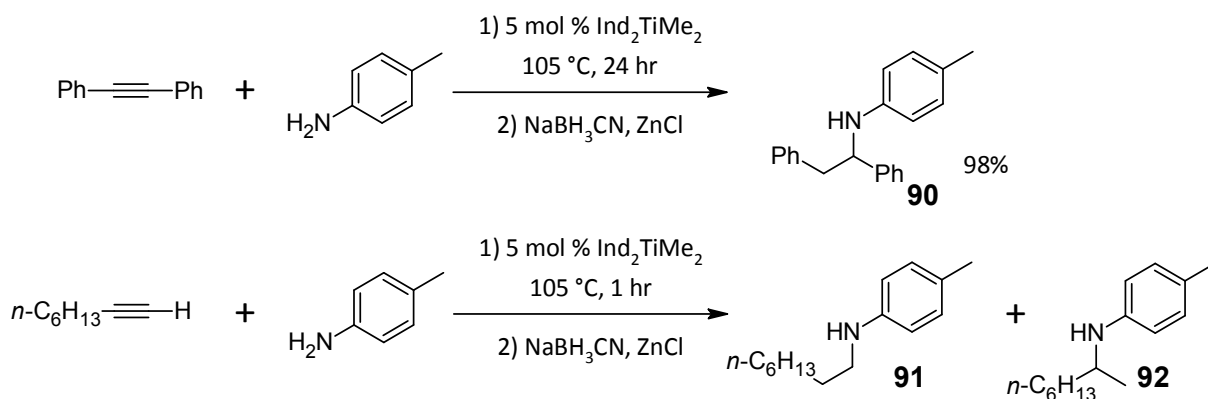


Scheme 25

The titanocene catalyst intermediate **89** (Scheme 25) formed appears to play a role in the regioselectivity of the reaction and it was found that for such catalyst systems steric factors played an important role in the regioselectivity. Bulky amines afforded the highest regioselectivity. However,

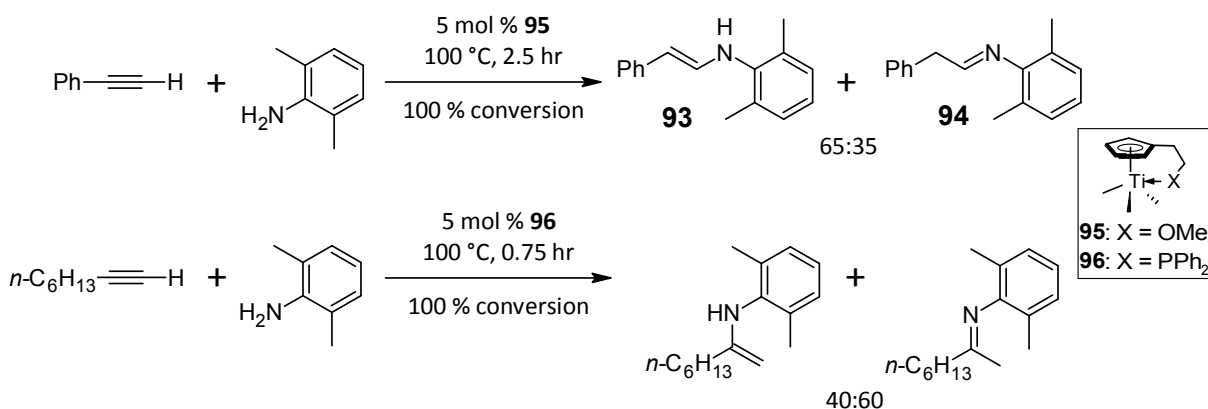
steric bulk in the amine is not the only factor influencing the regioselectivity as aniline gave the Markovnikov products preferentially. Higher anti-Markovnikov selectivities may be possible with even more sterically hindered titanocenes.⁵⁷

Another titanocene based catalyst, $\text{Ind}_2\text{TiMe}_2$ (Ind = indenyl), for intermolecular hydroamination of alkynes always affords the anti-Markovnikov product **90** for arylalkynes or *t*-BuNH₂. However, terminal alkylalkynes react with arylamines to give the Markovnikov isomer **91** preferentially (Scheme 26).⁴⁵



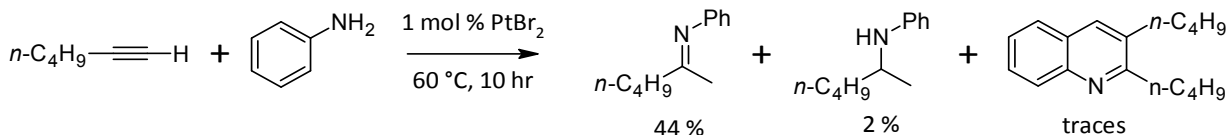
Scheme 26

Terminal and internal aromatic alkynes such as phenylacetylene and 1-phenylpropyne afford anti-Markovnikov products with 100 % regioselectivity, although a mixture of enamine **93** and imine **94** is obtained for CpTiMe_3X type catalysts **95** and **96**. On the other hand, aliphatic alkynes react to give Markovnikov products with the same catalyst (Scheme 27).⁴⁵



Scheme 27

Some late transition metal catalysts allow for selective formation of Markovnikov addition products from terminal alkynes. For example, the platinum catalyst PtBr₂ facilitates Markovnikov addition of terminal alkyl- and arylalkynes to aniline (Scheme 28). Phenylacetyline adds with complete Markovnikov selectivity. However, the selectivities for the addition to 1-hexyne to aniline decrease with an increase in reaction temperature (from 98:4 at 60 °C to 45:18 at 100 °C).⁴⁵



Scheme 28

1.3.5 Stereoselectivity of Hydroamination

The synthesis of enantiopure chiral compounds is of great importance in chemistry. Such chiral heterocompounds generally exhibit biological activity and are important in the pharmaceutical industry. Chiral hydroamination catalysts with significant steric bulk have allowed for enantioselective transformations. It has already been mentioned that Hultzsich and co-workers⁴⁷ have carried out a base catalysed asymmetric intramolecular hydroamination utilizing the chiral diamidobinaphthyl salt **81** (Scheme 16). An enantiomeric excess of 64 % (*S*) was achieved. It was also mentioned that Shapiro and co-workers⁵⁰ utilised a chiral Brønsted acid **86b** with a nucleophilic conjugate base to perform acid catalysed asymmetric intramolecular hydroaminations of 1,2- and 1,3-dienes (Scheme 21 and Figure 12). High yields and enantioselectivities up to 97 % were achieved.

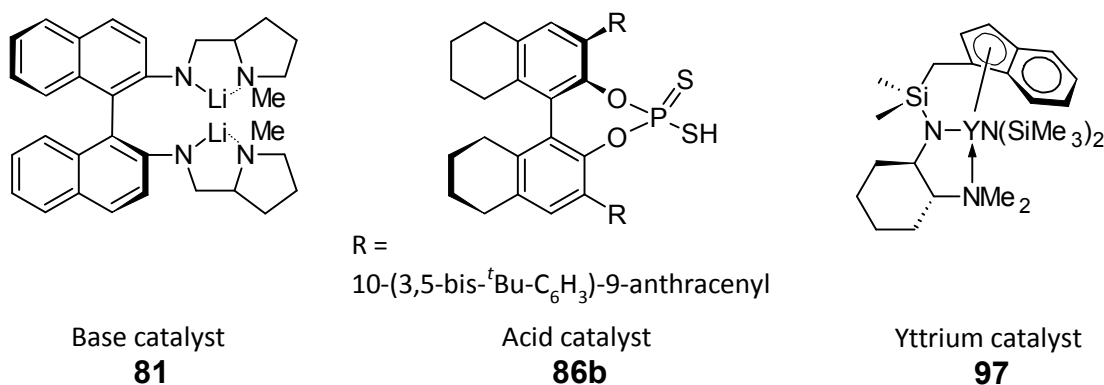


Figure 14: Catalysts for asymmetric hydroamination

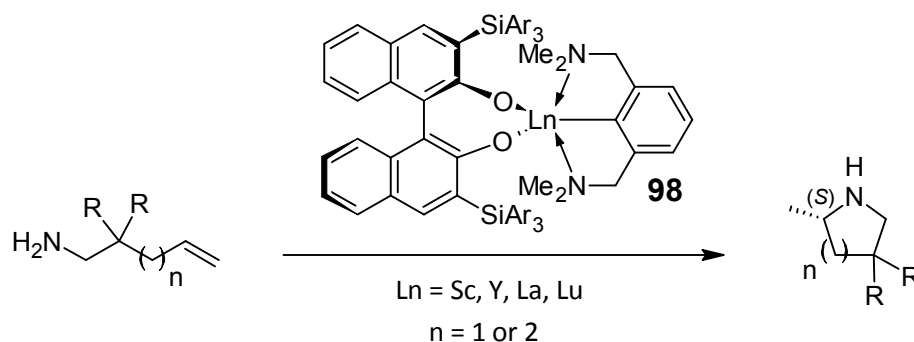
More recently, Chai and co-workers reported an yttrium complex **97** (Figure 14) which has facilitated enantioselective intramolecular hydroaminations.⁵⁸ Table 6 shows some of the hydroamination reactions. The enantiomeric excess of 97 % (entry 2) is the highest enantioselectivity reported for a rare-earth metal catalysed asymmetric hydroamination of non-activated olefins to date. Higher

reaction temperatures, larger precatalyst loadings and longer reaction times all had a negative effect on the enantioselectivities.⁵⁸ It has in fact been reported that enantioselectivities are improved with a decrease in reaction temperature,⁵⁹ but this was not the case for the yttrium catalyst **97**.

Table 6: Hydroamination of unactivated olefins catalysed by yttrium complex **97**

Entry	Substrate	Product	Time (h)	Conversion (%)	e.e. (%)
1			0.8	98 (96)	85
2			9.6	99 (97)	97
3			15.6	95 (94)	69
4			7.0	99	87

When transition metals have been utilised as hydroamination catalysts the ligands can be varied to control the regio- or stereochemistry of the products. Adjustments in both steric and electronic features can alter the selectivity. Sterically demanding substrates are more effective in facilitating enantioselectivity. Gribkov and co-workers⁵⁹ thus developed an asymmetric lanthanide and early transition metal based catalysts **98** with bulky substituents as shown in Scheme 29. They found that the enantioselectivity increased with a decrease in ionic radius of the metal. However, it was not only the catalyst that had an effect on the selectivity. For sterically unhindered amine substrates the most effective catalysts were those with increased steric bulk (Ar = 3,5-Me₂C₆H₃), but for sterically hindered amine substrates the slightly less bulky catalyst (Ar = Ph) was more effective. High enantioselectivities were also achieved with lower reaction temperatures (0 to 25 °C).⁵⁹



Scheme 29

The enantioselectivity can be understood by looking at the Ln-olefin transition state (Figure 15). If the olefin approaches with the *si* face there is an unfavourable steric interaction. If the olefin approaches from the *re* face instead, such unfavourable interactions are not present and the observed (*S*) stereochemistry is obtained.⁵⁹

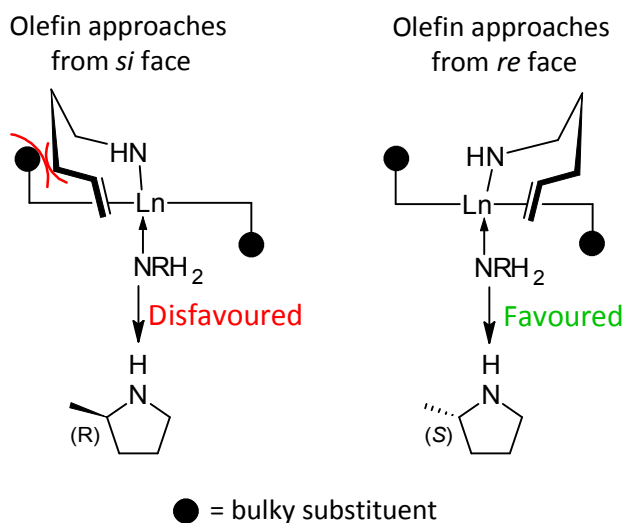
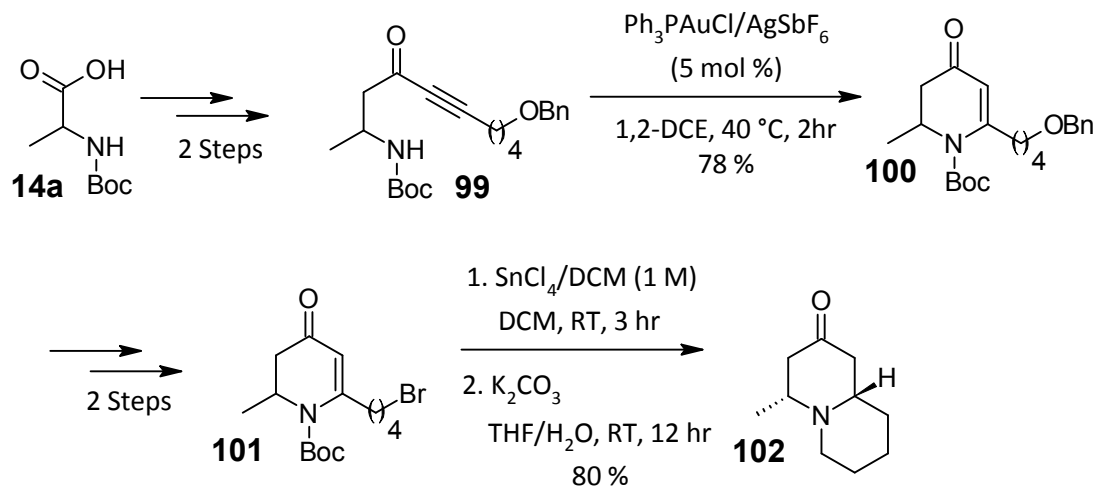


Figure 15

1.3.5 Hydroamination in Natural Product Synthesis

The hydroamination of alkenes, alkynes and allenes is a powerful method to access heterocyclic systems.⁶⁰ Many natural products, including alkaloids contain such heterocyclic systems.

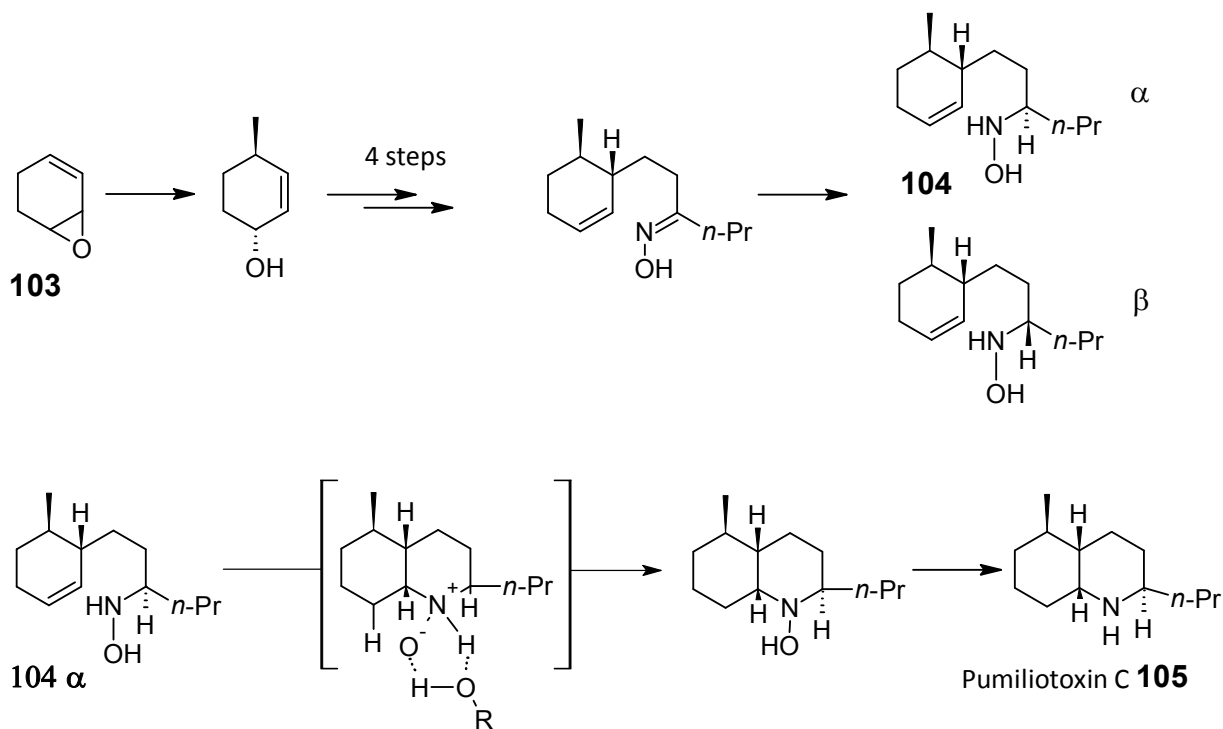
Trinh and co-workers completed a new route to the total synthesis of (-)-epimyrtine **102** from D-alanine. (-)-Epimyrtine is a quinolizidine alkaloid with a number of pharmacological properties including anticancer, antibacterial, antiviral and anti-inflammatory. The key step in their synthesis, as depicted in Scheme 30, was the gold(I)-catalysed hydroamination of a β -aminoynone **99**, which was stereoselectively prepared from *N*-Boc-D-alanine **14a** in two steps.⁶¹



Scheme 30

(-)-Epimyrtiline was synthesised over 6 steps in a 25 % yield from *N*-Boc-D-alanine by a gold mediated intramolecular hydroamination in a unique 6-endo-dig process.⁶¹

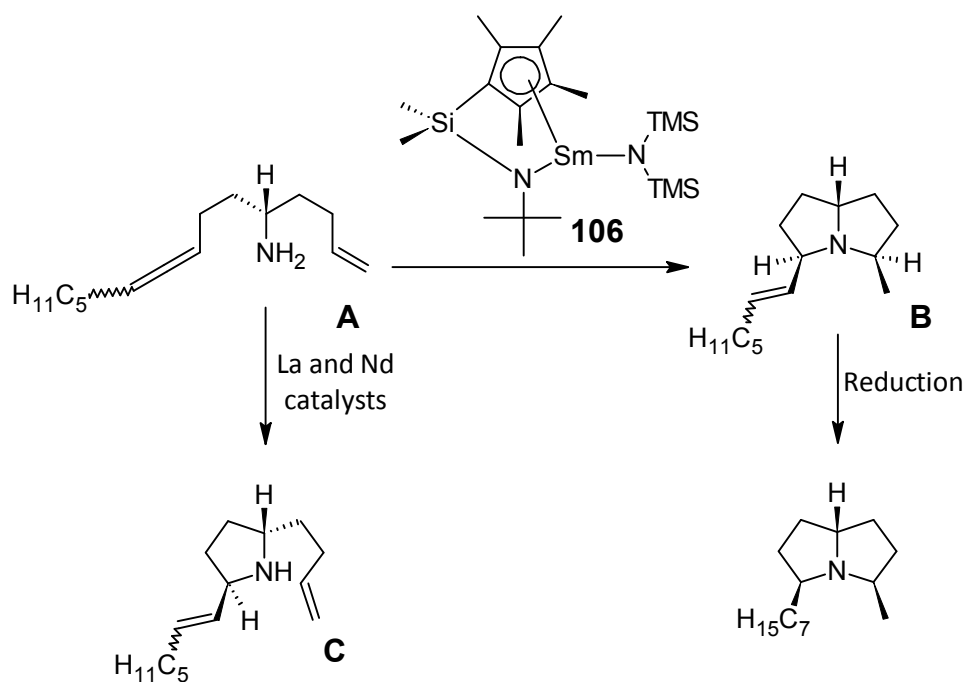
Pumiliotoxin C **105**, a potent toxin isolated from the poison frogs of Dendrobatidae, was synthesised *via* a Cope-type intramolecular hydroamination of **104**. The precursors for the hydroamination, **104** α and **104** β were synthesised in 8 steps from 3,4-epoxy-1-cyclohexene **103** (Scheme 31). The hydroamination proceeded smoothly in *n*-PrOH/H₂O in microwaves at 180 °C. **104** α was cyclised more readily than **104** β under the same conditions.⁶²



Scheme 31

The above Cope-type hydroamination reaction is of great significance since intramolecular hydroaminations of alkenes to form six-membered ring systems is very difficult and as such has rarely been successful.⁶²

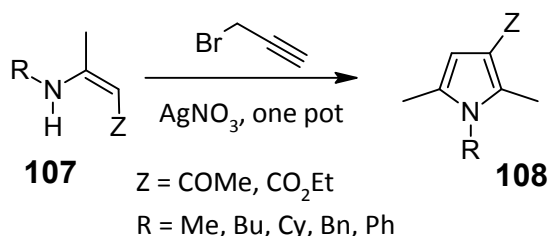
A total synthesis of (+)-xenovenine was carried out by Tian and co-workers utilising a Samarium based catalyst **106**. In comparison to more conventional La and Nd catalysts, the Sm catalyst allowed for tandem A → B bicyclisation rather than monocyclisation C (Scheme 32).⁶³



Scheme 32

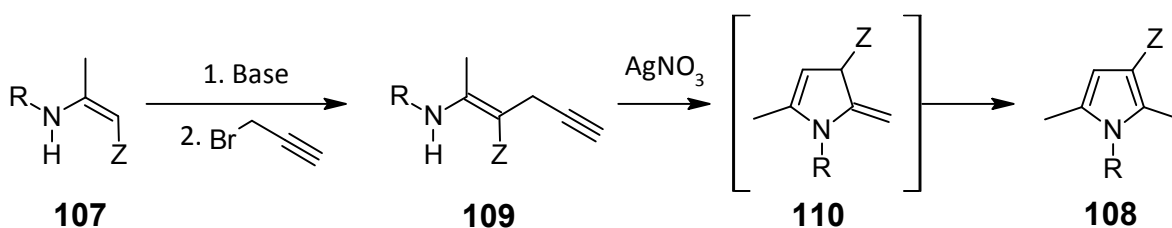
1.4 Previous Work within the Research Group

A novel one-pot silver nitrate mediated synthesis of functionalised pyrroles was first published in 2004 as shown in Scheme 33.⁶⁴ Secondary vinylogous amides or carbamates were reacted with propargyl bromide, mediated by silver nitrate. The reaction was found to be viable but not synthetically useful due to low yields (*ca.* 25 %). These low yields were attributed to the many possible reaction pathways prior to the hydroamination.⁶⁵



Scheme 33

The reaction was improved upon by Dovey by utilising a two-step procedure (Scheme 34).⁶⁵ The secondary enamines were first propargylated using *n*-BuLi or NaH and propargyl bromide followed by AgNO₃ catalysed intramolecular hydroamination. The hydroamination reaction proceeded in the presence of 0.2 equivalents of catalyst in acetonitrile at room temperature in good yields after 16-20 hours (Table 7).



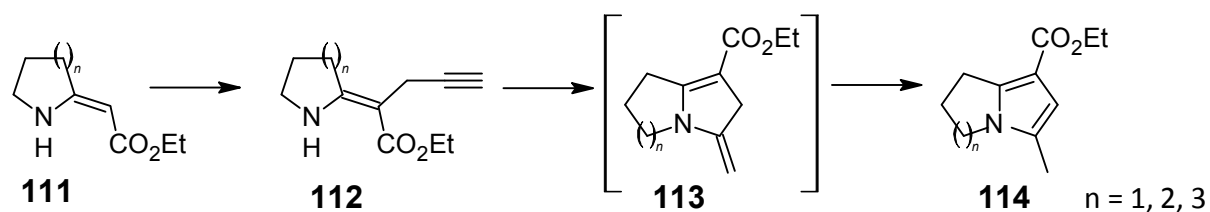
Scheme 34

Table 7: Synthesis of pyrroles **108** from vinyllogous amides **107** via hydroamination

Entry	R	Yield 107 (%)	Base	Yield 109 (%)	Yield 108 (%)
a	Me	80	<i>n</i> -BuLi	55	93
b	Me	80	NaH	46	93
c	<i>n</i> -Bu	76	<i>n</i> -BuLi	51	95
d	Cy	88	<i>n</i> -BuLi	52	87
e	<i>t</i> -Bu	6	—	—	—
f	Ph	94	<i>n</i> -BuLi	21	75
g	Bn	95	<i>n</i> -BuLi	—	43 ^a

^a**108g** was obtained directly from **107g**

The methodology was next applied to the synthesis of *N*-bridgehead pyrrole functionalities from cyclic secondary vinyllogous carbamates **111** as depicted in Scheme 35. Similarly, a one-pot synthesis afforded the desired products in low yields, whereas the two step process (*C*-propargylation to afford **112** followed by intramolecular hydroamination to afford **114** through the rearrangement of the cyclic enamine **113**) greatly improved the yields.⁶⁶



Scheme 35

For the one pot synthesis of *N*-bridgehead pyrroles the yields for $n = 1, 2$ and 3 were 13 %, 19 % and 14 % respectively. In utilising the two step procedure the yields (from **112** to **114**) for $n = 1, 2$ and 3 increased to 75 %, 75 % and 71 % respectively.⁶⁶

Prior utilised the novel approach developed by Dovey in a study on late transition metals as hydroamination catalysts.⁶⁷ The reaction chosen for the study is depicted in Scheme 34 where $R = \text{Bu}$ and $Z = \text{CO}_2\text{Et}$. The metals investigated were Cu(II), Ag(I), Zn(II), Cd(II) and Hg(II). Four counterions were used for each metal, namely oxide, acetate, nitrate and chloride. In contrast to the results reported by Dovey,⁶⁵ Prior successfully *C*-propargylated vinyllogous amides where $Z = \text{CO}_2\text{Et}$ in a yield of 80 %.⁶⁷ The hydroamination was microwave assisted with a catalyst loading of 0.04 equivalents in acetonitrile. Without the presence of a catalyst the hydroamination transformation was unsuccessful (Table 1, entry u). In the presence of all the transition metal catalysts the transformations were completely regioselective for the Markovnikov addition (attributed to the 5-*exo-dig* cyclisation to afford 5-membered pyrroles).⁶⁷

Table 8: Transition metal catalysts utilised for the hydroamination of vinyllogous amides 107 to pyrrole 108

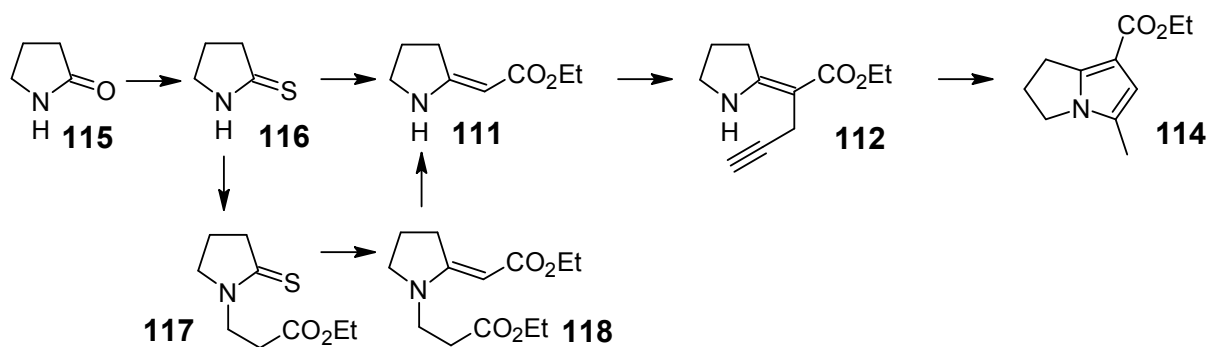
Entry	Catalyst	Yield 108 (%)	Entry	Catalyst	Yield 108 (%)
a	CuO	13	m	CdO	39
b	Cu(OAc) ₂	33	n	Cd(OAc) ₂	30
c	Cu(NO ₃) ₂	53	o	Cd(NO ₃) ₂	85
d	CuCl	65	p	CdCl	72
e	Ag ₂ O	6	q	HgO	24
f	AgOAc	7	r	Hg(OAc) ₂	68
g	AgNO ₃	14	s	Hg(NO ₃) ₂	57
h	AgCl	9	t	HgCl ₂	36
i	ZnO	3	u	None	3
j	Zn(OAc) ₂	96			
k	Zn(NO ₃) ₂	99			
l	ZnCl	93			

Under forcing conditions, the catalyst entries j–t yielded **108** in ≥ 96 % yield

The general trend observed for the metals from both Groups 11 and 12 was a decrease in activity down the Group (see Table 8). This decrease was attributed to the progressive decrease in Lewis acidity of the cationic metal centres. Thus Cu(II) was more active than Ag(I) and Zn(II) was more active than Cd(II) with Hg(II) being the least active of the Group 12 metals investigated. The counterions also influenced the activity of the catalysts with an increase in activity in the order of oxide < acetate < chloride < nitrate.⁶⁷

Thus the investigation found Zn(II) catalysts to afford the highest yields (with the exception of ZnO) under mild conditions and all Group 12 metal catalysts resulted in excellent yields under more forcing conditions.⁶⁷

Previously a method optimisation for the synthesis of ethyl 5-methyl-2,3-dihydro-1*H*-pyrrolizine-7-carboxylate from 2-pyrrolidinone was carried out as depicted in Scheme 36.



Scheme 36

2-Pyrrolidinone **115** was reacted with Lawesson's reagent to afford the thiolactam **116** in a 78 % yield. A direct Eschenmoser coupling from **116** to **111** was unsuccessful and thus the thiolactam **116** was first *N*-protected to give **117** in a 100 % yield. Eschenmoser coupling of **117** to bromoacetoacetate was successful to afford **118** in a 75 % yield. This was followed by deprotection utilising the strong non-nucleophilic base KHMDS to give **111** in a 72 % yield. *C*-propargylation of **111** gave 40 % **112** as well as a mixture of a dipropargylated species and starting materials. The desired product **112** was found to decompose on silica and thus the crude mixture was not purified before hydroamination of **112** catalysed by ZnCl₂ to give **114** (68% yield from **111**). An overall yield of 29 % over six steps was obtained.⁶⁸

1.5 Aims of the Project

Building upon previous work completed in the research group, the aim of this work is to synthesise the natural product **223H** (xenovenine) utilising a hydroamination approach. **223H** is a 3,5-disubstituted pyrrolizidine alkaloid first isolated from the Cryptic Thief ant.²¹ An aspect of the synthesis would be to control the asymmetric hydroamination to afford the natural product stereoselectively. Secondary to the aforementioned aim is to explore the possible mode of action and binding interactions of the alkaloid with biologically significant receptors.

Chapter 2: Results and Discussion

2.1 Focus of the Project

The focus of this project is to utilise the hydroamination methodology developed within our research group⁶⁶⁻⁶⁷ in the total synthesis of the pyrrolizidine alkaloid **223H** depicted in Figure 16. In particular, our focus is to complete the total synthesis of **223H** and to study the stereoselectivity of the hydroamination cyclisation.

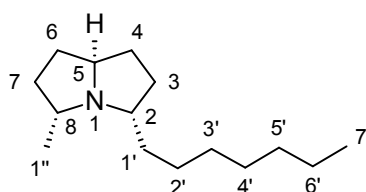


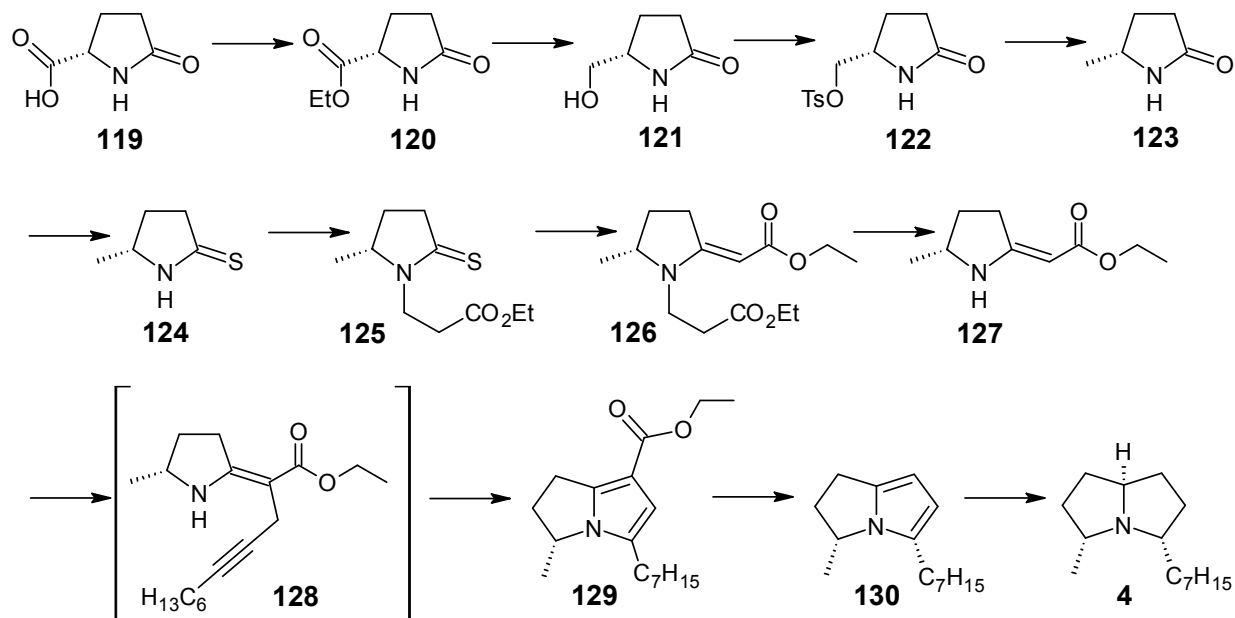
Figure 16

2.2 Proposed Synthetic Route

The proposed synthetic route (Scheme 37) for the synthesis of **223H** has been split into three distinct sections. The first section entails the synthesis of (5*R*)-5-methyltetrahydro-2*H*-pyrrol-2-one **123**. In order to synthesise the *R* enantiomer it is necessary to start the synthesis with (*S*)-pyroglutamic acid **119**, which is esterified to give **120**. This would be followed by reduction with NaBH₄ to afford **121** and the alcohol functionality is converted to a tosyl group as it is a much better leaving group than the alcohol. **122** would then be reduced to **123**.

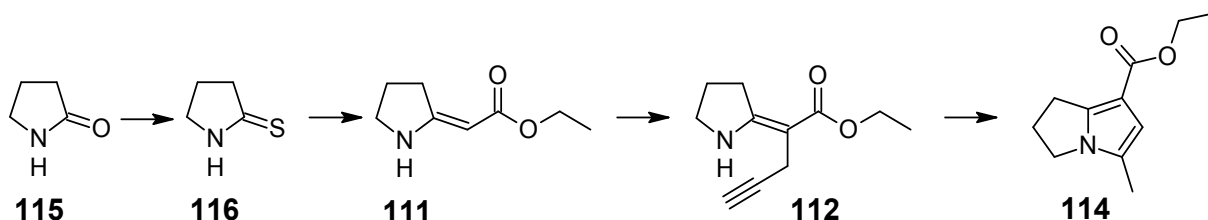
The second section includes the synthesis of ethyl 2-[(5*R*)-5-methyltetrahydro-2*H*-pyrrol-2-ylidene]acetate **127** as well as the synthesis of 1-bromo-2-nonyne **132**. The lactam **123** can be converted into its corresponding thiolactam **124** with Lawesson's Reagent. The thiolactam **124** can then be activated for the Eschenmoser sulfide contraction reaction by *N*-protection to give **125**. An Eschenmoser coupling would then afford **126** and deprotection would give the enaminoate **127** which, after alkylation with 1-bromo-2-nonyne **128** can undergo hydroamination.

The final section of the synthesis involves the hydroamination, decarboxylation and hydrogenation reactions to give **223H**. Once **127** has been alkylated, **128** can undergo the hydroamination to afford **129**. Decarboxylation and hydrogenation would then result in **223H**.



Scheme 37

This proposed synthetic route was based upon an optimisation study was completed by Prior⁶⁸ for the synthesis of **114** starting from 2-pyrrolidinone **115** as depicted in Scheme 38. This method utilises an Eschenmoser coupling reaction to give the carbamate **111**. Thus the lactam **115** is converted to the corresponding thiolactam **116** with Lawesson's reagent before an *N*-protection/activation necessary for a successful Eschenmoser coupling. Deprotection affords the carbamate **111**, which would subsequently be *C*-propargylated to afford **112** before hydroamination to give **114**.

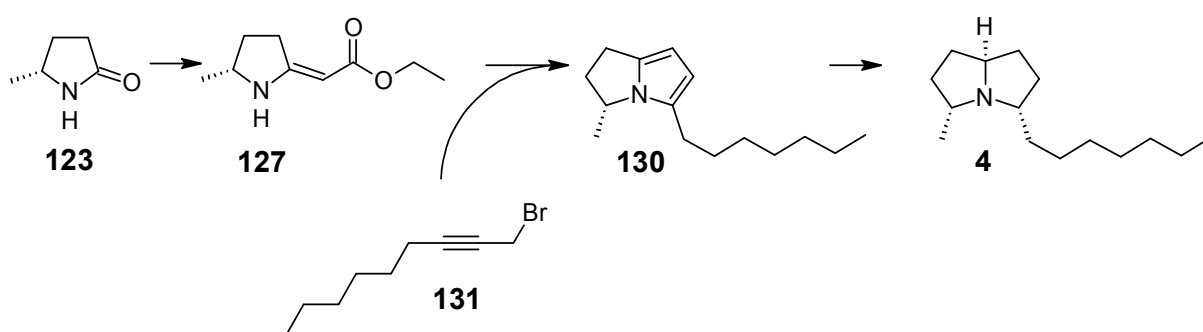


Scheme 38

2.3 Studies toward 223H

The complete synthesis of **223H** can be broken down into five small syntheses. These are the synthesis of (Scheme 39):

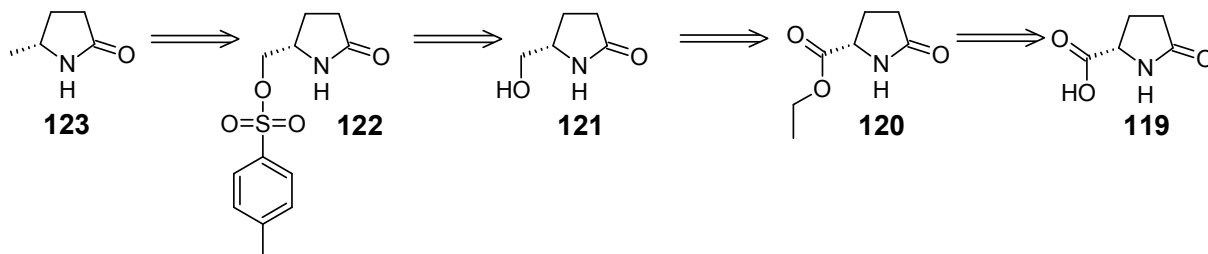
- Part 1: (5*R*)-5-methyltetrahydro-2*H*-pyrrol-2-one **123**
- Part 2: Ethyl [(5*R*)-5-methyltetrahydro-2*H*-pyrrol-2-ylidene]acetate **127**
- Part 3: 1-Bromo-2-nonyne **131**
- Part 6: (3*R*)-5-heptyl-3-methyl-2,3-dihydro-1*H*-pyrrolizidine **130**
- Part 5: Xenovenine **4** (**223H**)



Scheme 39

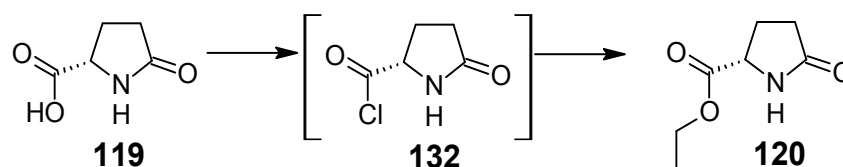
2.3.1 Part 1: Synthesis of (5*R*)-5-methyltetrahydro-2*H*-pyrrol-2-one

A retrosynthetic analysis shows that (5*R*)-5-methyltetrahydro-2*H*-pyrrol-2-one **123** can be synthesised from pyroglutamic acid **119** (Scheme 40). The methyl functionality is accessible by reduction of the corresponding tosylate derivatives using tributyltin hydride and AIBN. Alcohols are easily converted to tosylates⁶⁹ and alcohols can be obtained from esters (as well as acyl chlorides and aldehydes) by reduction with NaBH₄. Carboxylic acids can be converted into esters and thus the ester is available from pyroglutamic acid. In order to prepare the *R*-enantiomer of the methyl lactam (*S*)-pyroglutamic acid is used; it is commercially available at high optical purity and is inexpensive.



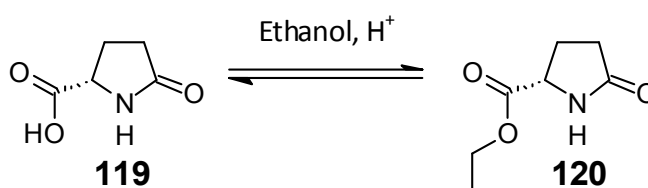
Scheme 40

The first step is to convert (*S*)-pyroglutamic acid **119** into its corresponding ester **120**. Common methods for this transformation are to either convert the carboxylic acid to an acyl chloride **132** with thionyl chloride (Scheme 41), or to employ a Fischer esterification (Scheme 42). High yields have been reported in the literature for both methods (80-95 %).⁷⁰⁻⁷⁴



Scheme 41

Considering the corrosive nature of thionyl chloride, we instead chose to use the Fischer esterification method. Applying Le Châtelier's Principle, the reaction can be driven towards products by using an excess of one of the reagents.



Scheme 42

(*S*)-Pyroglutamic acid was added to a 75 % ethanol-toluene solution with 1 cm³ 96 % sulfuric acid and refluxed for 12 hours with a Dean and Stark apparatus to afford a colourless oil after work up. Both ¹H NMR spectroscopy and GC-MS analysis showed the presence of two distinct compounds. The compounds were separated by vacuum distillation. The first fraction collected appeared to be a ring opened product as depicted in Figure 17, rather than the expected esterified pyroglutamic acid. This was confirmed by ¹H and ¹³C NMR spectroscopy as well as gas chromatography-mass spectroscopy.

The peak eluting at 10.51 minutes in the gas chromatograph (Figure 18) corresponds to the ring opened ester, whilst the peak eluting at 10.75 minutes corresponds to the pyroglutamic ester **120**. The mass spectrum possessed a parent molecular ion mass of 204 g mol^{-1} which correlates to the mass calculated for the ring opened ester of $203.236 \text{ g mol}^{-1}$. The presence of the ring opened product clearly lowered the yield of the desired ester.

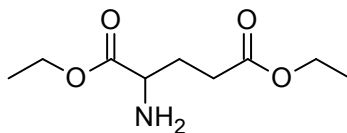


Figure 17

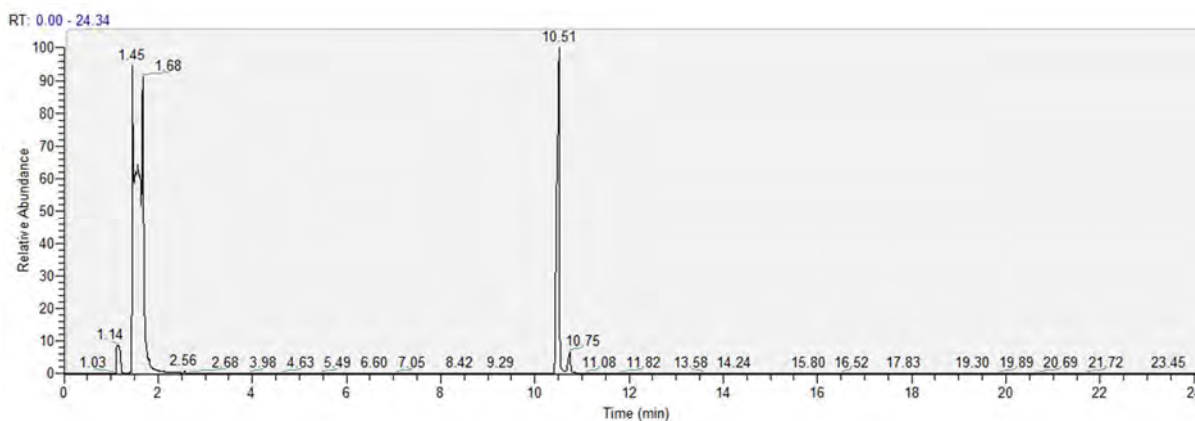


Figure 18

The ring opening was attributed to the high reaction temperature, as toluene has a boiling point of $110.6 \text{ }^{\circ}\text{C}$ and the energy put into the system seemed to facilitate ring opening. Therefore, in order to minimise the formation of the ring opened product benzene* (boiling point of $80 \text{ }^{\circ}\text{C}$) was used as a co-solvent rather than the less toxic toluene (the co-solvent is necessary for the azeotropic removal of water and the reaction does not proceed in absence of the co-solvent). The change to benzene did indeed minimise the ring opening. Based on these results an IR spectroscopically monitored reaction in toluene was instigated (Figure 19) and the temperature was not allowed to increase above $80 \text{ }^{\circ}\text{C}$. The peaks at 3320 cm^{-1} , 1744 cm^{-1} (1692 cm^{-1}) and 1204 cm^{-1} were monitored. As the reaction proceeded the peak at 3320 cm^{-1} corresponding to the $-\text{OH}$ of the carboxylic acid decreased in intensity as the carboxylic acid was converted to the ester. The peak at 1744 cm^{-1} corresponding to $\text{C}=\text{O}$ stretching of the carboxylic acid shifted towards 1735 cm^{-1} (with an increase in intensity) which corresponds to $\text{C}=\text{O}$ stretching of an ester. The peak at 1204 cm^{-1} also increased in intensity and corresponds to the $\text{C}-\text{O}$ stretching of an ester.

* Due caution was taken when working with benzene.

The reaction time was also decreased from 12 hours to 6 hours. This almost completely eliminated the formation of the side product and high yields (85-95 %) were obtained. Based on these results it was decided to attempt the reaction utilising microwave irradiation.

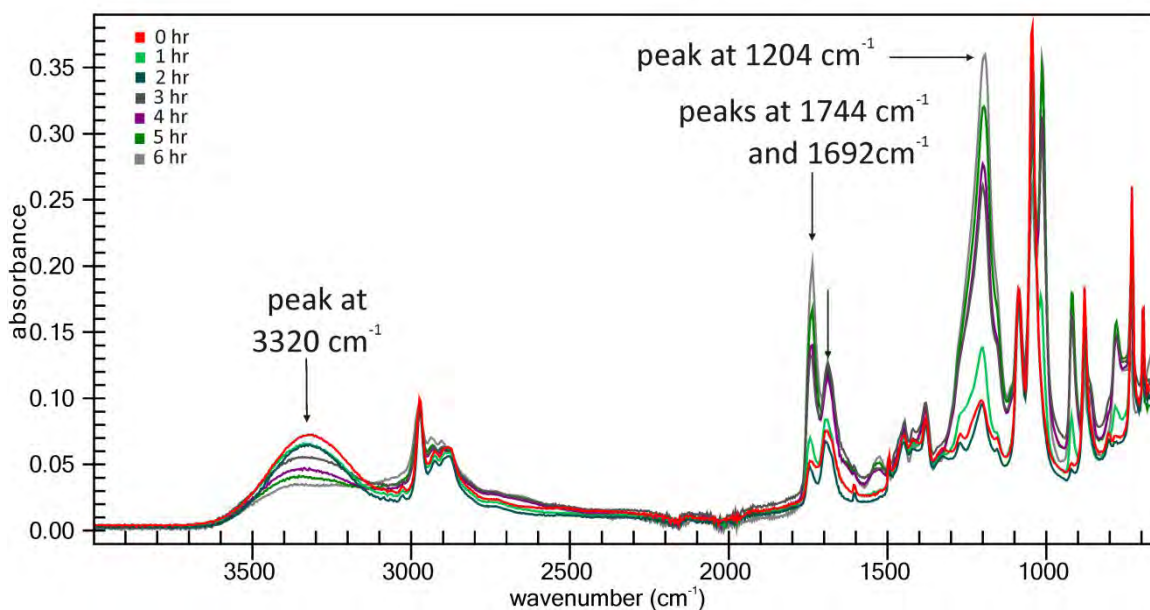


Figure 19: Infrared monitored Fischer esterification of (S)-pyroglutamic acid in toluene

The reaction was first attempted without a co-solvent on a 1 mmol scale in absolute ethanol with 0.5 cm³ H₂SO₄ and heated for 25 minutes to 60 °C. The resulting mixture was filtered and concentrated *in vacuo*. The ¹H NMR spectrum showed a mixture of starting materials and product, with a yield of only 10 %. For the next microwave reaction toluene was added as a co-solvent. The solution was heated to 80 °C for 10 minutes. The solution was next filtered and concentrated *in vacuo*. The ¹H NMR spectrum contained only the desired product in good yield of 95 %, with no ring opening observed.

Figure 20 shows an overlay for three ¹H NMR spectra for this transformation. The bottom spectrum depicts successful esterification with no ring opening under conventional heating in benzene. The middle spectrum depicts successful esterification under microwave heating in toluene and the top spectrum shows the result of conventional heating where toluene was used as the co-solvent and significant ring opening was observed.

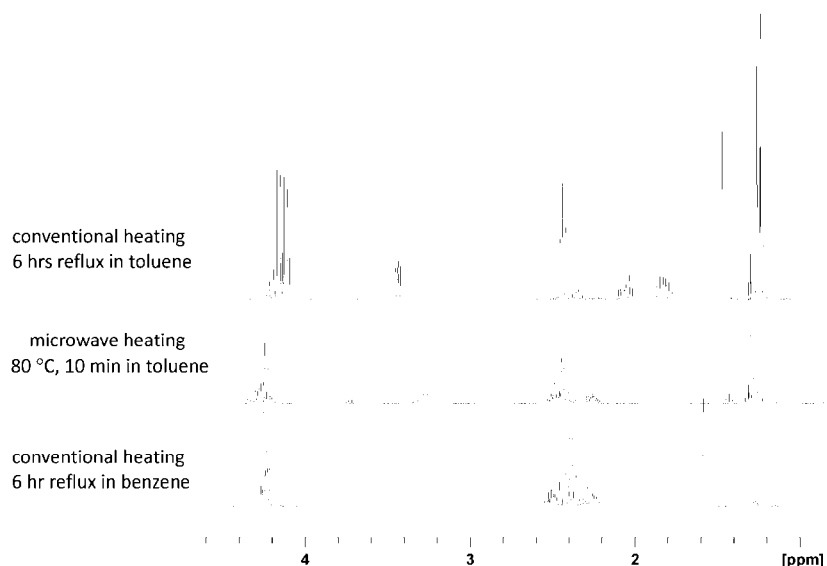


Figure 20

Having optimised the reaction conditions the structure was confirmed by NMR spectroscopy. The ^1H NMR spectrum (Figure 21) showed a characteristic broad singlet indicative of an N-H functionality resonating at 6.10 ppm and integrating for one proton. The triplet at 1.30 ppm integrating for two protons and the quartet at 4.22 ppm integrating for three protons have chemical shifts consistent with an ethyl ester functionality. Correlation between these two peaks was confirmed in the COSY spectrum (Figure 22). The remaining peaks in the ^1H NMR spectrum were assigned to the ring protons with the 3- H protons being non-equivalent as they are adjacent to a chiral centre. Thus the peaks at 2.21-2.30 ppm and 2.42-2.53 ppm were assigned to the 3- H protons. The peak at 4.20-4.25 ppm was assigned to the 2- H proton and the peak at 2.32-2.40 ppm to the 4- H protons. The COSY spectrum (Figure 22) also shows correlation between the 2- H proton and the 3- H protons as well as between the 3- H protons and the 4- H protons.

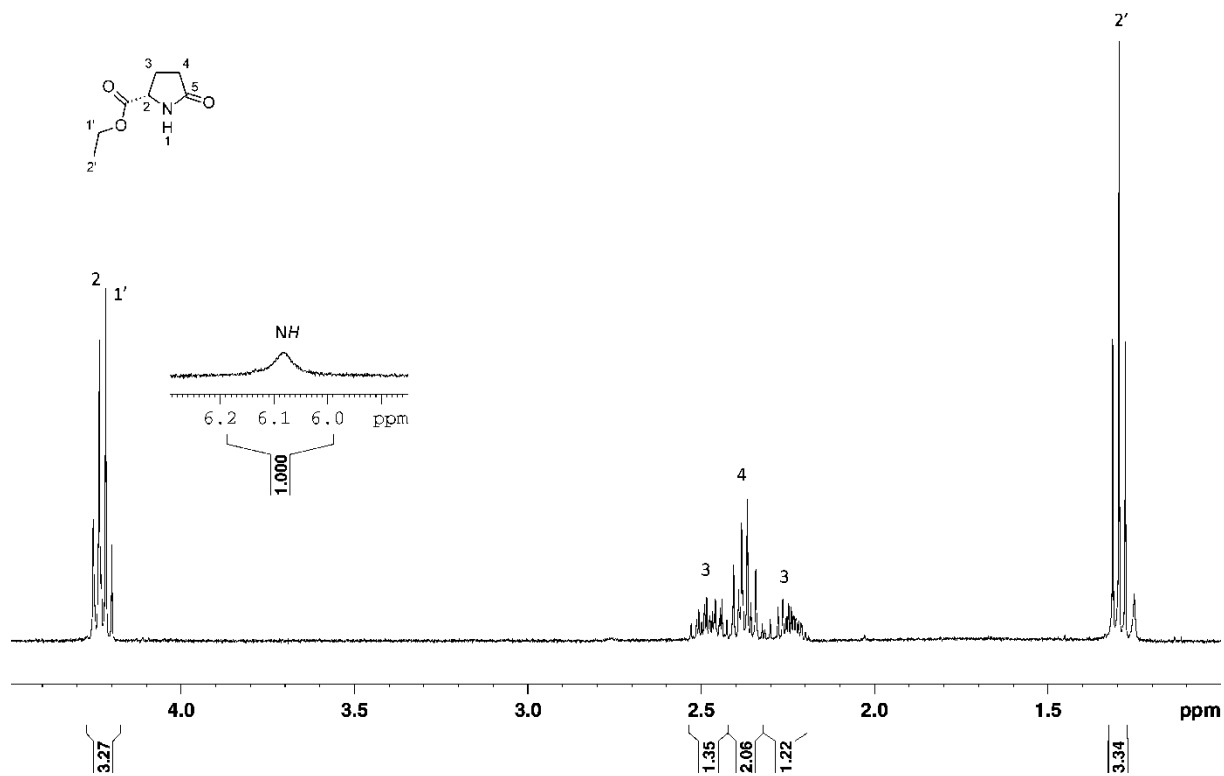


Figure 21: ¹H NMR Spectrum for ethyl (2S)-5-oxotetrahydro-1H-pyrrole-2-carboxylate*

* All integral traces have been omitted for clarity.

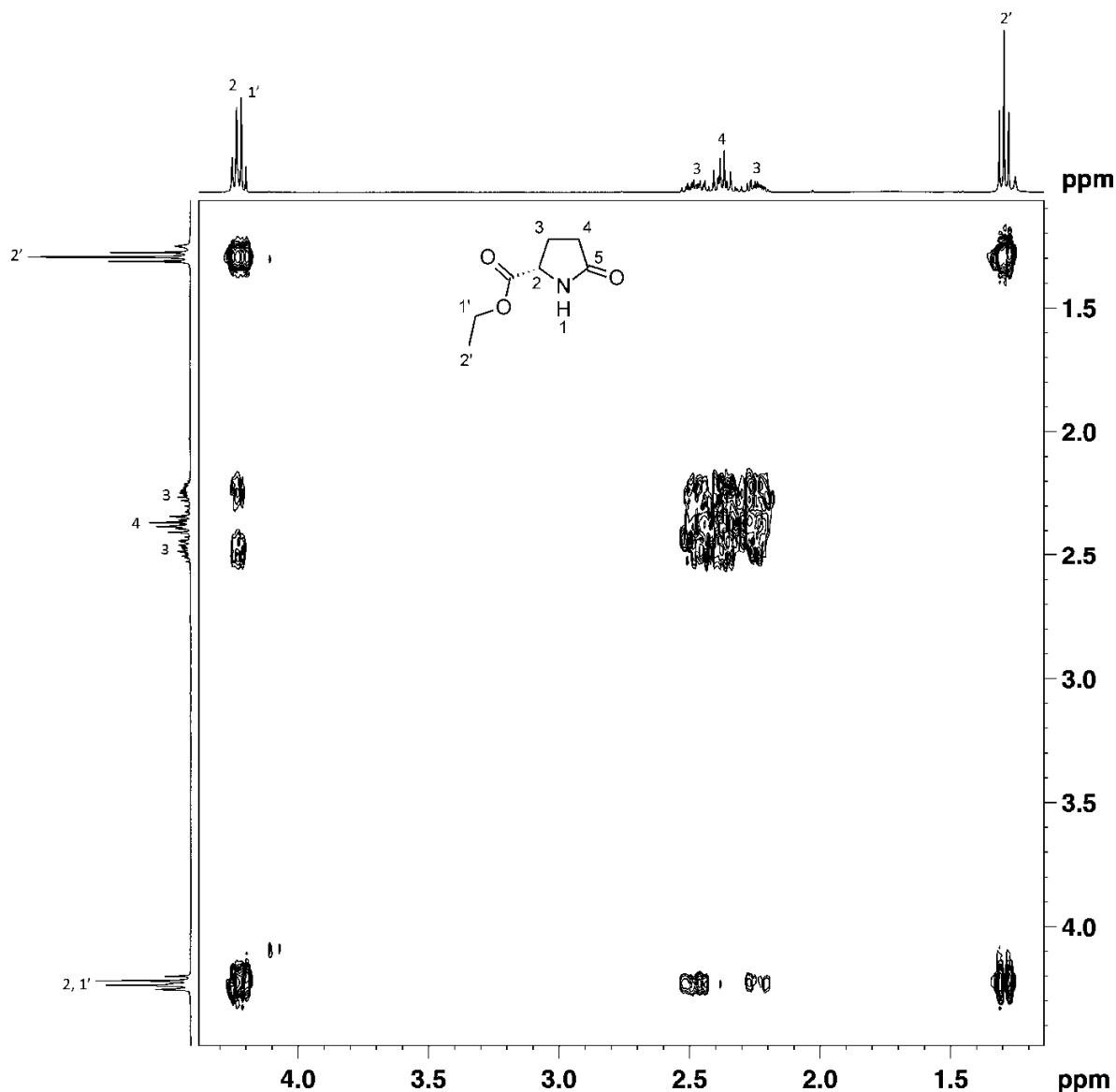


Figure 22: 2D COSY Spectrum for ethyl-(2S)-5-oxotetrahydro-1H-pyrrole-2-carboxylate

The ^{13}C NMR spectrum (Figure 23) showed the expected seven carbon peaks and the DEPT 135 spectrum (Figure 24) was used to distinguish between the primary, secondary and quaternary carbons. Two peaks were absent in the DEPT 135 spectrum that were present in the ^{13}C spectrum. These peaks resonated at 171.8 ppm and 177.7 ppm and are assigned to the 2- CCO_2 and 5-C respectively. The DEPT 135 spectrum also clearly showed three secondary carbon peaks. Two of these peaks resonated upfield at 24.8 and 29.1 ppm and were assigned as the ring carbons, 3-C and 4-C. The third peak was shifted downfield to 61.7 ppm and thus assigned as the ester CH_2 1'-C. The ester methyl peak 2'-C resonated at 14.1 ppm. The final peak at 55.3 ppm was assigned to the tertiary carbon 2-C.

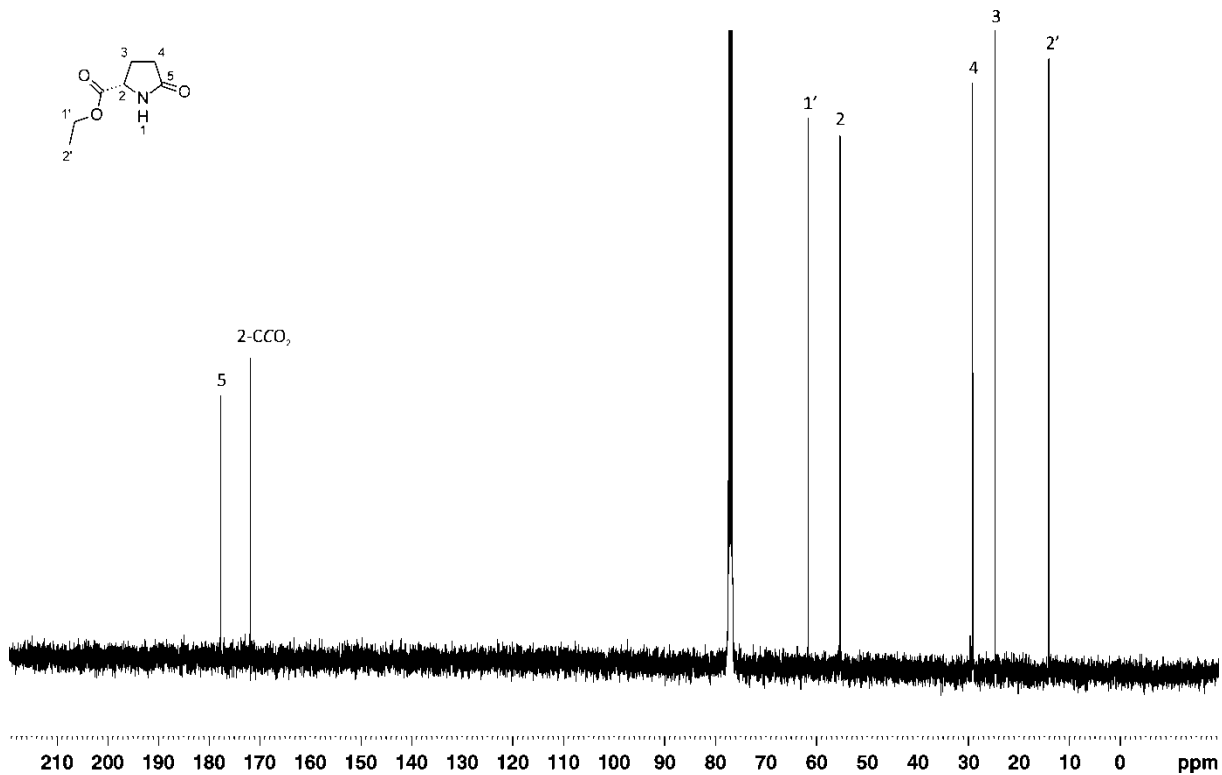


Figure 23: ^{13}C NMR Spectrum for ethyl-(2S)-5-oxotetrahydro-1H-pyrrole-2-carboxylate

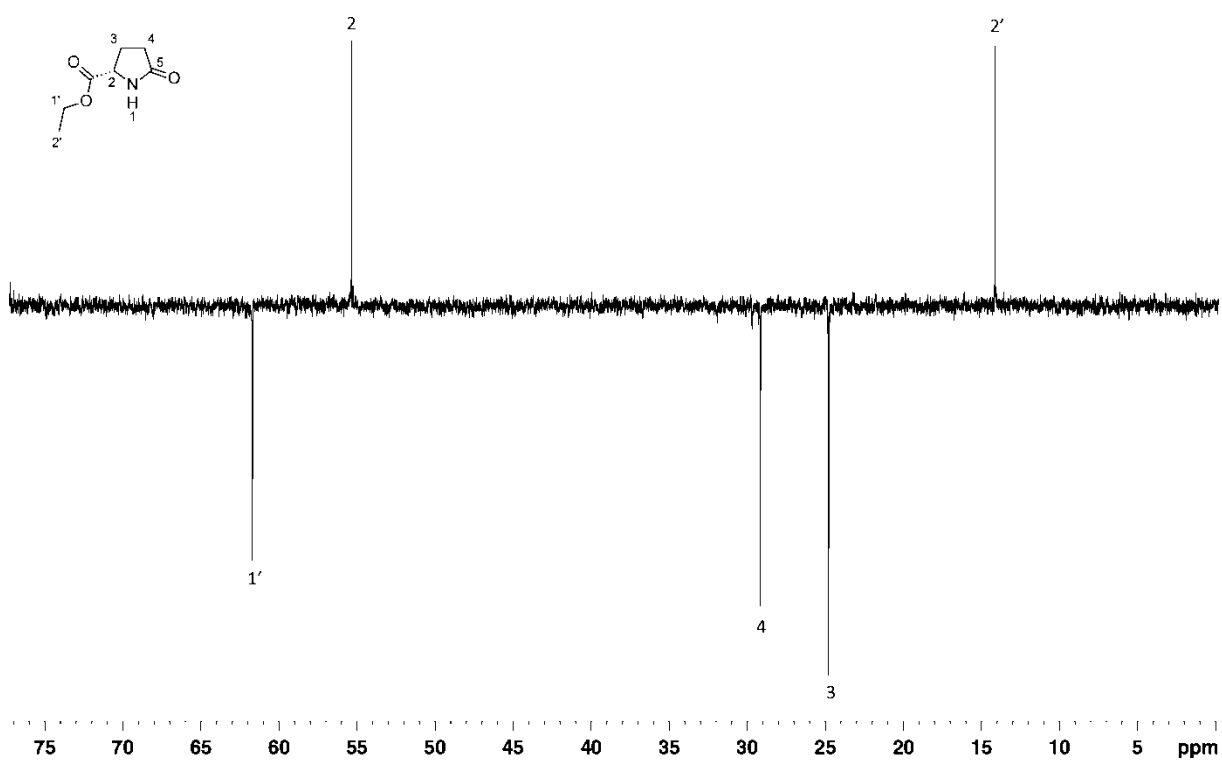


Figure 24: DEPT 135 NMR Spectrum for ethyl-(2S)-5-oxotetrahydro-1H-pyrrole-2-carboxylate

The two dimensional HSQC spectrum (Figure 25) was used to determine which protons were directly attached to which carbons. The peak resonating at 1.30 ppm in the ^1H NMR spectrum was directly coupled to the carbon at 14.1 ppm in the ^{13}C NMR spectrum. The HSQC also confirmed the 3-*H* protons to be non-equivalent as two peaks at 2.21-2.30 ppm and 2.42-2.53 ppm are directly coupled to the same carbon at 24.8 ppm. The peak at 2.32-2.40 ppm in the ^1H spectrum was directly coupled to the peak at 29.1 ppm in the ^{13}C spectrum. The only tertiary carbon in the molecule resonated at 55.3 ppm, which correlates to the proton 2-*H* at 4.20-4.25 ppm in the ^1H spectrum. Finally the peak at 4.22 ppm in the ^1H spectrum couples directly to the peak at 61.7 ppm in the ^{13}C spectrum.

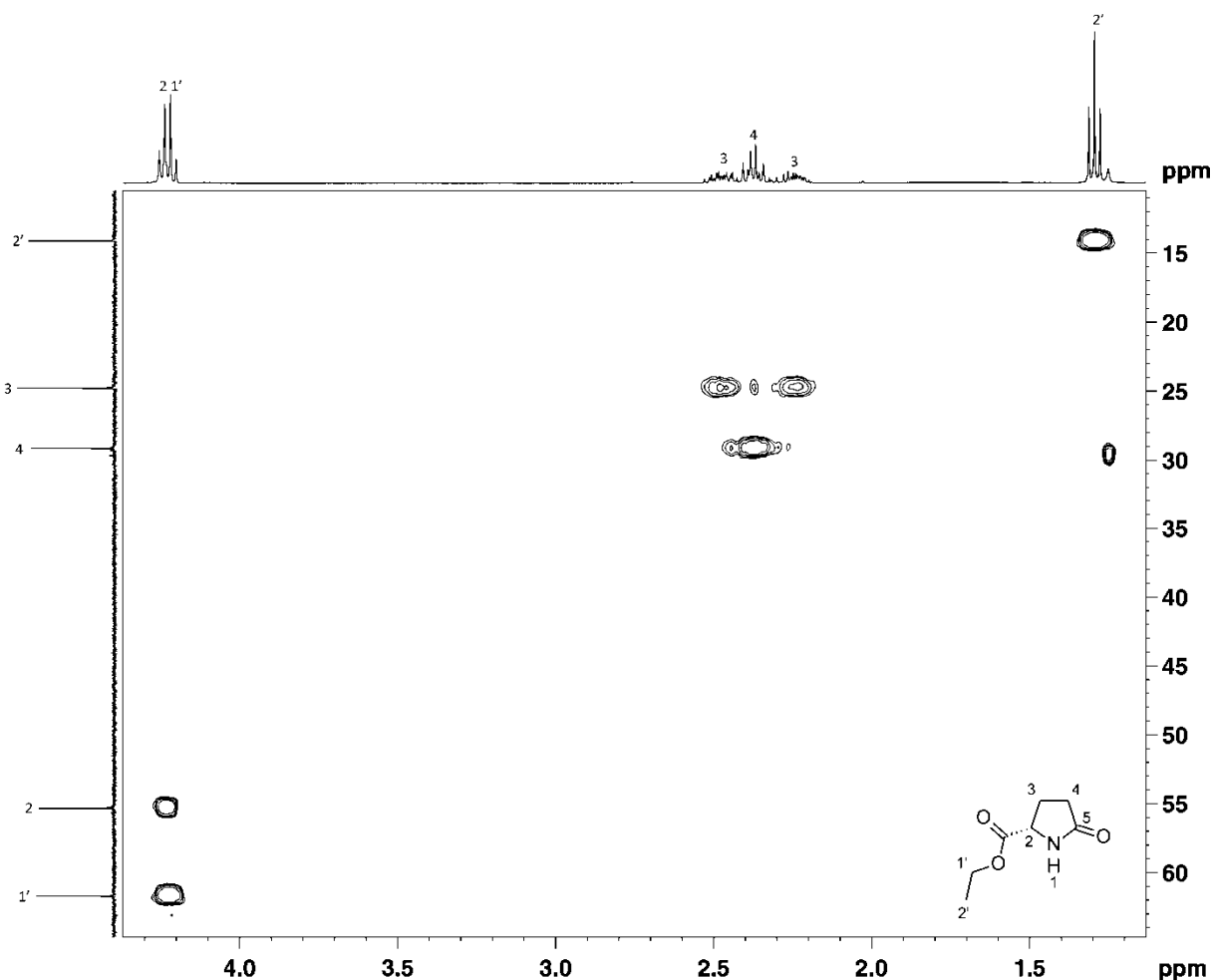


Figure 25: 2D HSQC NMR Spectrum for ethyl-(2S)-5-oxotetrahydro-1H-pyrrole-2-carboxylate

The carbonyl carbon 2- CCO_2 was expected to have long range coupling to both the 2-*H* and 1'-*H* protons, and this was confirmed in the two dimensional HMBC spectrum (Figure 26). Thus the peak at 171.8 ppm was assigned to the carbonyl carbon. The amide carbon was expected to have long range coupling to the ring protons 4-*H* and 3-*H*, and this too was confirmed in the HMBC spectrum. Thus the peak at 177.7 ppm was assigned to the amide carbon 5-*C*, and the chemical shift was consistent with an amide function.

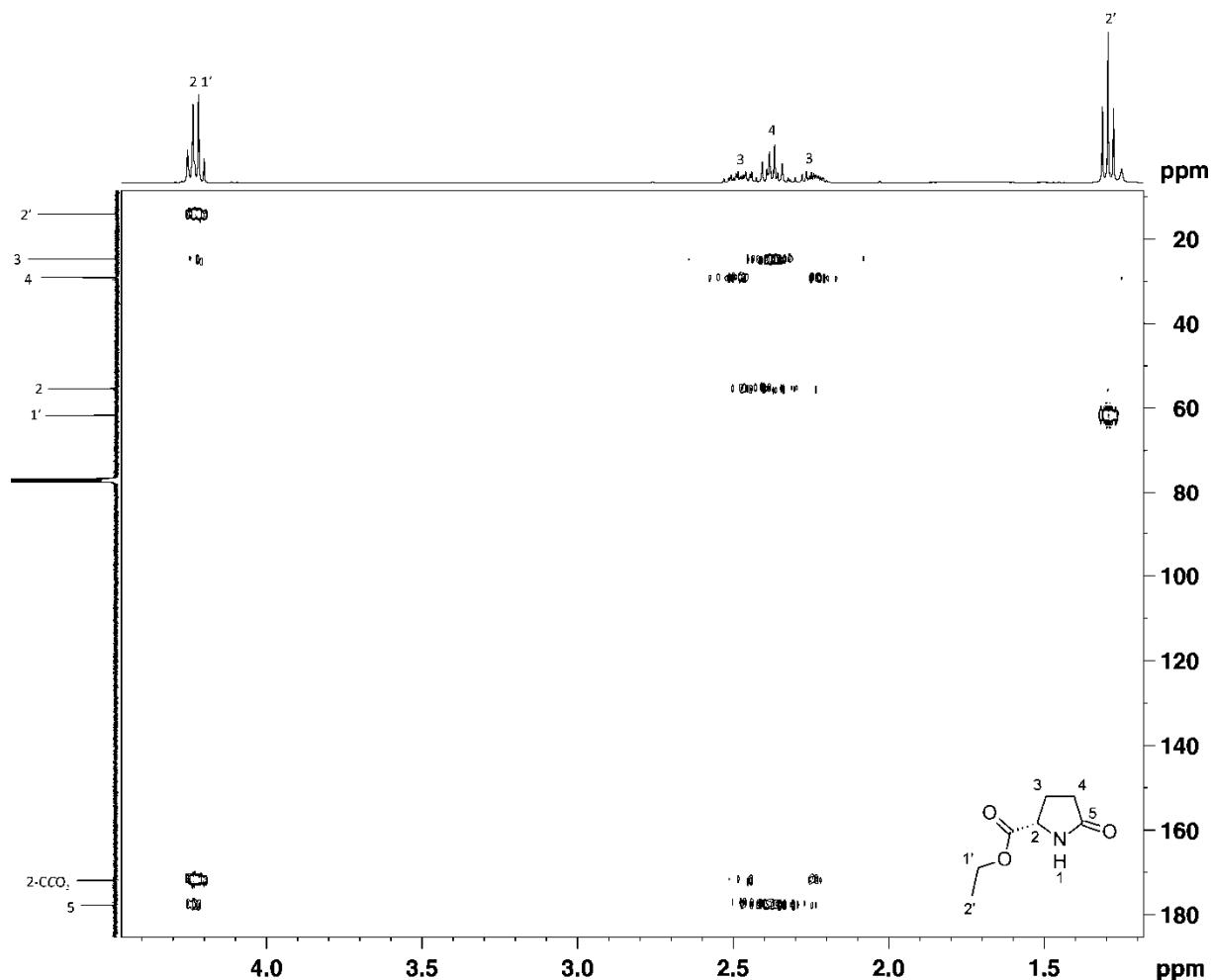
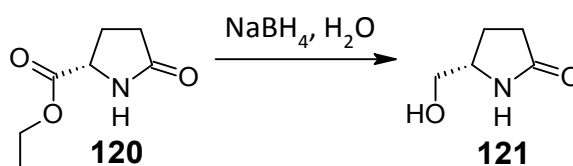


Figure 26: 2D HMBC NMR Spectrum for ethyl-(2S)-5-oxotetrahydro-1H-pyrrole-2-carboxylate

After confirming the structure of ethyl-(2S)-5-oxotetrahydro-1H-pyrrole-2-carboxylate **120** the next step involved the reduction of the ester to an alcohol **121** (Scheme 43). This was done with sodium borohydride, a mild reducing agent, to selectively reduce the ester and leave the amide unchanged.



Scheme 43

The reduction occurs by hydride transfer of $\text{H}-\text{BH}_3^- \text{Na}^+$ to the ester carbonyl to form an aldehyde intermediate. Further reduction by NaBH_4 followed by proton removal generates the alcohol. Each hydride removed from NaBH_4 is replaced by a hydroxide ion, to form NaOH and $\text{B}(\text{OH})_3$ as side products.⁷⁵

Sodium borohydride in distilled water was slowly added to a stirred solution of the ethyl ester **120** in distilled water at 0 °C. The solution was stirred for 3 hours whilst slowly warming to room temperature followed by quenching with acetone. Both TLC and NMR analysis indicated the presence of two compounds. A baseline spot on the TLC was presumed to be boric acid, a by-product formed from sodium borohydride reactions in water, and a spot with an $R_f = 0.36$ (2:1 ethyl acetate-methanol) was assumed to be the desired product. Filtering the solution through a short silica plug with vacuum removed the insoluble boric acid and allowed for much easier purification of the resulting milky white oil by column chromatography to afford a colourless oil which upon standing solidified to afford the product in a 96 % yield. NMR analysis of this compound indicated that it was indeed the desired alcohol (5S)-5-(hydroxymethyl)tetrahydro-2H-pyrrol-2-one **121**.

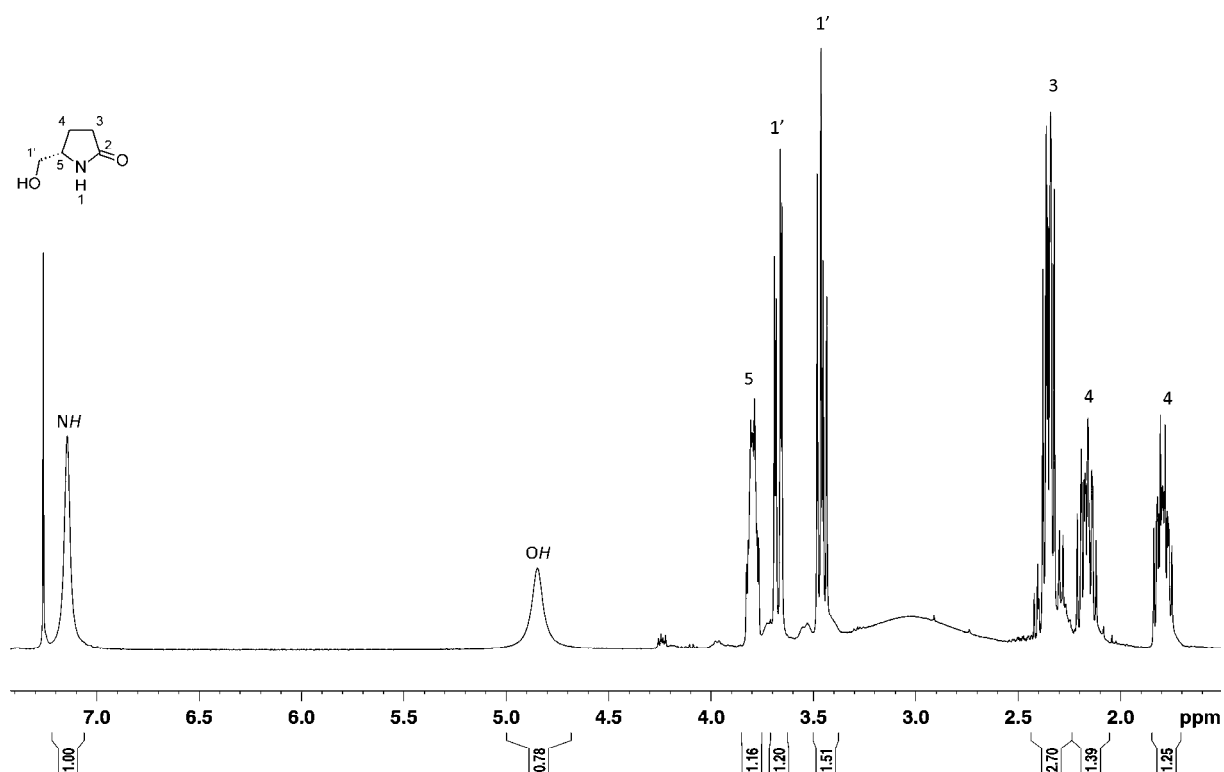


Figure 27: ¹H NMR Spectrum for (5S)-5-(hydroxymethyl)tetrahydro-2H-pyrrol-2-one

The ¹H NMR spectrum (Figure 27) showed two broad singlet peaks, integrating for one proton each. The peak resonating at 7.14 ppm was assigned as the amine and the peak resonating at 4.84 ppm as the alcohol. The chiral centre at 5-C was expected to lead to two pairs of non-equivalent pairs of protons 1'-H and 4-H. The 1'-H protons were expected to resonate more downfield due to their proximity to an alcohol functionality. Thus the peaks at 3.43-3.48 ppm and 3.65-3.68 ppm, both integrating for one proton, were assigned as the 1'-H protons. The 4-H protons were assigned to the peaks resonating at 1.75-1.84 ppm and 2.11-2.21 ppm. The remaining ring protons 3-H and 5-H were assigned to the peaks resonating at 2.32-2.38 ppm and 3.76-3.83 ppm respectively.

The COSY spectrum (Figure 28) showed the 4-*H* peaks were coupled to each other as well as to the 3-*H* and 5-*H* protons. The 1'-*H* peaks were also coupled to each other as well as to the 5-*H* proton. These observations indicated that the 4-*H* protons were indeed adjacent to the chiral centre and located in the ring, while the 1'-*H* protons were adjacent to the chiral centre and the alcohol.

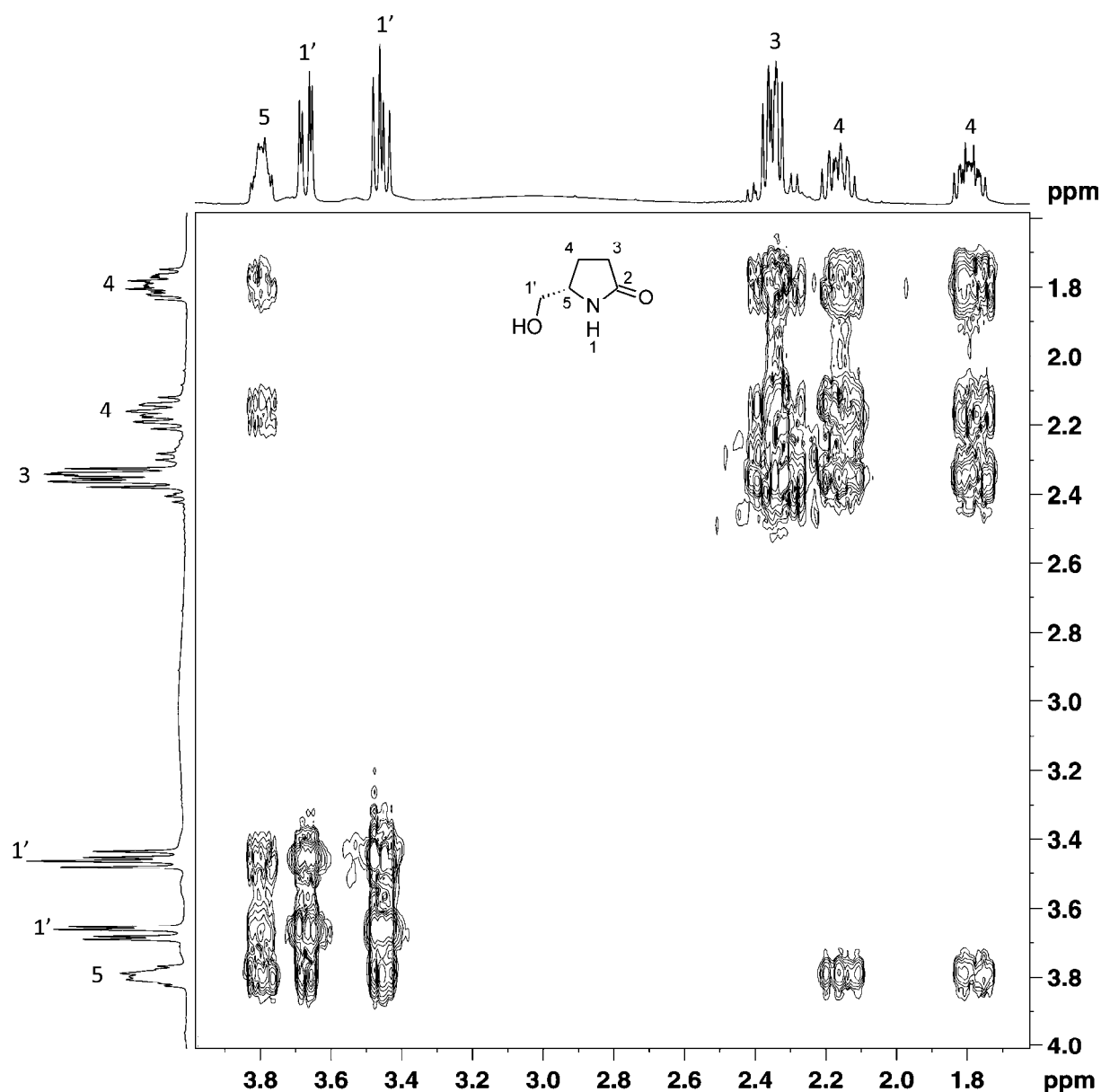


Figure 28: 2D COSY NMR Spectrum for (5S)-(hydroxymethyl)tetrahydro-2H-pyrrol-2-one

The ¹³C NMR spectrum (Figure 29) contained five peaks. The structure contains only one quaternary carbon, which would resonate downfield. One such signal was present in the ¹³C spectrum at 179.4 ppm, and was assigned to the amide carbon 2-C. Similarly, the structure contains only one tertiary carbon, 5-C, with a peak resonating at 56.4 ppm in the ¹³C spectrum. The remaining three peaks in the ¹³C spectrum all belonged to secondary carbons, as confirmed by the DEPT 135 spectrum

(Figure 30). The 1'-C peak was expected to resonate further downfield than the ring carbons due to its proximity to the alcohol functionality and was thus assigned as the peak resonating at 65.8 ppm. The remaining two peaks at 22.3 ppm and 30.2 ppm were assigned to 4-C and 3-C respectively. The two dimensional HSQC spectrum (Figure 31) confirmed these assignments, as the 4-C and the 1'-C carbons both coupled to non-equivalent protons.

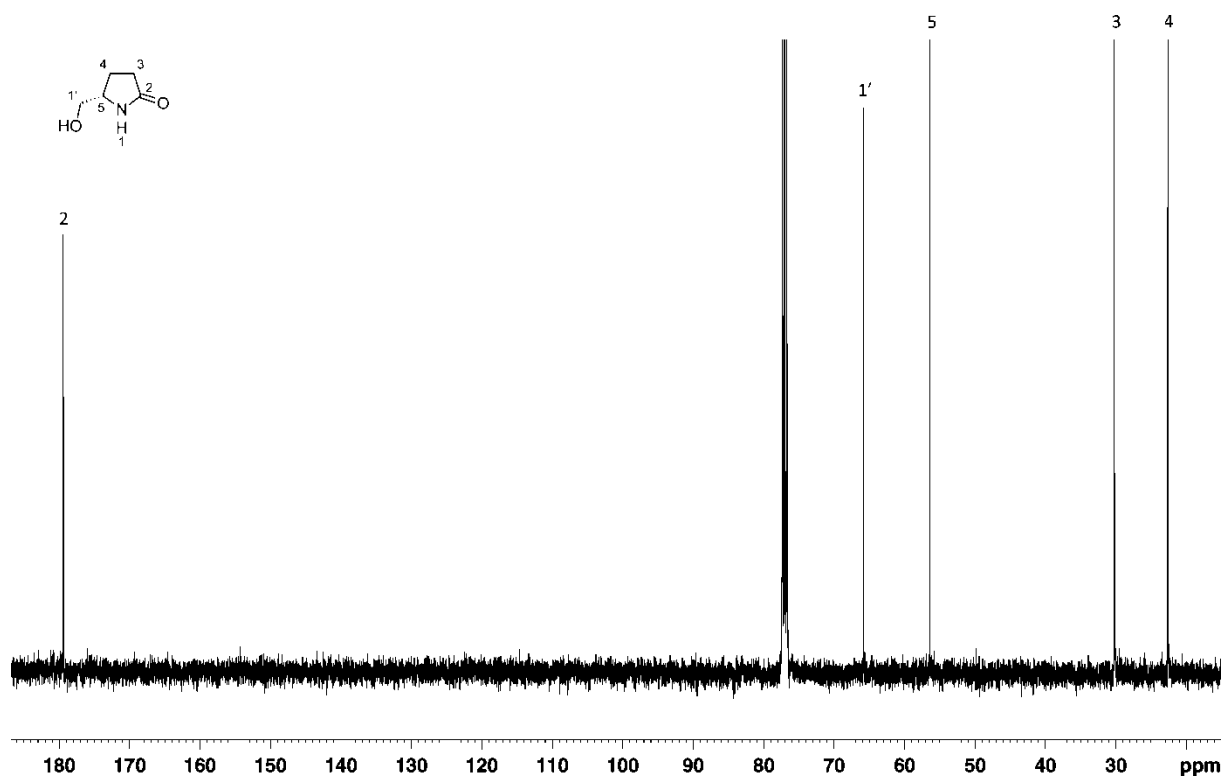


Figure 29: ¹³C NMR Spectrum for (5S)-(hydroxymethyl)tetrahydro-2H-pyrrol-2-one

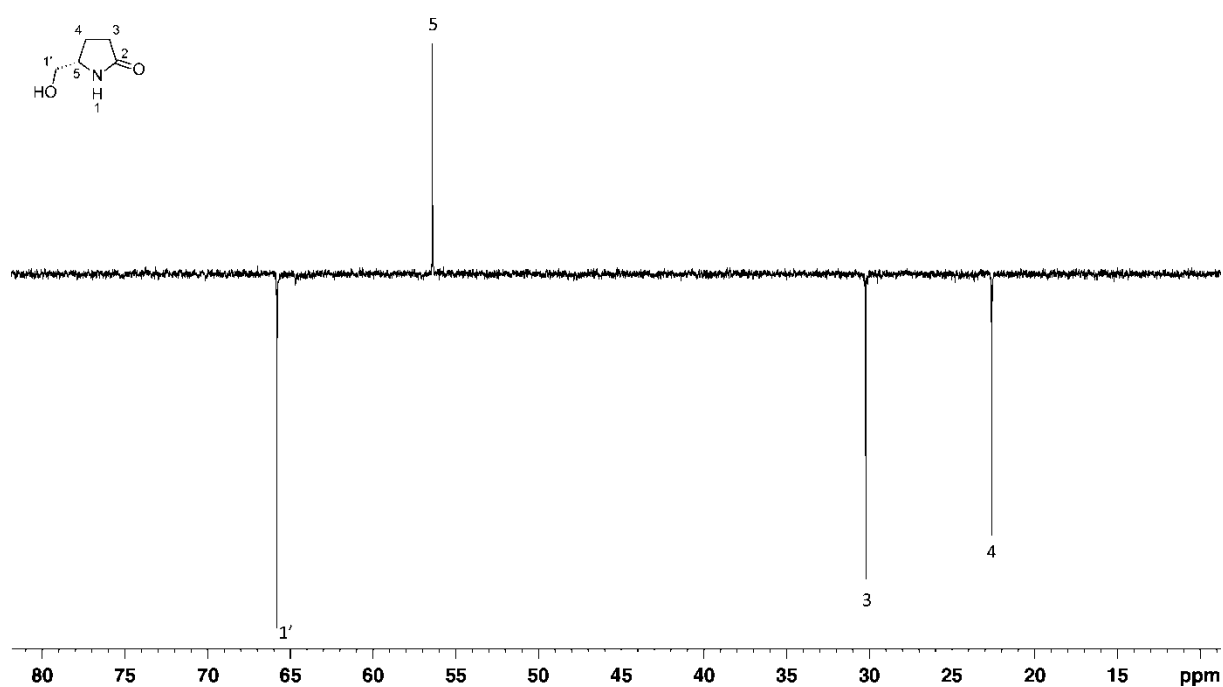


Figure 30: DEPT 135 NMR Spectrum for (5S)-(hydroxymethyl)tetrahydro-2H-pyrrol-2-one

The HSQC spectrum (Figure 31) also showed that the 5-*H* proton resonating at 3.76-3.83 ppm in the ^1H spectrum was directly attached to the tertiary carbon peak resonating at 56.4 ppm in the ^{13}C spectrum. The 3-*H* peak resonating at 2.32-2.38 ppm in the ^1H spectrum was directly attached to the peak resonating at 30.2 ppm in the ^{13}C spectrum.

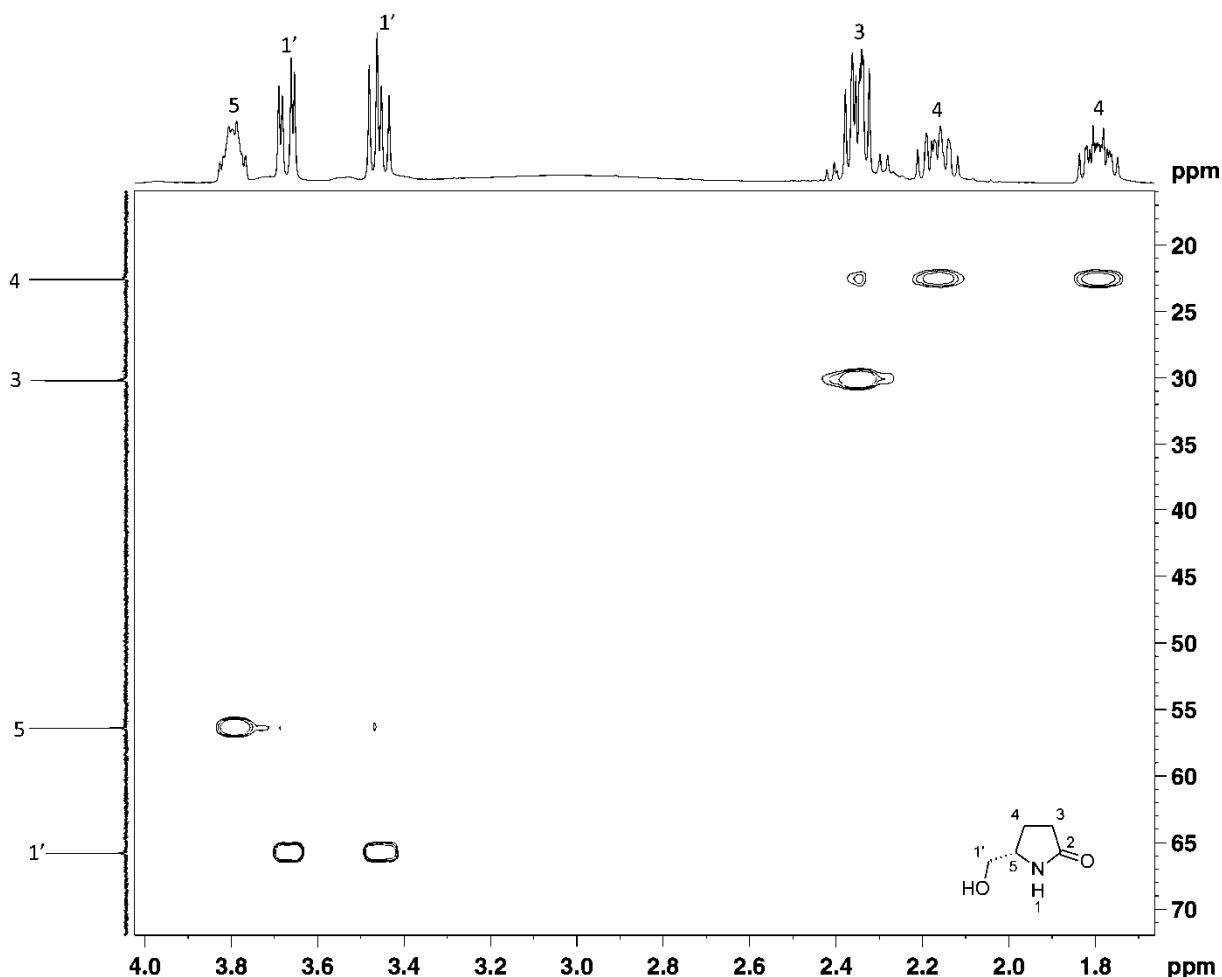
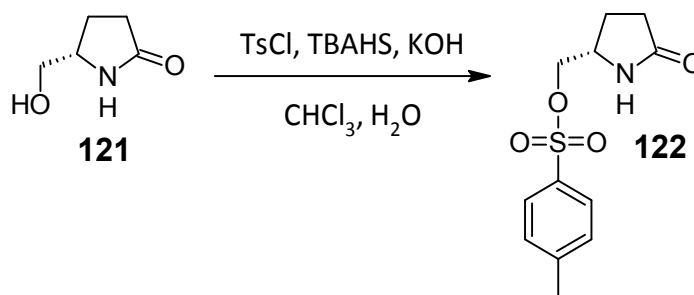


Figure 31: 2D HSQC NMR Spectrum for (5S)-(hydroxymethyl)tetrahydro-2H-pyrrol-2-one

The alcohol **121** was next converted into a good leaving group in order to be removed in a subsequent synthetic step (Scheme 44). Tosylate groups are known to be excellent leaving groups⁷⁶ as they are weak bases allowing for easy elimination. Tosylation has historically been achieved with tosyl chloride and a large excess of pyridine base.⁷⁷ However, due to the toxicity of pyridine as well as undesirable side reactions and anhydrous conditions required to prevent hydrolysis of tosyl chloride an alternative method was investigated. Morita *et al.*⁷⁷ have reported a so called green method for tosylation which does not require anhydrous conditions or the toxic pyridine as a base. They found that tosylations could be promoted by KOH using water as a solvent. The tosylations were carried out at high pH in order to prevent hydrolysis of tosyl chloride, making anhydrous conditions unnecessary. This method was thus modified for the tosylation reaction. A biphasic solvent system (Schotten-

Baumann conditions)⁷⁸ was used to eliminate the use of excess amine base (pyridine) to neutralise the acid by product, as the acid will move into the aqueous phase.



Scheme 44

Thus the alcohol **121** is treated with tosyl chloride and potassium hydroxide in a water-chloroform solution. A phase transfer catalyst, tetrabutylammonium hydrogen sulfate, is added to facilitate the transfer of the base into the organic phase where the amine is located. The solution was stirred with sonication for 48–96 hours. Sonication serves to improve the rate of reaction as well as the yield by cavitation.⁷⁹ Vigorous stirring along with sonication is essential for good yields. An off white solid remained after work up which was purified by recrystallisation from toluene afforded the product in yields ranging from 19 % (poor stirring and sonication) to 85 % (very good stirring and sonication). The structure of [(2*S*)-5-oxotetrahydro-1*H*-pyrrol-2-yl]methyl 4-methylbenzenesulfonate **122** was confirmed by NMR spectroscopy.

The ¹H NMR spectrum (Figure 32) showed the presence of an N–H functionality as a characteristic broad singlet at 5.65 ppm. The aromatic protons resonated downfield with the 2-*H* and 6-*H* protons further downfield than the 3-*H* and 5-*H* protons at 7.80 ppm and 7.38 ppm respectively. The tosyl methyl 4-*CH*₃ appeared as singlet at 2.47 ppm. The peak resonating at 2.29-2.34 ppm integrated for two protons and was assigned as the 4''-*H* protons. The protons adjacent to the chiral centre were expected to be non-equivalent and thus the peaks resonating at 3.85 ppm and 4.07 ppm were assigned to the 1'-*H* protons, while the peaks resonating at 1.72-1.80 ppm and 2.22-2.27 ppm were assigned to the 3''-*H* protons. Finally, the peak resonating at 3.90-3.96 ppm was assigned as the 2''-*H* proton.

The two dimensional COSY spectrum indicated that the 1'-*H* protons were indeed coupled to each other and the 3''-*H* protons were also coupled to each other. The 2- and 6-*H* protons of the aromatic ring were coupled to the aromatic the 3- and 5-*H* protons.

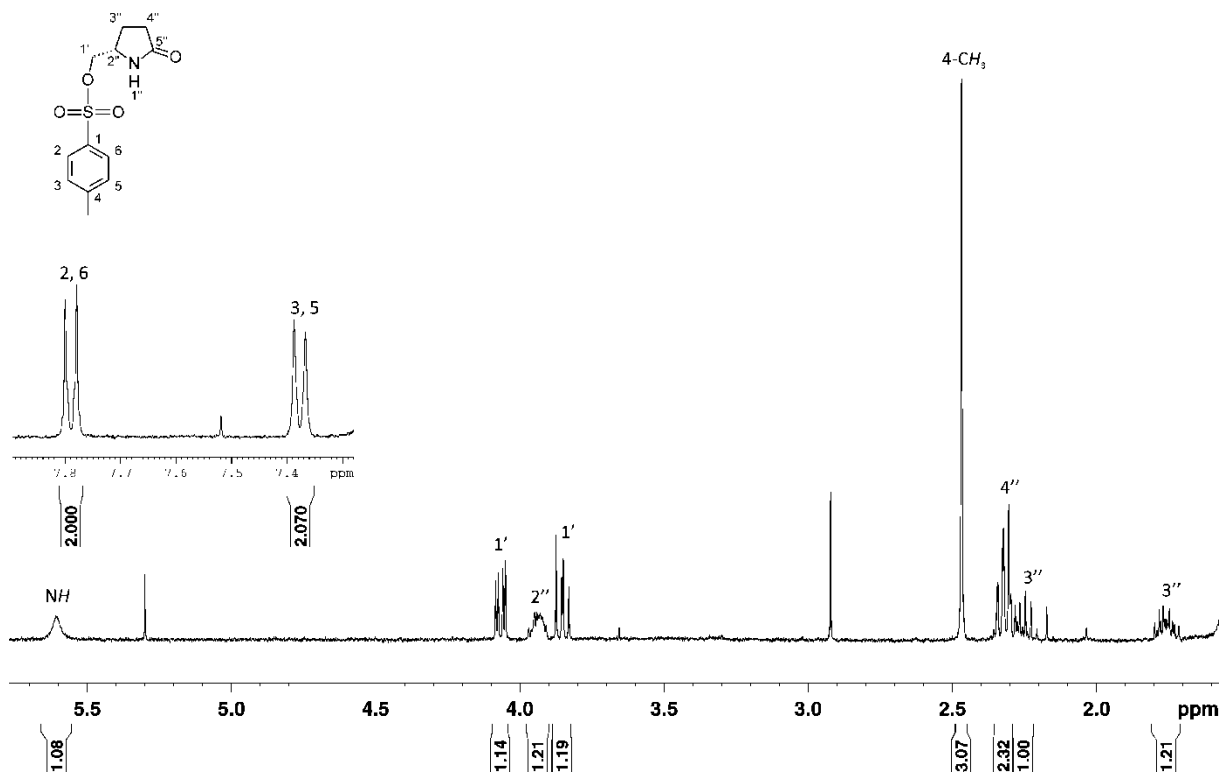


Figure 32: ^1H NMR Spectrum for [(2S)-5-oxotetrahydro-1H-pyrrol-2-yl]methyl 4-methylbenzenesulfonate

The ^{13}C NMR spectrum (Figure 33) showed only 10 peaks whereas the compound contains 12 carbons. However, two of the signals were of greater intensity than the other signals and had chemical shifts consistent with aromatic carbons. Thus the peaks resonating at 127.9 ppm and 130.1 ppm were assigned to the 2- and 6-C carbons and the 3- and 5-C carbons respectively. The carbons 2-C and 6-C give rise to only one signal as they are found in an identical environment. The same is true for the 3-C and 5-C carbons. The DEPT 135 spectrum (Figure 34) indicated the presence of only one methyl group and thus the peak resonating at 21.7 ppm was assigned as the 4-C CH_3 carbon. The structure also contains only one CH group 2''-C, which was assigned as the peak resonating at 52.5 ppm. Of the three quaternary carbons present the amide carbon 5''-C was expected to be the furthest downfield and was assigned as the peak resonating at 177.3 ppm. The 4-C carbon was expected to be more upfield in comparison to the other quaternary carbons and was assigned to the peak resonating at 132.5 ppm. Thus the final quaternary carbon 1-C was assigned to the peak resonating at 145.4 ppm. These three signals were not seen in the DEPT 135 spectrum indicating that they did indeed belong to quaternary carbons. The DEPT 135 spectrum also indicated the presence of three CH_2 groups. The 1'-C was expected to be further downfield and as assigned as the peak at 72.1 ppm. The 3''-C and 4''-C carbons were assigned to the peaks resonating at 22.8 ppm and 29.0 ppm respectively.

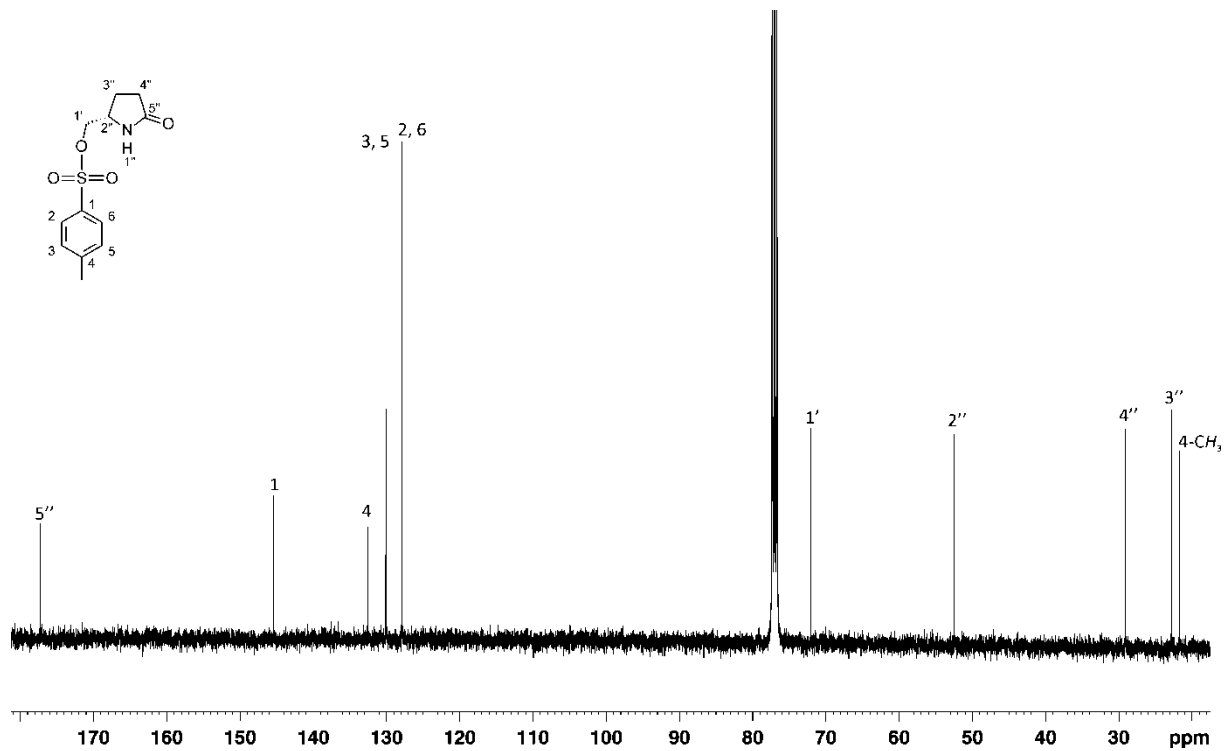


Figure 33: ^{13}C NMR Spectrum for [(2S)-5-oxotetrahydro-1H-pyrrol-2-yl]methyl 4-methylbenzenesulfonate

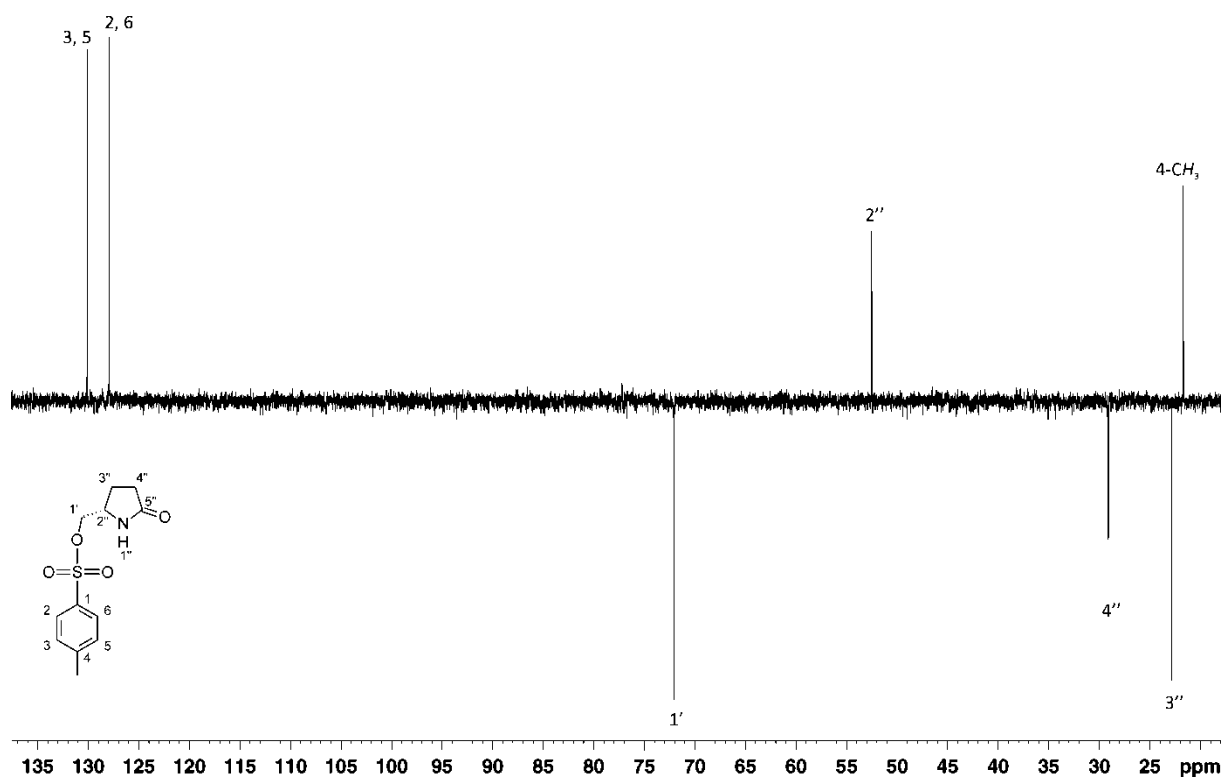


Figure 34: DEPT 135 NMR Spectrum for [(2S)-5-oxotetrahydro-1H-pyrrol-2-yl]methyl 4-methylbenzenesulfonate

In order to complete part one of the synthesis [(2*S*)-5-oxotetrahydro-1*H*-pyrrol-2-yl]methyl 4-methylbenzenesulfonate **122** required reduction to remove the tosyl group to afford (5*R*)-5-methyltetrahydro-2*H*-pyrrol-2-one **123**.

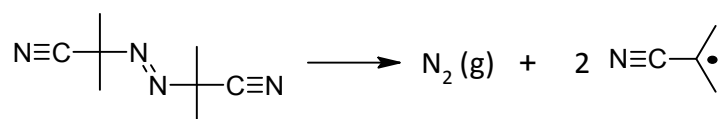
The substitution of a sulfone or tosyl group with hydrogen is widely utilised in organic synthesis and falls under the umbrella of reductive desulfonylation. Many reducing agents have been employed for this purpose such as samarium diiodide, hydrides in conjunction with transition metal catalysts such as platinum and tin hydrides,⁸⁰ where a radical reaction is used to replace a functional group, such as a halide, with a hydrogen. Such radical reactions are selective, and thus can be used for molecules containing more than one functional group.⁸¹ Halides, with the exception of fluorides, are easily reduced by tin, germanium or silicon hydrides.^{76, 81}

Thus, tributyltin hydride is employed as the reducing agent, with AIBN playing the role of the radical initiator. Tributyltin hydride is an ideal reagent for the reaction as the weak Sn–H bond is easily broken and the reaction is driven forward by the strength of the forming Sn–X bond, where X is a halogen (usually iodides or bromides).⁵⁴ The choice of initiator has a significant impact on the reactivity of the radicals and, if the radicals formed are too reactive it will lead to the formation of many side products as the radicals abstract any hydrogen, rather than just the Sn–H hydrogen. Thus AIBN is used as the radical formed is stabilised by the nitrile group, making it slightly less reactive, but still reactive enough to abstract the Sn–H proton.⁵⁴ An overall general reaction is illustrated in Scheme 45.



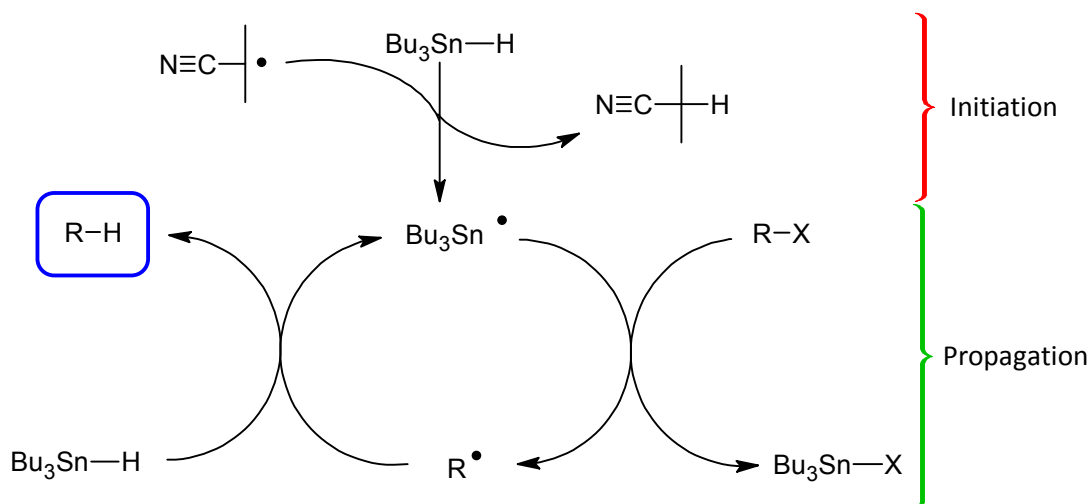
Scheme 45

Mill and Stringham⁸² in 1969 proposed that AIBN (and other compounds of the dialkyldiazene class) undergo photo-induced isomerisation from the *trans* isomer to the *cis* isomer and only upon heating of the *cis* isomer was the formation of radicals achieved (indicated by the liberation of N₂ (g)). Thermal homolysis at a temperature of 60 °C⁵⁴ is possible due to the presence of a weak azide bond (Scheme 46). Thus AIBN is an ideal source of radicals which in turn result in the formation of the tributyltin radicals necessary for the reaction.



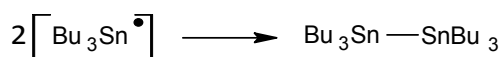
Scheme 46

There are three generally accepted steps to a radical chain reaction, namely initiation, propagation and termination.



Scheme 47

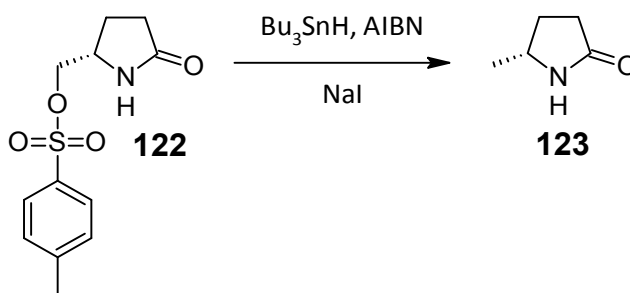
Scheme 47 illustrates the generally accepted initiation and propagation steps adapted from Clayden *et al.*⁵⁴ Initiation begins with homolysis of the free radical initiator and the resulting radical abstracting the proton from tributyltin hydride to form the tributyltin radical. Once generated, the tributyltin radical enters the propagation sequence where it abstracts a proton from the organic substrate R-X (X = halide, tosylate) to generate an organic radical species (the tosylate is usually converted to the iodide *in situ* with excess NaI, as the iodide is more susceptible to radical-mediated reduction). This then reacts with tributyltin hydride, abstracting a proton to form the product and regenerating the tributyltin radical in the process. The cycle continues until all of the R-X substrate has been consumed. Termination occurs when any of the radicals in solution combine with one another, for example if two tributyltin radicals combine to form a bis tributyltin species (Scheme 48).



Scheme 48

Tributyltin hydride and sodium iodide was added to a solution of 5-oxotetrahydro-1*H*-pyrrol-2-yl]methyl 4-methylbenzenesulfonate **122** and AIBN in dry toluene and refluxed for 14 hours (Scheme 49). A white precipitate (assumed to be a sodium-tosyl salt) formed and was removed by filtration and the filtrate was concentrated and purified by chromatography on silica to separate the (5*R*)-5-methyltetrahydro-2*H*-pyrrol-2-one **123** from the tributyltin iodide. High resolution mass

spectrometry confirmed the formation of **123** with an acquired mass of $122.0582 \text{ g mol}^{-1}$ which is in agreement with the calculated (M + H) mass of $122.0582 \text{ g mol}^{-1}$ for $\text{C}_6\text{H}_9\text{NONa}$.



Scheme 49

The structure was confirmed by NMR spectroscopy. The ^1H NMR spectrum (Figure 35) indicated that the tosyl group had been removed as there were no signals in the aromatic region. The doublet resonating at 1.13 ppm which integrated for 3 protons was assigned to the methyl protons $1'-\text{H}$. The peaks resonating at 1.51-1.60 ppm and 2.22-2.28 ppm were assigned to the 4-H protons, which are non-equivalent as they are adjacent to a chiral centre. The peak resonating at 2.22-2.28 ppm integrated for two protons and was assigned as the 3-H protons. Finally, the peak at 3.70 ppm integrating for one proton was assigned to the 5-H proton and the N-H proton resonated at 7.15 ppm.

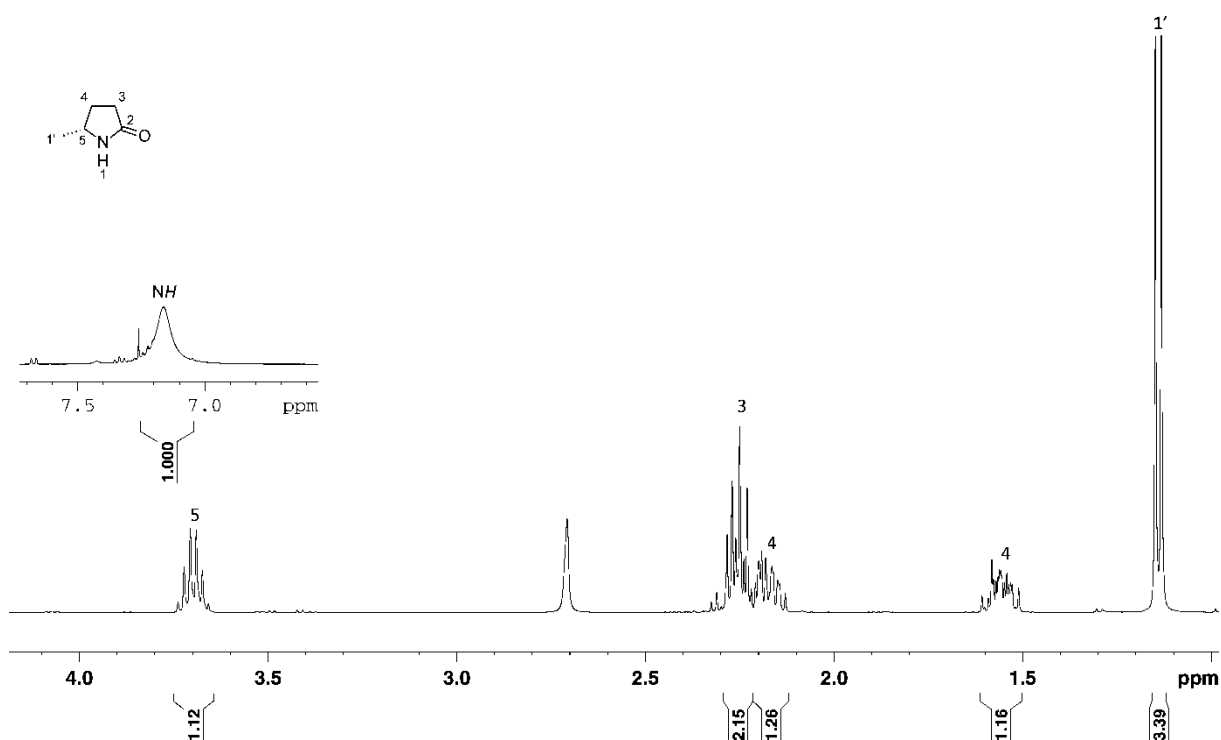


Figure 35: ^1H NMR Spectrum for (5R)-5-methyltetrahydro-2H-pyrrol-2-one

The ^{13}C NMR spectrum has five peaks (Figure 36). The peak resonating at 178.5 ppm was attributed to the only quaternary carbon in the compound 5-C. The peaks resonating at 28.9 ppm and 30.5 ppm attributed to secondary carbons 4-C and 3-C respectively as confirmed in the DEPT 135 spectrum. The peak resonating at 21.9 ppm was assigned to the primary carbon 1'-C and the final peak resonating at 50.1 ppm to the tertiary carbon 5-C.

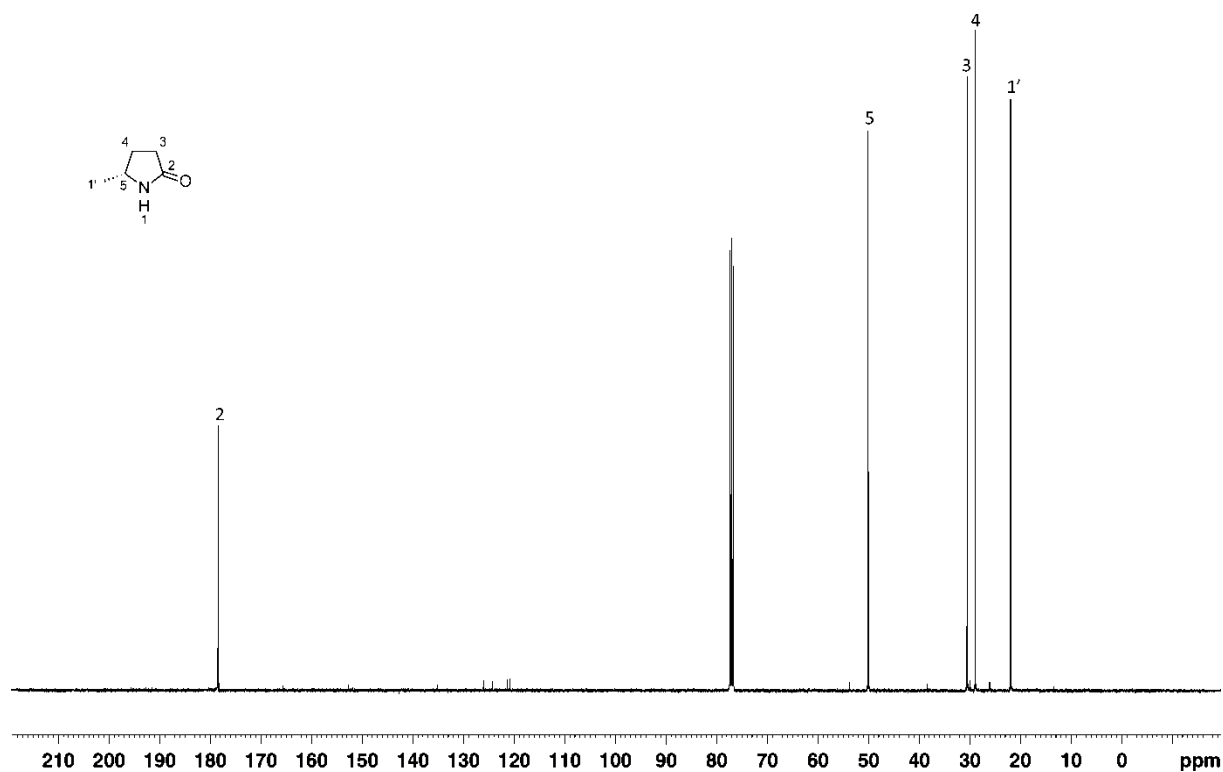
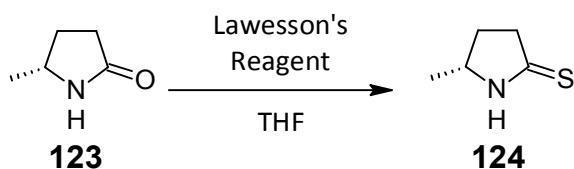


Figure 36: ^{13}C NMR Spectrum for (5*R*)-5-methyltetrahydro-2*H*-pyrrol-2-one

2.3.2 Part 2: Synthesis of ethyl 2-[(5*R*)-5-methyltetrahydro-2*H*-pyrrol-2-ylidene]acetate

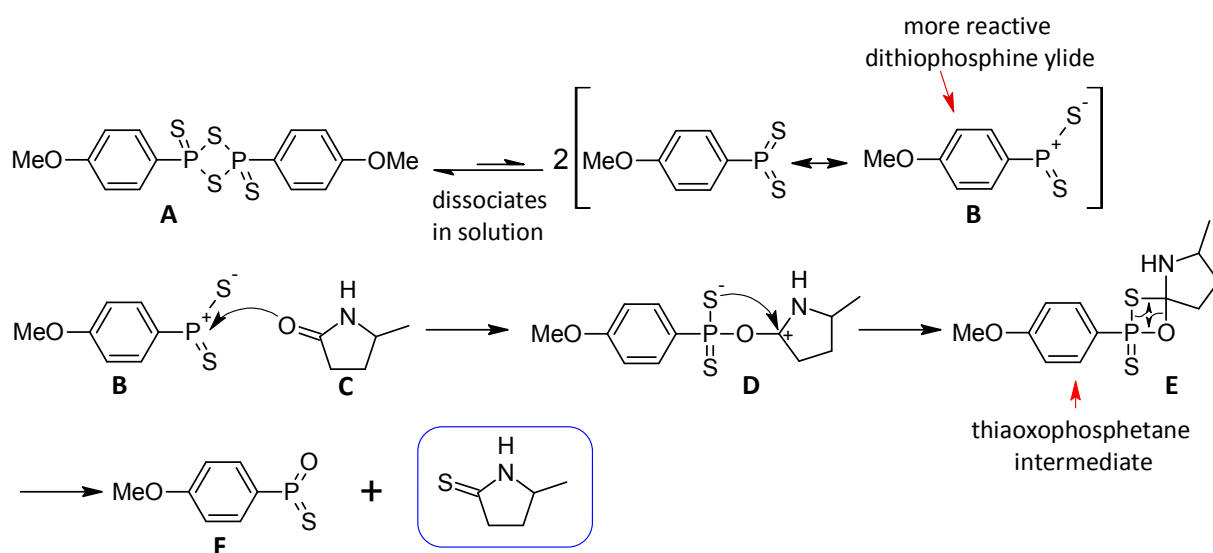
With (5*R*)-5-methyltetrahydro-2*H*-pyrrol-2-one in hand the next synthetic sequence could be undertaken. This began with the conversion of the methyl lactam **123** into its corresponding thiolactam **124**. There are a number of reagents available for thionation. Phosphorus pentasulfide (P_4S_{10}) was the most commonly utilised thionation agent before the discovery of 2,4-bis-(*p*-methoxyphenyl)-1,3-dithiadiphosphetane-2,4-disulfide (Lawesson's Reagent). Alternative thionation agents to P_4S_{10} such as hydrogen sulfide, boron sulfide, *O,O*-diethyldithiophosphonic acid and elemental sulfur have all been investigated for thionation.⁸³ However, since the discovery of the thionation ability of Lawesson's Reagent by Lawesson and co-workers in 1978, this reagent has dominated the literature for thionation chemistry.⁸⁴ The most widely used thionation agents today are Lawesson's Reagent and P_4S_{10} as both reagents have advantages and disadvantages associated

with them depending on particular reactions.⁸⁵ In general, Lawesson's Reagent results in much better yields than P₄S₁₀ and also allows for shorter reaction times, lower reaction temperatures and the use of better reaction solvents such as THF (as opposed to benzene, xylene and pyridine) and can be used for a wide range of carbonyl compounds.⁸³ Thus, in this synthesis Lawesson's Reagent was utilised as the thionation agent (Scheme 50).



Scheme 50

The mechanism reported in the literature⁸³⁻⁸⁵ for thionation by Lawesson's Reagent begins with the dissociation of the reagent in solution (Scheme 51). The more reactive dithiophosphine ylide **B** is responsible for the thionation.⁸³ Attack by the carbonyl **C** on the electrophilic phosphorus **B** followed by attack by the sulfur on the carbonyl carbon **D** results in the formation of a thioxophosphetane intermediate **E** (similar to a Wittig-type intermediate).⁸⁴ Cycloreversion of the thioxophosphetane intermediate results in the formation of the thionated lactam **124** and a by-product of Lawesson's Reagent **F**. The reaction is driven forward by the formation of the strong P=O bond of the thermodynamically stable by-product.⁸⁵



Scheme 51

(5*R*)-5-Methyltetrahydro-2*H*-pyrrol-2-one **123** in dry THF was added dropwise to a stirring solution of Lawesson's Reagent in dry THF and stirred for 24 hours at room temperature. The solvent was subsequently removed *in vacuo* followed by immediate purification by column chromatography on silica. The column was pre-warmed by heating with a heatgun as the crude oil is difficult to dissolve in any solvent once it has cooled and solidified. The column must be constantly warmed throughout the separation. However, impurities in the form of LR were present as can be seen in Figure 37 even after passing through the column. Purification of the thiolactam proved to be rather difficult and a disappointing yield of 33 % was obtained.

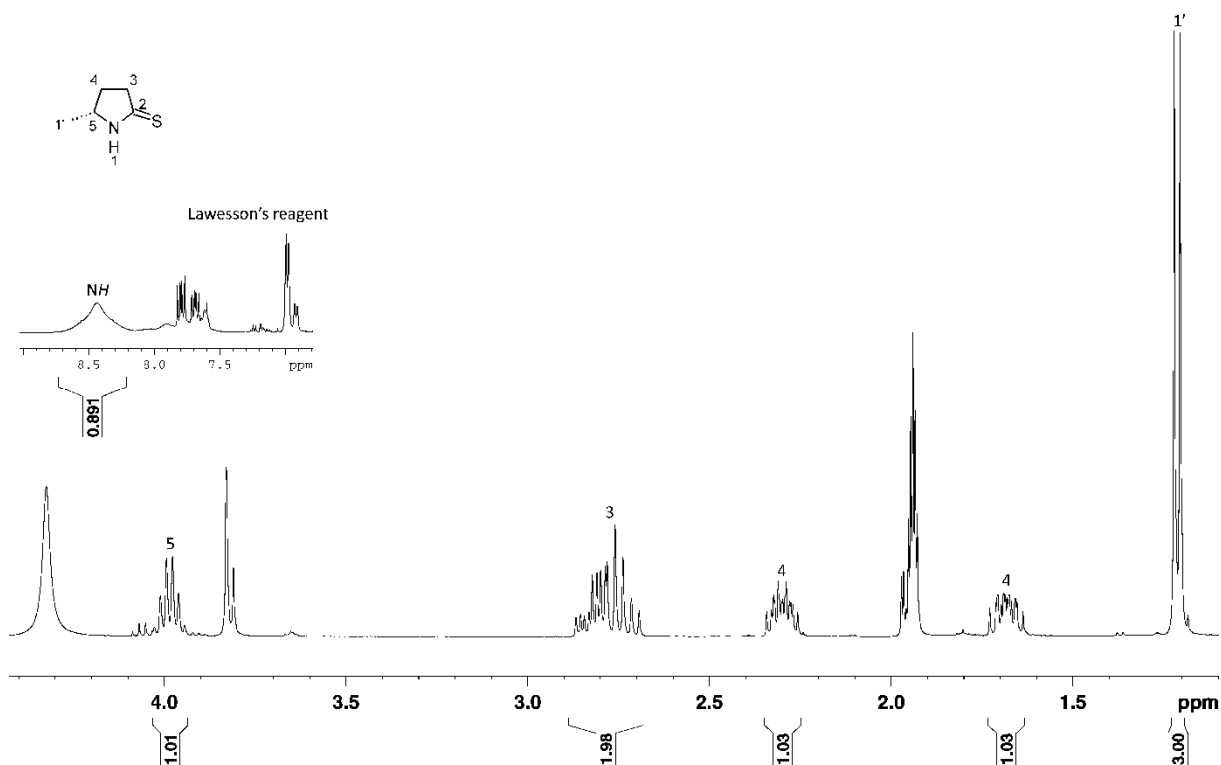
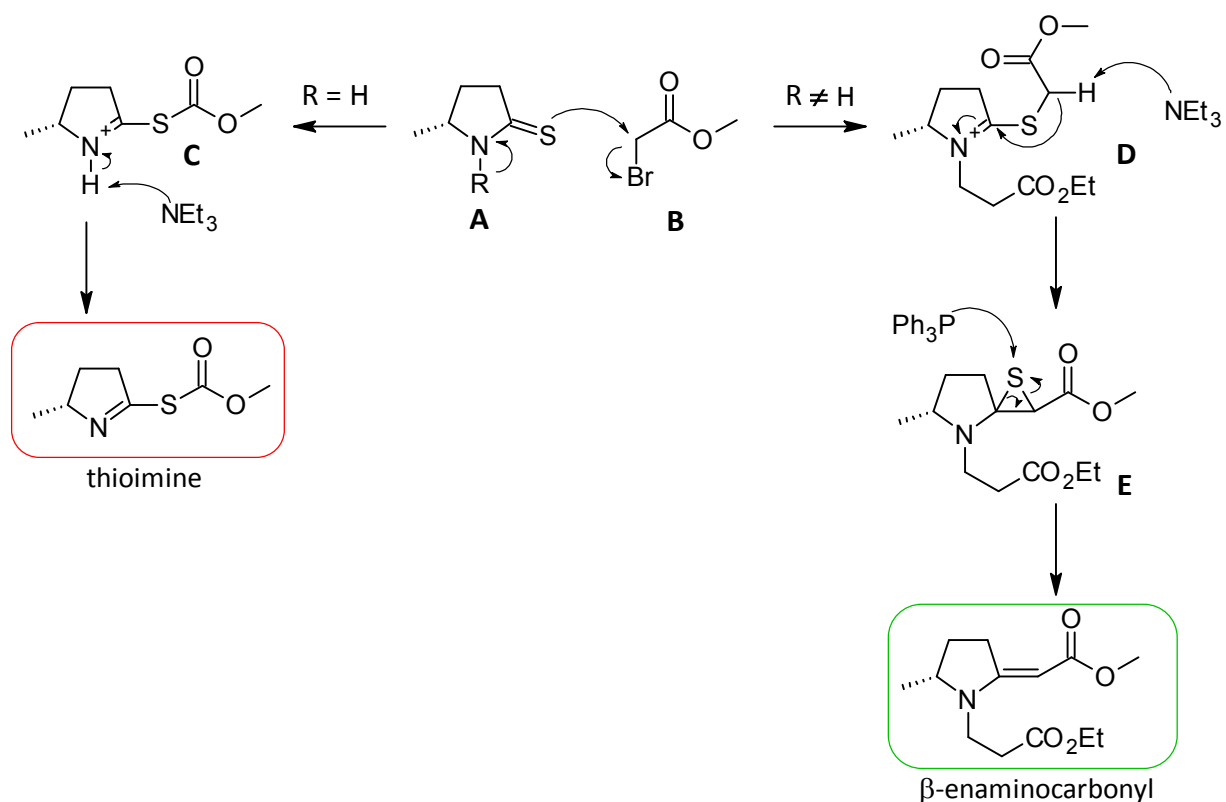


Figure 37: ^1H NMR spectrum of (5*R*)-5-methyltetrahydro-2*H*-pyrrole-2-thione

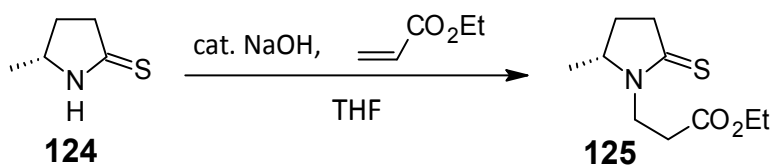
In order to access enaminoate **127** from the newly synthesised (5*R*)-5-methyltetrahydro-2*H*-pyrrole-2-thione **124** an activation step was required and the related reactions are outlined in detail below. Enaminoates can be prepared from alkenyl substituted β -enamino esters,⁸⁶ lactim ethers⁸⁷ and azido dicarbonyl compounds⁸⁸ and by lithiation of ketimines. However, the Eschenmoser sulfide contraction or Eschenmoser coupling reaction is the most used method for the preparation of enaminoates. Tertiary thiolactams can be converted into their corresponding enaminoates under mild conditions, by treatment with an activated alkyl halide, such as $\text{BrCH}_2\text{CO}_2\text{Et}$, a weak base (NEt_3) and a thiophile (PPh_3). However, secondary thiolactams require much harsher conditions to bring about the same transformation.⁸⁹ These include elevated reaction temperatures and times, a strong base like $\text{K}^t\text{O}^t\text{Bu}$ as well as a large excess of phosphine thiophile, which becomes difficult to remove. Therefore, before carrying out the Eschenmoser coupling *N*-protection/activation is essential to

prevent side product formation. Scheme 52 depicts two possible pathways for the Eschenmoser coupling postulated by Russowsky and Neto.⁹⁰⁻⁹¹ Initially, nucleophilic attack by the thiolactam on the bromoester forms a thioiminium cation. When R = H (i.e. when the lactam is secondary in nature) the NEt₃ preferentially removes the more acidic thioiminium proton to give the thioimine. However, when R ≠ H the more acidic proton in the α-proton of the bromoester carbonyl. This proton is thus removed to give a three membered sulfur ring at which point the thiophile attacks the sulfur atom to remove it, generating the β-enaminocarbonyl.⁹¹



Scheme 52

Following the protocol outlined above the secondary amine of (5*R*)-5-methyltetrahydro-2*H*-pyrrole-2-thione **124** had to be *N*-protected/activated (Scheme 53) before attempting the Eschenmoser coupling reaction. Acrylates are commonly used for functionalising the nitrogen of thiolactams by conjugate addition. The reaction is reversible by addition of a strong base.⁹²⁻⁹³



Scheme 53

(5*R*)-5-Methyltetrahydro-2*H*-pyrrole-2-thione **124** was dissolved in undried THF with solid NaOH added as a catalyst. The solution was stirred for about 5 minutes before the slow addition of ethyl acrylate. The solution was stirred for 5 hours at room temperature. This was followed by aqueous work up. It was evident from the ^1H NMR spectrum (Figure 38) that no product was obtained and the starting thiolactam and acrylate were present. Prior⁶⁸ reported yields of 95-100 % for this reaction and Dovey⁹⁴ reported yields of 75-95 % for analogue thiolactams. Our attempts of the same transformation utilising the procedures of Prior and Dovey however gave very low yields (10-40 %). It was therefore decided to go back to the model study for this reaction (previously completed by Prior). Thus 2-pyrrolidinone was converted to the pyrrolidine-2-thione by refluxing in dry toluene for 4 hours. The solution was concentrated and the residue recrystallised from chloroform/hexane (1:1). ^1H and ^{13}C NMR spectroscopic data was in close agreement to that reported by Prior⁶⁸ and Dovey.⁹⁴ With the thiolactam in hand the *N*-protection model study could be conducted.

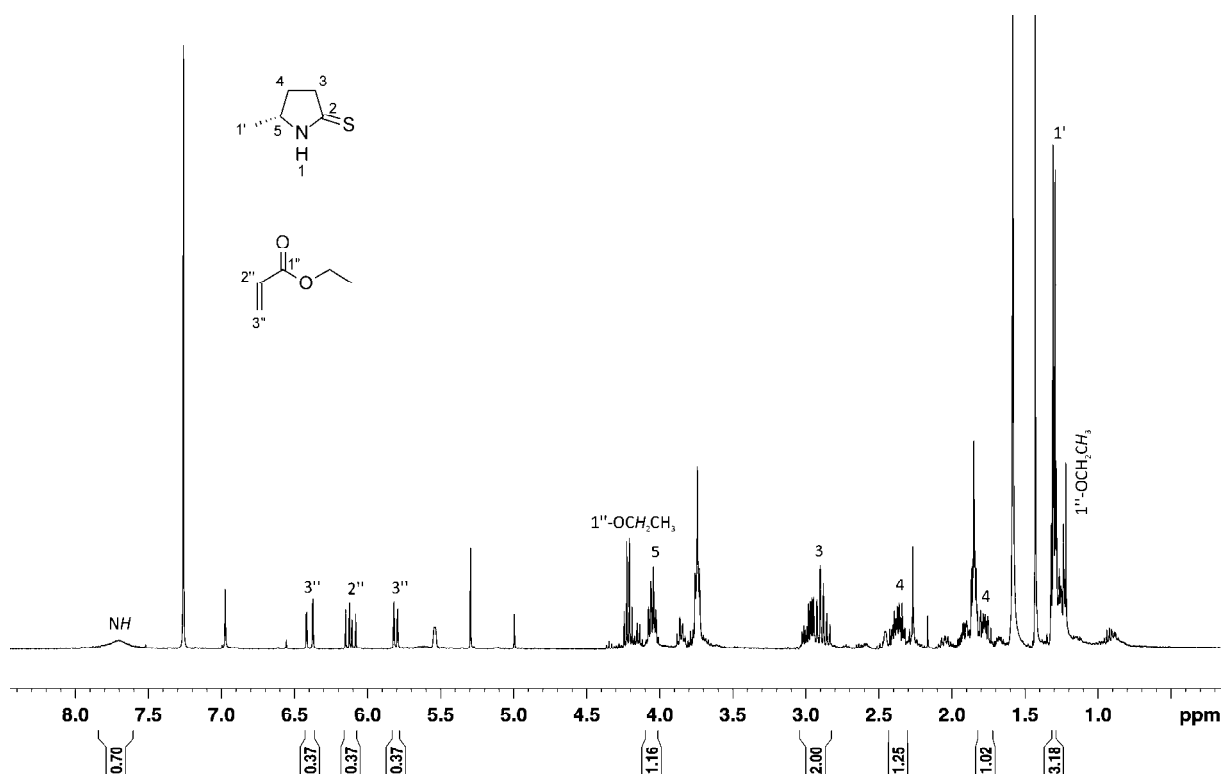


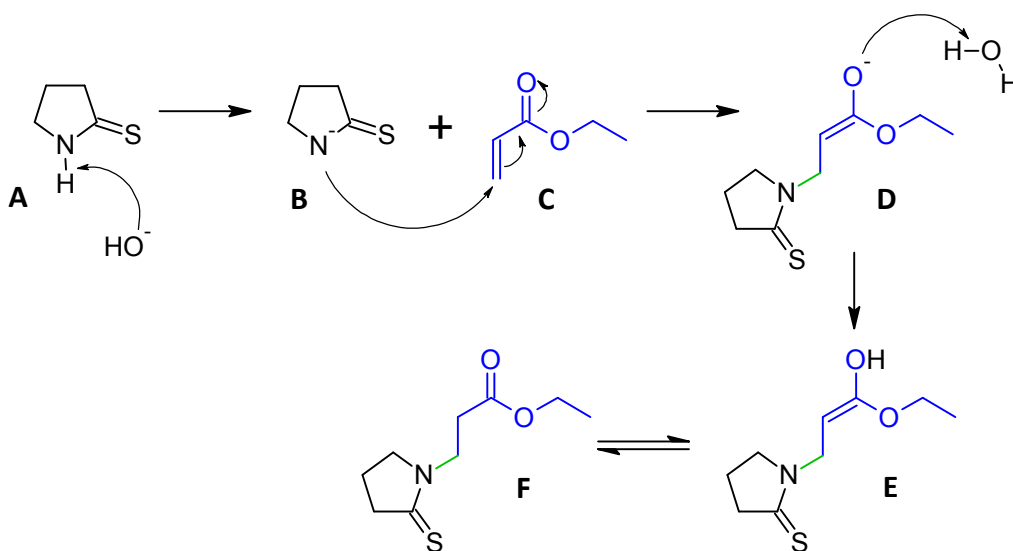
Figure 38: ^1H NMR spectrum of attempted *N*-alkylation of (5*R*)-5-methyltetrahydro-2*H*-pyrrol-2-thione

The study began by first trying to replicate the results of Prior⁶⁸ using the optimised conditions (see Chapter 1, Scheme 36). Therefore pyrrolidine-2-thione **116** was dissolved in undried THF and catalytic NaOH was added. The solution was stirred until most of the NaOH had dissolved before the dropwise addition of ethyl acrylate. The resulting solution was stirred for 5 hours at room

temperature before aqueous work up. Once again, ^1H NMR analysis showed very little product with a large amount of unreacted thiolactam.

At this point a new literature search seemed prudent and the method of Michael *et al.*⁹⁵ for similar transformations was attempted. Pyrrolidine-2-thione **116** was dissolved in dry THF and catalytic NaOH was added before the dropwise addition of ethyl acrylate. The solution was stirred at 40 °C for 16 hours before aqueous work up. However, the same problems were encountered; the majority of the thiolactam was un-reacted. This seemingly simple conjugate addition reaction became a serious obstacle to our synthesis.

A possible mechanism of such an addition is given in Scheme 54. The base (OH^- in this case) abstracts the proton of the secondary amine **A** (the thiolactam) giving a much better nucleophile and generating water in the process. The nucleophile **B** attacks the β -carbon of the acrylate **C** to give **D**. The newly formed oxygen nucleophile **D** abstracts a proton from water, regenerating the base. Keto-enol tautomerism of **E** gives the final conjugate addition product **F**. Thus, since the reaction generates water, dry THF is unnecessary. From this mechanism it can be seen that if the catalyst is not regenerated the reaction will not proceed any further.



Scheme 54

A number of different conditions and reagents were investigated. A different bottle of NaOH was used. A freshly made solution of 1M NaOH was used instead of solid NaOH. Stoichiometric amounts of NaOH were used instead of catalytic amounts. The base was changed from NaOH to NaH. Both dried and undried THF were used and freshly distilled THF was used. Ethanol was used as a solvent instead of THF. Different bottles of ethyl acrylate were used and the reaction was also attempted with methyl acrylate. The reaction temperature was increased from room temperature to 40 °C (Michael *et al.*)⁹⁵ to 50 °C, to reflux. In all of the above cases low yields were obtained with a large amount of unreacted thiolactam present. The best results were obtained when the thiolactam was

dissolved in THF and 1 cm³ 1M NaOH was added. The solution was stirred for 5 minutes before ethyl acrylate was added dropwise. The solution was placed in an ultrasonic bath for 30 seconds before stirring for 22 hours. After aqueous work up a yield of 55 % (NMR) was obtained. Having attempted this reaction under conventional conditions we decided to test the reaction under microwave irradiation. Table 9 illustrates the reaction conditions for all microwave reactions.

Table 9. Reaction conditions for *N*-alkylation of thiolactam with ethyl acrylate under microwave irradiation

Reaction	Thiolactam /mg	Acrylate /μL	Solvent /cm ³	Solvent volume /cm ³	1M NaOH volume /cm ³	Temp /°C	Time /min	Yield /%
1 ^a	99	188	THF	4	1	100	10	17
2	100	188	THF	2	1	80	10	28
3 ^a	99	188	EtOH	4	1	100	5 ^b	42
4 ^c	102	188	EtOH	2	1	80	10	46
5	99	188	EtOH	1.5	1.5	80	10	18
6	99	188	EtOH	1	2	80	10	9
7 ^c	100	188	EtOH	2	1	80	10	31
8	104	188	EtOH	2	1	80	20	46

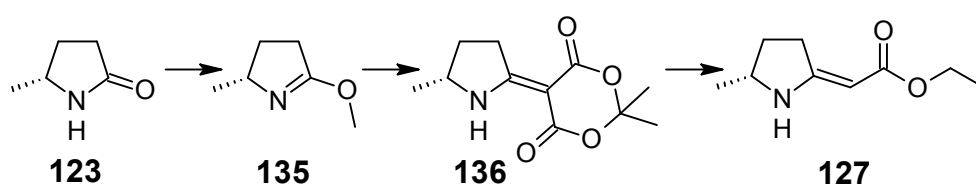
Work up: 3 cm³ distilled H₂O added and extracted into DCM (3 × 5 cm³) and concentrate.

^a reactions performed in an open vessel, ^b reaction stopped as vessel broke, ^c reaction 7 for reproducibility of reaction 4

It was clear from the microwave reactions that the yields were poor when the solvent and the 1M NaOH solution did not mix well. As such, the reactions worked better when absolute ethanol was used as the solvent. The open vessel reactions in both THF and EtOH (reactions 1 and 3) both gave lower yields than the closed vessel reactions (reactions 2 and 4) with all other conditions remaining unchanged. Therefore, all other reactions were carried out in ethanol under closed vessel conditions. The yield for reaction 4 was promising and so the conditions were altered (reactions 5 and 6) but low yields were obtained. A duplicate of reaction 4 was carried out to determine the reproducibility of the results and a lower yield was obtained (reaction 7). The reaction times were also increased and there was improvement in the yields but reaction times of more than 10 minutes in the microwave are undesired.

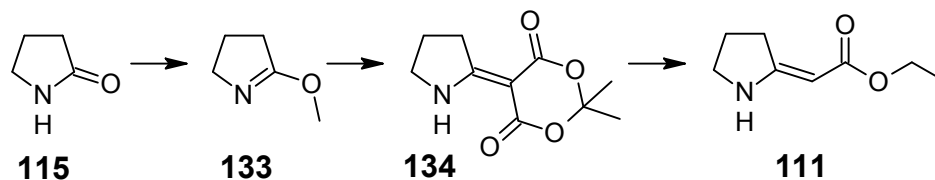
An alternative *N*-alkylation was also tried with 2-pyrrolidinone **115** instead of pyrrolidine-2-thione **116**. However, the yields were no better for this transformation than they were for the thiolactam. This route is, however, not an attractive alternative as the conversion of the *N*-alkylated pyrrolidinone to the *N*-alkylated pyrrolidine thione is poor.⁶⁸

Despite all efforts, the reaction would not proceed as expected (!) and the highest yield obtained was only 55 %, much lower than the yields reported in literature.^{66,95} At this point it was deemed prudent to find an alternative method towards the enaminoate **127**. As mentioned earlier, enaminoates are accessible from alkenyl substituted β -enamino esters, lactim ethers and azido dicarbonyl compounds and by lithiation of ketimines. We therefore chose to investigate the route *via* the lactim ether. In choosing the lactim ether route (Scheme 56) over the previously optimised Eschenmoser coupling route a brief model study was undertaken. This study was adapted from the work of Lhomett and co-workers⁹⁶ undertaken for the formation of **127** from the methyl lactam **123** (Scheme 55). In light of the difficulties encountered for the *N*-protection of the thiolactam **124**, it was decided that a study from the analogous compound **115** (Scheme 56) would be beneficial, so as to minimise further waste of the methyl lactam **123**.



Scheme 55

Before commencing with the synthesis a suitable methylating agent had to be chosen. There are a number of such agents available such as methyl iodide, dimethyl sulfate, trimethyloxonium tetrafluoroborate and tetramethyl ammonium salts.⁹⁷ The stronger the methylating agent is the more toxic it becomes, as these agents damage DNA by methylating DNA bases and interrupting DNA replication.⁹⁸ The less toxic methylating agents like dimethyl carbonate and tetramethyl ammonium salts require much harsher reaction conditions, particularly high temperatures (over 150 °C) and long reaction times.⁹⁹ More recently there has been success with dimethyl carbonate as a methylating agent at lower temperature when used in conjunction with K_2CO_3 and DBU.⁹⁷ Of the stronger methylating agents available, we looked at dimethyl sulfate and trimethyloxonium tetrafluoroborate ($Me_3O^+ \cdot BF_4^-$) for the transformation. Both reagents have advantages and disadvantages associated with them. Dimethyl sulfate is extremely hazardous and caution must be used when working with it, but it is a very effective methylating agent. $Me_3O^+ \cdot BF_4^-$ is a safer alternative but it is highly water sensitive, requiring strictly anhydrous conditions. Based on an analysis of the toxicity of dimethyl sulfate we chose to use $Me_3O^+ \cdot BF_4^-$.



Scheme 56

Thus 2-pyrrolidinone **115** was added to a stirring solution of $\text{Me}_3^+\text{BF}_4^-$ in anhydrous DCM and stirred at room temperature for 24 hours (Scheme 56). The solution was neutralised with NaHCO_3 and concentrated *in vacuo* to afford a colourless oil. ^1H NMR analysis showed the desired lactim ether **133** with no side products or impurities. High resolution mass spectrometry confirmed the presence of the lactim ether with an acquired mass of $100.0763 \text{ g mol}^{-1}$ which is in agreement with the calculated (M + H) mass of $100.0762 \text{ g mol}^{-1}$ for $\text{C}_5\text{H}_{10}\text{NO}$. The isolated yield was 70 % and may be improved upon as the lactim ether is very volatile. The lactim ether was next added to a solution of Meldrum's acid and $\text{Ni}(\text{acac})_2$ in dry CHCl_3 and refluxed overnight. Recrystallisation of the resulting yellow solid from ethanol afforded the cyclic dione **134** as a white solid in a 60 % yield. Once again, analysis of the ^1H NMR and high resolution mass spectrometry showed the desired product formation which could be used without further purification. To our delight the desired enaminoate **111** was obtained *via* ring opening of the cyclic dione **134** by refluxing in a solution of NaOEt and absolute ethanol overnight. The solution was concentrated and the resulting residue redissolved in water and the pH adjusted to 6. The aqueous phase was extracted into DCM and the combined organic phases dried over Na_2SO_4 and the solvent removed *in vacuo*. The ^1H NMR spectrum (Figure 39) was consistent with spectra reported in literature¹⁰⁰ and indicated that the enaminoate had been synthesised with no further purification necessary.

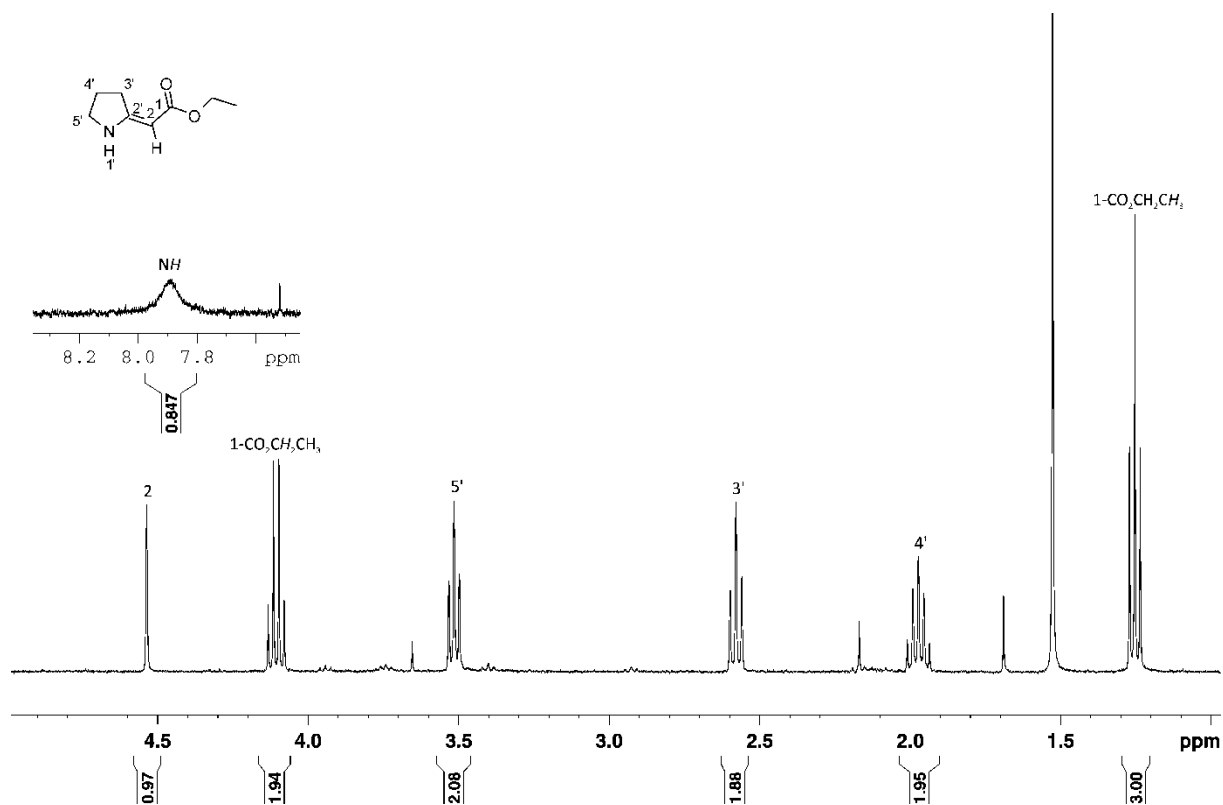


Figure 39: ¹H spectrum for ethyl [(2Z)-pyrrolidin-2-ylidene]acetate

A 2D NOESY experiment was conducted to determine the double bond geometry. A correlation between the ring protons 3'-H and the double bond proton 2-H was observed (Figure 40) indicating that the Z-isomer was present. No correlation was seen from 2-H to N-H suggesting that no E-isomer was present. This alternative route, *via* the lactim ether rather than the thiolactam, yields the Z-isomer exclusively (due to hydrogen bonding with the nitrogen),¹⁰¹ whereas the Eschenmoser route affords the E-isomer⁷⁵ as the major product, with very small amounts on the Z-isomer present.

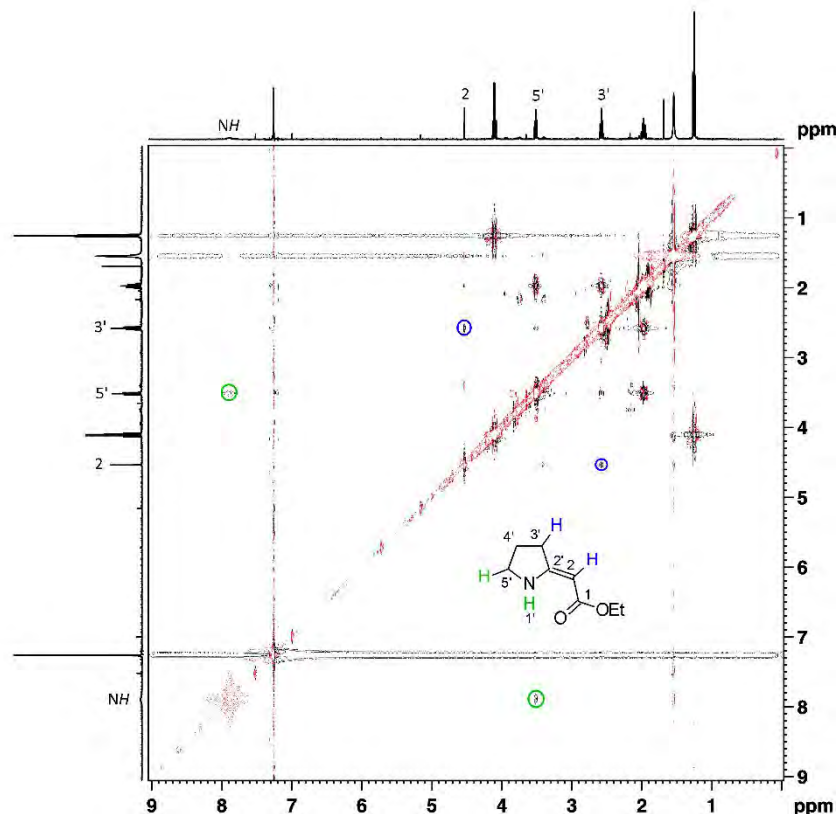
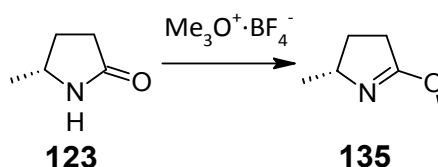


Figure 40: 2D NOESY NMR for ethyl [(2Z)-pyrrolidin-2-ylidene]acetate

Following the successful synthesis of **111** the model study was implemented for the same transformation of **123**.



Scheme 57

(5*R*)-5-methyltetrahydro-2*H*-pyrrol-2-one **123** was added to a stirring solution of $\text{Me}_3\text{O}^+\cdot\text{BF}_4^-$ in anhydrous DCM and stirred at room temperature for 24 hours (Scheme 57). The solution was diluted with anhydrous ether, quenched with NaHCO_3 and concentrated *in vacuo* to afford 3,4-dihydro-5-methoxy-2*H*-pyrrole **135** as a colourless oil in a 54 % yield. This low yield was attributed to the high volatility of the lactim and can therefore be improved upon with careful reaction planning. High resolution mass spectrometry indicated that the desired lactim was obtained with an acquired mass of $114.0918 \text{ g mol}^{-1}$ and a calculated ($M + H$) mass of $144.0919 \text{ g mol}^{-1}$ for $\text{C}_6\text{H}_{12}\text{NO}$. ^1H NMR analysis showed the desired lactim ether **135** with no side products and a small amount of ether (Figure 41). The absence of the characteristic broad singlet of an N-H functionality suggested the imine had indeed been formed. The singlet resonating at 3.79 ppm integrating for three protons is consistent

with a methyl group adjacent to an oxygen and was therefore assigned to the 1''-H protons. The doublet resonating at 1.23 ppm integrating for three protons was assigned to the 1''-H protons. The signals resonating at 1.50-1.57 ppm and 2.16-2.23 ppm both integrating for one proton were assigned to the 3-H protons adjacent to the chiral centre. The 4-H protons were assigned as the multiplet resonating at 2.41-2.49 ppm integrating for two protons. The 2-H proton was assigned to the peak resonating at 3.92-3.98 ppm. This downfield shift is consistent with a proton adjacent to an imine.

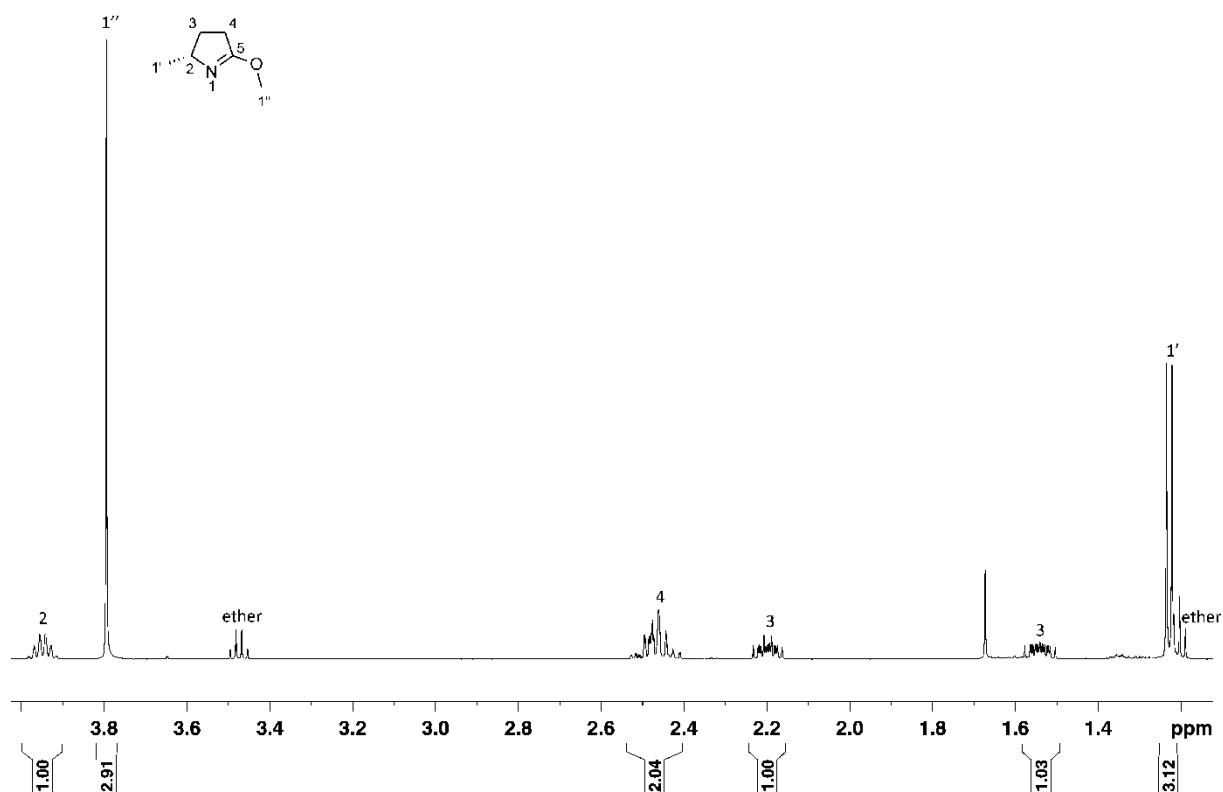


Figure 41: ¹H NMR spectrum of (2R)-3,4-dihydro-5-methoxy-2-methyl-2H-pyrrole

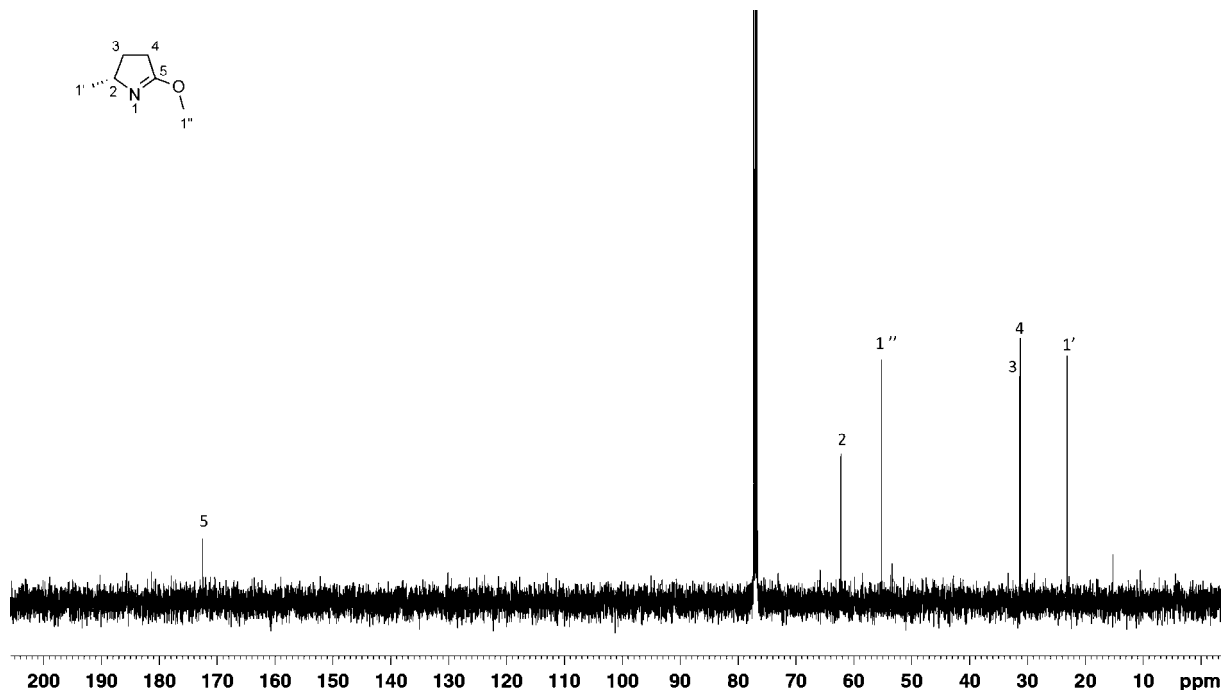


Figure 42: ^{13}C NMR spectrum of (2*R*)-3,4-dihydro-5-methoxy-2-methyl-2*H*-pyrrole

With (2*R*)-3,4-dihydro-5-methoxy-2*H*-pyrrole **135** successfully synthesised and no further purification necessary, it was carried through to the next synthetic step, a coupling reaction with Meldrum's acid (Scheme 59). Meldrum's acid was first reported in 1908 by A.N. Meldrum¹⁰² as the β -lactone β -hydroxyisopropylmalonic acid but the structure was correctly assigned by Davidson and Bernhard¹⁰³ in 1948 as 2,2-dimethyl-1,3-dioxane-4,6-dione (Figure 43).

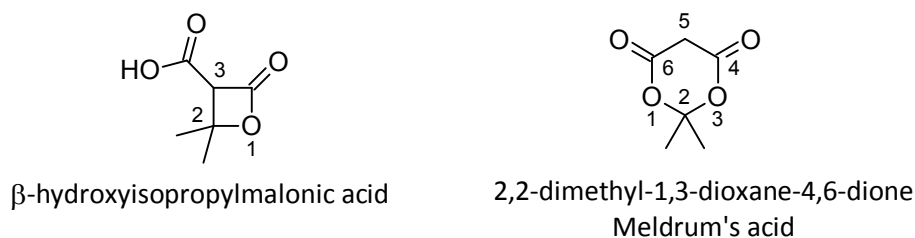
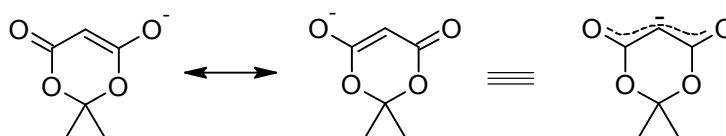


Figure 43

Meldrum's acid is an attractive reagent in synthetic chemistry for a number of reasons. It is easily accessible from malonic acid, acetone, acetic anhydride and H_2SO_4 (cat.); it is a strong organic acid (pK_a 4.83); it has a rigid structure.¹⁰⁴⁻¹⁰⁵ In particular, the acidity of the α -carbon is of great importance. The strong acid nature is attributed to the stability of the resonance anion (Scheme 58).

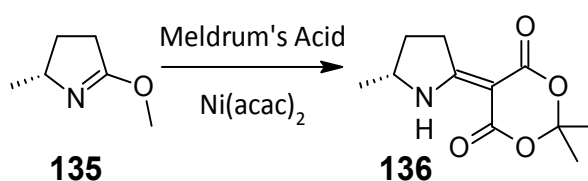


Scheme 58

The chemistry of Meldrum's acid is dominated by

1. Electrophilic attack *via* the anion at the 5-position (i.e. at the α -carbon), and
2. The susceptibility of the carbonyls at the 4- and 6- positions to nucleophilic attack.¹⁰⁴

Knoevenagel type condensations between Meldrum's acid and carbonyls do occur, some more readily than others. For instance, the condensation of Meldrum's acid with aromatic and hindered aliphatic aldehydes or aliphatic ketones occurs easily, while aromatic ketones require activation. This activation can occur in one of two ways, either by use of a catalyst or by conversion to ketimines.¹⁰⁴



Scheme 59

(2*R*)-3,4-Dihydro-5-methoxy-2*H*-pyrrole **135** was added to a stirring solution of Meldrum's acid and catalytic Ni(acac)₂ in anhydrous CHCl₃ and refluxed for 12 hours. Work up of the reaction mixture resulted in a yellow oil which was recrystallised with absolute ethanol to give 2,2-dimethyl-5-[(5*R*)-5-methyl-2-pyrrolidinylidene]1,3-dioxane-4,6-dione **136** as a white crystalline solid in a rather disappointing 25 % yield. However, the product was very clean and an X-ray crystal structure was obtained (the crystallographic data are summarized in Table 10). Inspection of the ¹H NMR spectrum revealed some interesting information with regard to the 3'-*H* and 2-CH₃ protons (Figure 44). Firstly, the two 2-CH₃ protons gave rise to two slightly overlapping singlets at 1.68 ppm and 1.69 ppm respectively. This is in contrast to the *des*-methyl analogue where the 2-CH₃ protons of the Meldrum acid moiety gave rise to one signal in the ¹H NMR spectrum. Similarly, the 3'-*H* protons are given by two separate multiplet signals at 3.22-3.32 ppm and 3.49-3.58 ppm. The 3'-*H* protons are distinguishable from the 4'-*H* diastereotopic protons at 1.67-1.74 ppm and 2.29-2.38 ppm as the 3'-*H* protons appear further downfield due to their proximity to the double bond. The characteristic broad singlet of an N-*H* functionality was once again present with a significant downfield shift of 10.04 ppm, which was attributed to H-bonding with the carbonyl oxygen (confirmed by X-ray crystallographic data). The doublet resonating at 1.36 ppm was assigned to the 1''-CH₃ protons and the multiplet at 4.08-4.16 ppm to the 5'-*H* proton. It is interesting to note that the two 2-CH₃ protons appear as two singlets when run in CDCl₃-*d*₁ but as one singlet when run in DMSO-*d*₆ with all signals shifted slightly upfield.

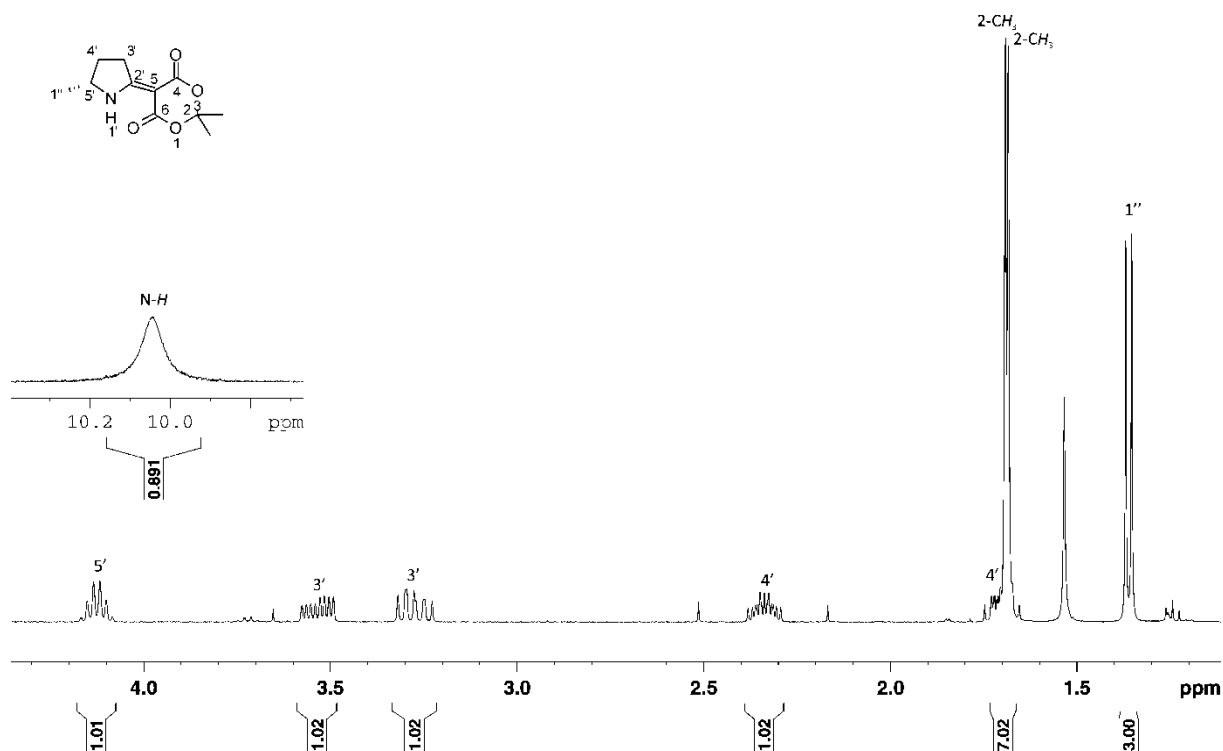


Figure 44: ¹H NMR spectrum of 2,2-dimethyl-5-[(5R)-5-methyl-2-pyrrolidinylidene]-1,3-dioxane-4,6-dione

The observed ¹H NMR spectrum in CDCl₃-d₁ is easily explained when looking at the X-Ray crystal structure. The dione system adopts what appears to be a half boat conformation with the lactone group (C–O–CO–C) in a planar orientation (Figure 45a). This is in line with the observed crystal structure of Meldrum's acid.¹⁰⁶ This planar orientation allows for maximum conjugation from the ether to the carbonyl. The significance of this half boat conformation is that the two methyl groups are in different planes – one is in the same plane as the dione ring whilst the other is above the plane – and therefore in slightly different environments, giving rise to two separate singlet signals in the ¹H NMR spectrum. The axial 3'-H proton is in closer proximity to one of the methyl groups of the dione and the equatorial 3'-H proton is in closer proximity to a carbonyl of the dione, giving rise to two signals for the 3'-H protons (Figure 45b).

Table 10: X-Ray crystallographic data for 2,2-dimethyl-5-[(5R)-5-methyl-2-pyrrolidinylidene]-1,3-dioxane-4,6-dione

Crystal Data	Structure	Data Collection	Structure
Formula	C ₁₁ H ₁₅ NO ₄	Diffractometer	Bruker APEX-II CCD
M _r	225.24	Absorption correction	Multi-scan SADABS, Bruker 2010
Crystal system, space group	Monoclinic, P 2 ₁	T _{min} , T _{max}	0.965, 0.988
a, b, c / Å	7.1937 (5), 10.2039 (7), 7.3613 (5)	No. of measured, independent and observed [<i>I</i> > 2 σ(<i>I</i>)] reflections	9928, 2823, 2747
β / °	91.096 (3)	R _{int}	0.019
T / K	100 (2)	Refinement	
Z	2	R[F ² > 2σ(F ²), wR(F ²), S	0.031, 0.084, 1.06
V / Å ³	540.25 (6)	No. of reflections	2823
R-Factor / %	3.21	No. of parameters	148
Radiation type	Mo Kα	No. of restraints	1
μ / mm ⁻¹	0.11	H-atom treatment	H atoms treated by a mixture of independent and constrained refinement
Crystal size / mm	0.34 × 0.23 × 0.11	Δρ _{max} , Δρ _{min} / e Å ⁻³	0.31, -0.22
		Absolute structure	Flack H D (1983), Acta Cryst. A39, 876-881
		Flack parameter	-0.1 (7)

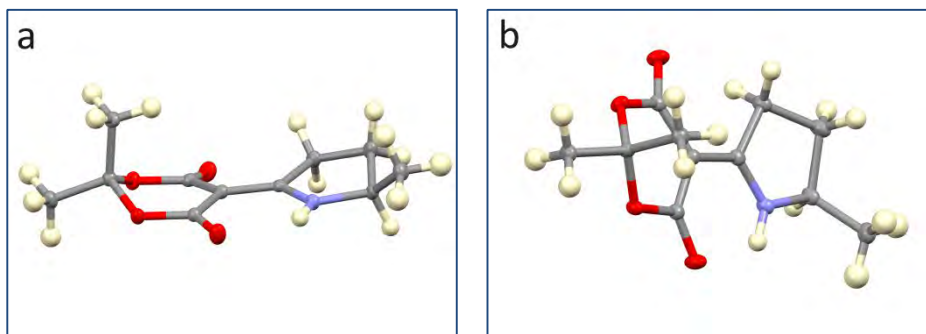


Figure 45: Two different views of the dione X-Ray structure; (a) illustration of the half boat conformation of the dione; (b) illustration of the axial and equatorial 3'-H protons in relation to the dione

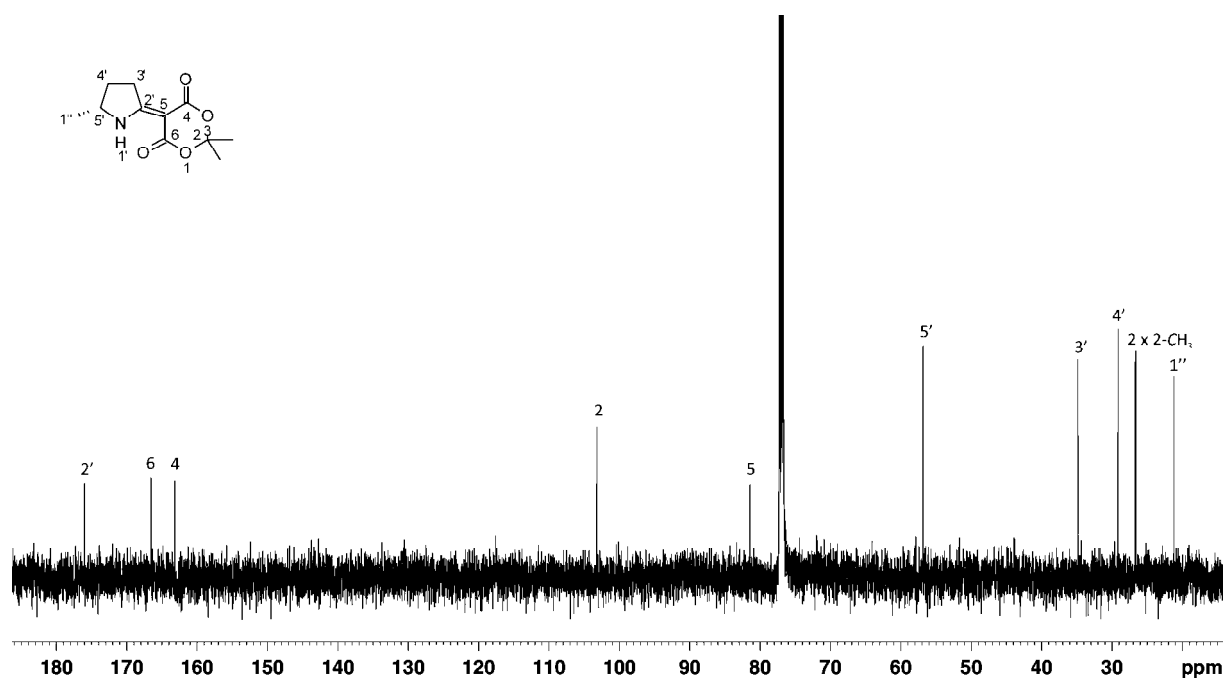
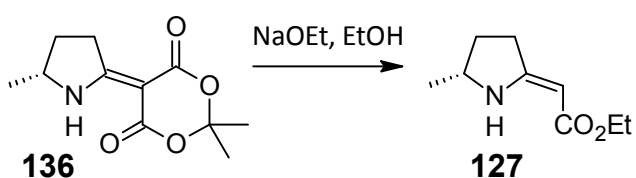


Figure 46: ^{13}C NMR spectrum of 2,2-dimethyl-5-[(5R)-5-methyl-2-pyrrolidinylidene]-1,3-dioxane-4,6-dione

The next step was to form ethyl 2-[(5R)-5-methyltetrahydro-2H-pyrrol-2-ylidene]acetate **127** by decarboxylation of 2,2-dimethyl-5-[(5R)-5-methyl-2-pyrrolidinylidene]-1,3-dioxane-4,6-dione **136** (Scheme 60).



Scheme 60

Thus 2,2-dimethyl-5-[(5*R*)-5-methyl-2-pyrrolidinylidene]1,3-dioxane-4,6-dione **136** was added to a solution of sodium ethoxide in absolute ethanol and refluxed for 16 hours. After pH adjustment and work up ethyl 2-[(5*R*)-5-methyltetrahydro-2*H*-pyrrol-2-ylidene]acetate **127** was furnished in a 95 % yield with no further purification required. This was a pleasing result as the previously utilised Eschenmoser coupling route deprotection used by Prior to give the enaminoate was difficult to purify and much lower yields (55 %) ⁶⁸ were obtained for the transformation. The decarboxylation was confirmed by NMR spectroscopy as the two lactone methyl groups were no longer present and the 3'-*H* protons gave only one signal. The presence of an ethyl group was also evident (Figure 47). There were 9 signals present in the ¹³C NMR spectrum (Figure 48), two less than for the starting dione. High resolution mass spectrometry confirmed the presence of the enaminoate with an acquired mass of 170.1180 g mol⁻¹ which is in agreement with the calculated (M + H) mass of 170.1181 g mol⁻¹ for C₉H₁₆NO₂.

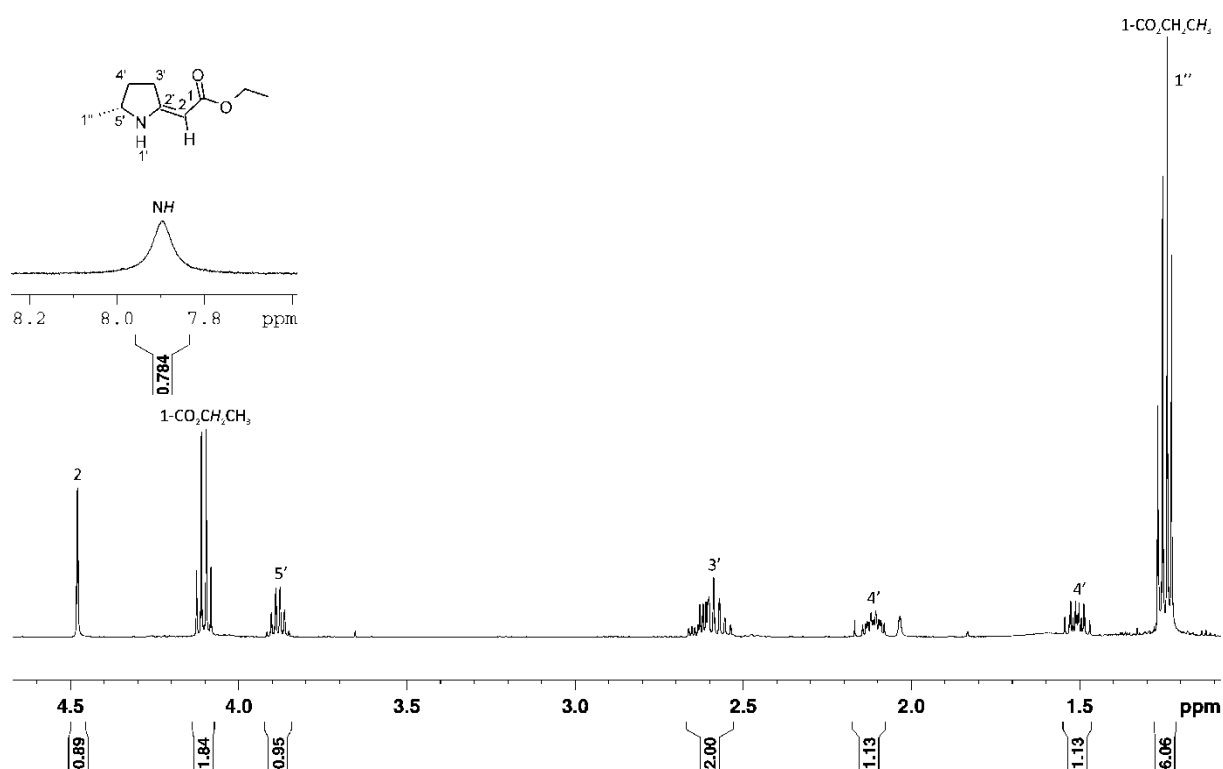


Figure 47: ¹H NMR spectrum of ethyl 2-[(5*R*)-5-methyltetrahydro-2*H*-pyrrol-2-ylidene]acetate

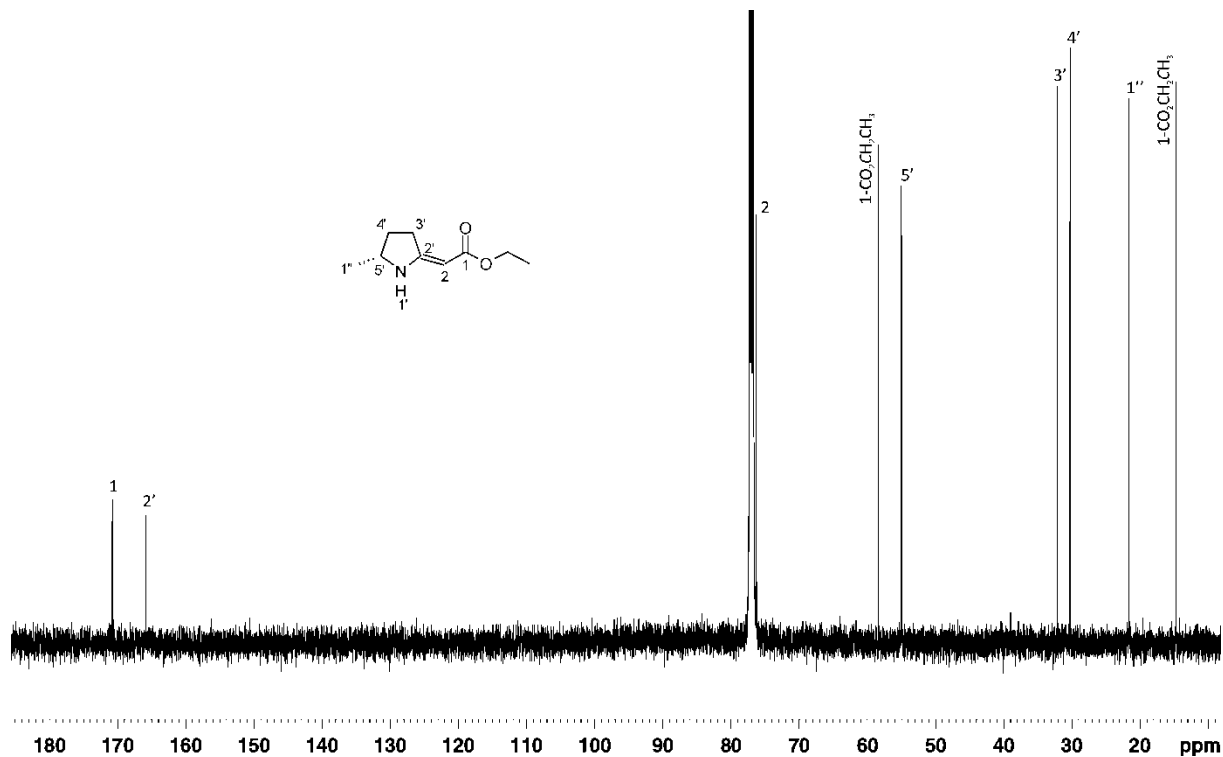


Figure 48: ¹³C NMR spectrum of ethyl 2-[(5R)-5-methyltetrahydro-2H-pyrrol-2-ylidene]acetate

A two dimensional NOE experiment was conducted to determine the geometry of the double bond. There were three protons of interest for this purpose, namely the 2-*H*, 3'-*H* and N-*H* protons. Correlation between the 2-*H* and N-*H* protons would suggest the *E*-isomer was present whilst correlation between the 2-*H* and 3'-*H* protons would suggest the *Z*-isomer was present. (When the Eschenmoser coupling route is employed **127** is obtained as the *E*-isomer. This may be due steric hindrance from the *N*-protected amine, favouring the formation of the *E*-isomer.) It appears from the 2D NOESY spectrum that there is correlation between both the 2-*H* and N-*H* protons and the 2'-*H* and 3'-*H* protons. However, the phase of the signals is also important to note. A positive phase (signals in black) signal signifies a true NOE interaction, a mixed phase signal is due to a COSY interaction and a negative phase signal (signals in red off the diagonal) are typically due to proton exchange. This therefore suggests that the *Z*-isomer is present. (In the lactim ether route the amine is unprotected and therefore there is no steric hindrance influencing the double bond geometry. The *Z*-isomer may be formed preferentially due to hydrogen bonding between the N-*H* proton and the carbonyl oxygen.) However, it is curious to see an exchange of a C-*H* proton. Therefore, in order to confirm that there was an exchange taking place between the 2-*H* and N-*H* protons a simple ¹H NMR experiment was performed. To start, a ¹H proton in CDCl₃-*d*₁ was run. The sample was removed and a drop of D₂O was added. The sample was allowed to stand for 22 hours before a new ¹H NMR was run and the two collected spectra were compared.

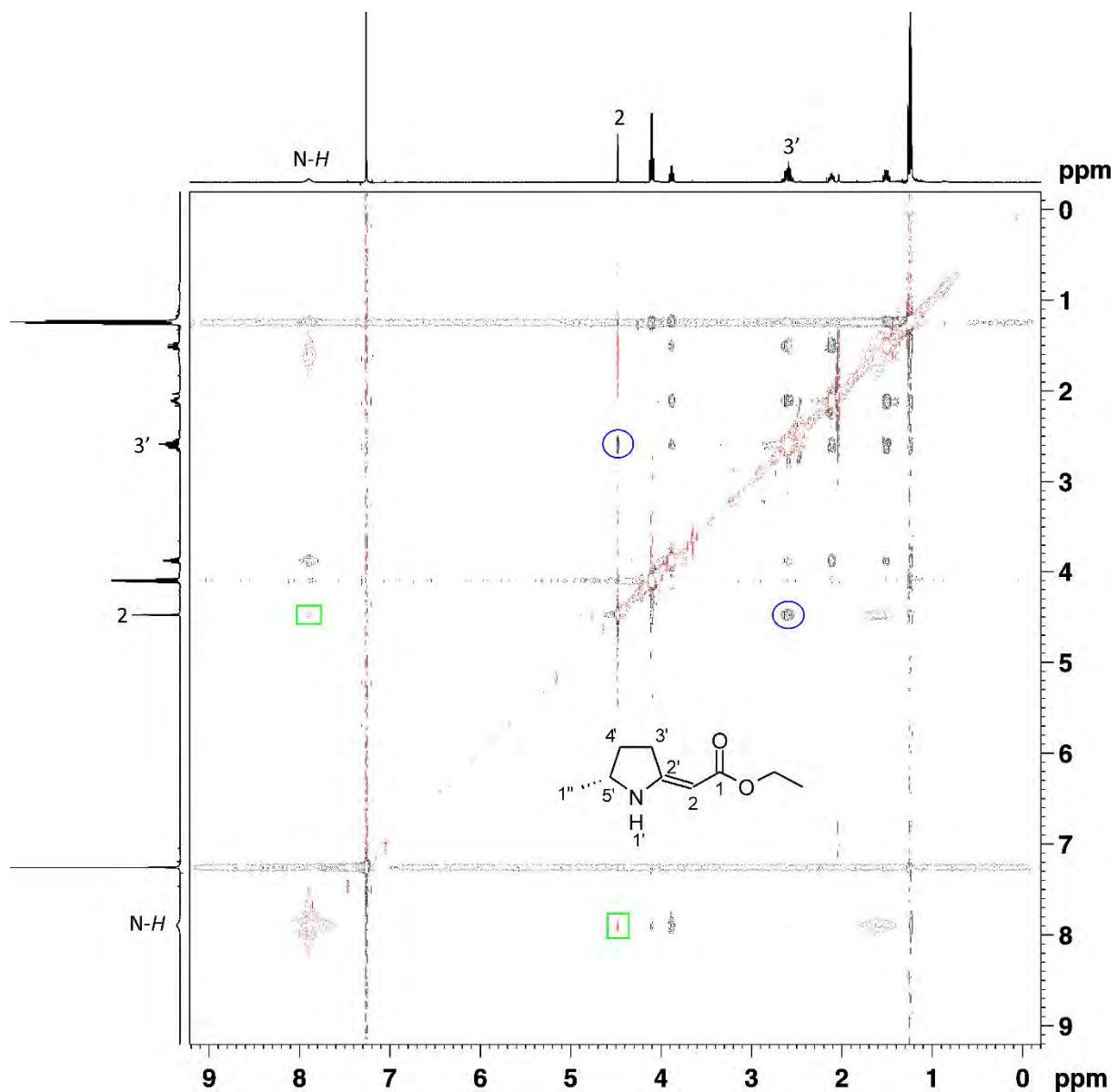


Figure 49: 2D NOE NMR spectrum of ethyl 2-[(5R)-5-methyltetrahydro-2H-pyrrol-2-ylidene]acetate

It is clear from Figure 50 that both the N-H and 2-H protons are no longer seen in the spectrum. This suggests that the N-H proton exchanges with a deuterium, which can in turn exchange with the 2-H proton as depicted in Scheme 61. The N-H proton can once again exchange with a deuterium and the signals for these protons are no longer seen.

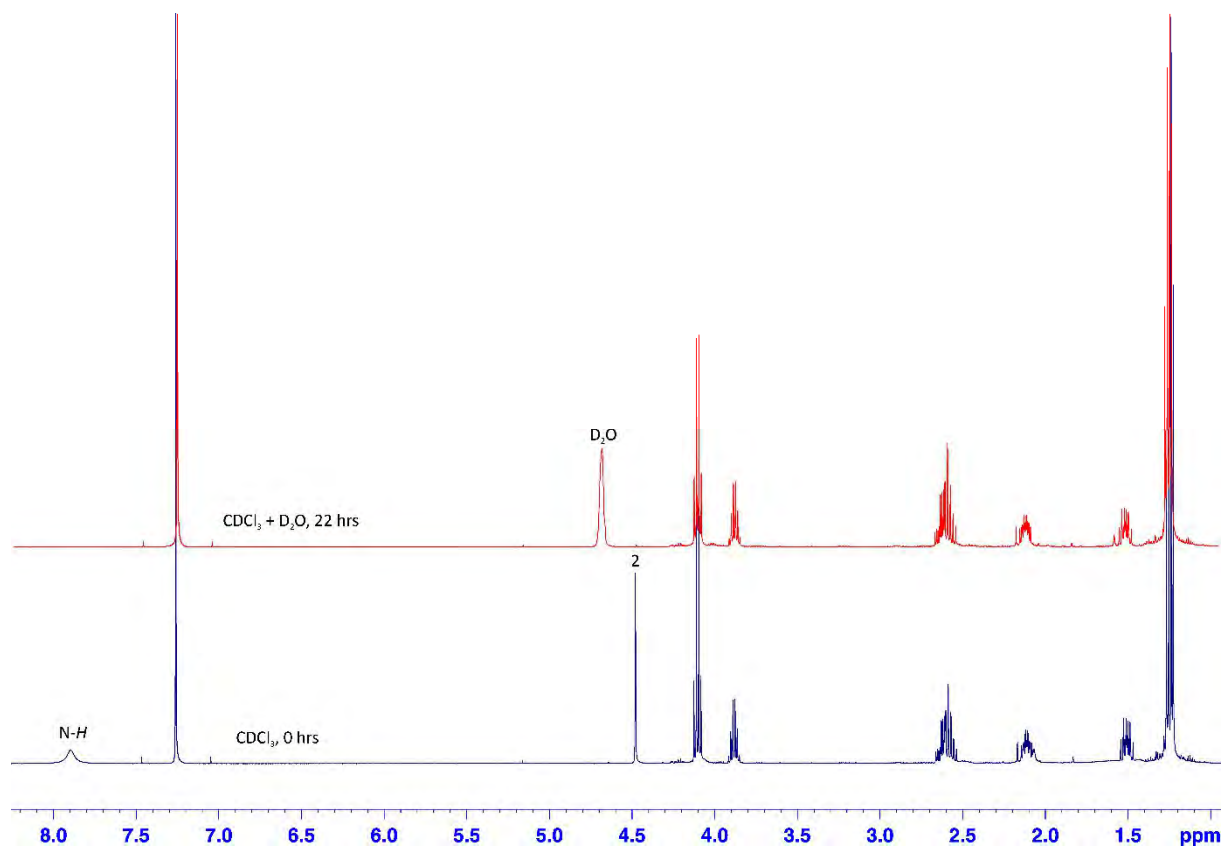
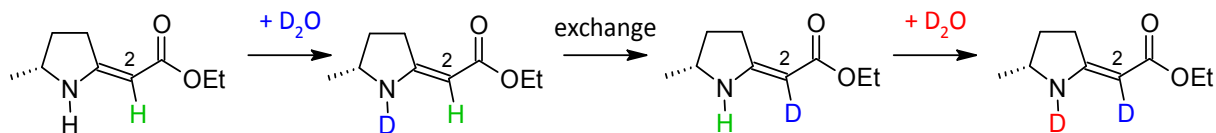


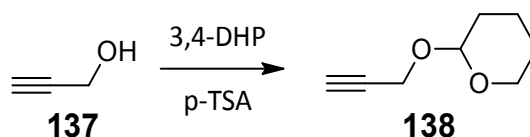
Figure 50: ^1H NMR spectrum of ethyl 2-[(5*R*)-5-methyltetrahydro-2*H*-pyrrol-2-ylidene]acetate before and after addition of D_2O



Scheme 61

2.3.3 Part 3: Synthesis of 1-bromo-2-nonyne

Before hydroamination the heptyl group must be introduced into the molecule and this is done with 1-bromo-2-nonyne **131**, which is easily accessible from propargyl alcohol **137** and 1-bromohexane **142**. The first step involves the protection of the alcohol functionality. This is to ensure that the alkyne proton is removed by butyl lithium in the subsequent step, rather than the more acidic proton of the alcohol. Thus propargyl alcohol **137** was treated with 3,4-dihydro-2*H*-pyran in the presence of a catalytic amount of *p*-toluenesulfonic acid in dichloromethane. The THP protected alcohol **138** was formed in a near quantitative yield as a pale yellow oil (Scheme 62). The structure was confirmed by NMR spectroscopy.



Scheme 62

The ^1H NMR spectrum (Figure 51) showed a triplet resonating at a shift characteristic of an alkyne proton at 2.41 ppm and was thus assigned as the 3'-H proton. Long range coupling across the triple bond is responsible for the observed triplet splitting. The 1'-H protons are expected to be fairly far downfield due to their proximity to oxygen. These protons are in fact non-equivalent due to the possible conformations the heterocycle can adopt, and thus give rise to an unusual splitting pattern and are assigned to the "quartet" peak resonating at 4.27 ppm. This quartet peak is actually a doublet of doublets as can be seen on inspection of the coupling constants. The $J = 15.73$ Hz is attributed to germinal coupling between the two non-equivalent 1'-H protons and the $J = 2.43$ Hz is attributed to the coupling between each of the 1'-H protons and the 3'-H proton. The triplet resonating at 4.82 ppm was assigned to the 2-H proton. The 6-H protons of the heterocycle were assigned as the peaks resonating at 3.51-3.56 ppm and 3.81-3.87 ppm. There are two signals due to the presence of axial and equatorial protons in the lower energy state chair conformation of the heterocycle. These shifts are consistent with heterocyclic protons adjacent to oxygen. The remaining heterocyclic protons were found in the range 1.50-1.79 ppm. The two dimensional COSY and HSQC spectra were utilised in order to distinguish between these protons. Thus the 3-H protons were assigned to the peaks resonating at 1.63-1.67 ppm and 1.70-1.78 ppm, the 4-H protons to the peaks at 1.50-1.54 ppm and 1.79-1.88 ppm, and the 5-H protons to the peak at 1.55-1.62 ppm.

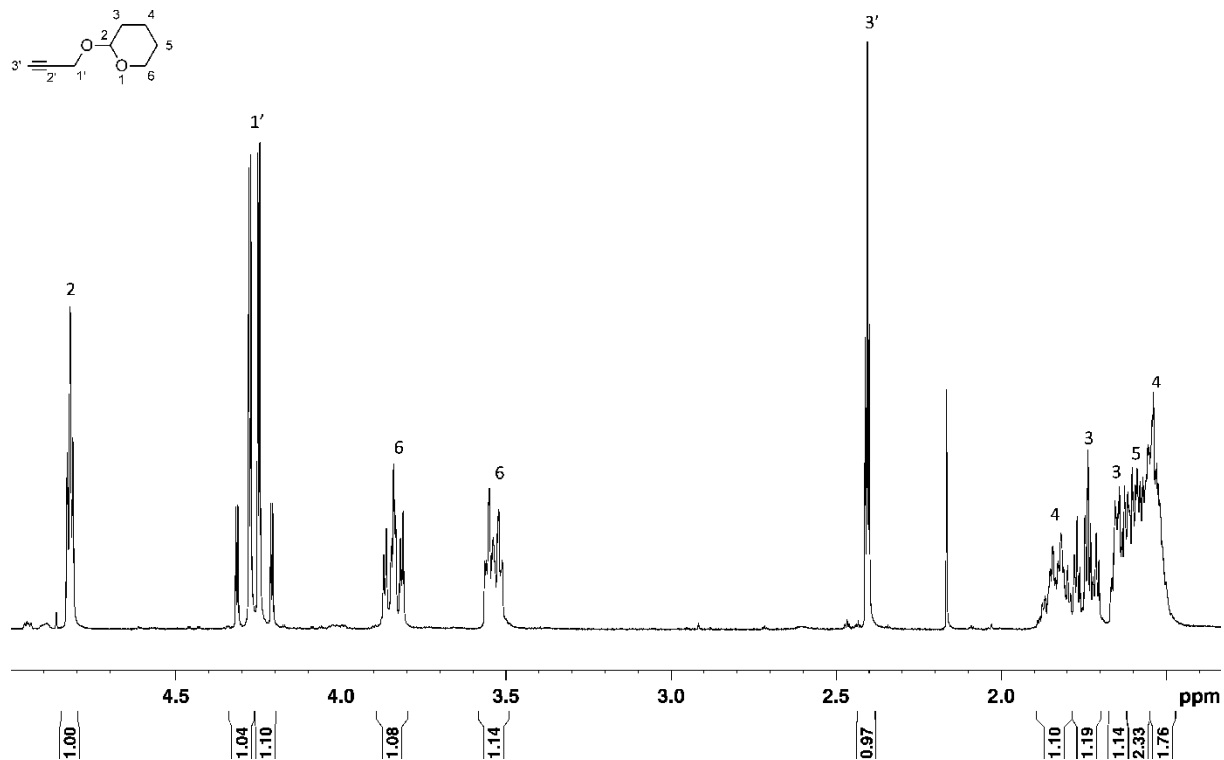


Figure 51: ^1H NMR Spectrum for 2-propynyl tetrahydro-2H-pyran-2-yl ether

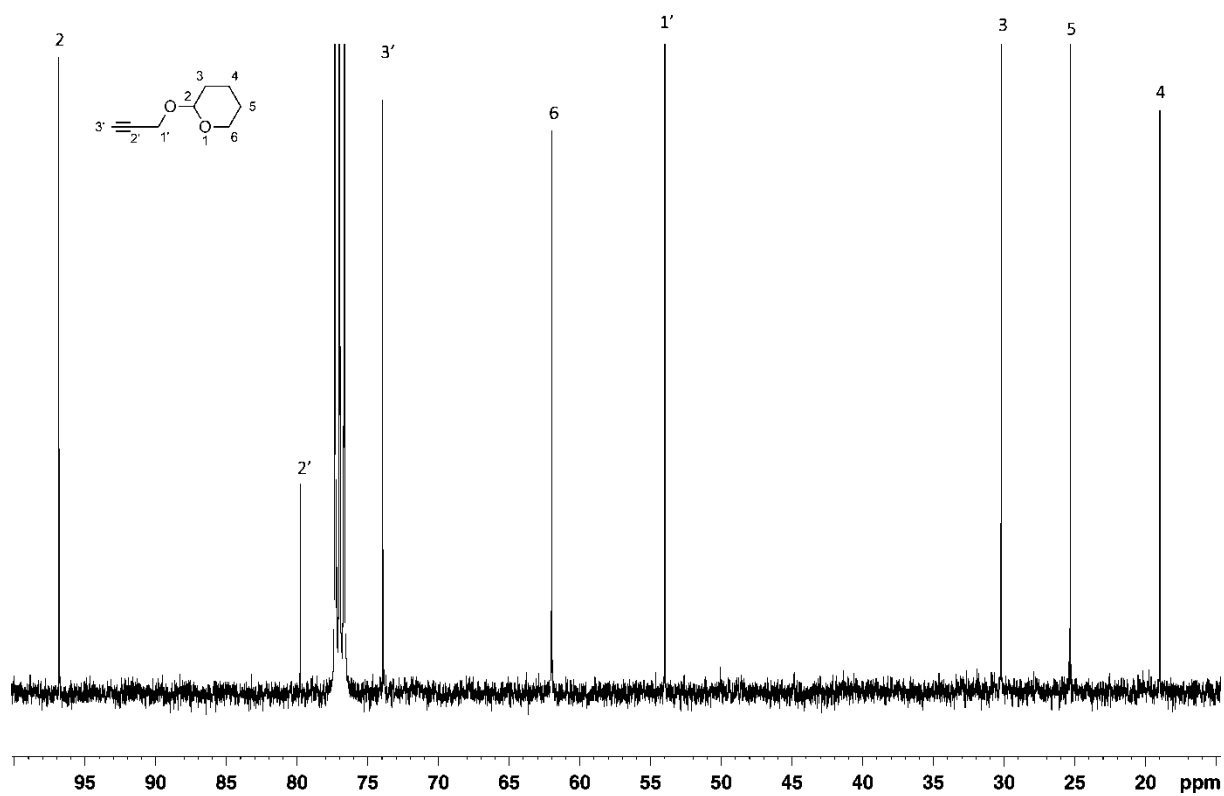
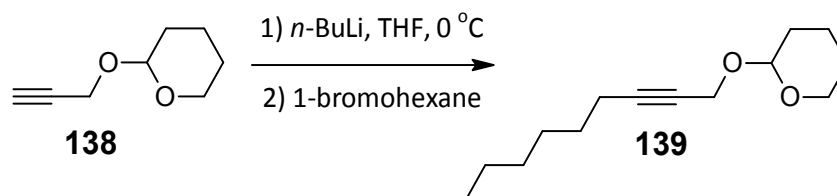


Figure 52: ^{13}C NMR Spectrum for 2-propynyl tetrahydro-2H-pyran-2-yl ether

There were 8 peaks present in the ^{13}C NMR spectrum (Figure 52) and only 6 peaks in the DEPT 135 spectrum. Thus the two peaks absent in the DEPT spectrum were assigned to the 2'-C and 3'-C

carbons resonating at 79.7 ppm and 73.9 ppm respectively in the ^{13}C spectrum. The secondary carbons 1'-C and 6-C were expected to resonate downfield due to their proximity to electron withdrawing groups. The two dimensional HSQC spectrum was used to distinguish between the two as the 6-C protons should appear as two proton signals coupled to one carbon signal, and the 1'-C protons should appear as one proton signal coupled to the carbon signal. This was indeed the case and to the 1'-C carbon was assigned to the peak resonating at 53.9 ppm and the 6-C carbon to the peak at 61.9 ppm. The remaining secondary carbons 3-C, 4-C and 5-C were assigned to the peaks resonating at 30.1 ppm, 18.9 ppm and 25.3 ppm respectively. Finally, the 2-C carbon was assigned to the most downfield peak resonating at 96.8 ppm.

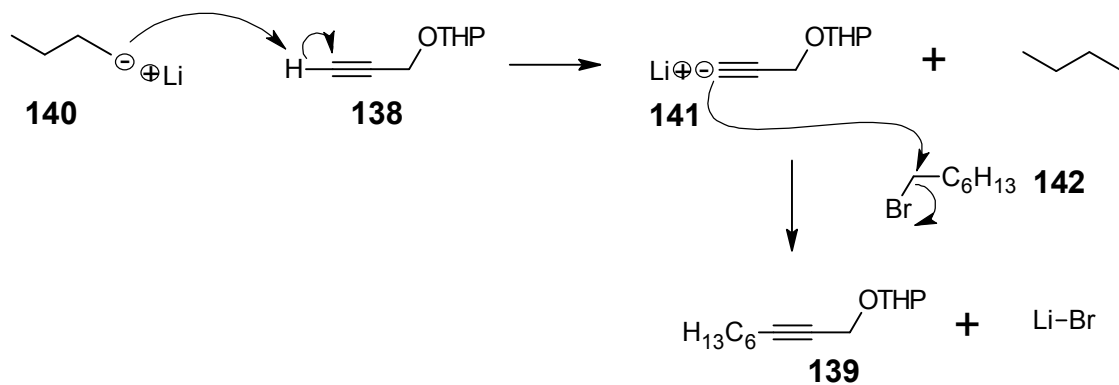
The THP protected propargyl alcohol **138** was next alkylated with 1-bromohexane (Scheme 63).



Scheme 63

Thus *n*-butyl lithium was added dropwise to a solution of 2-propynyl tetrahydro-2H-pyran-2-yl **138** ether in dry THF at 0 °C. The solution was stirred for 5 minutes before slowly warming to room temperature and stirred for a further one hour. The solution was again cooled to 0 °C before the addition of 1-bromohexane. The solution was then refluxed for 12 hours and then quenched with methanol. Work up and purification by column chromatography afforded 2-nonynyl tetrahydro-2H-pyran-2-yl ether **139** as a pale yellow oil in a yield of 30 % and the structure was confirmed by NMR spectroscopy. A high resolution mass spectrometry acquired mass of 247.1666 g mol⁻¹ was obtained, which compares favourably with the calculated (M + H) mass of 247.1674 g mol⁻¹ for C₁₄H₂₄O₂Na.

The following mechanism for the alkylation has been proposed (Scheme 64).^{68, 75} Firstly, *n*-butyllithium **140** abstracts the slightly acidic (pK_a ≈ 26) terminal acetylenic proton **138** resulting in the formation of a lithium salt intermediate **141**. What follows next is an S_N2 type nucleophilic substitution of the lithium salt with 1-bromohexane **142** to give the alkylated product **139**.



Scheme 64

The structure was confirmed by NMR spectroscopy. The ¹H spectrum showed (Figure 53) the disappearance of the alkyne proton at 2.41 ppm and a new triplet of triplets peak resonating at 2.21 ppm. The observed splitting is attributed to long range coupling across the triple bond (see Figure 55) and thus the peak was assigned to the 4'-H proton. Another distinctive new triplet peak was present at 0.88 ppm and was assigned as the methyl protons 9'-CH₃. The 2-H (4.81 ppm), and 6-H (3.49-3.55 ppm and 3.82-3.87 ppm) protons appear in similar shifts and splitting as seen in the protected propargyl alcohol spectrum (Figure 51). However, the 1'-H protons are now split into two separate doublets of triplets (4.21 and 4.29 ppm) as indicated by the coupling constants (see Figure 54). Each 1'-H proton is split by the 4'-H protons as well as the other 1'-H proton giving rise to *J* values of 15.25 Hz and 2.19 Hz respectively. The remaining heterocyclic protons resonate downfield relative to the remaining alkyl protons and at similar shifts to the protected propargyl alcohol with the 3-H protons resonating at 1.70-1.77 ppm, the 4-H protons at 1.55-1.57 ppm and 1.80-1.84 ppm, and the 5-H protons at 1.58-1.66 ppm. Coupling between these heterocyclic protons is clearly visible in the two dimensional COSY spectrum (Figure 56). The alkyl protons appear more upfield than the heterocyclic protons. The 5'-H proton peak resonates at 1.47-1.51 ppm, the 6'-H protons at 1.33-1.41 ppm, with the 7'-H protons at 1.26-1.28 ppm, and the 8'-H protons at 1.29-1.32 ppm.

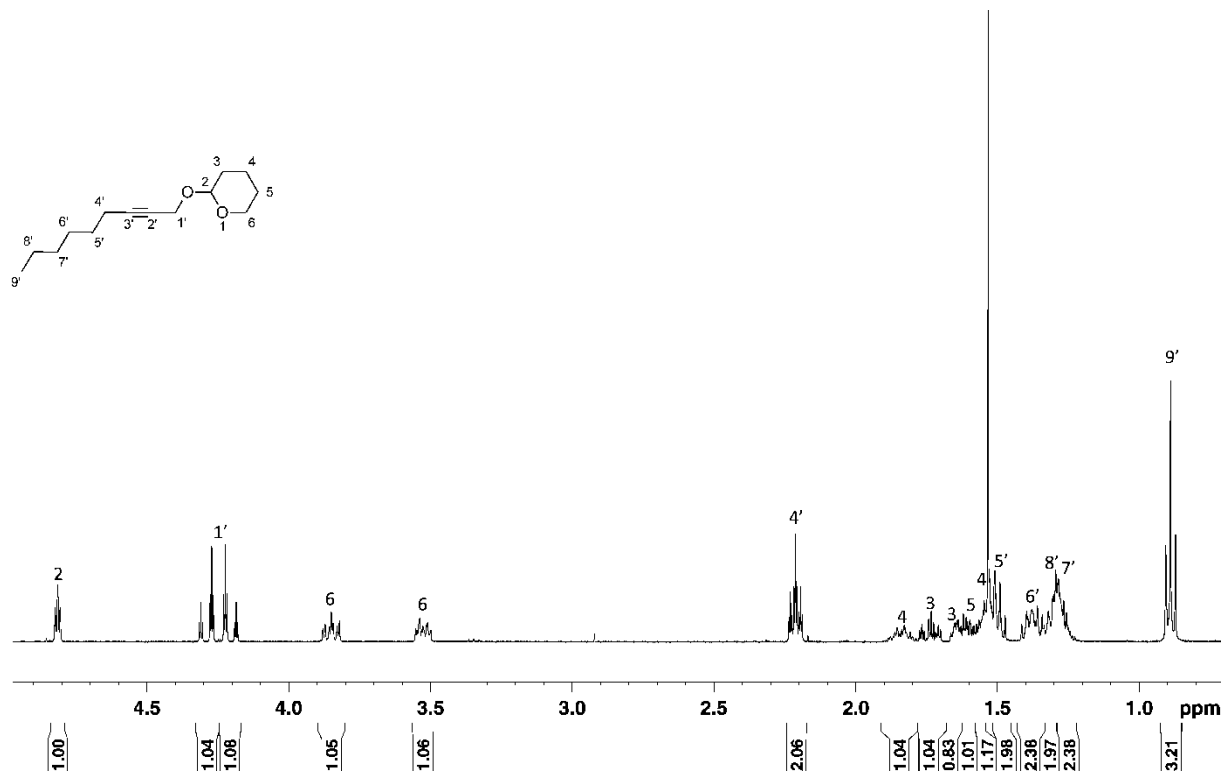


Figure 53: ^1H NMR Spectrum for 2-nonyl tetrahydro-2H-pyran-2-yl ether

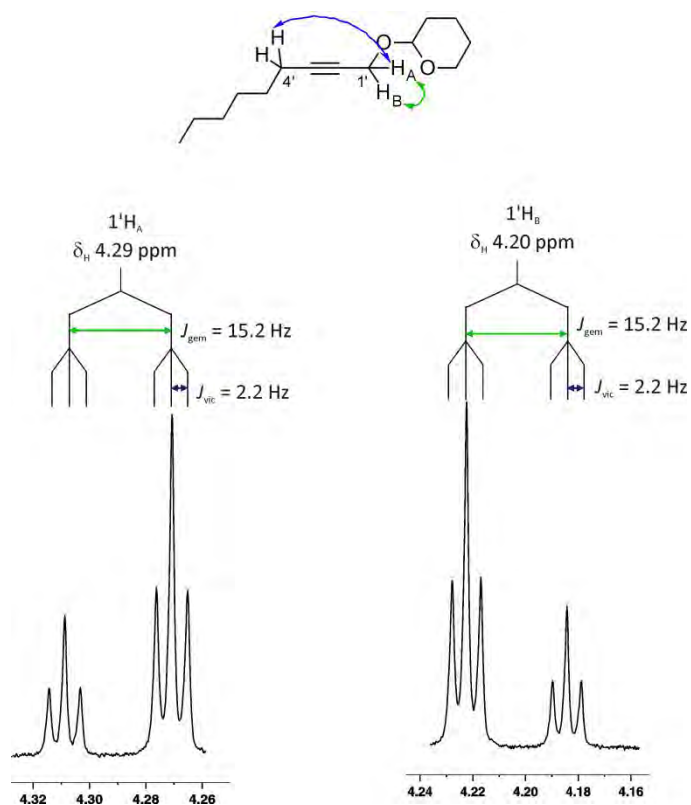


Figure 54

The magnetically non-equivalent $1'-\text{H}$ protons labelled at H_A and H_B in Figure 54 are split by one another into a doublet (geminal coupling shown by the green arrows, $J = 15.25$ Hz). The neighbouring

4'-H protons split each of the H_A and H_B protons into a triplet (vicinal coupling shown by the blue arrows, $J = 2.19$ Hz). This coupling gives rise to the observed doublet of triplets. The proximity of the two doublet of triplets to one another increases the intensity of the inner lines at the expense of the outer lines. This is known as the roofing effect,¹⁰⁷ and is what makes the splitting at first glance appear to be a quartet of triplets.

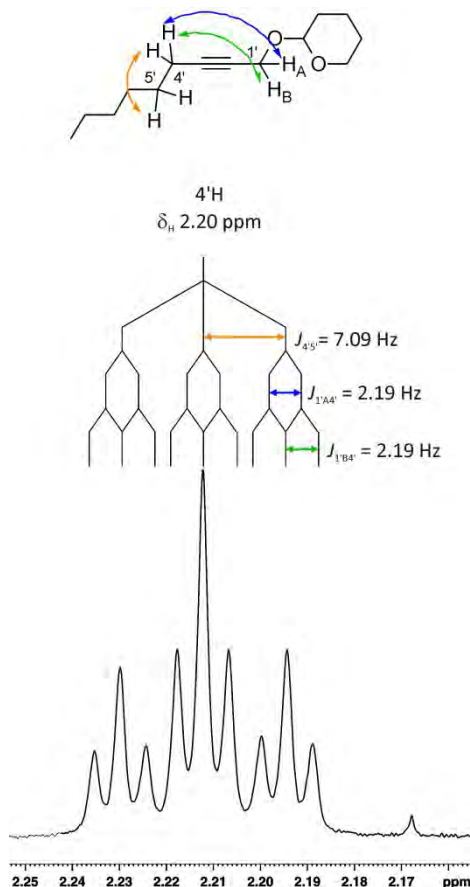


Figure 55

In the case of the triplet of triplets, the 4'-H protons are split into a triplet by the neighbouring 5'-H protons (vicinal coupling shown by the orange arrows, $J = 7.09$ Hz) as seen in Figure 55. The coupling constant is consistent with those seen for alkyl coupling. Further splitting occurs as each 1'-H proton H_A and H_B split the signal into a doublet. Since the coupling constant of H_A to 4'-H and H_B to 4'-H is the same ($J = 2.19$ Hz), the lines overlap giving rise to the observed triplet splitting.

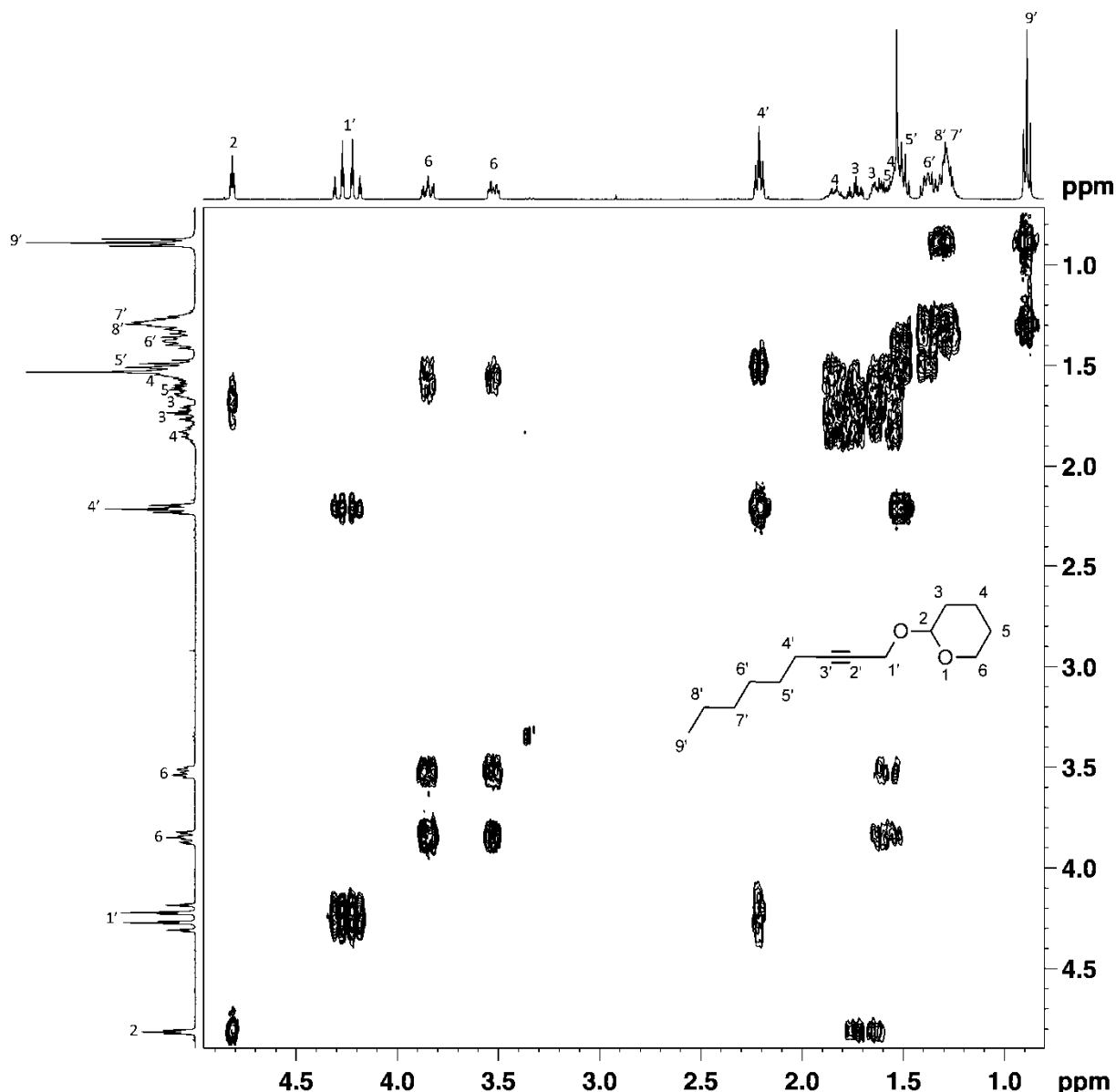


Figure 56: 2D COSY NMR Spectrum for 2-nonyl tetrahydro-2H-pyran-2-yl ether

On first inspection of the ¹³C NMR spectrum there appeared to be only 13 peaks, one less than required. On closer inspection it could be seen that two peaks were very close together, but were in fact two separate peaks. The DEPT 135 spectrum clearly distinguished the primary and tertiary carbon from the remaining secondary carbons. Thus the primary 9'-CH₃ carbon was assigned as the peak resonating at 14.0 ppm and tertiary 2-C carbon was assigned as the peak resonating at 96.7 ppm. The DEPT 135 spectrum also indicated two secondary carbons downfield relative to all the other secondary carbons. These signals at 54.7 ppm and 62.0 ppm were assigned to the 1'-C and 6-C carbons respectively. The quaternary carbons 2'-C and 3'-C were assigned as the peaks resonating at 86.7 ppm and 75.7 ppm respectively. The two dimensional HSQC and COSY spectra were used to distinguish between the remaining secondary carbons. The heterocyclic protons resonated in the region 1.55-1.77 ppm in the ¹H spectrum while the alkyl protons resonated in the region 1.26-1.51 ppm (Figure 53). This information along with the HSQC spectrum helped with the assignment of

the peaks in the ^{13}C spectrum. From this information the 3-C, 4-C and 5-C heterocyclic carbons were assigned as the peaks resonating at 30.3 ppm, 19.2 ppm, and 25.4 ppm respectively. The remaining alkyl carbons 5'-C (28.6 ppm), 6'-C (28.5 ppm), 7'-C (31.3 ppm) and 8'-C (22.5 ppm) were assigned.

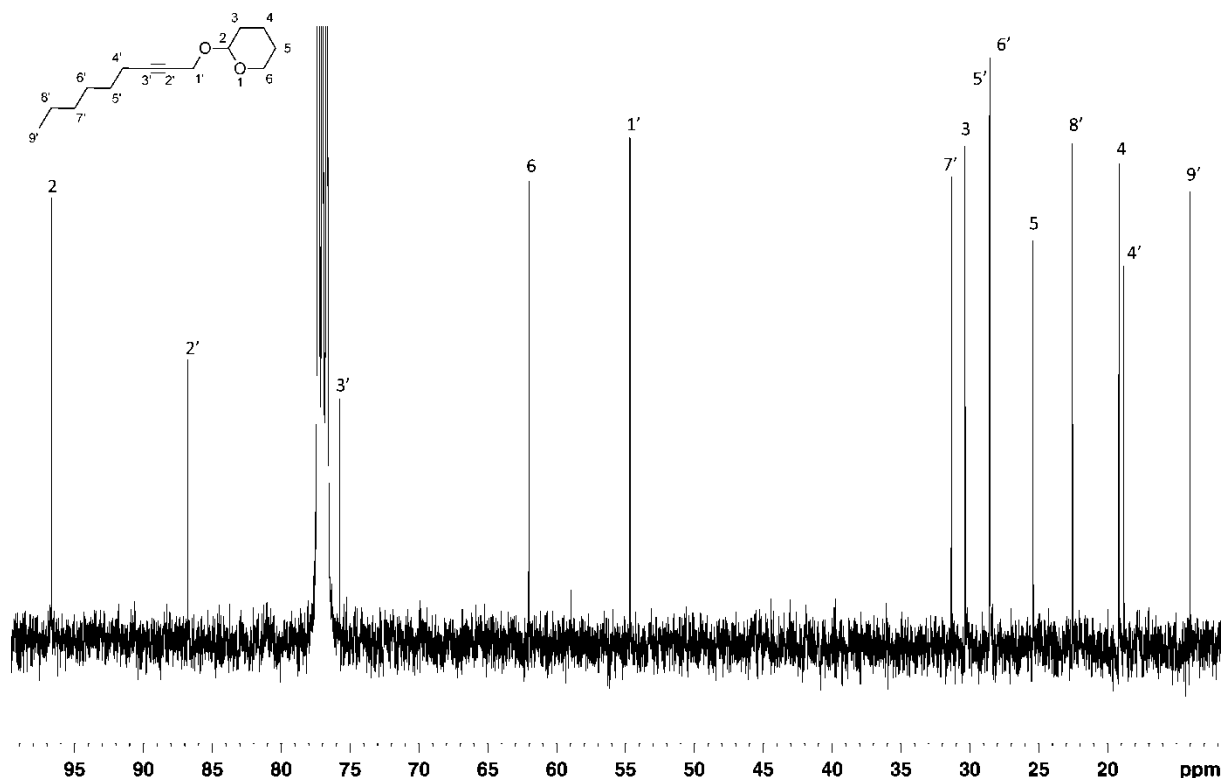
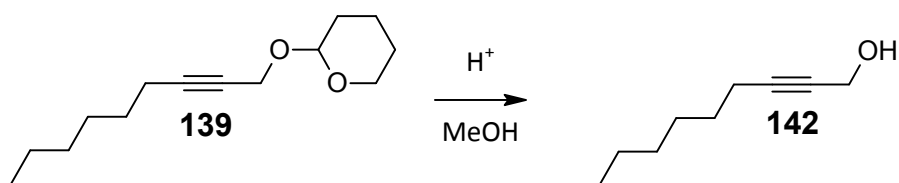


Figure 57: ^{13}C NMR Spectrum for 2-nonyl tetrahydro-2H-pyran-2-yl ether

Deprotection of 2-nonyl tetrahydro-2H-pyran-2-yl ether **139** generates 2-nonyl-1-ol **142** (Scheme 65). Thus 4M HCl was added to a solution of **139** in methanol and stirred for 4 hours. The solution was neutralised with K_2CO_3 . The solution was concentrated and to afford 2-nonyl-1-ol as a yellow oil which was used without further purification.



Scheme 65

The structure was confirmed by NMR spectroscopy. The ^1H NMR spectrum (Figure 58) indicated that the deprotection had successfully occurred as the spectrum was greatly simplified compared to Figure 53. The 1-H proton appears as a singlet at 4.25 ppm. The triplet of triplets at 2.21 ppm was

assigned as the 4-*H* protons, with coupling to the 5-*H* protons and long range coupling to the 1-*H* protons responsible for the observed splitting pattern. The methyl protons 9-*H* were assigned as the peak resonating at 0.89 ppm and the 1-*OH* proton was assigned as the broad singlet at 1.43 ppm. The remaining alkyl protons were assigned from correlations observed in the two dimensional COSY spectrum (Figure 59). The 9-*H* protons were seen to couple with the 8-*H* protons, which resonated at 1.25-1.33 ppm. Following the correlations seen in the COSY next gave the 7-*H* protons resonating at 1.25-1.33 ppm, followed by the 6-*H* protons at 1.34-1.40 ppm and finally the 5-*H* protons at 1.47-1.51 ppm.

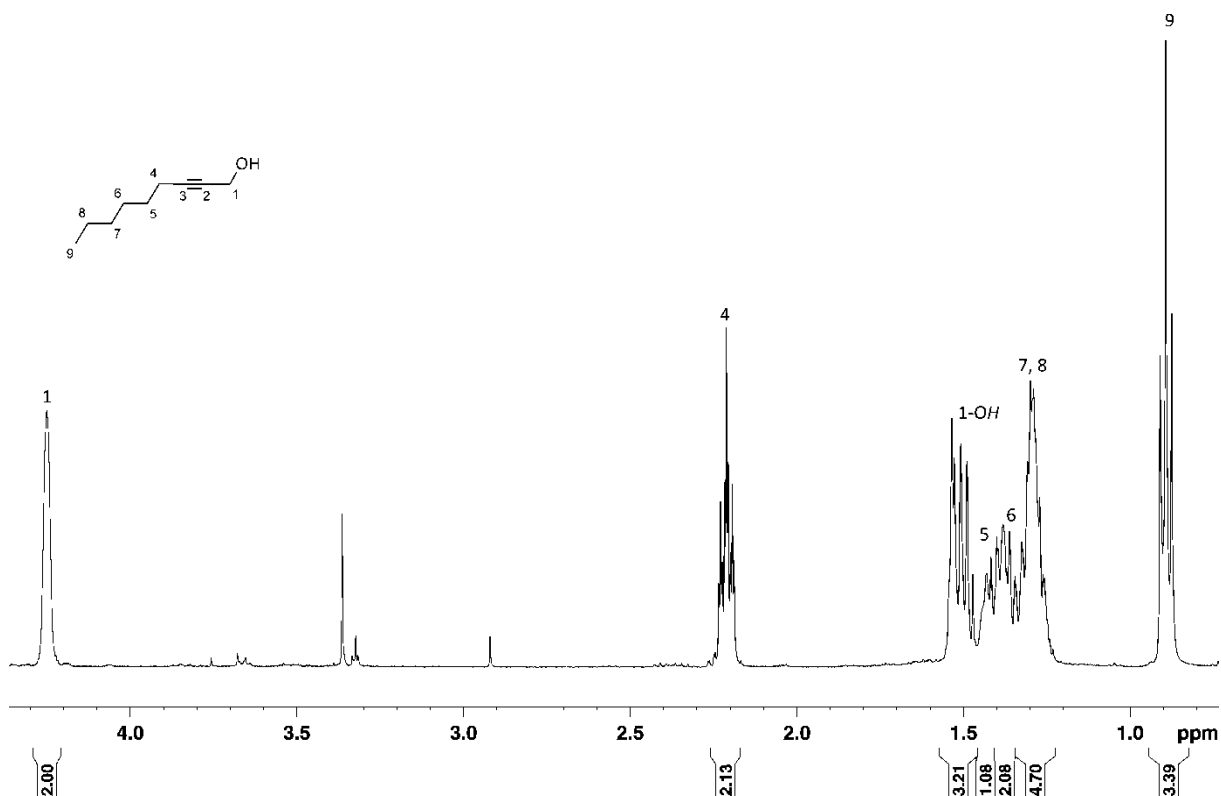


Figure 58: ¹H NMR Spectrum for 2-nonyn-1-ol

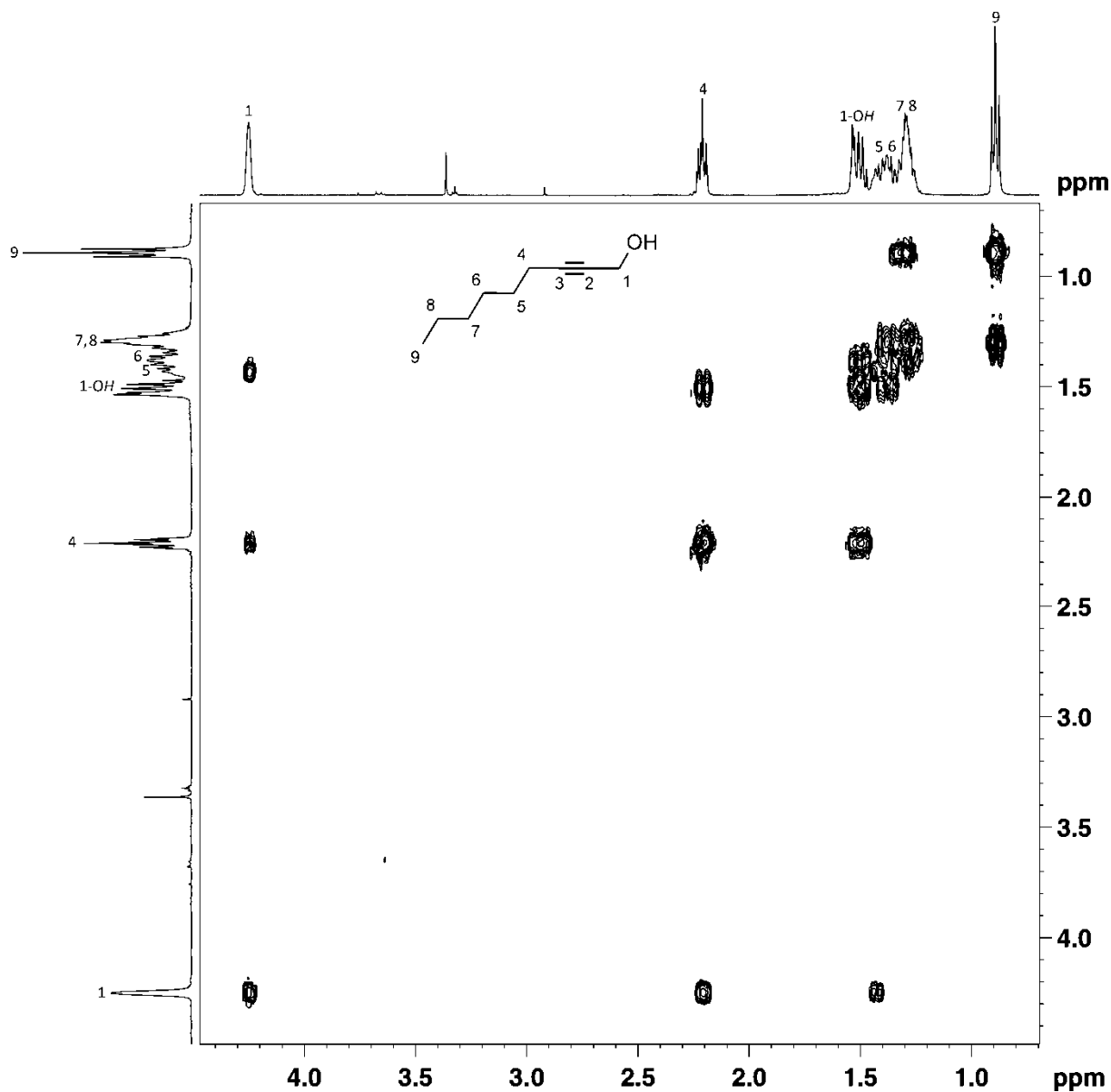


Figure 59: 2D COSY NMR Spectrum for 2-nonyn-1-ol

Interestingly, when at low concentrations in solution, coupling between the alcohol 1-OH and the adjacent methylene group 1-H gave rise to a triplet at 1.43 ppm with $J = 6.0233$ Hz. This in turn resulted in a doublet of triplet splitting at 4.25 ppm for the 1-H protons (Figure 60). The coupling constant for this alcohol splitting is not inconsistent with other observed alcohol splitting. For example, $J = 5.4$ Hz was observed for a methanol sample run in chloroform- d_1 with a quartet splitting of the OH and $J = 4.4$ Hz was observed for an ethanol sample run in chloroform- d_1 .

The triplet of triplet splitting for 4-H at 2.21 ppm arises from long range coupling across the alkyne bond to 1-H with $J = 2.18$ Hz and coupling to 5-H with $J = 7.08$ Hz.

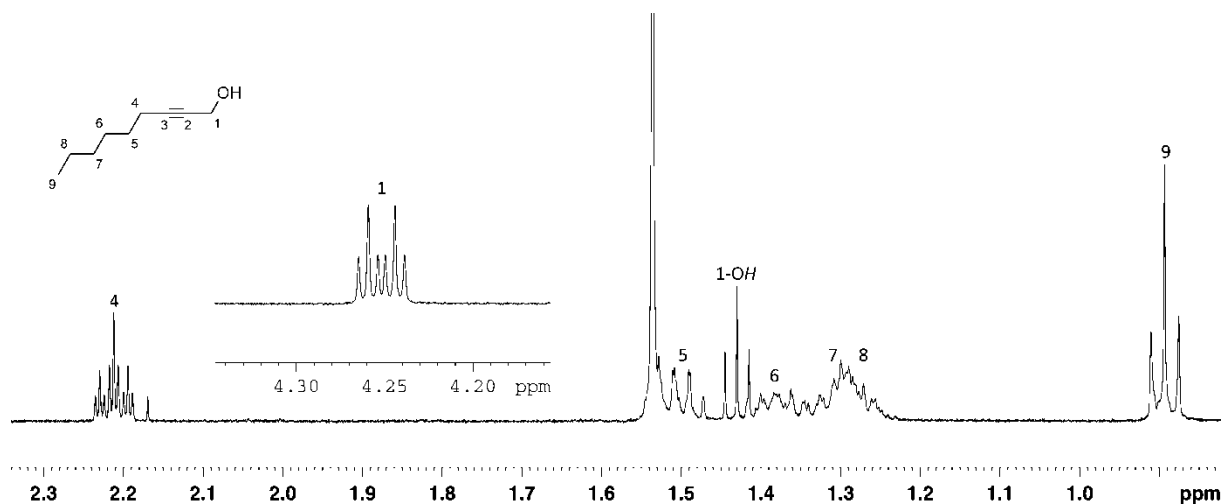


Figure 60: ^1H NMR Spectrum for 2-nonyn-1-ol at low concentration

These couplings were confirmed in a NMR experiment depicted in Figure 61. Firstly, a concentrated sample was run and the splitting at 4.25 ppm disappeared, leaving a broad singlet as hydrogen bonding is prevalent (trace **a**). The triplet at 1.43 ppm was not visible either. In the next run the sample was diluted by 0.75 fold (trace **b**). Splitting at 4.25 ppm becomes apparent and a triplet at 1.43 ppm begins to take shape. In the next run the sample was diluted another 0.75 fold (trace **c**). The splitting at 4.25 ppm is well resolved as a doublet of triplets and the triplet at 1.43 ppm becomes clearer. Further dilution had no effect on improving the observed splitting. Finally, deuterium oxide- d_2 was added to the sample (trace **d**). This destroyed the coupling between 1-OH and 1-H as the alcohol proton underwent exchange with deuterium, and the triplet is no longer visible. Similarly, the doublet of triplets changes, but maintains some splitting pattern due to long range coupling across the alkyne bond. The dilution has no effect on the peak at 2.21 ppm.

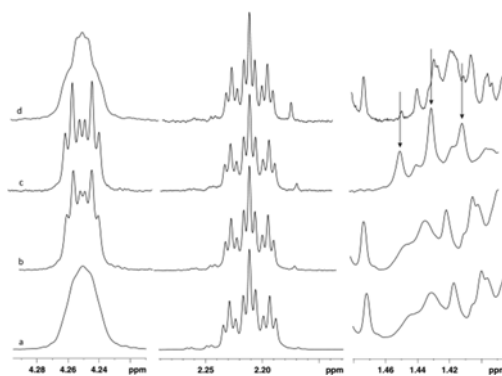


Figure 61: The effect of dilution on three peaks in the ^1H NMR spectrum of 2-nonyn-1-ol

The ^{13}C spectrum appeared to show only 8 peaks (Figure 62). However, two peaks were found to be close together, the two dimensional HSQC spectrum (Figure 63) confirmed that the 5-C and 6-C peaks

couple to different protons in the ^1H spectrum, accounting for the apparent absence of a peak in the ^{13}C NMR spectrum. The 1-C carbon adjacent to the alcohol group was expected to resonate fairly far downfield and was assigned as the peak resonating at 51.5 ppm. The 4-C carbon was assigned to the peak resonating at 18.7 ppm based on evidence in the HSQC spectrum. The quaternary carbons 2-C and 3-C were assigned as the peaks resonating at 78.3 ppm and 86.7 ppm respectively. These shifts are consistent with quaternary alkyne carbon shifts. The only primary carbon 9-C was assigned as the peak resonating at 14.0 ppm. The 5-C and 6-C secondary carbons appeared at very similar shifts (28.6 ppm and 28.5 ppm respectively) as seen in the HSQC spectrum. Finally, the 7-C and 8-C secondary carbons were assigned as the peaks resonating at 31.3 ppm and 22.5 ppm respectively.

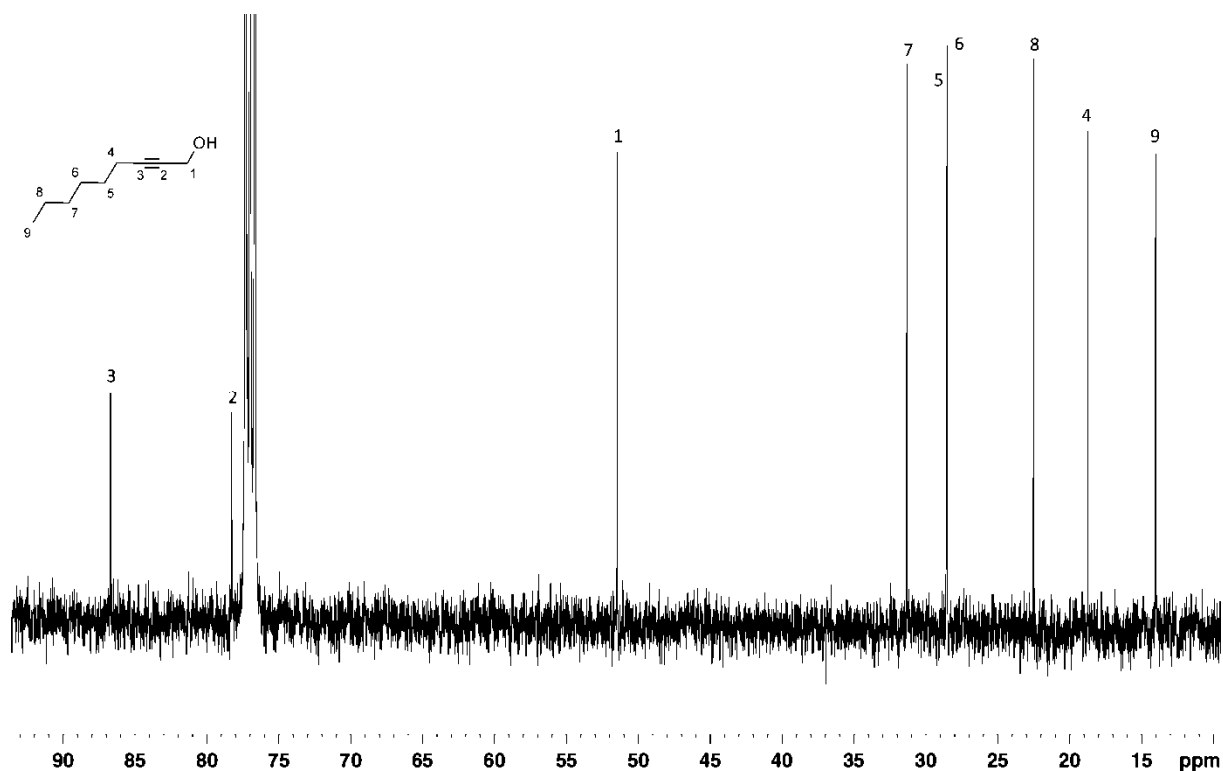


Figure 62: ^{13}C NMR Spectrum for 2-nonyn-1-ol

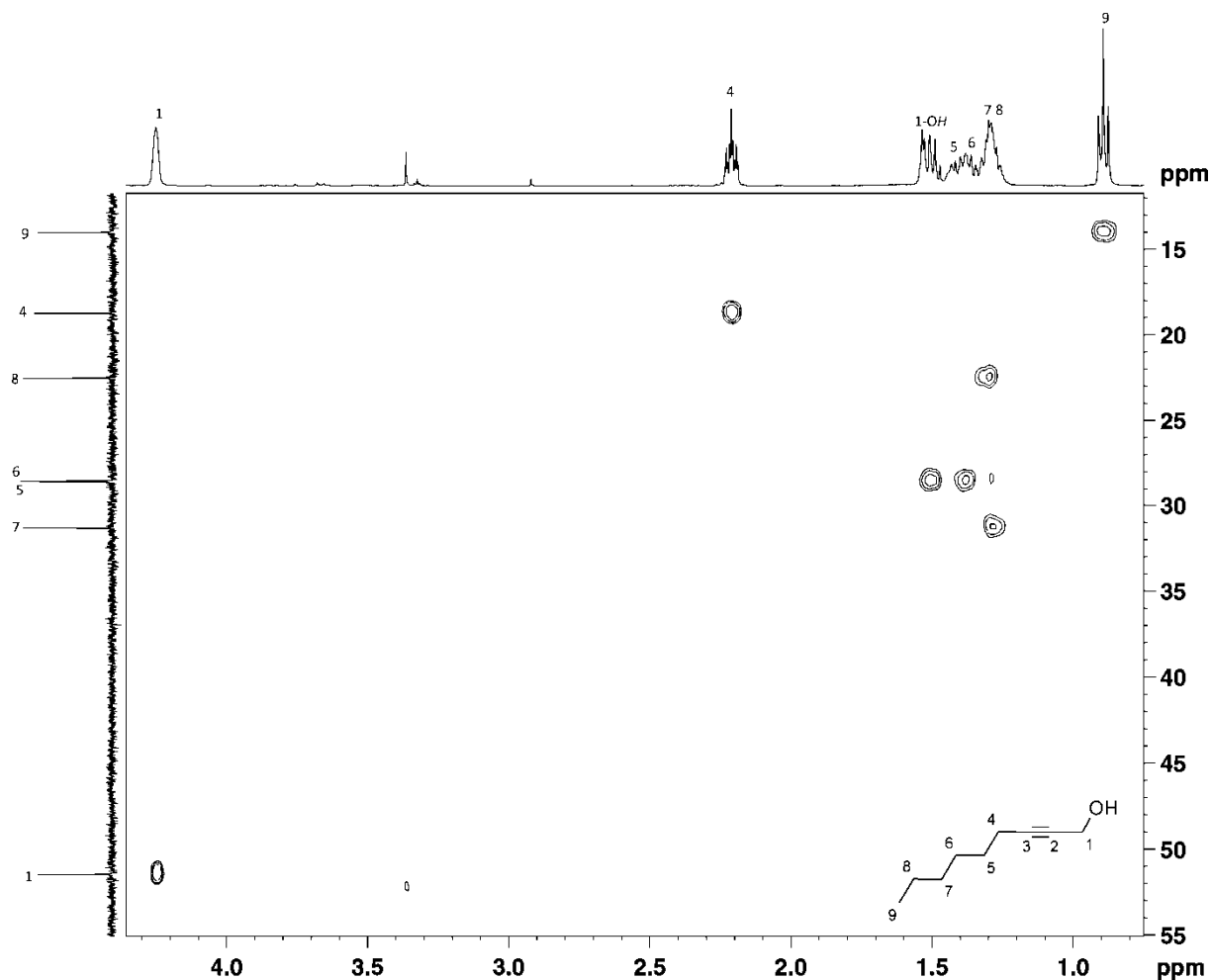
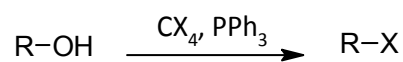


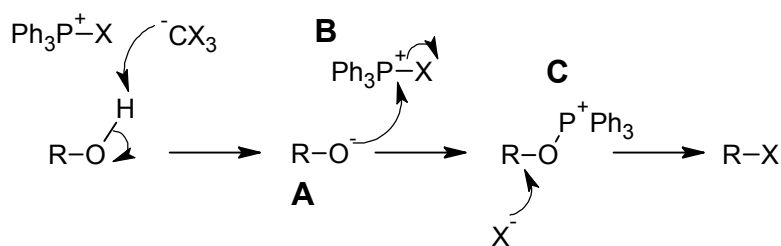
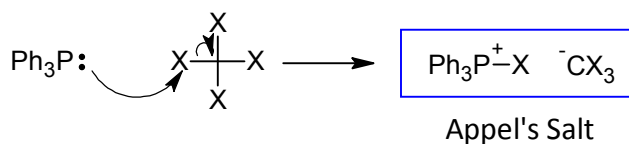
Figure 63: 2D HSQC NMR Spectrum for 2-nonyn-1-ol

Finally, the alcohol functionality could be converted to a bromide to give 1-bromo-2-nonyne **132**. The alcohol was converted into the bromide *via* the Appel reaction (named after Rolf Appel), which involves a reaction between triphenylphosphine and a tetrahalomethane such as CCl_4 or CBr_4 . This results in the formation of a salt known as Appel's salt.



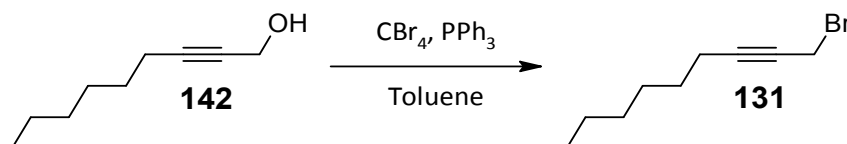
Scheme 66

The mechanism for this reaction is depicted in Scheme 67. The first step in the mechanism involves the formation of Appel's salt. The reaction then proceeds *via* nucleophilic attack of the halogen-phosphonium salt on the hydroxyl group¹⁰⁸ to form the intermediate **A**. Nucleophilic attack by the anion on the halogen-phosphonium ion **B** forms the intermediate **C**, which undergoes nucleophilic attack from the halide, forming the alkyl halide R-X and regenerating the triphenylphosphine.



Scheme 67

Thus the alcohol **142** was converted to the bromide **131** utilising the Appel reaction (Scheme 68). 2-Nonyn-1-ol was added to a stirring solution of carbon tetrabromide and triphenylphosphine in dry toluene and stirred for four hours. The resulting solution was purified by column chromatography after work up to give 1-bromo-2-nonyne. High resolution mass spectrometry confirmed the formation of the brominated product **131** with an acquired mass of $124.1246 \text{ g mol}^{-1}$ which compares favourably with the calculated ($M + H$) mass of $124.1252 \text{ g mol}^{-1}$ for C_9H_{16} .



Scheme 68

The structure was confirmed by NMR spectroscopy. The spectra are similar in appearance to those of the starting material. The ^1H NMR spectrum showed two differences when compared to the starting material (Figure 58). The first difference was the absence of the triplet assigned to the OH proton, and the second difference was the broad singlet at 4.25 ppm was now a triplet at 3.90 ppm (Figure 64). These changes were expected, as there is no longer any coupling from the OH proton to the 1- H protons, and therefore the 1- H protons appear as a triplet due to long range coupling with the 4- H protons. These observations suggest that the alcohol has indeed been converted into a bromide. Thus the peak resonating at 3.90 ppm was assigned to the 1- H protons (which is consistent with the shifts for methylene protons adjacent to bromide groups), and the peak at 2.21 ppm to the 4- H protons. The peak resonating at 0.87 ppm was assigned to the 9- H protons, with the chemical shift in the appropriate range for a methyl group. The remaining peaks resonating at 1.24-1.31 ppm,

1.32-1.38 ppm and 1.45-1.52 ppm were assigned to the remaining methylene protons 7-H, 8-H, 6-H and 5-H protons respectively.

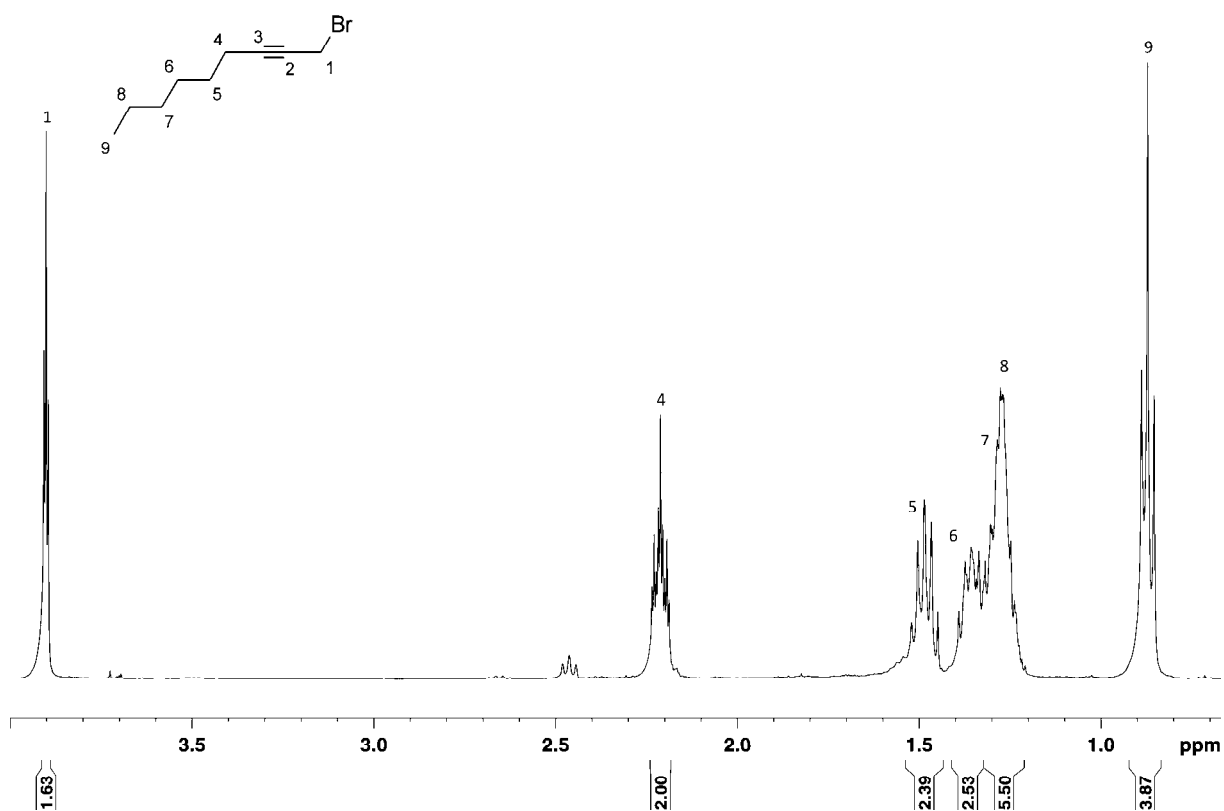


Figure 64: ¹H NMR Spectrum for 1-bromo-2-nonyne

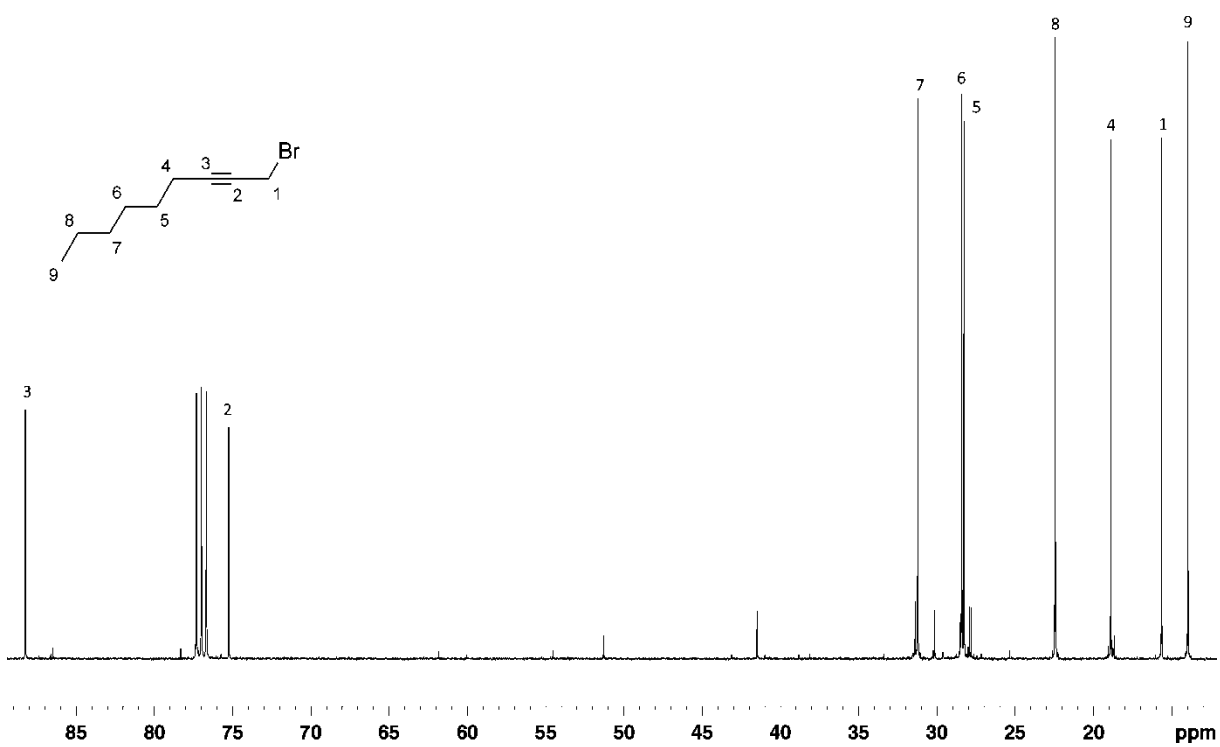


Figure 65: ¹³C NMR Spectrum for 1-bromo-2-nonyne

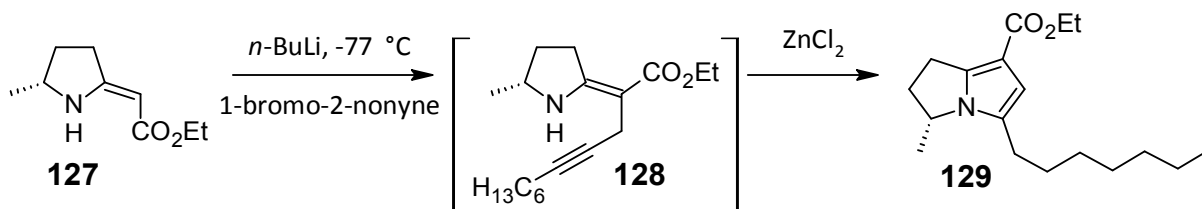
The ^{13}C and DEPT 135 NMR spectra were used to assign the carbons and assignments were confirmed with the two dimensional HSQC and HMBC spectra. There were nine peaks in the ^{13}C spectrum (Figure 65). The only primary carbon 9-C was assigned as the peak resonating at 14.0 ppm. The quaternary carbons were expected to resonate quite far downfield and thus the 2-C and 3-C carbons were assigned as the peaks resonating at 75.3 ppm and 88.2 ppm respectively. The 4-C (18.9 ppm) and 1-C (15.7 ppm) carbons were fairly easily assigned through the proton coupling in the HSQC spectrum. The remaining peaks at 28.3 ppm, 28.4 ppm, 31.2 ppm and 22.4 ppm were assigned as the 5-C, 6-C, 7-C and 8-C carbons.

2.4 Catalytic Hydroamination Study

With the enaminoate **127** in hand the hydroamination cyclisation could be attempted by one of two synthetic methods. The first method is a one-pot procedure for the C-propargylation-hydroamination sequence and the second method is a two-step procedure where the hydroamination is only initiated after the C-propargylation (see Chapter 1, page 41). Regardless of the chosen method, a catalyst for the hydroamination is required. A study by Prior⁶⁷ indicated ZnCl_2 would be a good catalyst for the hydroamination, whilst Dovey⁹⁴ used AgNO_3 for the same transformations. ZnCl_2 was chosen for the reaction as there was not enough material to test both catalysts.

2.4.1 Part 4: Synthesis of ethyl (3*R*)-5-heptyl-3-methyl-2,3-dihydro-1*H*-pyrrolizidine-7-carboxylate

A two-step process for the propargylation-hydroamination sequence was shown by Dovey⁶⁶ to afford higher yields and as such was implemented for our synthesis (Scheme 69).



Scheme 69

Ethyl 2-[(5*R*)-5-methyltetrahydro-2*H*-pyrrol-2-ylidene]acetate **127** in dry THF was cooled to $-77\text{ }^{\circ}\text{C}$ before the slow addition of 2.5*M* *n*-BuLi and left to stir at $-77\text{ }^{\circ}\text{C}$ for 30 minutes. The solution was slowly warmed to room temperature and allowed to stir for a further 30 minutes before it was once again cooled to $-77\text{ }^{\circ}\text{C}$ after which 1-bromo-2-nonyne in dry THF was added dropwise and stirred for 30 minutes. The solution was once again slowly warmed to room temperature and stirred for 14 hours. The reaction was then quenched with 2*M* NH_4Cl and concentrated *in vacuo*. ZnCl_2 and dry acetonitrile were added to the resulting brown oil and the solution was refluxed for 5 hours. The solution was passed through a silica plug before it was concentrated *in vacuo* and immediately purified by column chromatography. Unfortunately inspection of the ^1H NMR spectrum indicated that the reaction was unsuccessful (Figure 66). This is evident as the starting enamine 2-*H* proton signal was absent in the spectrum as was the 6-*H* proton of the *N*-bridgehead pyrrolidine (Scheme 70). Also, the splitting observed for the protons neighbouring the alkyne of 1-bromo-2-nonyne was still present, and this would be absent if the hydroamination cyclisation had been successful.

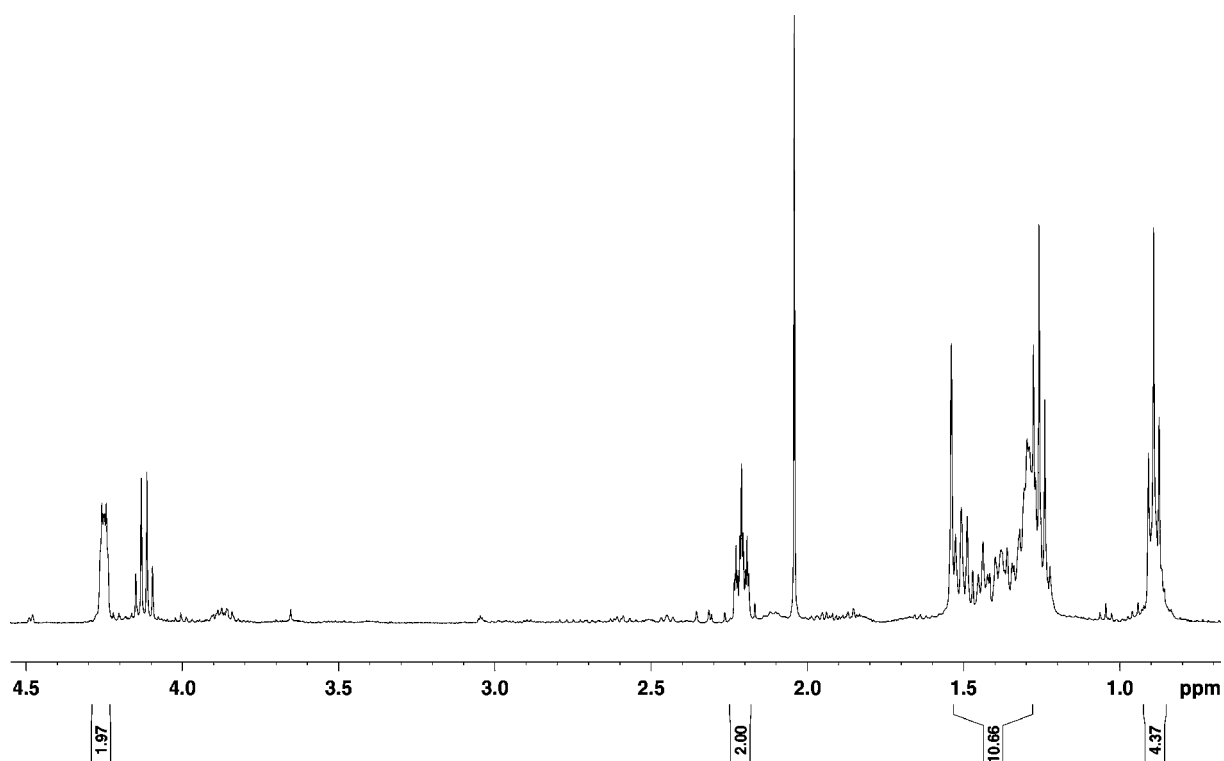
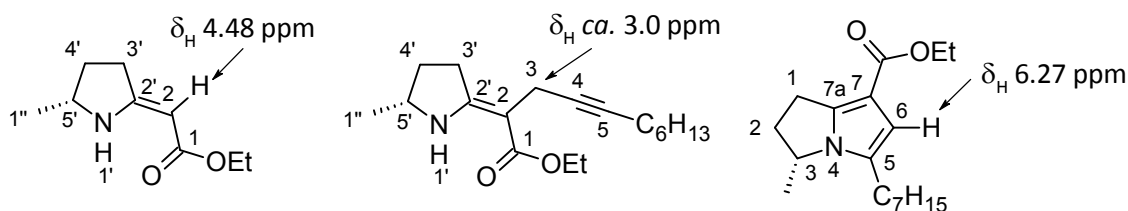


Figure 66



Scheme 70

The hydroamination cyclisation could have failed for a number of reasons. It is possible (the ^1H NMR spectrum suggests it) that the C-propargylation failed. If this is the case then there would not have been a multiple bond over which the amine could add and therefore the hydroamination could not have occurred. The intermediate C-propargylated compound was not isolated as both Prior⁶⁸ and Dovey⁹⁴ have shown that the compound either decomposes on silica or decomposes on exposure to atmosphere. Thus the hydroamination cyclisation was attempted without confirmation of successful C-propargylation. Another possibility is the formation of a di-propargylated compound shown in Figure 67. However, no evidence of such a compound was found.

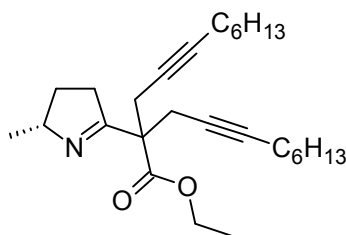
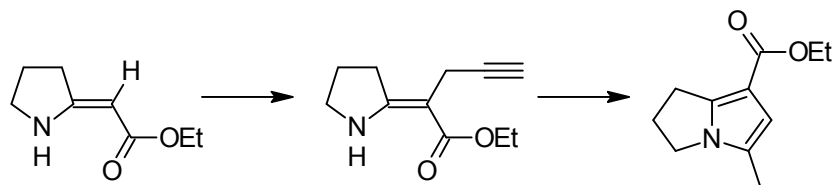


Figure 67

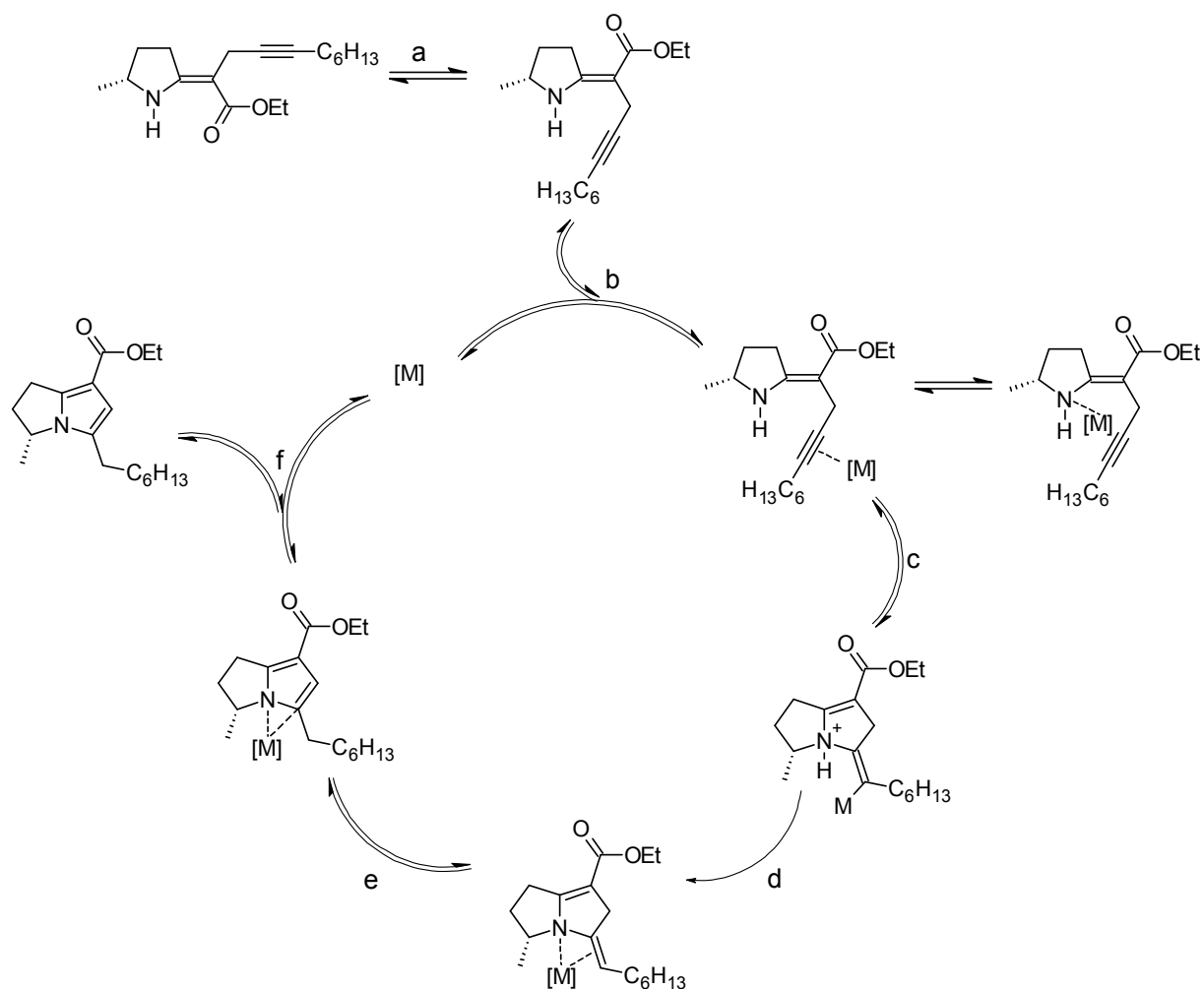
Presuming the C-propargylation was successful, the hydroamination may have failed due to the choice in, and amount of catalyst used. Prior found that the optimum amount of catalyst required for the hydroamination of similar acyclic compounds was 0.04 equivalents⁶⁷ and unfortunately the catalyst loading in the hydroamination attempt was 0.9 equivalents.

In Prior's synthesis the hydroamination catalysed by ZnCl_2 was successful but as the synthesis proceeded through the Eschenmoser coupling pathway the *E*-isomer of the enaminoate was formed.⁶⁸ In our synthesis through the lactim ether pathway the *Z*-isomer of the enaminoate was formed, putting the alkyne multiple bond and the amine in a *trans* orientation. The concern here was that the hydroamination would not occur readily. However, it has been suggested that metal mediated isomerisation occurs before the hydroamination putting the C—C triple bond and the amine in a *cis* orientation.^{67, 109} This geometric isomerisation is rationalised as a metal-olefin complex in equilibrium with a polarised form which may allow for the isomerisation to occur.⁶⁷ In a study conducted by Prior, acyclic C-propargyl vinylogous amides in the *Z*-configuration were successfully cyclised by microwave mediated hydroamination into pyrroles with a number of metal catalysts, including ZnCl_2 (see Chapter 1, Scheme 34).⁶⁷ The C-propargylated *E*-isomer (Scheme 69) in the hands of Prior underwent a ZnCl_2 catalysed hydroamination in a 43 % yield over two steps.⁶⁸ On the other hand, the *Z*-isomer depicted in Scheme 71 underwent successful AgNO_3 catalysed microwave mediated hydroamination in a 50 % yield over two steps (66 % for the C-propargylation and 75 % for the hydroamination).⁹⁴



Scheme 71

This is in contrast to the study conducted by Prior which suggested that AgNO_3 was not a viable catalyst for the transformation.⁶⁷ However, due to time constraints the reaction could not be reattempted but will form part of future work. Therefore, once the C-propargylated enamine is successfully synthesised the hydroamination will be reattempted with both ZnCl_2 and AgNO_3 and under both conventional and microwave methods.



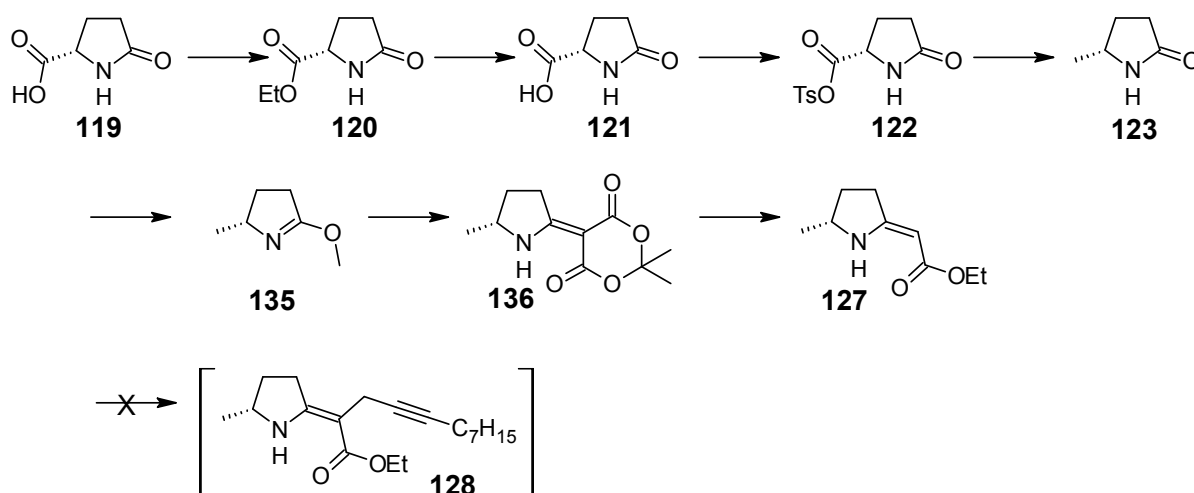
Scheme 72

The following mechanism adapted from Muller *et al.*¹⁰⁹ accounts for the ability of Zn(II) to catalyse the hydroamination (Scheme 72). Geometrical isomerisation **A** must occur before the

hydroamination. The C—C triple bond is next activated by π -coordination to the metal centre **B**. This is followed by nucleophilic attack on the C—C triple bond by the nitrogen lone pair of electrons in a 5-*exo*-dig cyclisation **C**. A 1,3-hydrogen shift follows at **D** and again at **E**. Regeneration of the catalyst **F** affords the hydroamination product.

2.4 Summary of Synthesis

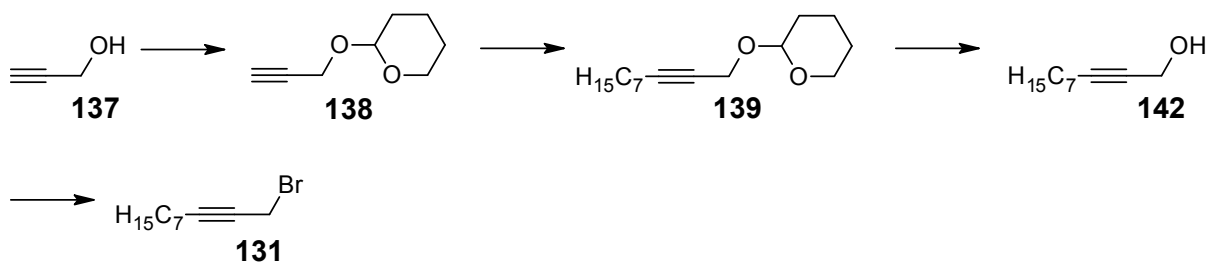
Scheme 73 depicts the overall synthetic scheme employed in the attempted synthesis of the pyrrolizidine alkaloid xenovenine. (*S*)-pyroglutamic acid **119** was converted into the corresponding ethyl ester **120** in a 97 % yield by Fischer esterification. Reduction of the ethyl ester **120** with sodium borohydride in water afforded the corresponding alcohol **121** in a 96 % yield. The tosylated derivative **122** was obtained from tosyl chloride, KOH and tetrabutylammonium hydrogen sulfate in a water/chloroform mixture in a 60 % yield. Reduction of the tosyl derivative **122** with tributyltin hydride and AIBN afforded the methyl lactam **123** in a 45 % yield. The methyl lactam **123** was converted into its corresponding methyl lactim ether **135** with trimethyloxonium tetrafluoroborate in a 54 % yield. The methyl lactim ether **135** was coupled with Meldrum's acid, catalysed by Ni(acac)₂, to give **136** in a 30 % yield. Decarboxylation of **136** afforded the methyl enaminoate **127** in a 98 % yield and in an overall 4 % yield from (*S*)-pyroglutamic acid **119**. The attempted C-propargylation was unsuccessful and thus this, as well as the remaining decarboxylation and reduction, will be the focus of future studies.



Scheme 73

Scheme 74 depicts the synthetic scheme utilised in the synthesis of 1-bromo-2-nonyne **131**. Propargyl alcohol **137** was protected with 3,4-dihydropyran in a 99 % yield before it was alkylated

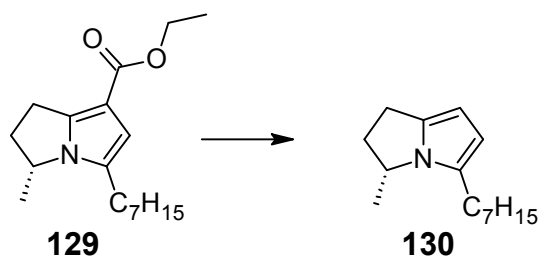
with 1-bromohexane to afford **139** in a 30 % yield. **139** was deprotected with 4M HCl in methanol to give the alcohol **142** in a 99 % yield. The alcohol **142** was then converted into the corresponding bromide **131** with carbon tetrabromide and triphenyl phosphine in a 40 % yield.



Scheme 74

2.5 Future Work

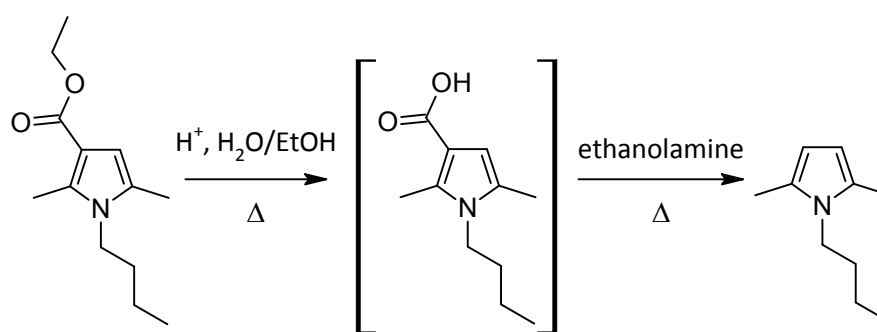
Whilst progress was made in the attempt to synthesis xenovenine, in particular a new pathway in this synthesis, a major challenge was encountered in the synthesis of the protected thiolactam, and much time was spent in trying to overcome the problems encountered. For this reason, and will little time available to complete this work, the final steps to afford xenovenine could not be completed. Therefore, a number of points are to be addressed in future work. First and foremost is the completion of the synthesis, beginning with the *C*-propargylation-hydroamination cyclisation. As mentioned in Section 2.5.1 it appeared that the *C*-propargylation was unsuccessful and must therefore be completed before attempting the hydroamination. The study completed by Prior has indicated that a more detailed analysis of the ZnCl_2 and AgNO_3 systems is required as this may be help in the optimisation the hydroamination step. Once the *C*-propargylation and hydroamination cyclisation have been completed the pyrrolidine **129** must be decarboxylated to afford the pyrrolizidine **130** (Scheme 75).



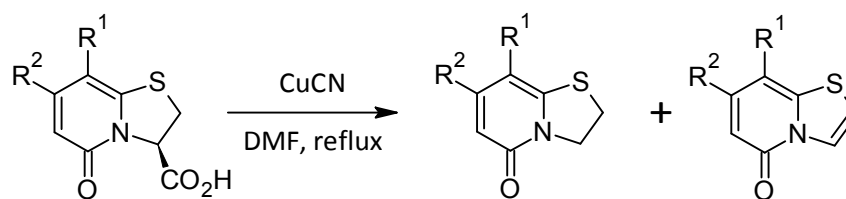
Scheme 75

Prior has shown that a plausible method for decarboxylation is a reverse Fischer esterification type reaction. The monocyclic derivate used in Priors study was successfully decarboxylated by employing

the reverse Fischer esterification method followed by reflux in ethanolamine to afford the decarboxylated species in a 31 % yield (Scheme 76).⁶⁸

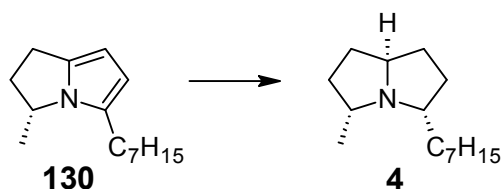


The low yields of this reaction may be improved upon in a microwave assisted decarboxylation. For example, Aberg *et al.*¹¹⁰ improved the yields of decarboxylation under conventional heating from 30 % to 80-99 % under microwave irradiation for the reaction shown in Scheme 77.



Therefore, a microwave assisted decarboxylation is a feasible alternative which may provide higher yields for the transformation.

After decarboxylation the final remaining step is the reduction of the pyrrolizidine **130** to xenovenine **4** (Scheme 78).



This is arguably one of the most important steps in the synthesis as the final two stereocentres will be introduced here. Both the metal and ligand of the chosen catalyst are important in such an asymmetric hydrogenation. A DFT study on the asymmetric reduction may provide insight into the choice of catalyst for the reaction. One option is to attempt the reduction with $H_2(g)$ over $Pd/CaCO_3$ at a low temperature. The question that arises here is on the final stereochemistry at the two new stereocentres. Firstly, due to steric hindrance, the pyrrolidine should be hydrogenated on the opposite face to the existing 3-C stereocentre, and as such the 5-C stereocentre should in fact form the desired stereocentre. However, the 7a-C stereocentre should give the opposite stereocentre as the hydrogen should add from the same side (Figure 68).

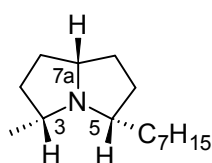
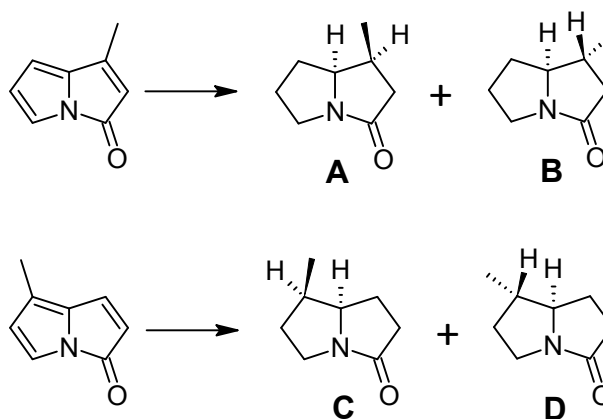


Figure 68

Despinoy and McNab¹¹¹ have had success with rhodium based catalysts for the asymmetric hydrogenation of pyrrolizin-3-ones to afford pyrrolizidines with high diastereoselectivity. The ratio of **A:B** where hydrogenation was carried out with 5 % Rh/Al_2O_3 in ethanol was 91:1 and the ratio of **C:D** where hydrogenation was carried out with 5 % Rh/C in hexane was 98:2 (Scheme 79).



Scheme 79

2.6 Conclusion

The focus of this work was to synthesis the pyrrolizidine alkaloid xenovenine **223H** utilising the hydroamination cyclisation developed within our research group. To this end, enantiomerically pure (*S*)-pyroglutamic acid **119** was converted into the corresponding methyl lactam **123**, which could next be transformed into the methyl enaminoate **127** *via* an Eschenmoser coupling reaction. It was therefore necessary to convert the methyl lactam **123** into the methyl thiolactam **124**, with a protection/activation step required before the Eschenmoser coupling could be attempted. The methyl thiolactam **124** was synthesised and purified with some difficulty and the protection/activation was attempted. However, this reaction did not proceed at all as expected, and very low yields were obtained. Much time was spent on altering the conditions of the reaction in an attempt to achieve the desired results. This became a major obstacle to the synthesis as the Eschenmoser coupling reaction could not proceed without this step.

Fortunately, on careful review of the literature a work around to this obstacle was identified. The method in question was *via* conversion to the lactim ether **135** and a brief model study proved to be extremely successful and the enaminoate **111** was obtained. This model study was carried over into the main synthesis and the methyl enaminoate **127** was obtained shortly thereafter. At this point the *C*-propargylation-hydroamination cyclisation was put in motion but was unfortunately unsuccessful as the *C*-propargylation was believed to have failed and with a limited amount of time available the required methyl enaminoate **127** could not be resynthesised. Therefore, the asymmetric hydrogenation to afford the final pyrrolizidine xenovenine **4** could not be conducted as desired, and will thus be addressed in future work, along with the *C*-propargylation, hydroamination and decarboxylation.

Careful spectroscopic analysis of all compounds was carried out. NMR spectroscopy was utilised and both one dimensional (^1H , ^{13}C , DEPT 135) and two dimensional (COSY, HSQC, HMBC, NOESY) techniques were used. In some cases it was necessary to analyse the coupling constants to determine the connectivity of the compounds and two dimensional NOE spectroscopy gave insight to the geometries of some compounds (**111** and **127**). Infrared spectroscopy and mass spectrometry were also used. An X-Ray crystallographic analysis gave useful insight into the observed ^1H NMR spectrum of compound **136**.

Chapter 3: Experimental

3.1 General information

^1H , ^{13}C and ^{15}N NMR spectra were recorded on either a Bruker Avance III 500 or Bruker Avance III 400 spectrometer at frequencies of 500 MHz/400 MHz (^1H), 125 MHz/100 MHz (^{13}C) and 51 MHz (^{15}N) using one of a 5 mm BBOZ probe 19F-31P-109Ag-[1H], 5 mm BBIZ probe 1H-[31P-109Ag], or a 5 mm TBIZ probe 1H-[31P]-[31P-103Rh]. All proton and carbon chemical shifts are quoted in ppm and are relative to the relevant solvent signal (e.g. CDCl_3 : ^1H , 7.26 ppm, ^{13}C , 77.0 ppm; D_2O : ^1H , 4.79 ppm). Proton-proton coupling constants are reported in Hertz. All experiments were conducted at 30 °C unless otherwise specified. Abbreviations used: s – singlet; d – doublet; t – triplet; q – quartet; dd – doublet of doublets.

High-resolution Mass Spectrometry was carried out on a Waters Acquity UPLC + LCT Premier TOF-MS, with either electrospray (ES) or atmospheric pressure chemical ionisation (AP) acquisition modes in either + or – mode.

Low-resolution Mass Spectrometry was carried out on two GC-MS instruments with instrument grade helium carrier gas. The first GC-MS instrument used was a Thermofinnigan Trace GC coupled with a Polaris-Q Mass Spectrometer. The Trace GC column used was an SGE, ID-BPX5, 30 m, ID: 0.25 μm , diameter 0.32 mm. The GC oven temperature was held at 40 °C for 1 minute followed by a 12 °C per minute ramp to 200 °C and held for 10 minutes. The spectral window for the mass spectrometer was 35 – 600 m/z with a source temperature of 200 °C. The second GC-MS instrument used was a Shimadzu QP-2010. The column used was an InertCap 5MS/Sil, 30 m, ID: 0.25 μm , diameter 0.25 mm. The GC oven temperature was held at 40 °C for 1 minute followed by a 12 °C per minute ramp to 200 °C and held for 10 minutes. The spectral window for the mass spectrometer was 50 – 700 m/z with a source temperature of 200 °C.

FT-IR were recorded with a Smiths Identify IR with an ATR diamond (64 scans collected) as thin films (neat) or thin films (chloroform).

Optical rotations were obtained using a Bellingham + Stanley Ltd. ADP 440+ Polarimeter with an LED/Interference filter (589.3 nm) light source and a photodiode detector. A path length of 1 cm was used and all concentrations are quoted in $\text{g}/100\text{cm}^3$.

Melting points were measured with either a Kofler Hotstage melting point apparatus or a Stuart™ SMP3 melting point apparatus.

All microwave reactions were performed using a CEM Discover Microwave System™.

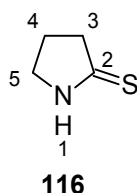
The X-ray data were recorded on a Bruker Apex Duo equipped with an Oxford Instruments Cryojet operating at 100(2) K and an Incoatec microsource operating at 30 W power. Crystal and structure refinement data are given in Table 10 (pg 81). The data were collected with Mo K α ($\lambda = 0.71073 \text{ \AA}$) radiation at a crystal-to-detector distance of 50 mm. The following conditions were used for the data collection: omega and phi scans with exposures taken at 30 W X-ray power and 0.50° frame widths using APEX2.¹¹² The data were reduced with the programme SAINT¹¹² using outlier rejection, scan speed scaling, as well as standard Lorentz and polarisation correction factors. A SADABS semi-empirical multi-scan absorption correction¹¹² was applied to the data. Direct methods, SHELX-2014¹¹³ and WinGX¹¹⁴ were used to solve the structure. All non-hydrogen atoms were located in the difference density map and refined anisotropically with SHELX-2014.¹¹³ All hydrogen atoms were included as idealised contributors in the least squares process. Their positions were calculated using a standard riding model with C–H_{aromatic} distances of 0.93 \AA and $U_{\text{iso}} = 1.2 \text{ Ueq}$, C–H_{methylene} distances of 0.99 \AA and $U_{\text{iso}} = 1.2 \text{ Ueq}$ and C–H_{methyl} distances of 0.98 \AA and $U_{\text{iso}} = 1.5 \text{ Ueq}$. The amine N–H was located in the difference density map and refined isotropically.

Column chromatography was performed using Macherey-Nagel Kieselgel 60 (0.063 -0.2 mm particle size and 70 – 230 mesh) or with a Grace Reveleris® Flash System. Thin layer chromatography (TLC) was performed using Merck silica gel 60F₂₅₄ supported on an aluminium backing and was visualised under UV-light (254 or 365 nm) and/or by exposure to iodine vapour or anisaldehyde staining solution.

All chemicals were purchased from Sigma-Aldrich or Merck and used without further purification.

3.2 Preparative Procedures and Spectrometric Data

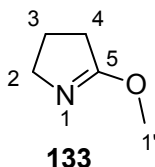
Synthesis of 2-Pyrrolidinethione (116)



Lawesson's reagent (4.838 g, 11.96 mmol) was weighed out into a nitrogen flushed round bottom flask and dissolved in dry toluene (150 cm^3) before the addition of 2-pyrrolidinone (1.75 cm^3 , 22.95 mmol). The mixture was refluxed for 4 hours after which distilled water (100 cm^3) was added and the aqueous phase was extracted with diethyl ether ($3 \times 70 \text{ cm}^3$). The combined organic extracts

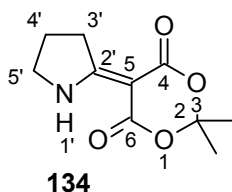
were concentrated *in vacuo* to yield a viscous yellow oil which solidified on standing. The resulting solid was recrystallised from CHCl₃-Hex 1:1 to afford 2-pyrrolidinethione (1.165 g, 11.51 mol, 50 %) as a white crystalline solid; R_f (EtOAc-Hex 1:1); mp [lit. 109-110 °C]; $\nu_{\max}/\text{cm}^{-1}$ 2882, 1533, 1417, 1291, 1110 and 782; ¹H NMR δ_{H} (400 MHz; CDCl₃) 2.16-2.23 (m, 2 H, 4-*H*), 2.89 (t, 2 H, *J* = 7.96 Hz, 3-*H*), 3.64 (t, 2 H, *J* = 7.22 Hz, 5-*H*), 8.63 (s, 1 H, N-*H*); ¹³C NMR δ_{C} (100MHz, CDCl₃) 22.9 (4-*C*), 43.2 (3-*C*), 49.6 (5-*C*), 205.9 (2-*C*); LRMS *m/z* (EI) 100.9 (100), 102.9 (5).

Synthesis of 3,4-Dihydro-5-methoxy-2*H*-pyrrole (133)



2-Pyrrolidinone (0.467 cm³, 6.15 mmol) in anhydrous dichloromethane (10 cm³) was added to a stirring solution of trimethyloxonium tetrafluoroborate (1.00 g, 6.76 mmol) in anhydrous dichloromethane (20 cm³) and stirred at room temperature for 22 hours. The resulting solution was diluted with anhydrous diethyl ether (30 cm³) and cooled to 0 °C. Cold saturated NaHCO₃ (30 cm³) was added dropwise over 15 minutes. The layers were separated and the organic phase washed once with NaHCO₃ (30 cm³). The organic phase was dried over Na₂SO₄ and filtered. The filtrate was carefully concentrated *in vacuo* (product is extremely volatile!) to afford 3,4-dihydro-5-methoxy-2*H*-pyrrole as a colourless oil (0.430 g, 4.34 mmol, 70 %); $\nu_{\max}/\text{cm}^{-1}$ 1647, 1196 and 1002; ¹H NMR δ_{H} (400 MHz; CDCl₃) 1.99-2.07 (m, 2 H, 3-*H*), 2.43-2.47 (m, 2 H, 2-*H*), 3.65-3.68 (m, 2 H, 4-*H*), 3.81 (s, 3 H, 1'-CH₃); ¹³C NMR δ_{C} (100MHz, CDCl₃) 23.3 (3-*C*), 30.8 (4-*C*), 54.9 (2-*C*), 55.2 (1'-*C*), 173.7 (5-*C*); HRMS (ES⁺) found 100.0763 (C₅H₁₀NO), calculated 100.0762.

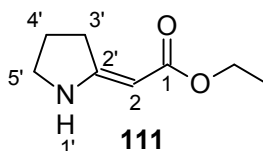
Synthesis of 2,2-Dimethyl-5-(2-pyrrolidinylidene)-1,3-dioxane-4,6-dione (134)



3,4-Dihydro-5-methoxy-2*H*-pyrrole (0.397 g, 4.01 mmol) was added to a stirred solution of Meldrum's acid (0.578 g, 4.01 mmol) and Ni(acac)₂ (1.0 mg, 0.006 mmol) in anhydrous chloroform (30 cm³) and refluxed for 12 hours. The solvent was removed under vacuum and the resulting yellow solid was recrystallised from absolute ethanol to give 2,2-dimethyl-5-(2-pyrrolidinylidene)-1,3-dioxane-4,6-dione as a crystalline white solid (0.311 g, 1.47 mmol, 38 % over two steps); R_f 0.30

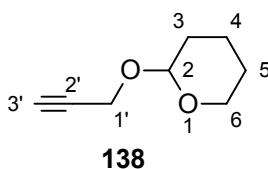
(EtOAc-Hex 1:1); mp 43-45 °C; $\nu_{\max}/\text{cm}^{-1}$ 3309, 1712, 1649, 1580, 1261, 995 and 914; $^1\text{H NMR } \delta_{\text{H}}$ (400 MHz; CDCl_3) 1.68 (s, 6 H, 2 × 2- CH_3), 2.17 (p, 2 H, $J=7.89$ Hz, 4'-H), 3.40 (t, 2 H, $J=7.84$ Hz, 5'-H), 3.72-3.76 (m, 2 H, 3'-H), 10.12 (s, 1 H, N-H); $^{13}\text{C NMR } \delta_{\text{C}}$ (100MHz, CDCl_3) 20.8 (4'-C), 26.7 (2 × 2- CH_3), 34.9 (5'-C), 48.3 (3'-C), 81.8 (5-C), 103.2 (2-C), 163.1 (4-C), 166.6 (6-C), 177.0 (2'-C); HRMS (ES^+) found 234.0736 ($\text{C}_{10}\text{H}_{13}\text{NO}_4\text{Na}$), calculated 234.0742.

Synthesis of (2Z)-pyrrolidinylidene ethyl ester (111)



2,2-Dimethyl-5-(2-pyrrolidinylidene)1,3-dioxane-4,6-dione (0.285 g, 1.373 mmol) was added to a stirring solution of sodium ethoxide (32 mg) and absolute ethanol (2 cm^3) and refluxed overnight. The solvent was removed *in vacuo* and the resulting residue was dissolved in distilled water. The pH was adjusted to 6 with chilled 1M HCl. The aqueous phase was extracted with chloroform (3 × 30 cm^3) and the combined organic extracts were dried over Na_2SO_4 and filtered. The filtrate was concentrated *in vacuo* to give (2Z)-pyrrolidinylidene ethyl ester as a clear liquid which solidified on standing (81 mg, 0.52 mmol, 38 %); R_f 0.60 (EtOAc-Hex 1:1); mp 59-61 °C [lit. 60-62 °C]⁶⁶; $\nu_{\max}/\text{cm}^{-1}$ 3376, 2975, 1715, 1658, 1595, 1235, 1144 and 1056; $^1\text{H NMR } \delta_{\text{H}}$ (400 MHz; CDCl_3) 1.25 (t, 3 H, $J=7.10$ Hz, CH_3), 1.97 (p, 2 H, $J=7.23$ Hz, 4'-H), 2.58 (t, 2 H, $J=7.78$ Hz, 5'-H), 3.52 (m, 2 H, 3'-H), 4.12 (q, 2 H, $J=7.10$ Hz, CH_2), 4.54 (s, 1 H, 2-H), 7.89 (s, 1 H, N-H); $^{13}\text{C NMR } \delta_{\text{C}}$ (100MHz, CDCl_3) 14.7 (1- $\text{CO}_2\text{CH}_2\text{CH}_3$), 22.0 (4'-C), 32.2 (3'-C), 47.0 (5'-C), 58.4 (1- $\text{CO}_2\text{CH}_2\text{CH}_3$), 76.6 (2-C), 166.5 (2'-C), 170.8 (1-C); HRMS (ES^+) found 219.1118 ($\text{C}_{10}\text{H}_{16}\text{N}_2\text{O}_2\text{Na}$) [M^+ + acetonitrile + Na], calculated 219.1109.

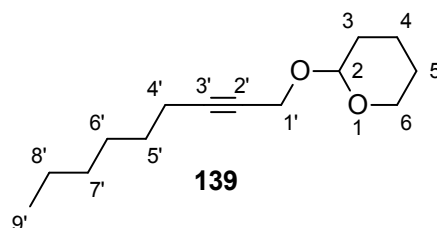
Synthesis of 2-Propynyl tetrahydro-2H-pyran-2-yl ether (138)



p-Toluenesulfonic acid (70 mg) was added to a stirring solution of 3,4-dihydro-2H-pyran (3.7 cm^3 , 41 mmol), propargyl alcohol (2.0 cm^3 , 34 mmol) and dichloromethane (100 cm^3) in a 250 cm^3 round bottom flask and stirred for 6 hours. Distilled water (125 cm^3) was added and the aqueous phase extracted into dichloromethane (3 × 80 cm^3). The combined organic extracts were filtered through a 2 cm silica plug and then dried over Na_2SO_4 and then concentrated *in vacuo* to give 2-propynyl

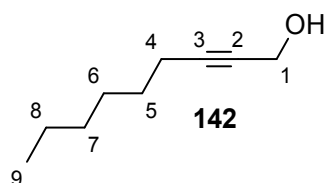
tetrahydro-2*H*-pyran-2-yl ether (4.701 g, 34 mmol, 99 %) as a yellow liquid; R_f 0.61 (EtOAc-Hex 1:1); ν_{\max} (thin film)/ cm^{-1} 3284, 2939, 2867, 2850, 1201, 1183, 1119, 1078, 1056, 1020, 974 and 814; ^1H NMR δ_{H} (400MHz, CDCl_3) 1.50-1.54 (m, 1 H, 4-*H*), 1.55-1.62 (m, 2 H, 5-*H*), 1.63-1.67 (m, 1 H, 3-*H*), 1.70-1.78 (m, 1 H, 3-*H*), 1.79-1.88 (m, 1 H, 4-*H*), 2.41 (t, 1 H, $J = 2.4$ Hz, 3'-*H*), 3.51-3.56 (m, 1 H, 6-*H*), 3.81-3.87 (m, 1H, 6-*H*), 4.27 (dq, 2 H, $J = 2.4$ Hz, $J = 15.8$ Hz, 1'-*H*), 4.82 (t, 1 H, $J = 3.4$ Hz, 2-*H*); ^{13}C NMR δ_{C} (100MHz, CDCl_3) 18.9 (4-*C*), 25.3 (5-*C*), 30.1 (3-*C*), 53.9 (1'-*C*), 61.9 (6-*C*), 73.9 (3'-*C*), 79.7 (2'-*C*), 96.8 (2-*C*); LRMS m/z (EI) 101 (2), 93 (2), 85 (100), 67 (51), 55 (31), 41 (43).

Synthesis of 2-Nonynyl tetrahydro-2*H*-pyran-2-yl ether (139)



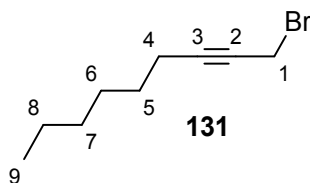
2.5 M *n*-BuLi (26 cm^3 , 65 mmol) was added dropwise with a dropping funnel over a period of 10 minutes to a stirring solution of 2-propynyl tetrahydro-2*H*-pyran-2-yl ether (9.185 g, 54 mmol) in dry THF at 0 °C in a vacuum dried and evacuated 250 cm^3 two neck round bottom flask under nitrogen atmosphere and stirred for 5 minutes. The solution was then allowed to slowly warm to room temperature and stirred for a further 1 hour. The solution was then cooled to 0 °C followed by the dropwise addition of 1-bromohexane (10 cm^3 , 71 mmol) over 10 minutes and then refluxed for 12 hours. The reaction was quenched with methanol (1 cm^3) followed by the addition of distilled water (100 cm^3). The aqueous phase was extracted into dichloromethane (3 \times 80 cm^3) and the combined organic extracts were filtered through a 2 cm silica plug, and then dried over Na_2SO_4 before concentrating *in vacuo* to give a brown oil, which was purified by chromatography on a Grace Resolve system to afford 2-nonynyl tetrahydro-2*H*-pyran-2-yl ether (3.315 g, 15 mmol, 28 %) as a pale yellow oil; R_f 0.70 (EtOAc-Hex 1:1); ν_{\max} (thin film)/ cm^{-1} 2929, 2856, 1453, 1343, 1261, 1200, 1029; ^1H NMR δ_{H} (400MHz, CDCl_3) 0.88 (t, 3 H, $J = 6.9$ Hz, 9'-*H*), 1.26-1.28 (m, 2 H, 7'-*H*), 1.29-1.32 (m, 2 H, 8'-*H*), 1.33-1.41 (m, 2 H, 6'-*H*), 1.47-1.51 (m, 2 H, 5'-*H*), 1.55-1.57 (m, 1 H, 4-*H*), 1.58-1.62 (m, 2H, 5-*H*), 1.63-1.66 (m, 1 H, 3-*H*), 1.70-1.77 (m, 1 H, 3-*H*), 1.83-1.88 (m, 1 H, 4-*H*), 2.21 (tt, 2 H, $J = 2.19$ Hz, $J = 7.09$ Hz, 4'-*H*), 3.49-3.55 (m, 1 H, 6-*H*), 3.82-3.87 (m, 1 H, 6-*H*), 4.21 (dd, 1 H, $J = 2.19$ Hz, $J = 15.25$ Hz, 1'-*H*), 4.29 (dd, 1 H, $J = 2.19$ Hz, $J = 15.25$ Hz, 1'-*H*), 4.81 (t, 1 H, $J = 3.44$ Hz, 2-*H*); ^{13}C NMR δ_{C} (100MHz, CDCl_3) 14.0 (9'-*C*), 18.8 (4'-*C*), 19.2 (4-*C*), 22.5 (8'-*C*), 25.4 (5-*C*), 28.5 (6'-*C*), 28.6 (5'-*C*), 30.3 (3-*C*), 31.3 (7'-*C*), 54.7 (1'-*C*), 62.0 (6-*C*), 75.7 (2'-*C*), 86.7 (3'-*C*), 96.7 (2-*C*); m/z (EI) 224 (M^+ , 0.03 %), 153 (0.64), 101 (27), 93 (27), 85 (57), 81 (10), 79 (83), 67 (100), 55 (11), 41 (41); HRMS (ES^+) found 247.1666 ($\text{C}_{14}\text{H}_{24}\text{O}_2\text{Na}$), calculated 247.1674.

Synthesis of 2-Nonyl-1-ol (142)



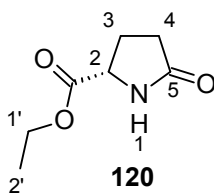
4M HCl (1 cm³) was added to a stirring solution of 2-nonyl tetrahydro-2H-pyran-2-yl ether (1.452 g, 6.5 mmol) and methanol (25 cm³) and stirred for 4 hours. The solution was neutralised with K₂CO₃ and filtered twice. The solvent was removed *in vacuo* to afford 2-nonyl-1-ol (0.910 g, 6.4 mmol, 99 %) as a yellow oil; R_f 0.62 (EtOAc-Hex 1:1); ν_{\max} (thin film)/cm⁻¹ 3337, 2927, 2858, 1457, 1136, 1010; ¹H NMR δ_{H} (400MHz, CDCl₃) 0.89 (t, 3 H, *J* = 6.9 Hz, 9-*H*), 1.25-1.33 (m, 4 H, 7-*H*, 8-*H*), 1.34-1.40 (m, 2 H, 6-*H*), 1.43 (t, 1 H, *J* = 2.2 Hz, *J* = 6.0 Hz, 1-OH), 1.47-1.51 (m, 2 H, 5-*H*), 2.21 (tt, 2 H, *J* = 2.2 Hz, *J* = 7.1 Hz, 4-*H*), 4.25 (dt, 2 H, *J* = 2.2 Hz, *J* = 6.0 Hz, 1-*H*); ¹³C NMR δ_{C} (100MHz, CDCl₃) 14.0 (9-C), 18.7 (4-C), 22.5 (8-C), 28.5 (6-C), 28.6 (5-C), 31.3 (7-C), 51.5 (1-C), 78.3 (2-C), 86.7 (3-C); *m/z* (EI) 139 (M⁺, 15 %), 109 (7), 93 (1), 67 (9), 55 (7), 41 (13), 39 (5).

Synthesis of 1-Bromo-2-nonyne (131)



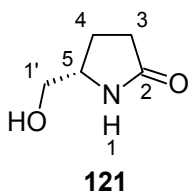
2-Nonyl-1-ol (0.910 g, 6.49 mmol) was added to a stirring solution of carbon tetrabromide (2.176 g, 6.54 mmol) and triphenylphosphine (1.716 g, 6.54 mmol) in dry toluene (35 cm³) and stirred for 4 hours. Distilled water (25 cm³) was added and the aqueous phase extracted into hexane (3 × 20 cm³). The combined organic extracts were concentrated *in vacuo* and purified by column chromatography on silica (EtOAc-Hex 1:1) to afford 1-bromo-2-nonyne (0.492 g, 2.42 mmol, 37 %) as a yellow oil; R_f 0.84 (EtOAc-Hex 1:1); ν_{\max} (thin film)/cm⁻¹ 2953, 2929, 2858, 1725, 1457 and 1215; ¹H NMR δ_{H} (400MHz, CDCl₃) 0.87 (t, 3 H, *J* = 6.9 Hz, 9-*H*), 1.24-1.31 (m, 4 H, 7-*H*, 8-*H*), 1.32-1.38 (m, 2 H, 6-*H*), 1.45-1.52 (m, 2 H, 5-*H*), 2.21 (tt, 2 H, *J* = 2.4 Hz, *J* = 7.1 Hz, 4-*H*), 3.90 (t, 2 H, *J* = 2.4 Hz, 1-*H*); ¹³C NMR δ_{C} (100MHz, CDCl₃) 14.0 (9-C), 15.7 (1-C), 18.9 (4-C), 22.4 (8-C), 28.3 (5-C), 28.4 (6-C), 31.2 (7-C), 75.3 (2-C), 88.2 (3-C); HRMS (AP⁺) found 124.1246 (C₉H₁₆), calculated 124.1252.

Synthesis of Ethyl (2*S*)-5-oxopyrrolidine-2-carboxylate (120)



5-Oxopyrrolidine-2-carboxylic acid (12.853 g, 0.10 mol) was added to a stirring solution of absolute ethanol (80 cm³) and benzene (40 cm³) in a 500 cm³ round bottom flask. Concentrated sulphuric acid (0.5 cm³) was added and the solution refluxed with a Dean and Stark apparatus for 6 hours. The solution was then cooled and concentrated *in vacuo*. The resulting oil was dissolved in chloroform and potassium carbonate (2 g) added, after which the solution was stirred for 30 min. The potassium carbonate was removed by filtration and the filtrate concentrated *in vacuo*. The resulting pale yellow oil was purified by distillation with the impurities distilled out at 30 mmHg to furnish ethyl (2*S*)-5-oxopyrrolidine-2-carboxylate (15.33g, 97 mmol, 97%) as a white solid; *R_f* 0.64 (100% EtOH); mp 43-47 °C [lit. 50-51 °C]¹¹⁷; [α]_D²¹ +3.3° (c. 5.0, EtOH)[lit.+3.5°]¹¹⁸; IR ν_{\max} (thin film)/cm⁻¹ 3227, 2977, 1735, 1689, 1419, 1192, 1151, 1027; ¹H NMR δ_{H} (400MHz, CDCl₃) 1.30 (t, 3 H, *J* = 7.0 Hz, 2'-*H*), 2.21-2.30 (m, 1 H, 3-*H*), 2.32-2.40 (m, 2 H, 4-*H*), 2.42-2.53 (m, 1 H, 3-*H*), 4.22 (q, 2 H, *J* = 7.0 Hz, 1'-*H*), 4.20-4.25 (m, 1 H, 2-*H*), 6.10 (s, 1 H, N-*H*); ¹³C NMR δ_{C} (100MHz, CDCl₃) 14.1 (2'-C),24.8 (3-C),29.1 (4-C),55.3 (2-C),61.7, (1'-C),171.8 (2-CCO₂),177.7 (5-C); LRMS *m/z* (EI) 158 (10), 84 (100), 56 (20), 41 (70), 39 (24).

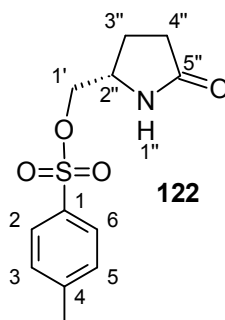
Synthesis of (5*S*)-5-(Hydroxymethyl)tetrahydro-2*H*-pyrrol-2-one (121)



Sodium borohydride (3.100 g, 82 mmol) was added in small portions to a stirring solution of (5*S*)-ethyl 5-oxopyrrolidine-2-carboxylate (11.63 g, 74 mmol) in absolute ethanol (100 cm³) in a 500 cm³ conical flask at 0 °C after which the solution was allowed to warm to room temperature and stirred for 2 hours followed by dropwise addition of acetone (7 cm³).The mixture was filtered through a 2 cm silica plug to remove the boric acid derivative and then concentrated *in vacuo* to afford a milky white oil which was purified by column chromatography on silica (EtOAc-MeOH 2:1) to afford (5*S*)-5-(hydroxymethyl)tetrahydro-2*H*-pyrrol-2-one (8.147 g, 71 mmol, 96 %) as a colourless oil; *R_f* 0.36 (EtOAc-MeOH 2:1); mp 81-83 °C [lit. 86-87 °C]¹¹⁹; [α]_D¹⁹ +25.9° (c. 4.9, EtOH) [lit. +28.0° (c 5.0, EtOH)]¹²⁰; IR ν_{\max} (thin film)/cm⁻¹ 3247, 2934, 1652, 1646, 1436, 1281, 1088, 1054; ¹H NMR

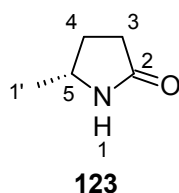
δ_{H} (400MHz, CDCl_3) 1.75-1.84 (m, 1 H, 4-H), 2.11-2.21 (m, 1 H, 4-H), 2.32-2.38 (m, 2 H, 3-H), 3.43-3.48 (m, 1 H, 1'-H), 3.65-3.68 (m, 1 H, 1'-H), 3.76-3.83 (m, 1 H, 5-H), 4.84 (s, 1 H, 1'-OH), 7.14 (s, 1 H, N-H); ^{13}C NMR δ_{C} (100MHz, CDCl_3)22.6 (4-C), 30.2 (3-C),56.4 (5-C),65.8 (1'-C), 179.4 (2-C); LRMS m/z (EI) 115 (M^+ , 5%), 84 (100), 72 (3), 56 (15).

Synthesis of [(2S)-5-Oxotetrahydro-1H-pyrrol-2-yl]methyl 4-methylbenzenesulfonate (122)



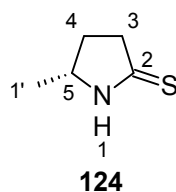
4-Methylbenzenesulfonyl chloride (8.246 g, 43 mmol) was added to a solution of (5S)-5-(hydroxymethyl)tetrahydro-2H-pyrrol-2-one (4.490 g, 39 mmol), potassium hydroxide (2.819 g, 50 mmol), tetrabutylammonium hydrogen sulfate (0.397 g, 1.17 mmol) and distilled water (50 cm^3) in chloroform (150 cm^3) in a 500 cm^3 reaction vessel fitted with an overhead stirrer. The solution was stirred whilst submerged in an ultrasonic bath for 18 hours a day for 3 days. The solution was concentrated *in vacuo* to afford a brown solid which was recrystallized four times from hot toluene to give [(2S)-5-oxotetrahydro-1H-pyrrol-2-yl]methyl 4-methylbenzenesulfonate (2.083 g, 7.7 mmol, 20%) as a shiny white crystalline solid; R_f 0.84 (EtOH-Ether 1:1); mp 125-127 $^{\circ}\text{C}$ [lit. mp 128-130 $^{\circ}\text{C}$]¹²¹; $[\alpha]_D^{25} +6.25^{\circ}$ (c. 1.6, EtOH) [lit. +7.9 $^{\circ}$ (c 1.0 EtOH)]¹²²; IR ν_{max} (thin film)/ cm^{-1} 3298, 2970, 1699, 1651, 1461, 1397, 1349; ^1H NMR δ_{H} (400MHz, CDCl_3) 1.72-1.80 (m, 1 H, 3''-H), 2.22-2.27 (m, 1 H, 3''-H), 2.29-2.34 (m, 2 H, 4''-H), 2.47 (s, 3 H, 4'- CH_3), 3.85 (dd, 1 H, $J = 7.8$ Hz, $J = 9.8$ Hz, 1'-H), 3.90-3.96 (m, 1 H, 2''-H), 4.07 (dd, 1 H, $J = 3.6$ Hz, $J = 9.8$ Hz, 1'-H), 5.65 (s, 1 H, N-H), 7.38 (d, 2 H, $J = 8.3$ Hz, 3-H, 5-H), 7.80 (d, 2 H, $J = 8.3$ Hz, 2-H, 6-H); ^{13}C NMR δ_{C} (100MHz, CDCl_3) 21.7 (4-C CH_3), 22.8 (3'-C), 29.0 (4''-C), 52.5 (2''-C), 72.1 (1'-C), 127.9 (2-C, 6-C), 130.1 (3-C, 5-C), 132.5 (4-C), 145.4 (1-C), 177.3 (5''-C); HRMS (ES^+) found 292.0616 ($\text{C}_{12}\text{H}_{15}\text{NO}_4\text{NaS}$), calculated 292.0619.

Synthesis of (5*R*)-5-Methyltetrahydro-2*H*-pyrrol-2-one (123)



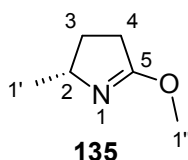
Tributyltin hydride (0.27 cm³, 1.0 mmol) was added dropwise to a stirring solution of [(2*S*)-5-oxotetrahydro-1*H*-pyrrol-2-yl]methyl 4-methylbenzenesulfonate (0.268 g, 1.0 mmol), sodium iodide (0.252 g, 1.68 mmol) and 2,2'-azobisisobutyronitrile (0.06 cm³, 0.40 mmol) in dry toluene (40 cm³) under nitrogen and refluxed for 14 hours. The precipitate was removed *via* filtration and the filtrate was concentrated *in vacuo*. The resulting colourless oil was purified by column chromatography on silica, eluting first with diethyl ether to remove the tributyltin iodide, and then with diethyl ether-isopropanol (8:1) to give 5-methyltetrahydro-2*H*-pyrrol-2-one (0.024 g, 0.25 mmol, 25%) as a colourless oil; *R*_f 0.21 (Ether); $[\alpha]_D^{20} +15.0^\circ$ (c. 0.020, EtOH) [lit.+15.8° (c. 0.023, EtOH)];⁷⁰ IR ν_{\max} (thin film)/cm⁻¹ 3238, 2964, 2926 and 1661, 1652, 1423 and 1278; ¹H NMR δ_{H} (400MHz, CDCl₃) 1.13 (d, 3 H, *J* = 6.3 Hz, 1'-*H*), 1.51-1.60 (m, 1 H, 4-*H*), 2.13-2.21 (m, 1 H, 4-*H*), 2.22-2.28 (m, 2 H, 3-*H*), 3.70 (m, 1 H, 5-*H*), 7.15 (s, 1 H, N-*H*); ¹³C NMR δ_{C} (100MHz, CDCl₃) 21.9 (1'-*C*), 28.9 (4-*C*), 30.5 (3-*C*), 50.1 (5-*C*), 178.3 (2-*C*); HRMS (ES⁺) found 122.0582 (C₅H₉NONa), calculated 122.0582.

Synthesis of (5*R*)-5-Methyltetrahydro-2*H*-pyrrole-2-thione (124)



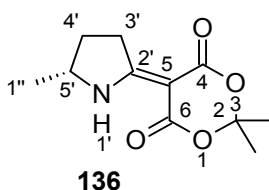
(5*R*)-5-Methyltetrahydro-2*H*-pyrrol-2-one (0.198 g, 2.0 mmol) was added to a stirring solution of Lawesson's reagent (0.405 g, 1.0 mmol) in dry THF (50 cm³) and stirred at room temperature for 17 hours. The solution was concentrated *in vacuo* and purified immediately by column chromatography on pre-warmed silica (EtOAc-Hex 1:1). The column was warmed continuously with a heat gun during separation to give (5*R*)-5-Methyltetrahydro-2*H*-pyrrole-2-thione (0.074 g, 0.65 mmol, 33 %) as an off white solid; *R*_f 0.38 (EtOAc-Hex 1:1); $[\alpha]_D^{29} +17.3^\circ$ (c. 0.1, EtOH) [lit.+13.8° (c. 4.8, EtOH)];⁶⁸ IR ν_{\max} 3134, 2949, 1535, 1293, 1218, 1112, 1062 and 782; ¹H NMR δ_{H} (400MHz, CD₃CN) 1.21 (d, 3 H, *J* = 6.36 Hz, 1'-*H*), 1.64-1.73 (m, 1 H, 4-*H*), 2.26-2.34 (m, 1 H, 4-*H*), 2.69-2.87 (m, 2 H, 3-*H*), 3.96-4.00 (m, 1 H, 5-*H*), 8.47 (s, 1 H, N-*H*); ¹³C NMR δ_{C} (100MHz, CD₃CN) 19.3, (1'-*C*), 30.8 (4-*C*), 43.0 (3-*C*), 57.4 (5-*C*), 205.1 (2-*C*).

Synthesis of (2*R*)-3,4-Dihydro-5-methoxy-2-methyl-2*H*-pyrrole (135)



(5*R*)-5-methyltetrahydro-2*H*-pyrrol-2-one (1.626 g, 16.4 mmol) in anhydrous dichloromethane (10 cm³) was added to a stirring solution of trimethyloxonium tetrafluoroborate (2.668 g, 18.0 mmol) in anhydrous dichloromethane (50 cm³) in an oven dried 100 cm³ round bottom flask and stirred at room temperature for 24 hours. The resulting solution was diluted with anhydrous diethyl ether (50 cm³) and cooled to 0 °C. Cold saturated NaHCO₃ (60 cm³) was added dropwise over 20 minutes. The layers were separated and the organic phase washed once with NaHCO₃ (60 cm³). The organic phase was dried over Na₂SO₄ and filtered. The filtrate was carefully concentrated *in vacuo* (product is extremely volatile!) to afford 3,4-dihydro-5-methoxy-2*H*-pyrrole as a yellow oil (0.998 g, 8.82 mmol, 54 %); $[\alpha]_D^{25} +50.0^\circ$ (c. 0.04, CHCl₃) [lit.+46.7° (c. 0.96, EtOH)];¹²³ $\nu_{\max}/\text{cm}^{-1}$ 1654 and 1164; ¹H NMR δ_{H} (400 MHz; CDCl₃) 1.23 (d, 3 H, *J* = 6.6 Hz, 1'-CH₃), 1.50-1.57 (m, 1 H, 3-*H*), 2.16-2.23 (m, 1 H, 3-*H*), 2.41-2.49 (m, 2 H, 4-*H*), 3.79 (s, 3 H, 1''-CH₃), 3.92-3.98 (m, 1 H, 2-*H*); ¹³C NMR δ_{C} (100MHz, CDCl₃) 23.1 (1'-C), 31.2 (4-C), 31.3 (3-C), 55.2 (1''-C), 62.2 (2-C), 172.5 (5-C); HRMS (ES⁺) found 114.0918 (C₆H₁₂NO), calculated 114.0919.

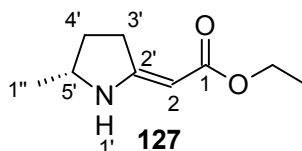
Synthesis of 2,2-Dimethyl-5-[(5*R*)-5-methyl-2-pyrrolidinylidene]-1,3-dioxane-4,6-dione (136)



(2*R*)-3,4-dihydro-5-methoxy-2*H*-pyrrole (0.683 g, 6.0 mmol) was added to a stirred solution of Meldrum's acid (0.860 g, 6.0 mmol) and Ni(acac)₂ (5 mg) in anhydrous chloroform (20 cm³) in an oven dried 50 cm³ round bottom flask and refluxed for 12 hours. The solution was filtered through a 0.5 cm silica plug to remove the Ni(acac)₂ and the solvent was removed under vacuum and the resulting yellow oil was recrystallised from absolute ethanol to give 2,2-dimethyl-5-[(5*R*)-5-methyl-2-pyrrolidinylidene]1,3-dioxane-4,6-dione as a crystalline white solid (0.445 g, 1.97 mmol, 25 %); *R*_f 0.71 (EtOAc-Hex 1:1); mp 149.6-150.3 °C [lit. 150 °C¹²⁴;]; $[\alpha]_D^{27} +25.9^\circ$ (c 1.0, CHCl₃) [lit.+26.0° (c. 1.08, CHCl₃)]¹²⁴; $\nu_{\max}/\text{cm}^{-1}$ 3286, 2983, 1705, 1658, 1571, 1442 and 1261; ¹H NMR δ_{H} (400 MHz; CDCl₃) 1.36 (d, 3 H, *J* = 6.40 Hz, 1''-CH₃), 1.68 (s, 3 H, 2-CH₃), 1.69 (s, 3 H, 2-CH₃), 1.67-1.74 (m, 1 H,

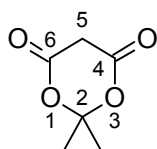
4'-H), 2.29-2.38 (m, 1 H, 4'-H), 3.22-3.32 (m, 1 H, 3'-H), 3.49-3.58 (m, 1 H, 3'-H), 4.08-4.16 (m, 1 H, 5'-H), 10.04 (s, 1 H, N-H); ^{13}C NMR δ_{C} (100MHz, CDCl_3) 21.2 (1''-C), 26.6 (2- CH_3), 26.7 (2- CH_3), 29.1 (4'-C), 4.8 (3'-C), 56.8 (5'-C), 81.4 (5-C), 103.2 (2-C), 163.2 (4-C), 166.6 (6-C), 175.9 (2'-C); HRMS (ES^+) found 248.0894 ($\text{C}_{11}\text{H}_{15}\text{NO}_4\text{Na}$), calculated 248.0899.

Synthesis of Ethyl 2-[(5R)-5-methyltetrahydro-2H-pyrrol-2-ylidene]acetate (127)



2,2-Dimethyl-5-[(5R)-5-methyl-2-pyrrolidinylidene]1,3-dioxane-4,6-dione (0.380 g, 1.68 mmol) was added to a stirring solution of sodium ethoxide (40 mg Na) in absolute ethanol (3 cm^3) in a 10 cm^3 round bottom flask and refluxed for 16 hours. The solution was concentrated *in vacuo* and the resulting yellow residue was dissolved in distilled water. The pH was adjusted to 6 with chilled 1M HCl. The aqueous solution was extracted with CHCl_3 (3 \times 30 cm^3). The combined organic extracts were dried over Na_2SO_4 and filtered. The filtrate was concentrated *in vacuo* to afford ethyl 2-[(5R)-5-methyltetrahydro-2H-pyrrol-2-ylidene]acetate as a pale yellow oil (0.280 g, 1.65 mmol, 98 %) and used without further purification; R_f 0.70 (EtOAc-Hex 1:1); $[\alpha]_D^{27} -19.7^\circ$ (c 0.035, CHCl_3) [lit. -11.0° (c 1.315, CHCl_3)]¹²⁴; $\nu_{\text{max}}/\text{cm}^{-1}$ 3355, 2966, 1654, 1591, 1230, 1140, 1045 and 778; ^1H NMR δ_{H} (400 MHz; CDCl_3) 1.23-1.27 (m, 6 H, 1''- CH_3 , 1-O CH_2CH_3), 1.46-1.53 (m, 1 H, 4'-H), 2.07-2.15 (m, 1 H, 4'-H), 2.53-2.67 (m, 2 H, 3'-H), 3.84-3.92 (m, 1 H, 5'-H), 4.10 (q, 2 H, $J = 7.11$ Hz, 1-O CH_2CH_3), 4.48 (s, 1 H, 2-H), 7.90 (s, 1 H, N-H); ^{13}C NMR δ_{C} (100MHz, CDCl_3) 14.7 (1-O CH_2CH_3), 21.6 (1''-C), 30.3 (4'-C), 32.1 (3'-C), 54.9 (5'-C), 58.3 (1-O CH_2CH_3), 76.3 (2-C), 165.8 (2'-C), 170.8 (1-C); HRMS (ES^+) found 170.1180 ($\text{C}_9\text{H}_{16}\text{NO}_2$), calculated 170.1181.

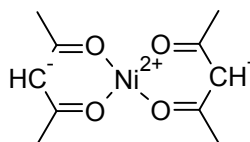
Synthesis of 2,2-Dimethyl-1,3-dioxane-4,6-dione (Meldrum's acid)



Malonic acid (4.16 g, 40 mmol) in acetic anhydride (4.8 cm^3) was cooled to 0 $^\circ\text{C}$ in an ice bath with stirring. Once at 0 $^\circ\text{C}$ concentrated H_2SO_4 (0.16 cm^3) was added and the solution stirred until all of the malonic acid had dissolved. Acetone (4.0 cm^3 , 68 mmol) was added dropwise and the mixture was stirred for 6 hours at 0 $^\circ\text{C}$. The resulting yellow solution was then stirred overnight at 4 $^\circ\text{C}$. Cold distilled water was added precipitating orange crystals which were vacuum filtered and washed with

cold distilled water until all of the orange colour was removed yielding Meldrum's acid as a white crystalline solid (2.67 g, 18.5 mmol, 46 %); R_f 0.51 (EtOAc-Hex 1:1); mp 90-93 °C [lit. 94-96 °C];¹¹⁵ $\nu_{\max}/\text{cm}^{-1}$ 3003, 2928, 1786, 1747, 1397, 1279, 1199, 1067, 1013, 974 and 953; $^1\text{H NMR } \delta_{\text{H}}(400 \text{ MHz}; \text{CDCl}_3)$ 1.78 (s, 6 H, 2 × 2- CH_3), 3.62 (s, 2 H, 5- H); $^{13}\text{C NMR } \delta_{\text{C}}(100\text{MHz}, \text{CDCl}_3)$ 27.6 (2- CH_3), 36.1 (5-C), 106.2 (2-C), 162.8 (4-C, 6-C).

Synthesis of Nickel(II) acetylacetonate [$\text{Ni}(\text{acac})_2$]



Nickel(II) nitrate hexahydrate (4.57 g, 25 mmol) was dissolved in distilled water (25 cm³) in a 250 cm³ conical flask. Acetylacetonone (5.00 g, 50 mmol) was dissolved in methanol (10 cm³) and was added dropwise over 20 minutes to the nickel solution. Excess sodium acetate (6.8 g) was dissolved in distilled water (15 cm³) and was added dropwise over 5 minutes to the nickel and acetylacetonone solution, precipitating a blue solid. The resulting mixture was heated to approximately 80 °C for 15 minutes with rapid stirring. The mixture was then cooled to room temperature and then to 0 °C in an ice bath. The blue precipitate was vacuum filtered and washed with cold distilled water. The precipitate was suction dried for 15 minutes before drying in an oven at 120 °C overnight to yield an emerald green solid $\text{Ni}(\text{acac})_2$ (3.572 g, 13.7 mmol, 84 %); mp 228-229 °C [lit. 230 °C]¹¹⁶; $\nu_{\max}/\text{cm}^{-1}$ 3359, 1582, 1507, 1445, 1386, 1257, 1194, 1017 and 924.

Chapter 4: References

1. Hesse, M., *Alkaloids: nature's curse or blessing?* Wiley-VCH: Weinheim, 2002.
2. Cordell, G. A.; Quinn-Beattie, M. L.; Farnsworth, N. R., *Phytotherapy Research* **2001**, *15* (3), 183-205.
3. Cordell, G. A., *Introduction to Alkaloids: a biogenetic approach*. Wiley: New York, 1981.
4. Evans, W. C., *Trease and Evans-Pharmacology*. 16th ed.; Saunders Elsevier: Edinburgh, 2009.
5. Dewick, P. M., *Medicinal Natural Products: a biosynthetic approach*. 2nd ed.; Wiley: West Sussex, 2001.
6. Andriamaharavo, N. R.; Garraffo, H. M.; Saporito, R. A.; Daly, J. W.; Razafindrabe, C. R.; Andriantsiferana, M.; Spande, T. F., *Journal of Natural Products* **2010**, *73* (3), 322-330.
7. Gärtner, M.; Weihofen, R.; Helmchen, G., *Chemistry – A European Journal* **2011**, *17* (27), 7605-7622.
8. Mota, Antonio J.; Chiaroni, A.; Langlois, N., *European Journal of Organic Chemistry* **2003**, *2003* (21), 4187-4198.
9. Felluga, F.; Forzato, C.; Nitti, P.; Pitacco, G.; Valentin, E.; Zangrando, E., *Journal of Heterocyclic Chemistry* **2010**, *47* (3), 664-670.
10. Harris, J. B., *Natural Toxins: Animal, Plant, and Microbial*. Oxford University Press: Oxford, 1986; p 86-87.
11. Dalton, D. R., *The Alkaloids: the fundamental chemistry: a biogenetic approach*. Marcel Inc.: New York, 1979; p 85-96.
12. Mattocks, A. R., *Chemistry and Toxicology of Pyrrolizidine Alkaloids*. Academic Press: London, 1986.
13. Fang, L.; Xiong, A.; Yang, X.; Cheng, W.; Yang, L.; Wang, Z., *Journal of Separation Science* **2014**, (00), 1-7.
14. Xiong, A.; Yang, F.; Fang, L.; Yang, L.; He, Y.; Wan, Y. Y.-J.; Xu, Y.; Qi, M.; Wang, X.; Yu, K.; Tsim, K. W.-K.; Wang, Z., *Chemical Research in Toxicology* **2014**, *27* (5), 775-786.

15. Argyropoulos, N. G.; Sarli, V. C.; Gdaniec, M., *European Journal of Organic Chemistry* **2006**, *2006* (16), 3738-3745.
16. Zimmer, R.; Collas, M.; Czerwonka, R.; Hain, U.; Reissig, H.-U., *Synthesis* **2008**, *2008* (02), 237-244.
17. Ruan, J.; Yang, M.; Fu, P.; Ye, Y.; Lin, G., *Chemical Research in Toxicology* **2014**, *27*, 1030-1039.
18. Wiedenfeld, H.; Edgar, J., *Phytochem Reviews* **2011**, *10* (1), 137-151.
19. Legeay, J.-C.; Lewis, W.; Stockman, R. A., *Chemical Communications* **2009**, (16), 2207-2209.
20. Jiang, T.; Livinghouse, T., *Organic Letters* **2010**, *12* (19), 4271-4273.
21. Jones, T. H.; Blum, M. S.; Fales, H. M.; Thompson, C. R., *The Journal of Organic Chemistry* **1980**, *45* (23), 4778-4780.
22. Liu, X.-K.; Zheng, X.; Ruan, Y.-P.; Ma, J.; Huang, P.-Q., *Organic & Biomolecular Chemistry* **2012**, *10* (6), 1275-1284.
23. McNaught, A. D.; Wilkinson, A., *IUPAC. Compendium of Chemical Terminology: The Gold Book*. 2nd ed.; Blackwell Scientific Publications: Oxford, 1997.
24. Clark, V. C.; Raxworthy, C. J.; Rakotomalala, V.; Sierwald, P.; Fisher, B. L., *Proceedings of the National Academy of Sciences of the United States of America* **2005**, *102* (33), 11617-11622.
25. Daly, J. W.; Spande, T. F.; Garraffo, H. M., *Journal of Natural Products* **2005**, *68* (10), 1556-1575.
26. Toyooka, N.; Zhou, D.; Nemoto, H.; Tezuka, Y.; Kadota, S.; Andriamaharavo, N. R.; Garraffo, H. M.; Spande, T. F.; Daly, J. W., *The Journal of Organic Chemistry* **2009**, *74* (17), 6784-6791.
27. Uchiyama, K.; Hayashi, Y.; Narasaka, K., *Tetrahedron* **1999**, *55* (29), 8915-8930.
28. Pedder, D. J.; Fales, H. M.; Jaouni, T.; Blum, M.; MacConnell, J.; Crewe, R. M., *Tetrahedron* **1976**, *32* (19), 2275-2279.
29. Barthelme, A.; Richards, D.; Mellor, I. R.; Stockman, R. A., *Chemical Communications* **2013**, *49* (89), 10507-10509.

30. Takahata, H.; Takahashi, S.; Azer, N.; Eldefrawi, A. T.; Eldefrawi, M. E., *Bioorganic & Medicinal Chemistry Letters* **2000**, *10* (11), 1293-1295.
31. Diseases and Conditions: Congenital myasthenic syndromes. <http://www.mayoclinic.org/diseases-conditions/congenital-myasthenic-syndrome/basics/definition/con-20034998> (accessed 16 September 2014).
32. Takano, S.; Otaki, S.; Ogasawara, K., *Journal of the Chemical Society, Chemical Communications* **1983**, (20), 1172-1174.
33. Takahata, H.; Bando, H.; Momose, T., *The Journal of Organic Chemistry* **1992**, *57* (16), 4401-4404.
34. Xiang, Y.-G.; Wang, X.-W.; Zheng, X.; Ruan, Y.-P.; Huang, P.-Q., *Chemical Communications* **2009**, (45), 7045-7047.
35. Vavrecka, M.; Janowitz, A.; Hesse, M., *Tetrahedron Letters* **1991**, *32* (40), 5543-5546.
36. Ciganek, E., *The Journal of Organic Chemistry* **1995**, *60* (18), 5803-5807.
37. Scarpi, D.; Occhiato, E. G.; Guarna, A., *The Journal of Organic Chemistry* **1999**, *64* (5), 1727-1732.
38. Dhimane, H.; Vanucci-Bacqué, C.; Hamon, L.; Lhommet, G., *European Journal of Organic Chemistry* **1998**, *1998* (9), 1955-1963.
39. Nobis, M.; Drießen-Hölscher, B., *Angewandte Chemie International Edition* **2001**, *40* (21), 3983-3985.
40. Yamamoto, Y.; Radhakrishnan, U., *Chemical Society Reviews* **1999**, *28* (3), 199-207.
41. Senn, H. M.; Blöchl, P. E.; Togni, A., *Journal of the American Chemical Society* **2000**, *122* (17), 4098-4107.
42. Pohlki, F.; Doye, S., *Chemical Society Reviews* **2003**, *32* (2), 104-114.
43. Enders, D.; Schaumann, E., *Science of Synthesis: Houben-Weyl Methods of Molecular Transformations*. Georg Thieme Verlag KG: Stuttgart, 2009; Vol. 40a, p 241-304.
44. Togni, A.; Grützmaier, H., *Catalytic Heterofunctionalization*. Wiley-VCH: Weinheim, 2001.
45. Severin, R.; Doye, S., *Chemical Society Reviews* **2007**, *36* (9), 1407-1420.

46. Cornils, B.; Herrmann, W. A., *Applied Homogeneous Catalysis with Organometallic Compounds*. Wiley-VCH: Weinheim, 2000.
47. Martinez, P. H.; Hultsch, K. C.; Hampel, F., *Chemical Communications* **2006**, (21), 2221-2223.
48. Siddiqui, I. R.; Abumhdi, A. A. H.; Shamim, S.; Shireen; Waseem, M. A.; Rahila; Srivastava, A.; Srivastava, A., *RSC Advances* **2013**, 3 (26), 10173-10176.
49. Li, Z.; Zhang, J.; Brouwer, C.; Yang, C.-G.; Reich, N. W.; He, C., *Organic Letters* **2006**, 8 (19), 4175-4178.
50. Shapiro, N. D.; Rauniyar, V.; Hamilton, G. L.; Wu, J.; Toste, F. D., *Nature* **2011**, 470 (7333), 245-249.
51. Straub, T.; Haskel, A.; Neyroud, T. G.; Kapon, M.; Botoshansky, M.; Eisen, M. S., *Organometallics* **2001**, 20 (24), 5017-5035.
52. Casalnuovo, A. L.; Calabrese, J. C.; Milstein, D., *Journal of the American Chemical Society* **1988**, 110 (20), 6738-6744.
53. Mizushima, E.; Hayashi, T.; Tanaka, M., *Organic Letters* **2003**, 5 (18), 3349-3352.
54. Clayden, J.; Greeves, N.; Warren, S.; Wothers, P., *Organic Chemistry*. 1st ed.; Oxford University Press: Oxford, 2009; p 1040-1041.
55. Deslongchamps, P., *Stereoelectronic Effects in Organic Chemistry*. 1st ed.; Pergamon Press: Oxford, 1983; Vol. 1.
56. Alabugin, I. V.; Gilmore, K., *Chemical Communications* **2013**, 49 (96), 11246-11250.
57. Tillack, A.; Garcia Castro, I.; Hartung, C. G.; Beller, M., *Angewandte Chemie International Edition* **2002**, 41 (14), 2541-2543.
58. Chai, Z.; Hua, D.; Li, K.; Chu, J.; Yang, G., *Chemical Communications* **2014**, 50 (2), 177-179.
59. Gribkov, D. V.; Hultsch, K. C.; Hampel, F., *Journal of the American Chemical Society* **2006**, 128 (11), 3748-3759.
60. Molander, G. A.; Dowdy, E. D., *The Journal of Organic Chemistry* **1998**, 63 (24), 8983-8988.
61. Trinh, T. T. H.; Nguyen, K. H.; de Aguiar Amaral, P.; Gouault, N., *Beilstein Journal of Organic Chemistry* **2013**, 9, 2042-2047.

62. Dion, I.; Vincent-Rocan, J.-F.; Zhang, L.; Cebrowski, P. H.; Lebrun, M.-E.; Pfeiffer, J. Y.; Bédard, A.-C.; Beauchemin, A. M., *The Journal of Organic Chemistry* **2013**, *78* (24), 12735-12749.
63. Tian, S.; Arredondo, V. M.; Stern, C. L.; Marks, T. J., *Organometallics* **1999**, *18* (14), 2568-2570.
64. Gravestock, D.; Dovey, M. C., *Synthesis* **2003**, *2003* (09), 1470-1470.
65. Robinson, R. S.; Dovey, M. C.; Gravestock, D., *Tetrahedron Letters* **2004**, *45* (36), 6787-6789.
66. Robinson, R. S.; Dovey, M. C.; Gravestock, D., *European Journal of Organic Chemistry* **2005**, *2005* (3), 505-511.
67. Prior, A. M.; Robinson, R. S., *Tetrahedron Letters* **2008**, *49* (3), 411-414.
68. Prior, A. M. The Use of Hydroamination in the Attempted Synthesis of Ant Alkaloid 223H (xenovevine). Master's Thesis, University of KwaZulu-Natal, 2008.
69. Ding, R.; He, Y.; Wang, X.; Xu, J.; Chen, Y.; Feng, M.; Qi, C., *Molecules* **2011**, *16* (7), 5665-5673.
70. Williams, G. D.; Wade, C. E.; Clarkson, G. J.; Wills, M., *Tetrahedron: Asymmetry* **2007**, *18* (5), 664-670.
71. Feng, M.; Jiang, X., *Chemical Communications* **2014**, *50* (68), 9690-9692.
72. Harris, P. W. R.; Brimble, M. A., *Organic & Biomolecular Chemistry* **2006**, *4* (14), 2696-2709.
73. Moloney, M. G.; Panchal, T.; Pike, R., *Organic & Biomolecular Chemistry* **2006**, *4* (21), 3894-3897.
74. Villeneuve, P.; Barēa, B.; Sarrazin, P.; Davrieux, F.; Boulanger, R.; Caro, Y.; Figueroa-Espinoza, M. C.; Pina, M.; Graille, J., *Enzyme and Microbial Technology* **2003**, *33* (1), 79-84.
75. Janse Van Rensburg, C. K. A. Progress Towards the Synthesis of Indolizidine Alkaloid 223AB. Master's Thesis, University of KwaZulu-Natal, 2008.
76. Alonso, D. A.; Ájera, C. N., Desulfonylation Reactions. In *Organic Reactions*, Denmark, S. E., Ed. John Wiley & Sons, Inc.: New Jersey, 2004; Vol. 72, pp 367-656.
77. Morita, J.-i.; Nakatsuji, H.; Misaki, T.; Tanabe, Y., *Green Chemistry* **2005**, *7* (10), 711.
78. March, J., *Advanced Organic Chemistry: Reactions, Mechanisms, and Structure*. 4th ed.; Wiley Interscience: New York, 1992; p 392, 418.

79. Mason, T. J., *Chemical Society Reviews* **1997**, 26 (6), 443-451.
80. Nájera, C.; Yus, M., *Tetrahedron* **1999**, 55 (35), 10547-10658.
81. Fossey, J.; Lefort, D.; Sorba, J., *Free Radicals in Organic Chemistry*. John Wiley & Sons: Chichester, 1997.
82. Mill, T.; Stringham, R. S., *Tetrahedron Letters* **1969**, 10 (23), 1853-1856.
83. Cava, M. P.; Levinson, M. I., *Tetrahedron* **1985**, 41 (22), 5061-5087.
84. Jesberger, M.; Davis, T. P.; Barner, L., *Synthesis* **2003**, 2003 (13), 1929-1958.
85. Ozturk, T.; Ertas, E.; Mert, O., *Chemical Reviews* **2007**, 107 (11), 5210-5278.
86. Ferraz, H. M. C.; de Oliveira, E. O.; Payret-Arrua, M. E.; Brandt, C. A., *The Journal of Organic Chemistry* **1995**, 60 (22), 7357-7359.
87. Celerier, J. P.; Deloisy, E.; Lhommet, G.; Maitte, P., *The Journal of Organic Chemistry* **1979**, 44 (17), 3089-3089.
88. Lambert, P. H.; Vaultier, M.; Carrie, R., *The Journal of Organic Chemistry* **1985**, 50 (25), 5352-5356.
89. Trost, B. M., *Comprehensiv Organic Synthesis*. Pergamon Press: Oxford, UK, 1991; Vol. 2, p 865-892.
90. Neto, B. A. D.; Lapis, A. A. M.; Bernd, A. B.; Russowsky, D., *Tetrahedron* **2009**, 65 (12), 2484-2496.
91. Russowsky, D.; da Silveira Neto, B. A., *Tetrahedron Letters* **2004**, 45 (7), 1437-1440.
92. Michael, J. P.; Jungmann, C. M., *Tetrahedron* **1992**, 48 (46), 10211-10220.
93. Michael, J. P.; Parsons, A. S., *Tetrahedron* **1996**, 52 (6), 2199-2216.
94. Dovey, M. C. Silver-catalysed hydroamination: synthesis of functionalised pyrroles. Doctoral Thesis, University of Kwa-Zulu Natal, 2004.
95. Michael, J. P.; Koning, C. B.; San Fat, C.; Natrass, G. L., *Archive of Organic Chemistry* **2002**, (ix), 62-77.

96. Bacos, D.; Célérier, J. P.; Marx, E.; Rosset, S.; Lhommet, G., *Journal of Heterocyclic Chemistry* **1990**, 27 (5), 1387-1392.
97. Lamourex, G.; Agüero, C., *Archive of Organic Chemistry* **2009**, 2009 (1), 251-264.
98. Wyatt, M. D.; Pittman, D. L., *Chemical Research in Toxicology* **2006**, 19 (12), 1580-1594.
99. Tundo, P.; Selva, M., *Accounts of Chemical Research* **2002**, 35 (9), 706-716.
100. Elliott, M. C.; Wordingham, S. V., *Synthesis* **2006**, 2006 (07), 1162-1170.
101. Michael, J. P.; Koning, C. B.; Gravestock, D.; Hosken, G. D.; Howard, A. S.; Jungmann, C. M.; Krause, R., W.M.; Parsons, A. S.; Pelly, S.; Stanbury, T. V., *Pure and Applied Chemistry* **1999**, 71, 979-988.
102. Meldrum, A. N., *Journal of the Chemical Society, Transactions* **1908**, 93 (0), 598-601.
103. Davidson, D.; Bernhard, S. A., *Journal of the American Chemical Society* **1948**, 70 (10), 3426-3428.
104. McNab, H., *Chemical Society Reviews* **1978**, 7 (3), 345-358.
105. Oikawa, Y.; Hirasawa, H.; Yonemitsu, O., *Tetrahedron Letters* **1978**, 19 (20), 1759-1762.
106. Pflüger, C. E.; Boyle, P. D., *Journal of the Chemical Society, Perkin Transactions 2* **1985**, (10), 1547-1549.
107. Harwood, L. M.; Claridge, T. D. W., *Introduction to organic spectroscopy*. Oxford University Press: Oxford, 1997; p 42-53.
108. Mackie, R. K.; Smith, D. M., *Guidebook to Organic Synthesis*. Longman: Essex, 1982; p 268-269.
109. Müller, T. E.; Grosche, M.; Herdtweck, E.; Pleier, A.-K.; Walter, E.; Yan, Y.-K., *Organometallics* **2000**, 19 (2), 170-183.
110. Aberg, V.; Norman, F.; Chorell, E.; Westermark, A.; Olofsson, A.; Sauer-Eriksson, A. E.; Almqvist, F., *Organic & Biomolecular Chemistry* **2005**, 3 (15), 2817-2823.
111. Despinoy, X. L. M.; McNab, H., *Organic & Biomolecular Chemistry* **2009**, 7 (21), 4502-4511.
112. Bruker APEX2, SAINT and SADABS. Bruker AXS Inc., Madison, Wisconsin, USA., 2012.

113. Sheldrick, G., *Acta Crystallographica Section A* **2008**, *64* (1), 112-122.
114. Farrugia, L., *Journal of Applied Crystallography* **2012**, *45* (4), 849-854.
115. Xiao, J.-M.; Feng, L.; Zhou, L.-S.; Gao, H.-Z.; Zhang, Y.-L.; Yang, K.-W., *European Journal of Medicinal Chemistry* **2013**, *59*, 150-159.
116. Nickel(II) acetylacetonate.
<http://www.sigmaaldrich.com/catalog/product/aldrich/283657?lang=en®ion=ZA>
(accessed 23 November 2015).
117. Elliott, M. C.; Long, M. S., *Organic & Biomolecular Chemistry* **2004**, *2* (14), 2003-2011.
118. L-Pyroglutamic acid ethyl ester.
<http://www.sigmaaldrich.com/catalog/product/sial/83175?lang=en®ion=ZA> (accessed 11 November 2015).
119. Hashimoto, M.; Matsumoto, M.; Terashima, S., *Tetrahedron* **2003**, *59* (17), 3019-3040.
120. Bateman, L.; Breeden, S. W.; O'Leary, P., *Tetrahedron: Asymmetry* **2008**, *19* (3), 391-396.
121. Hjelmgard, T.; Sjøtofte, I.; Tanner, D., *The Journal of Organic Chemistry* **2005**, *70* (14), 5688-5697.
122. Occhiato, E. G.; Prandi, C.; Ferrali, A.; Guarna, A., *The Journal of Organic Chemistry* **2005**, *70* (11), 4542-4545.
123. Provot, O.; Celerier, J. P.; Petit, H.; Lhommet, G., *The Journal of Organic Chemistry* **1992**, *57* (7), 2163-2166.
124. Calvet-Vitale, S.; Vanucci-Bacqu , C.; Fargeau-Bellassoued, M.-C.; Lhommet, G., *Tetrahedron* **2005**, *61* (32), 7774-7782.

Appendix

All IR data, GC-MS data, HRMS data and original NMR fid files are available on the accompanying CD. All NMR data not included in this document are also available. The X-ray cif file is included as well as a pdf copy of this thesis.

Appendix

A. Infrared Spectra

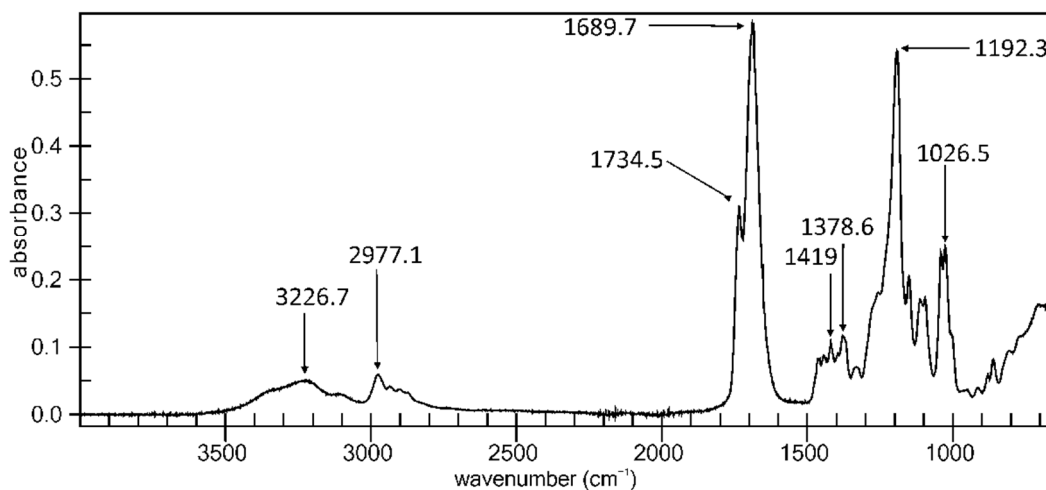


Figure A1: Infrared spectrum for ethyl (2S)-5-oxopyrrolidine-2-carboxylate 120

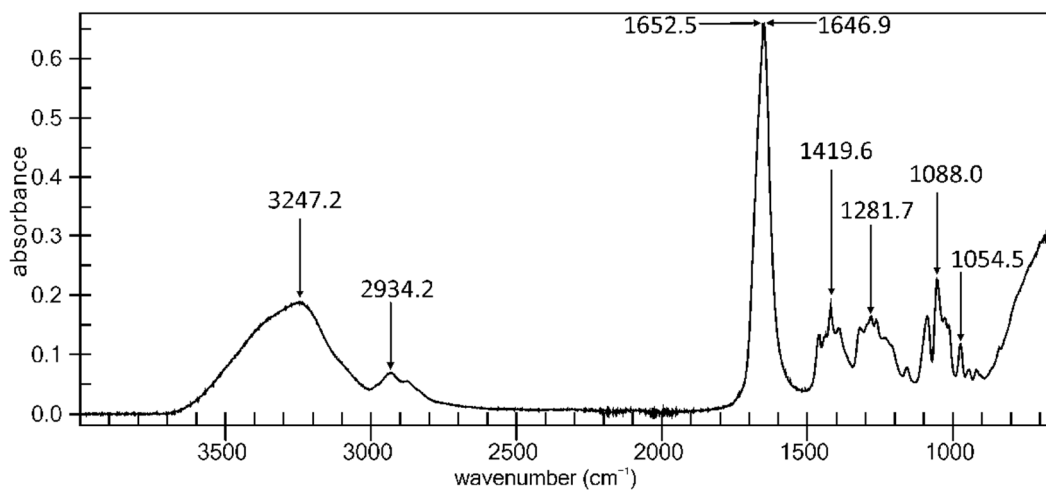


Figure A2: Infrared spectrum for (5S)-5-(hydroxymethyl)tetrahydro-2H-pyrrol-2-one 121

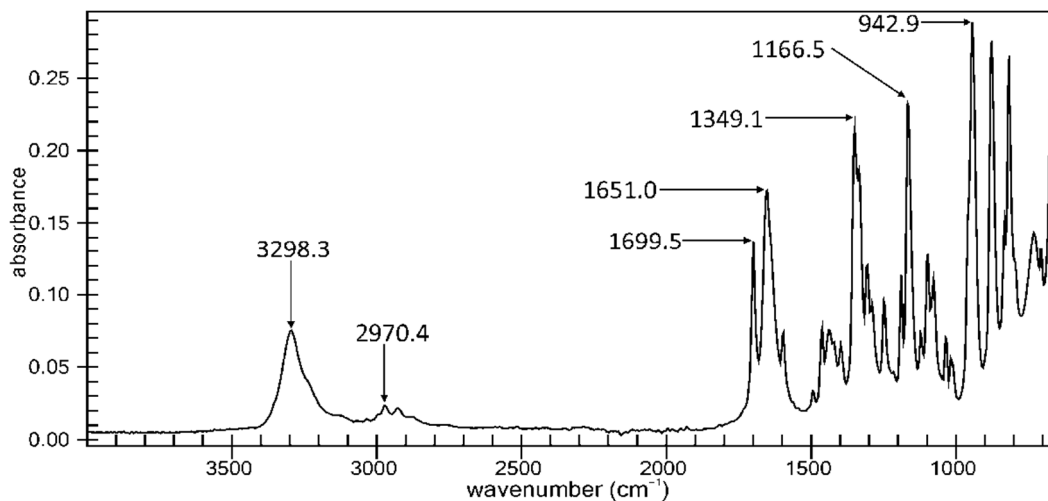


Figure A3: Infrared spectrum for [(2S)-5-oxotetrahydro-1H-pyrrol-2-yl]methyl 4-methylbenzenesulfonate 122

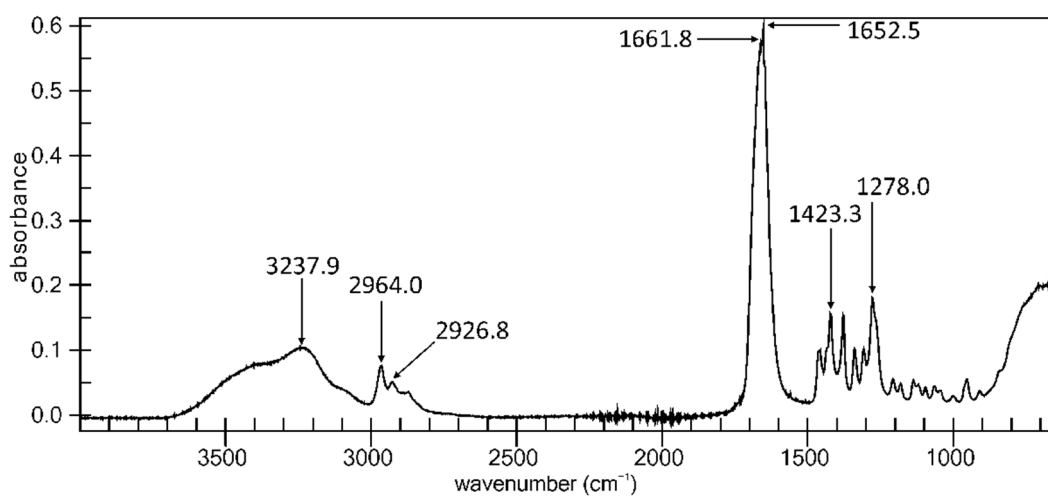


Figure A4: Infrared spectrum for (5R)-5-methyltetrahydro-2H-pyrrol-2-one 123

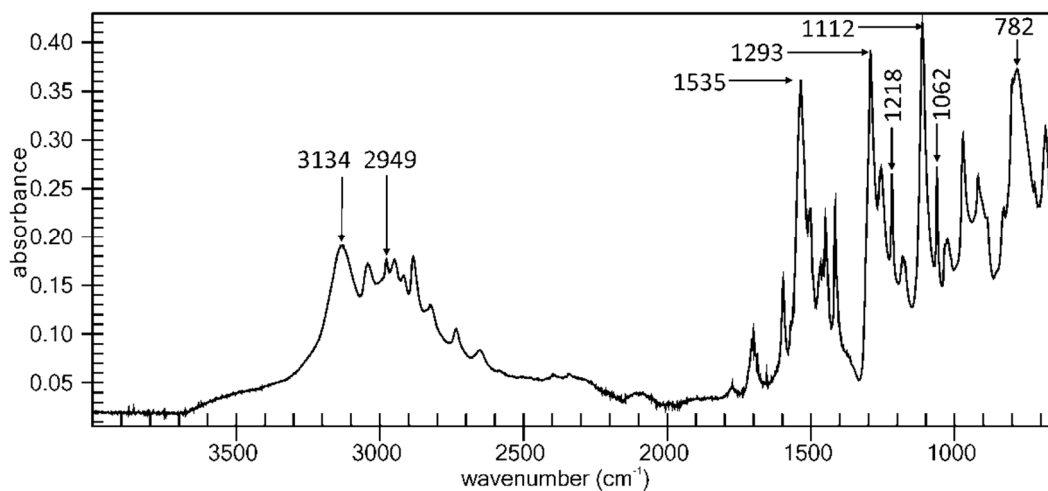


Figure A5: Infrared spectrum for (5R)-5-methyltetrahydro-2H-pyrrole-2-thione 124

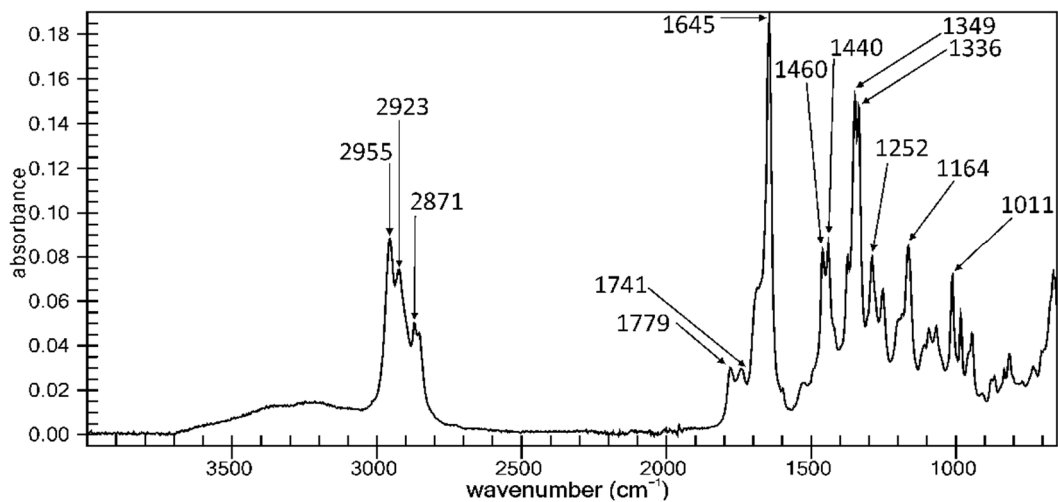


Figure A6: Infrared spectrum for (2R)-3,4-dihydro-5-methoxy-2-methyl-2H-pyrrole 135

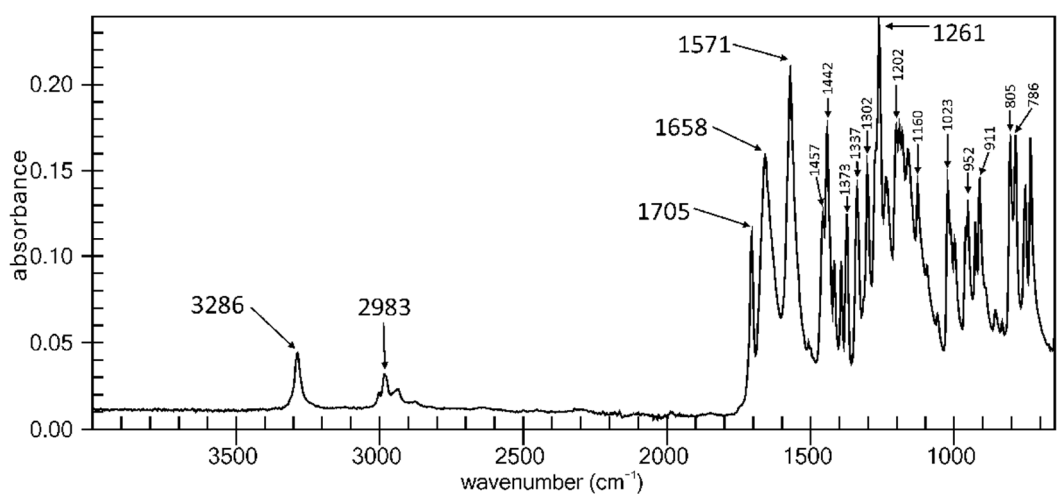


Figure A7: Infrared spectrum for 2,2-dimethyl-5-[(5R)-5-methyl-2-pyrrolidinylidene]-1,3-dioxane-4,6-dione 136

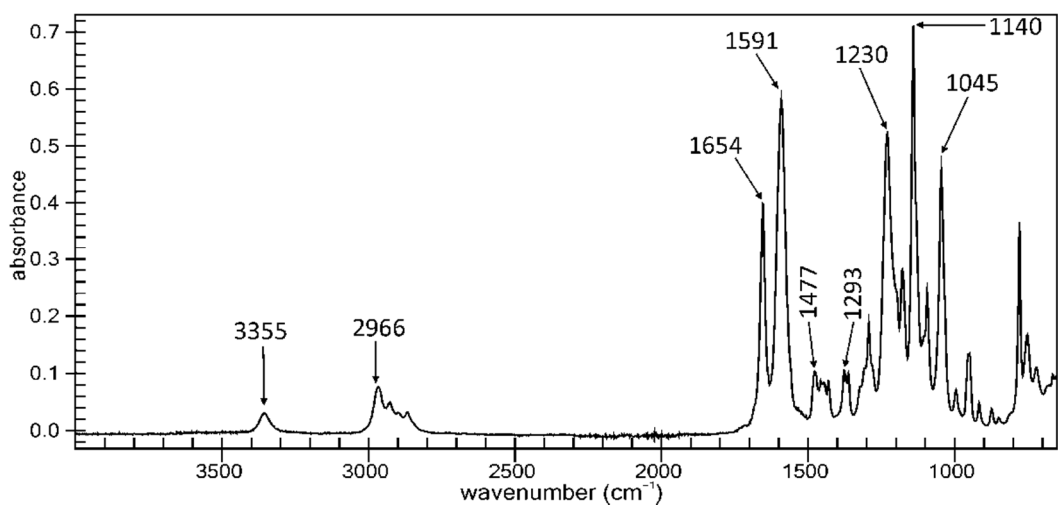


Figure A8: Infrared spectrum for ethyl 2-[(5R)-5-methyltetrahydro-2H-pyrrol-2-ylidene]acetate 127

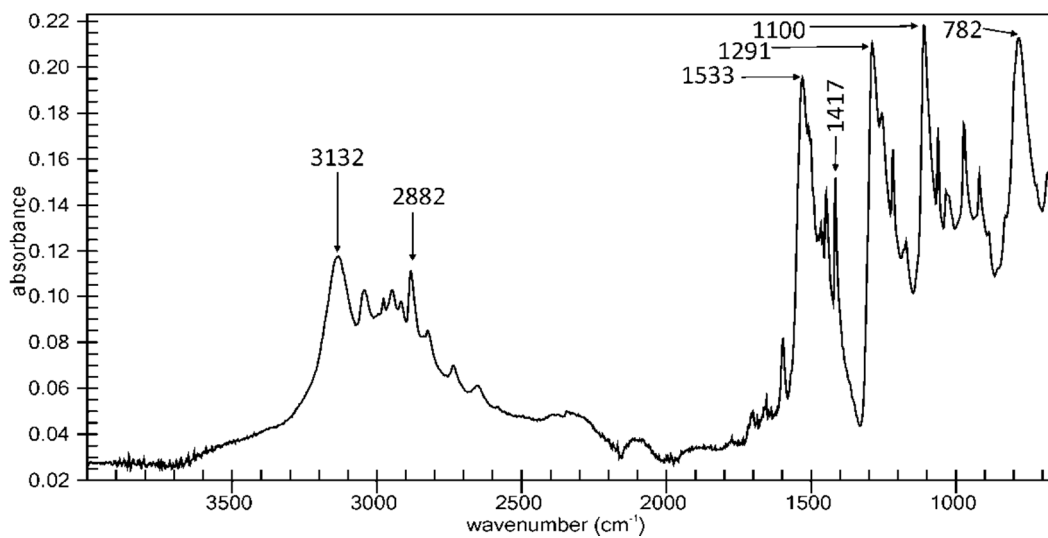


Figure A9: Infrared spectrum for 2-pyrrolidinethione 116

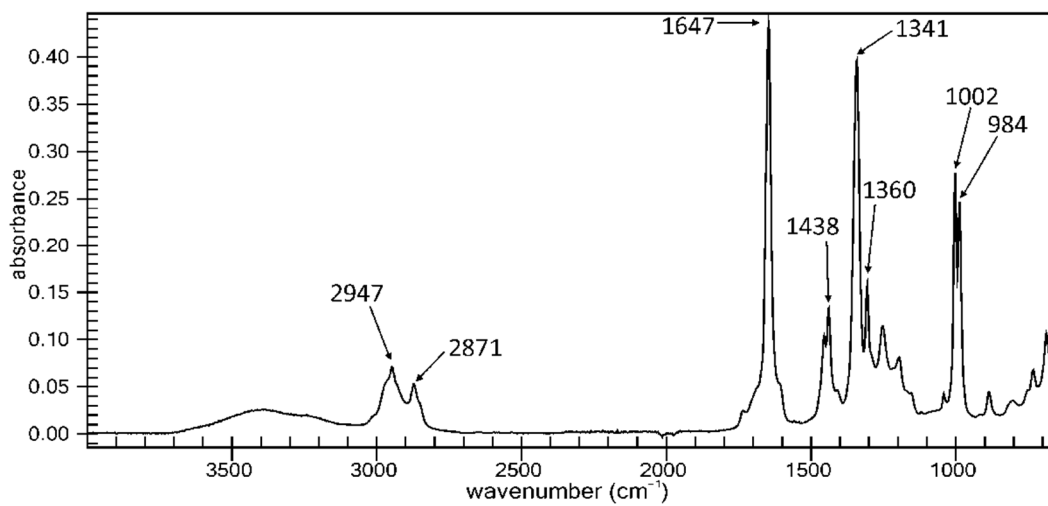


Figure A10: Infrared spectrum for 3,4-dihydro-5-methoxy-2H-pyrrole 133

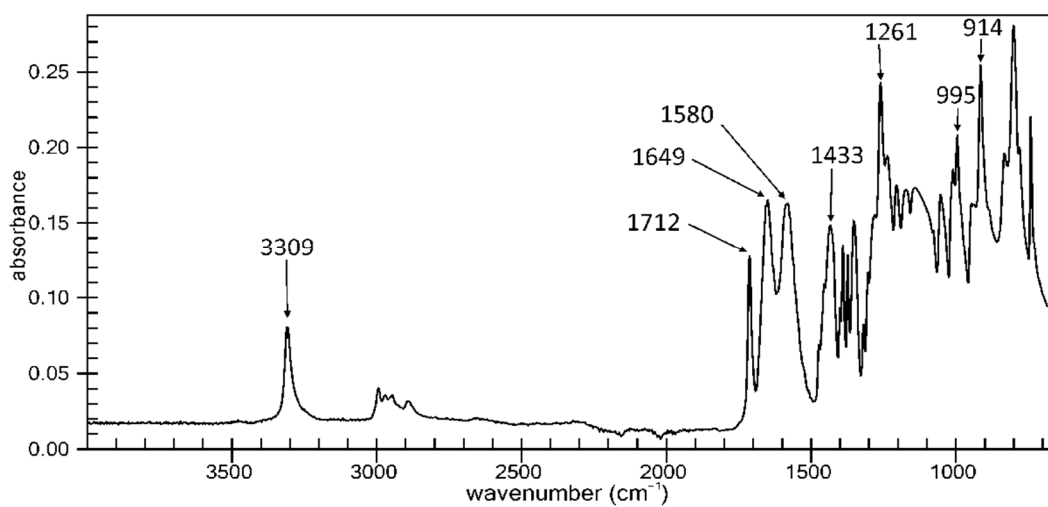


Figure A11: Infrared spectrum for 2,2-dimethyl-5-(2-pyrrolidinylidene)1,3-dioxane-4,6-dione 134

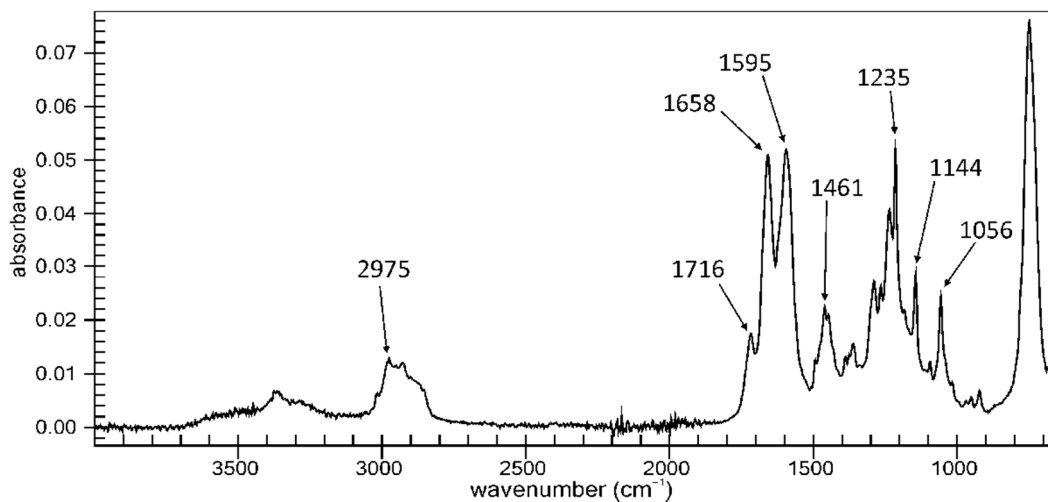


Figure A12: Infrared spectrum for (2Z)-pyrrolidinylidene ethyl ester 111

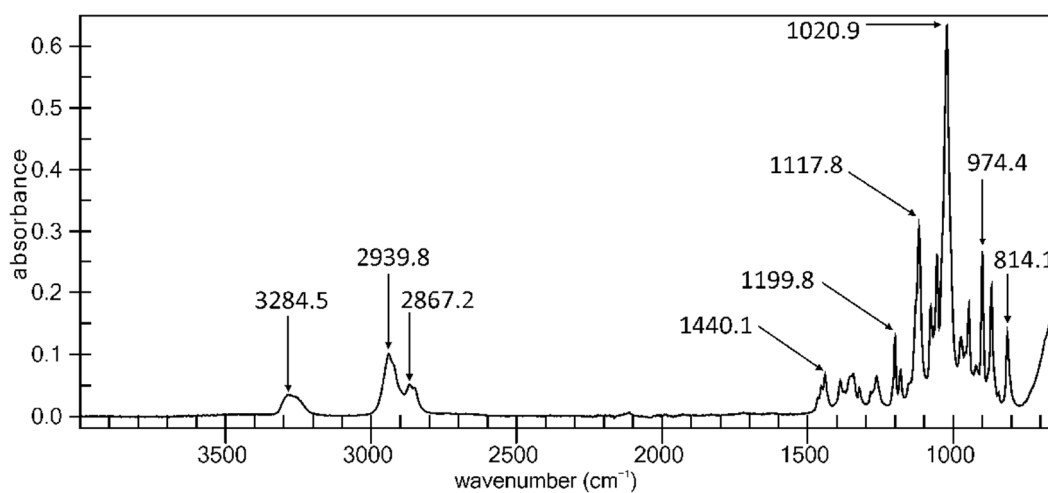


Figure A13: Infrared spectrum for 2-propynyl tetrahydro-2H-pyran-2-yl ether 138

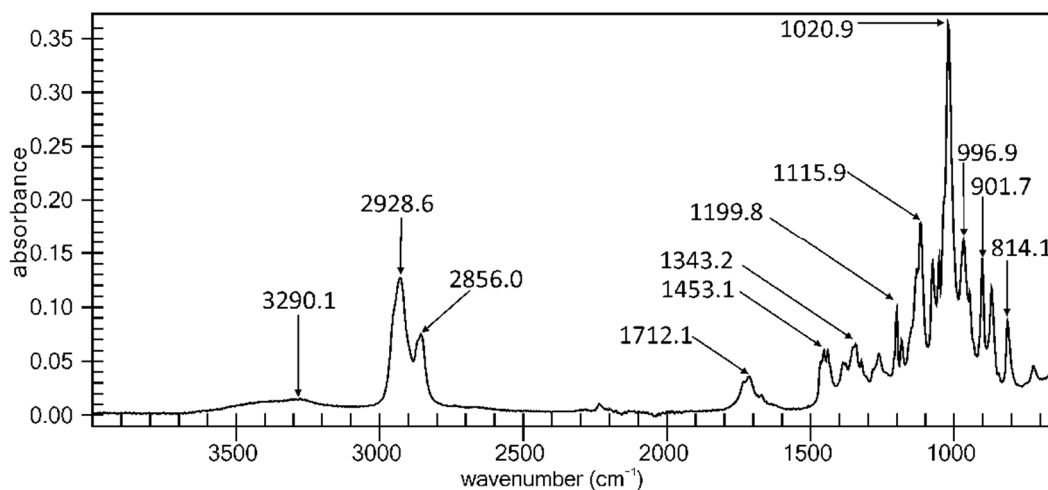


Figure A14: Infrared spectrum for 2-nonyl tetrahydro-2H-pyran-2-yl ether 139

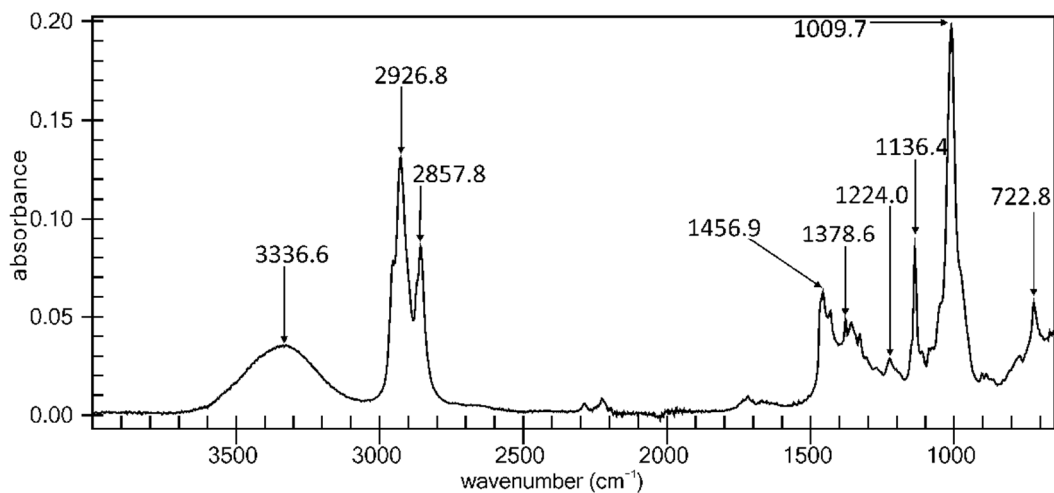


Figure A15: Infrared spectrum for 2-nonyl-1-ol 142

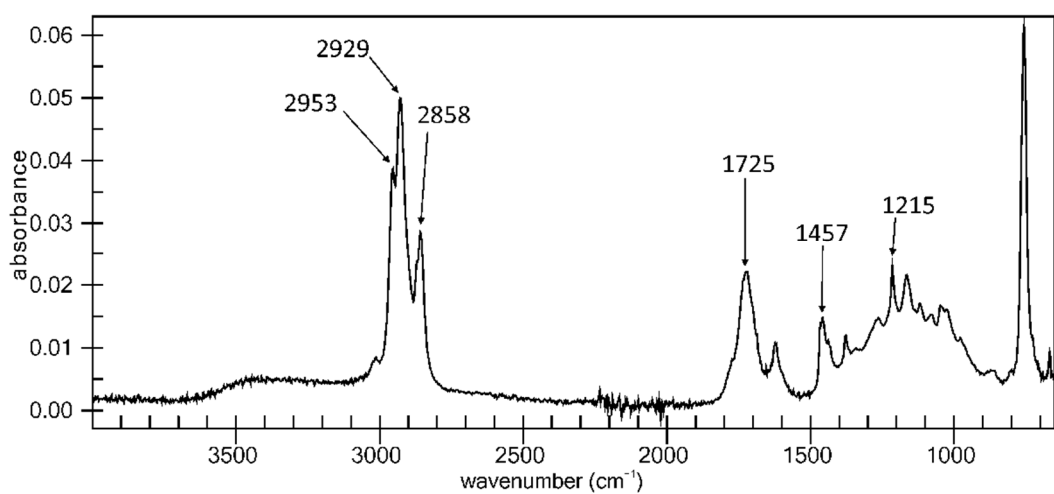


Figure A16: Infrared spectrum for 1-bromo-2-nonyne 131

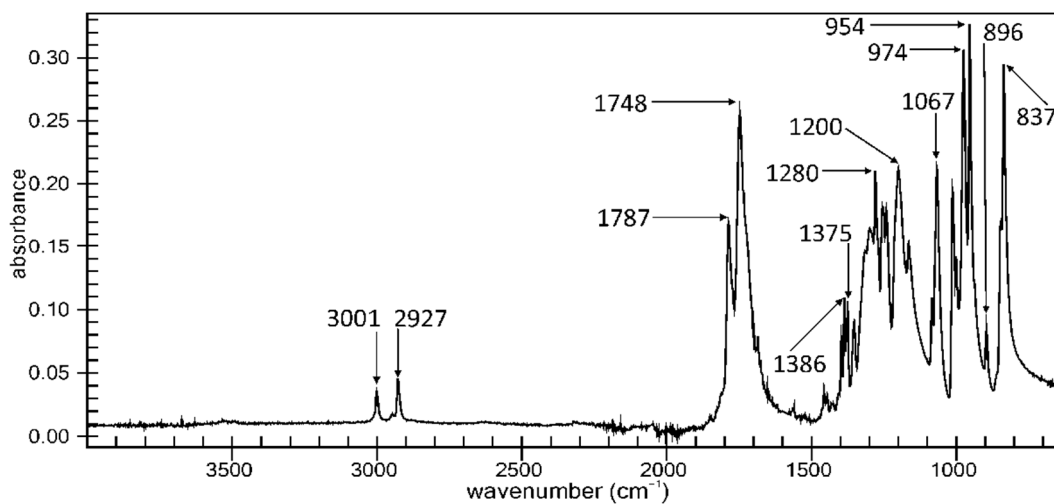


Figure A17: Infrared spectrum for 2,2-dimethyl-1,3-dioxane-4,6-dione (Meldrum's acid)

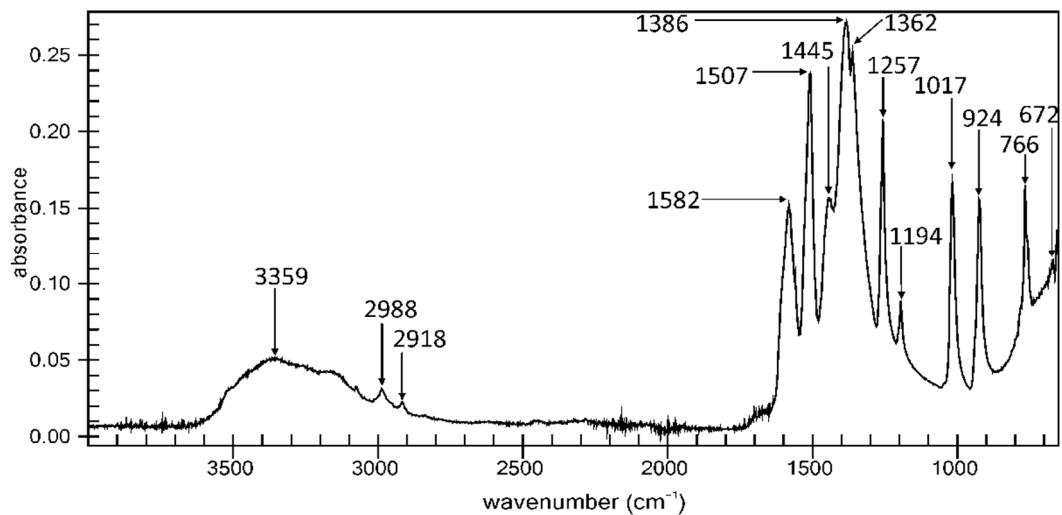


Figure A18: Infrared spectrum for nickel(II) acetylacetonate [Ni(acac)₂]

Appendix

B. CheckCIF for X-ray crystallographic data

checkCIF/PLATON report

Structure factors have been supplied for datablock(s) shelx

THIS REPORT IS FOR GUIDANCE ONLY. IF USED AS PART OF A REVIEW PROCEDURE FOR PUBLICATION, IT SHOULD NOT REPLACE THE EXPERTISE OF AN EXPERIENCED CRYSTALLOGRAPHIC REFEREE.

No syntax errors found. CIF dictionary Interpreting this report

Datablock: shelx

Bond precision:	C-C = 0.0026 Å	Wavelength=0.71073	
Cell:	a=7.1937 (5)	b=10.2039 (7)	c=7.3613 (5)
	alpha=90	beta=91.096 (3)	gamma=90
Temperature:	100 K		

	Calculated	Reported
Volume	540.25 (6)	540.25 (6)
Space group	P 21	P 21
Hall group	P 2yb	P 2yb
Moiety formula	C11 H15 N O4	C11 H15 N O4
Sum formula	C11 H15 N O4	C11 H15 N O4
Mr	225.24	225.24
Dx, g cm ⁻³	1.385	1.385
Z	2	2
Mu (mm ⁻¹)	0.106	0.106
F000	240.0	240.0
F000'	240.13	
h, k, lmax	9, 13, 10	9, 13, 10
Nref	2844 [1498]	2823
Tmin, Tmax	0.971, 0.988	0.965, 0.988
Tmin'	0.965	

Correction method= # Reported T Limits: Tmin=0.965 Tmax=0.988
AbsCorr = MULTI-SCAN

Data completeness= 1.88/0.99 Theta (max)= 28.973

R(reflections)= 0.0310 (2745) wR2(reflections)= 0.0845 (2823)

S = 1.073 Npar= 148

The following ALERTS were generated. Each ALERT has the format
test-name ALERT alert-type alert-level.
Click on the hyperlinks for more details of the test.

Alert level C

STRVA01_ALERT_4_C Flack parameter is too small
From the CIF: `_refine_ls_abs_structure_Flack -0.300`
From the CIF: `_refine_ls_abs_structure_Flack_su 0.300`

Alert level G

PLAT007_ALERT_5_G Number of Unrefined Donor-H Atoms 1 Report
PLAT032_ALERT_4_G Std. Uncertainty on Flack Parameter Value High . 0.300 Report
PLAT066_ALERT_1_G Predicted and Reported Tmin&Tmax Range Identical ? Check
PLAT791_ALERT_4_G The Model has Chirality at C6 (Chiral SPGR) R Verify
PLAT912_ALERT_4_G Missing # of FCF Reflections Above STh/L= 0.600 3 Note

0 **ALERT level A** = Most likely a serious problem - resolve or explain
0 **ALERT level B** = A potentially serious problem, consider carefully
1 **ALERT level C** = Check. Ensure it is not caused by an omission or oversight
5 **ALERT level G** = General information/check it is not something unexpected
1 ALERT type 1 CIF construction/syntax error, inconsistent or missing data
0 ALERT type 2 Indicator that the structure model may be wrong or deficient
0 ALERT type 3 Indicator that the structure quality may be low
4 ALERT type 4 Improvement, methodology, query or suggestion
1 ALERT type 5 Informative message, check

It is advisable to attempt to resolve as many as possible of the alerts in all categories. Often the minor alerts point to easily fixed oversights, errors and omissions in your CIF or refinement strategy, so attention to these fine details can be worthwhile. In order to resolve some of the more serious problems it may be necessary to carry out additional measurements or structure refinements. However, the purpose of your study may justify the reported deviations and the more serious of these should normally be commented upon in the discussion or experimental section of a paper or in the "special_details" fields of the CIF. checkCIF was carefully designed to identify outliers and unusual parameters, but every test has its limitations and alerts that are not important in a particular case may appear. Conversely, the absence of alerts does not guarantee there are no aspects of the results needing attention. It is up to the individual to critically assess their own results and, if necessary, seek expert advice.

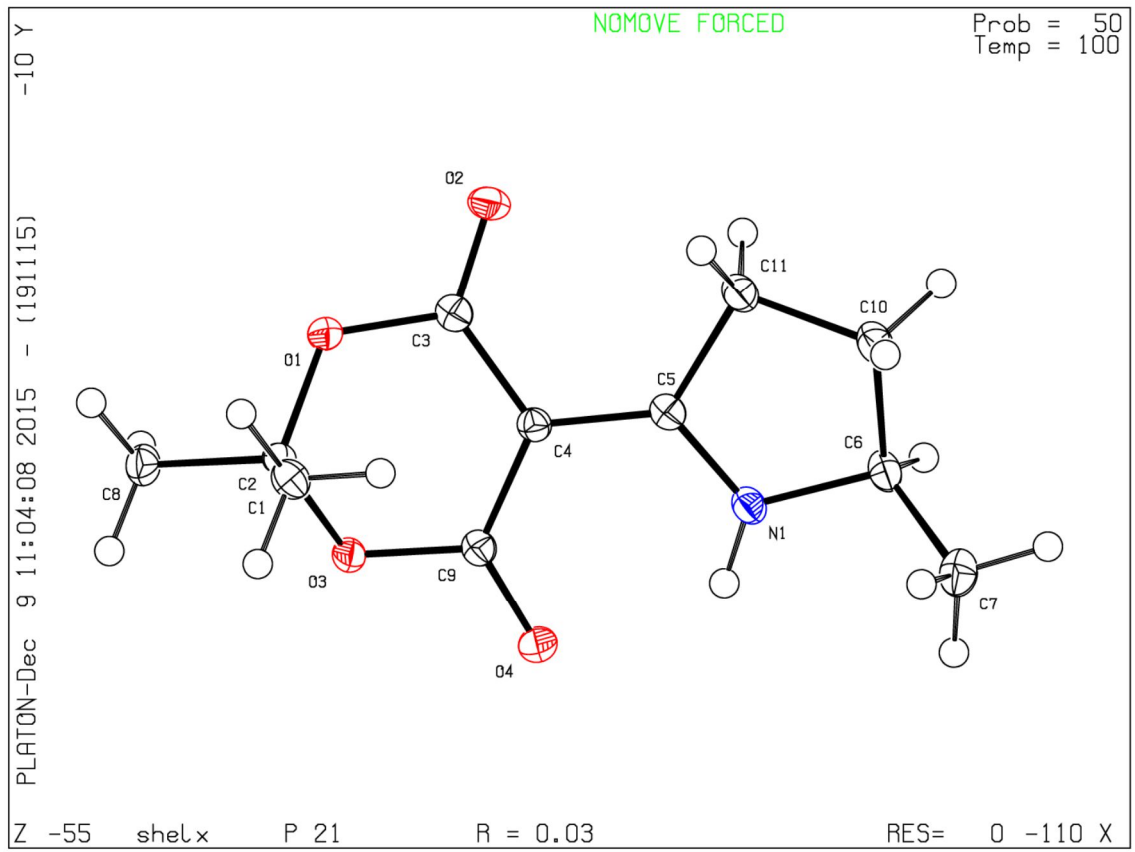
Publication of your CIF in IUCr journals

A basic structural check has been run on your CIF. These basic checks will be run on all CIFs submitted for publication in IUCr journals (*Acta Crystallographica*, *Journal of Applied Crystallography*, *Journal of Synchrotron Radiation*); however, if you intend to submit to *Acta Crystallographica Section C* or *E*, you should make sure that full publication checks are run on the final version of your CIF prior to submission.

Publication of your CIF in other journals

Please refer to the *Notes for Authors* of the relevant journal for any special instructions relating to CIF submission.

PLATON version of 19/11/2015; check.def file version of 17/11/2015



Appendix

C. NMR Spectra

The following spectra were not included in Chapter 2: Results and Discussion. The fid files for all spectra are included on the accompanying CD.

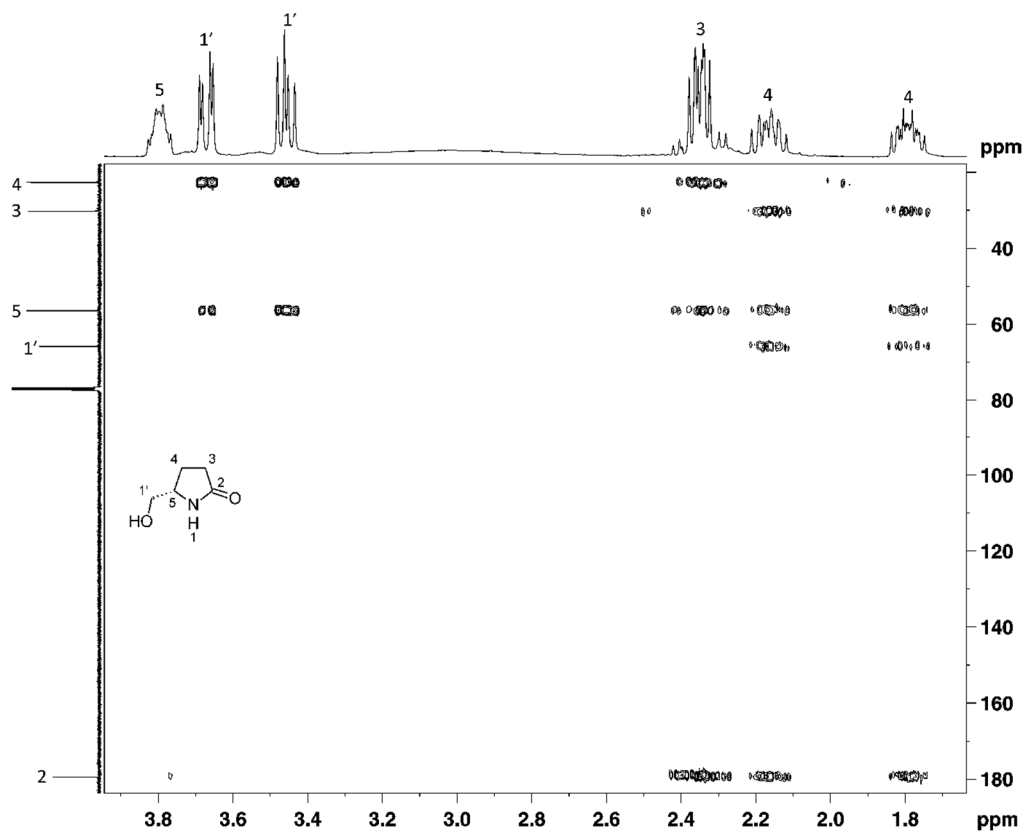


Figure C1: 2D HMBC Spectrum for (5S)-(hydroxymethyl)tetrahydro-2H-pyrrol-2-one 121

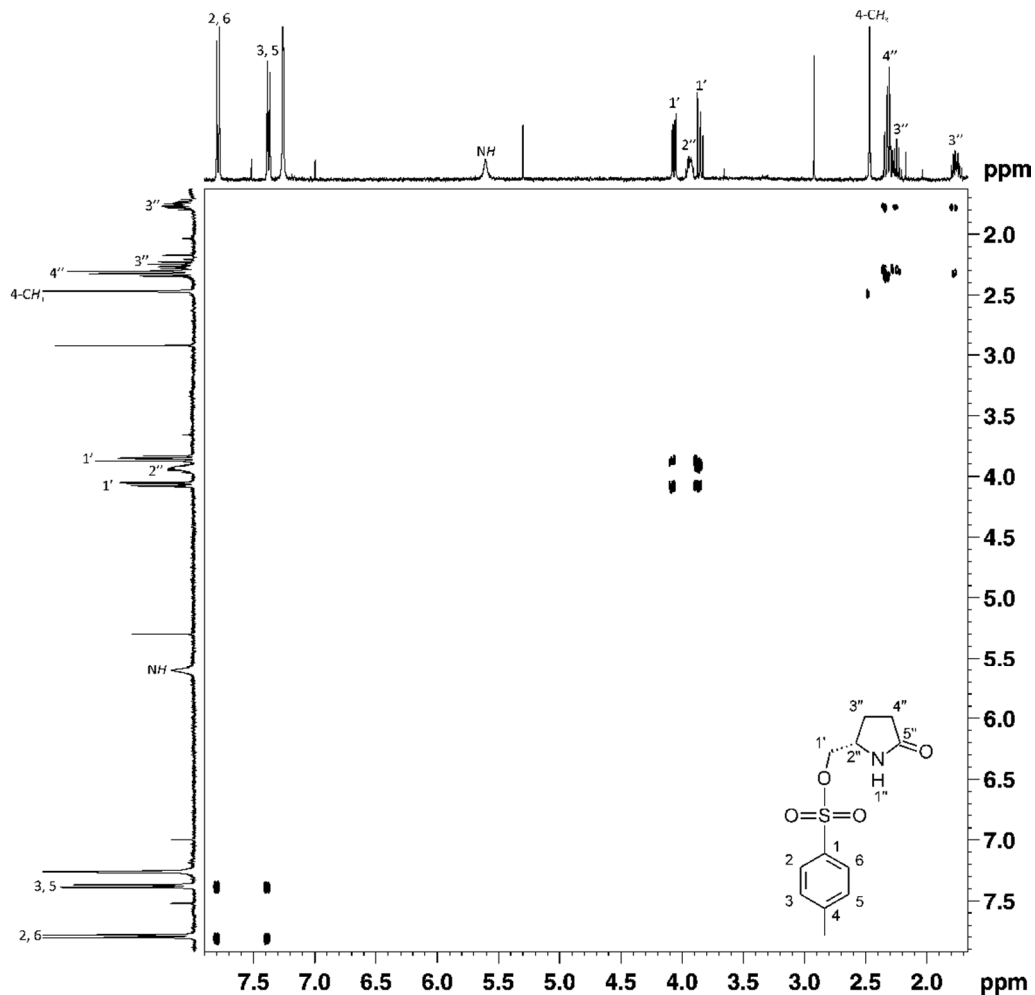


Figure C2: 2D COSY NMR Spectrum for [(2S)-5-oxotetrahydro-1H-pyrrol-2-yl]methyl 4-methylbenzenesulfonate 122

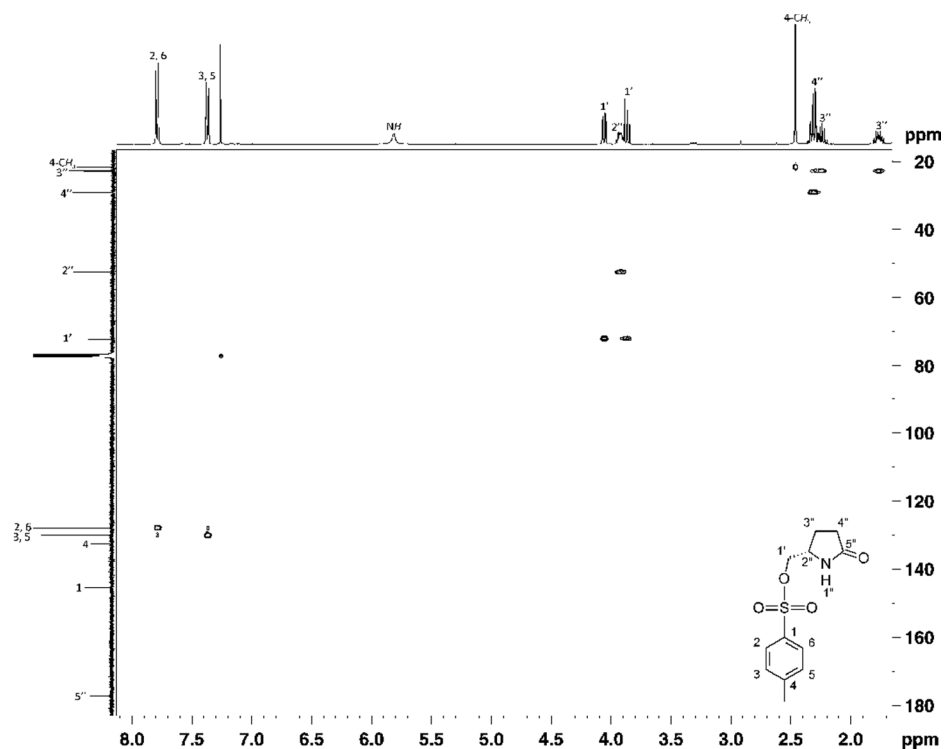


Figure C3: 2D HSQC NMR Spectrum for [(2S)-5-oxotetrahydro-1H-pyrrol-2-yl]methyl 4-methylbenzenesulfonate 122

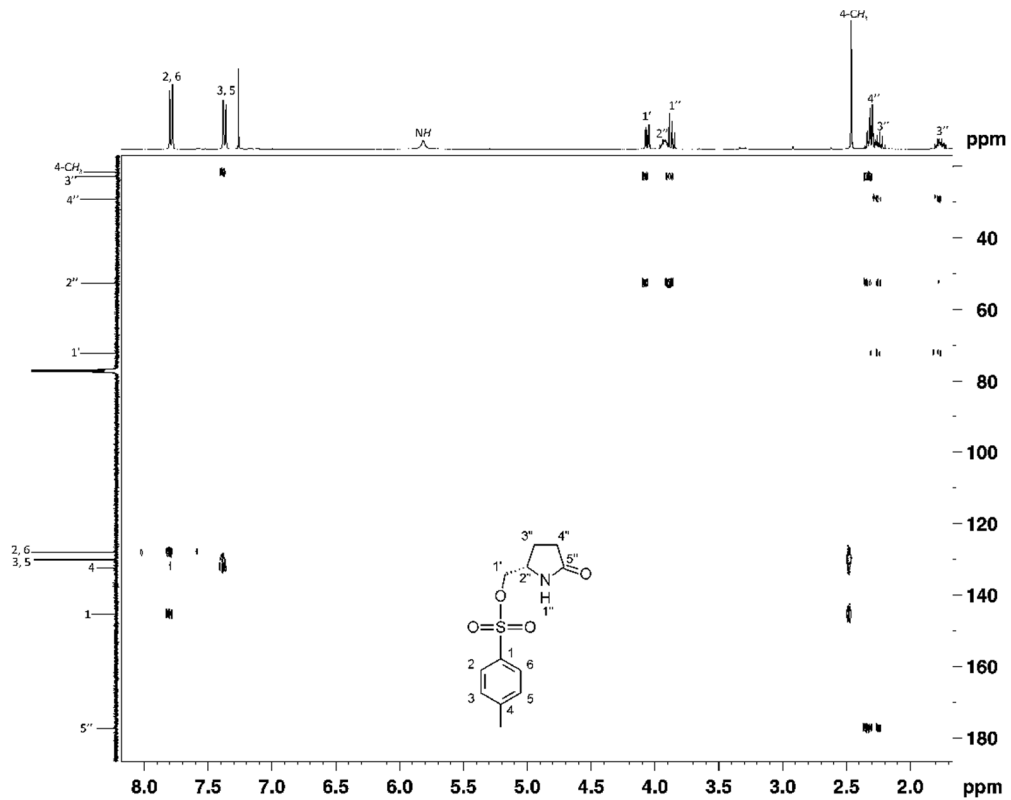


Figure C4: 2D HMBC NMR Spectrum for [(2S)-5-oxotetrahydro-1H-pyrrol-2-yl]methyl 4-methylbenzenesulfonate 122

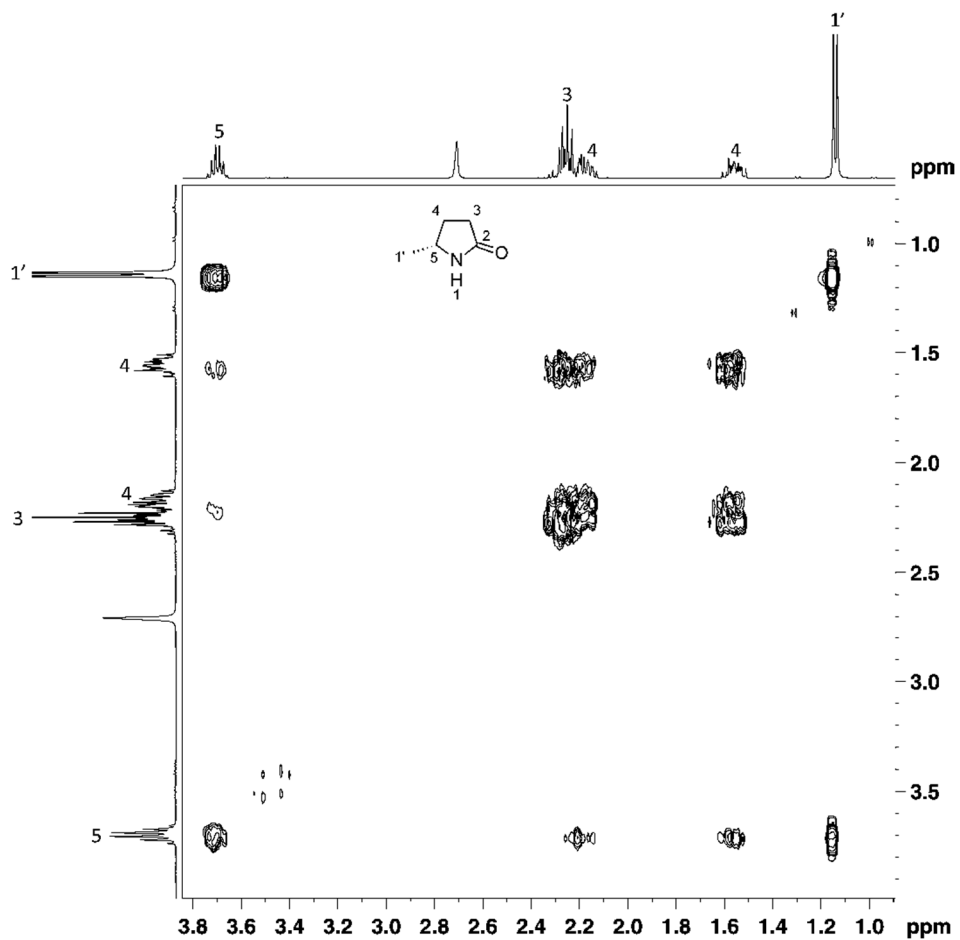


Figure C5: 2D COSY NMR Spectrum for (5R)-5-methyltetrahydro-2H-pyrrol-2-one 123

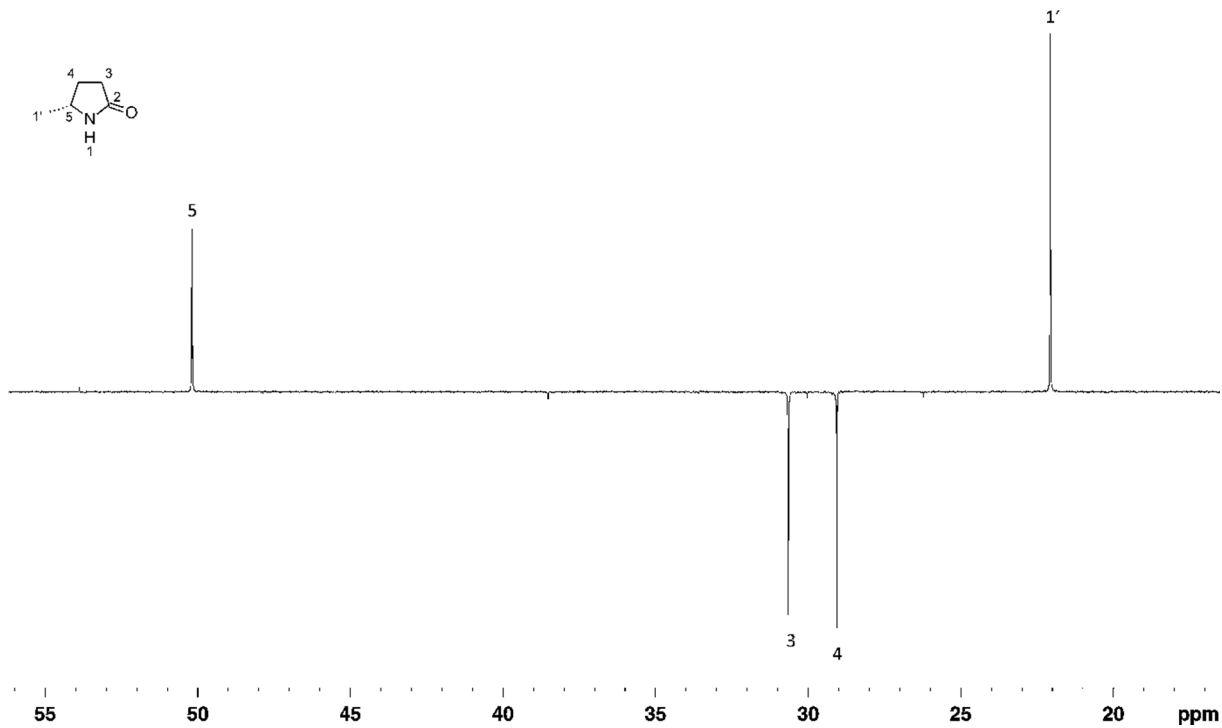


Figure C6: DEPT 135 NMR Spectrum for (5R)-5-methyltetrahydro-2H-pyrrol-2-one 123

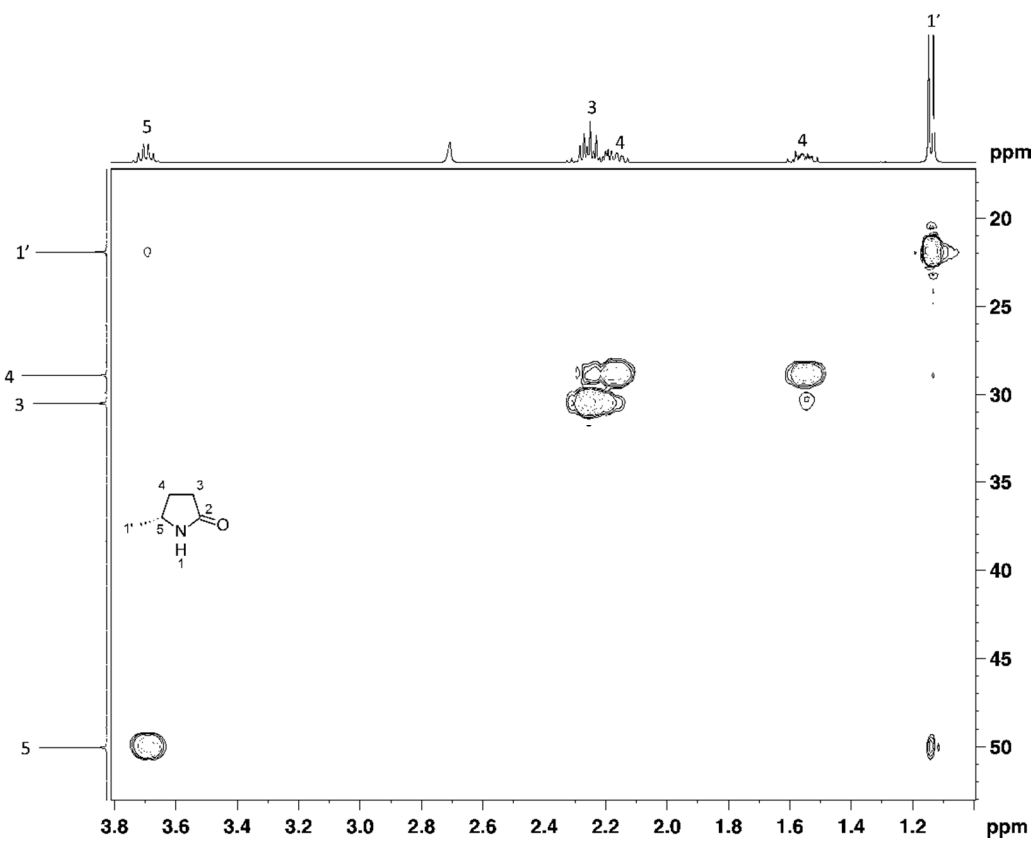


Figure C7: 2D HSQC NMR Spectrum for (5R)-5-methyltetrahydro-2H-pyrrol-2-one 123

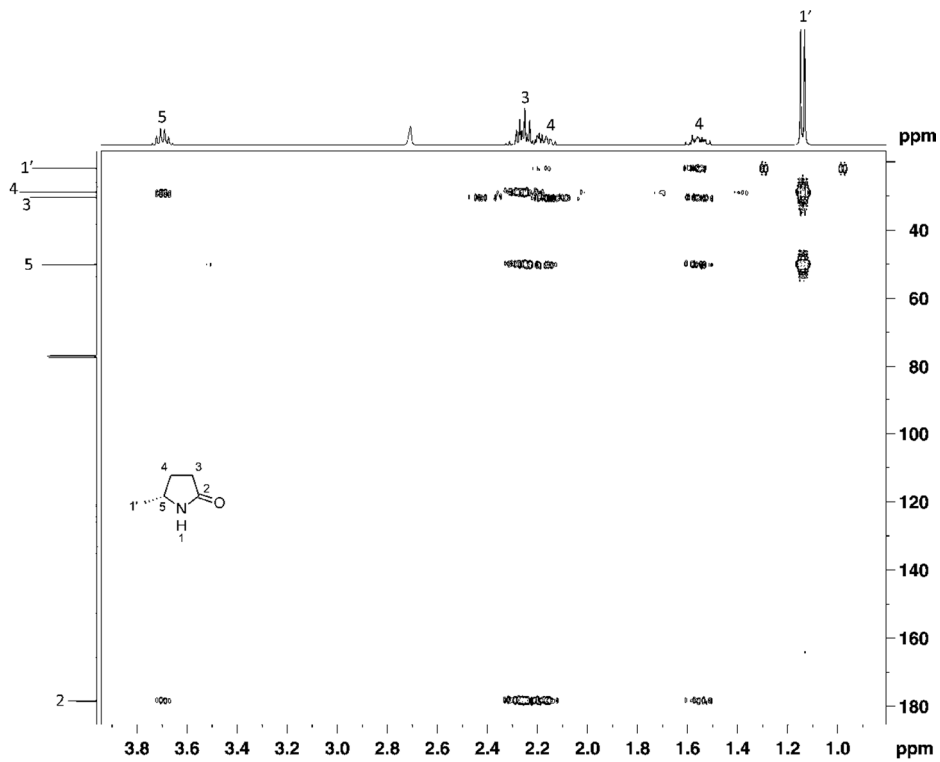


Figure C8: 2D HMBC NMR Spectrum for (5R)-5-methyltetrahydro-2H-pyrrol-2-one 123

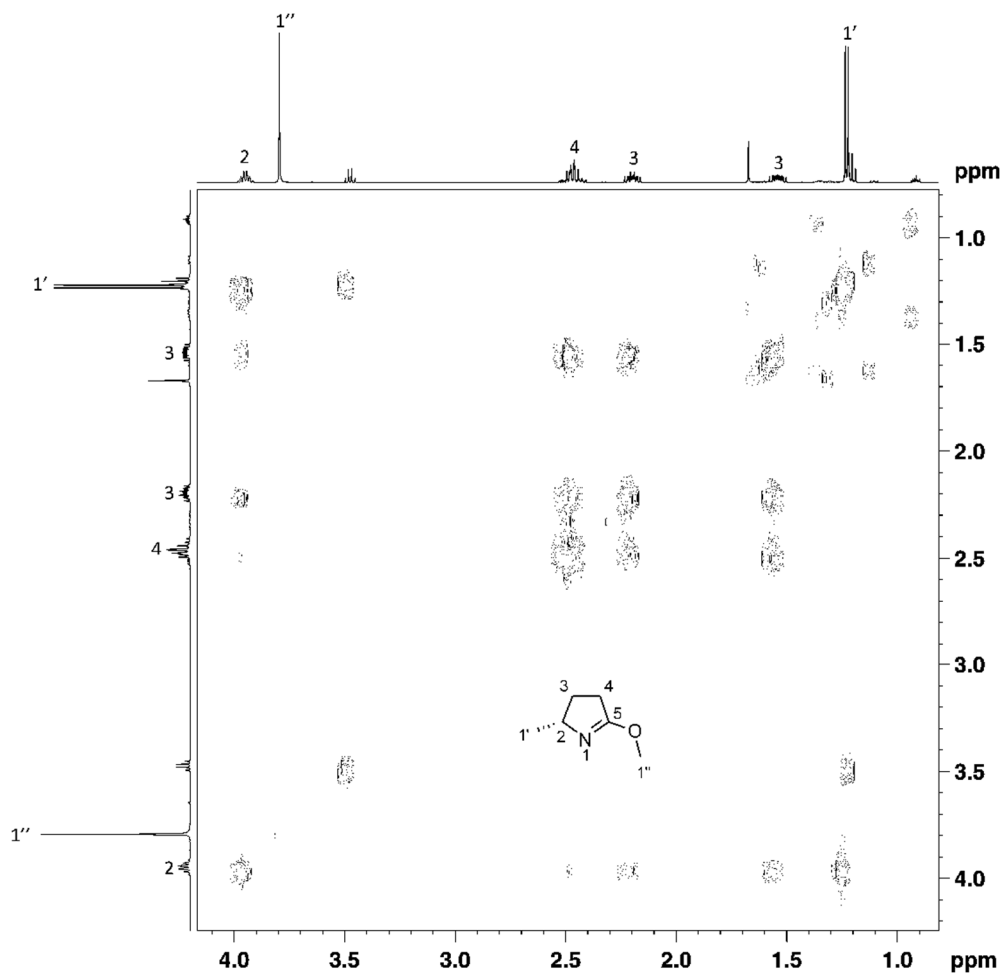


Figure C9: 2D COSY NMR Spectrum for (2R)-3,4-dihydro-5-methoxy-2-methyl-2H-pyrrole 135

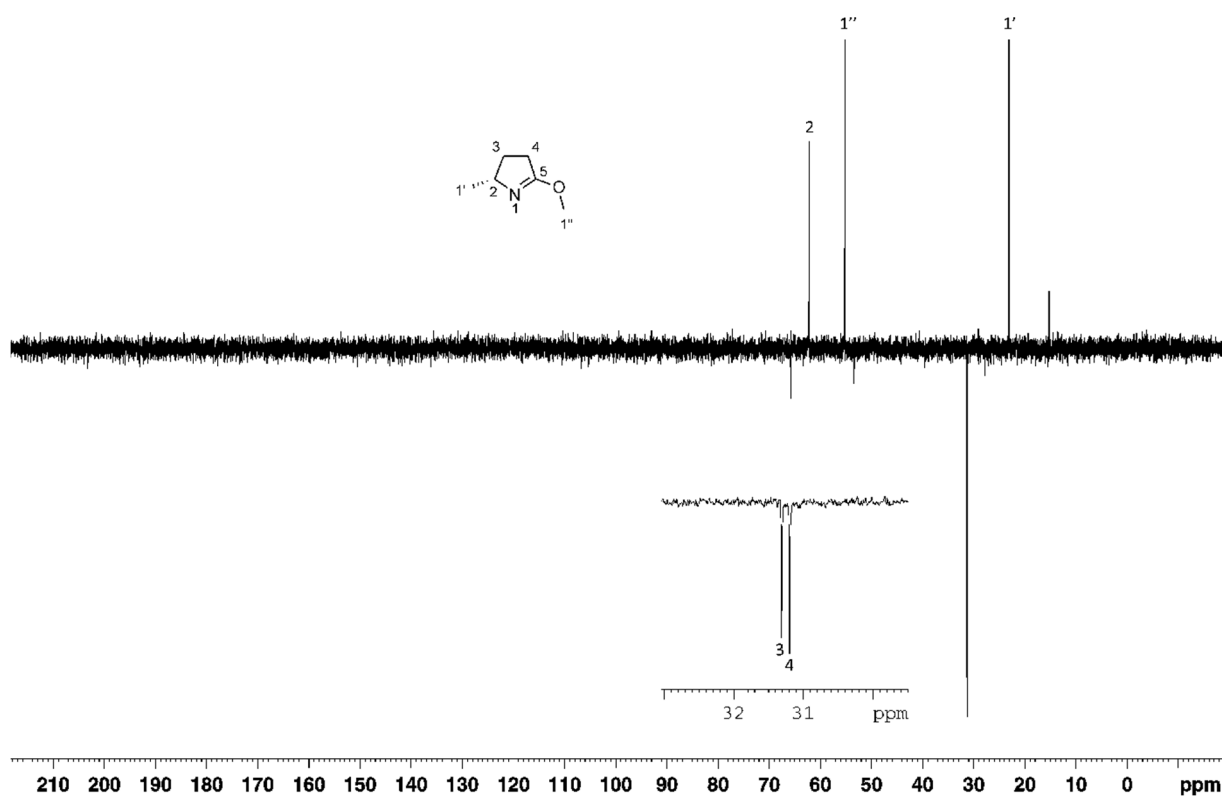


Figure C10: DEPT 135 NMR Spectrum for (2R)-3,4-dihydro-5-methoxy-2-methyl-2H-pyrrole 135

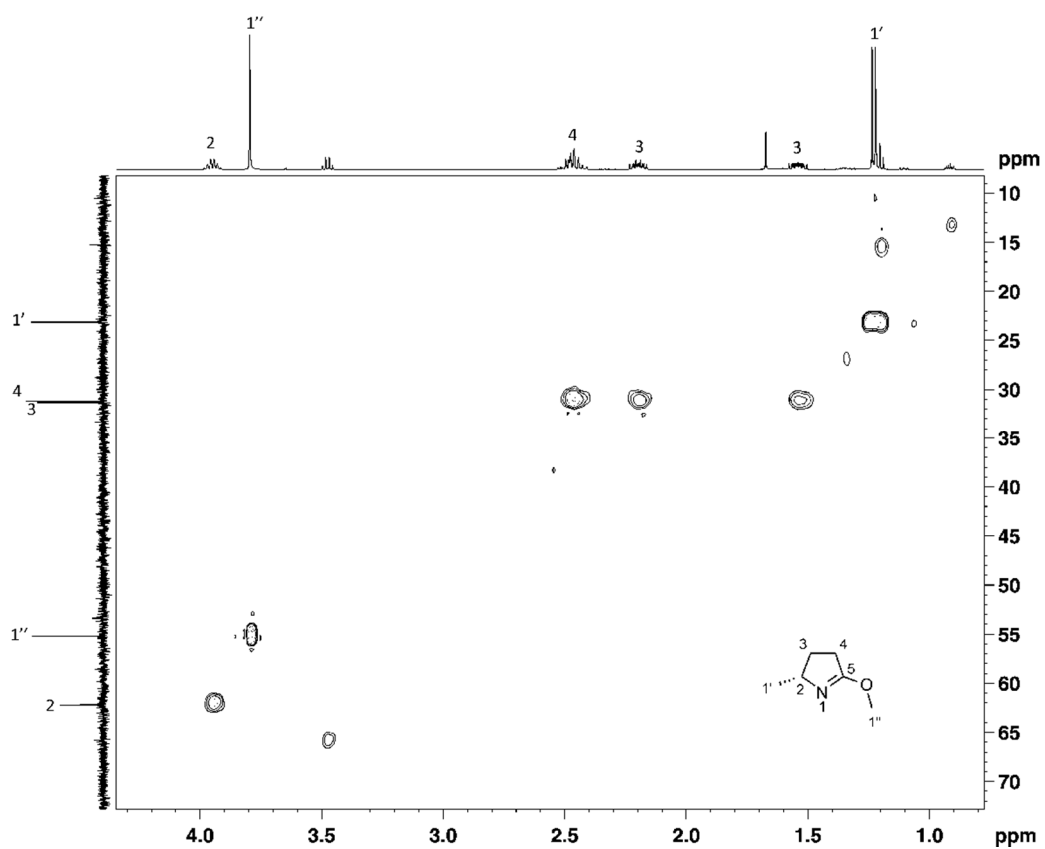


Figure C11: 2D HSQC NMR Spectrum for (2R)-3,4-dihydro-5-methoxy-2-methyl-2H-pyrrole 135

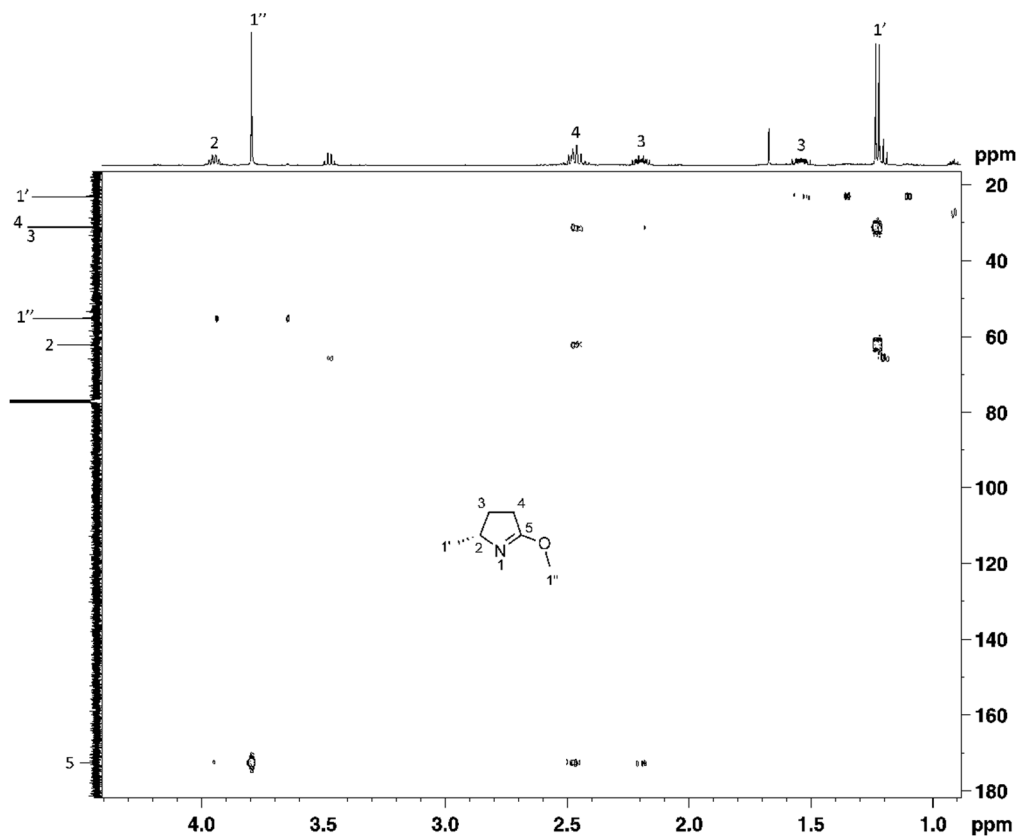


Figure C12: 2D HMBC NMR Spectrum for (2R)-3,4-dihydro-5-methoxy-2-methyl-2H-pyrrole 135

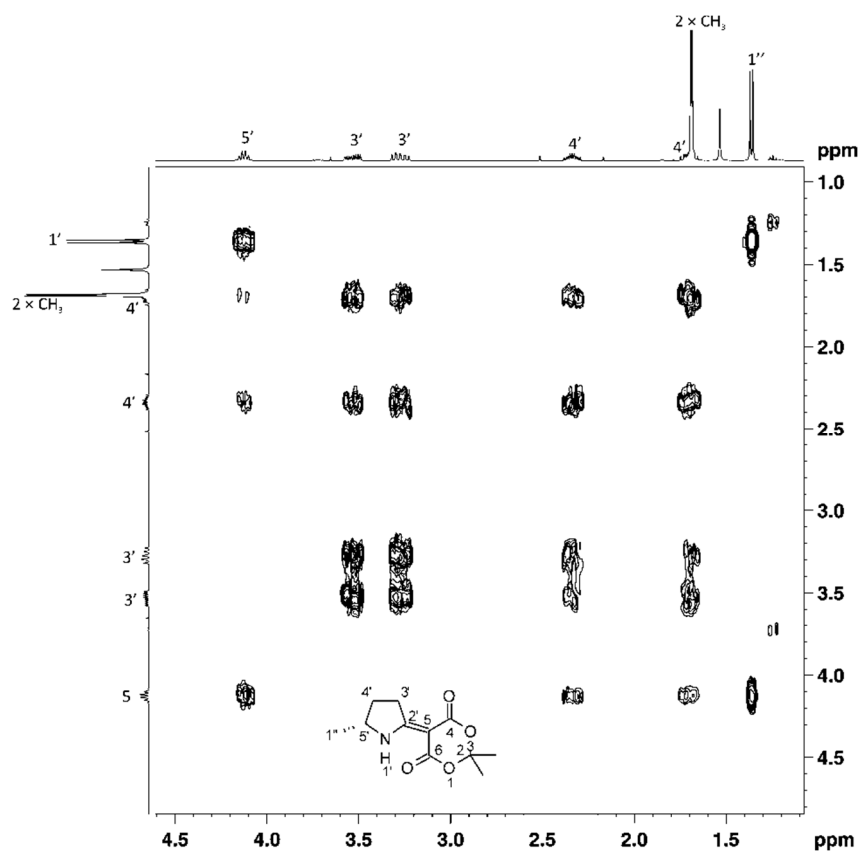


Figure C13: 2D COSY NMR Spectrum for 2,2-dimethyl-5-[(5R)-5-methyl-2-pyrrolidinylidene]-1,3-dioxane-4,6-dione 136

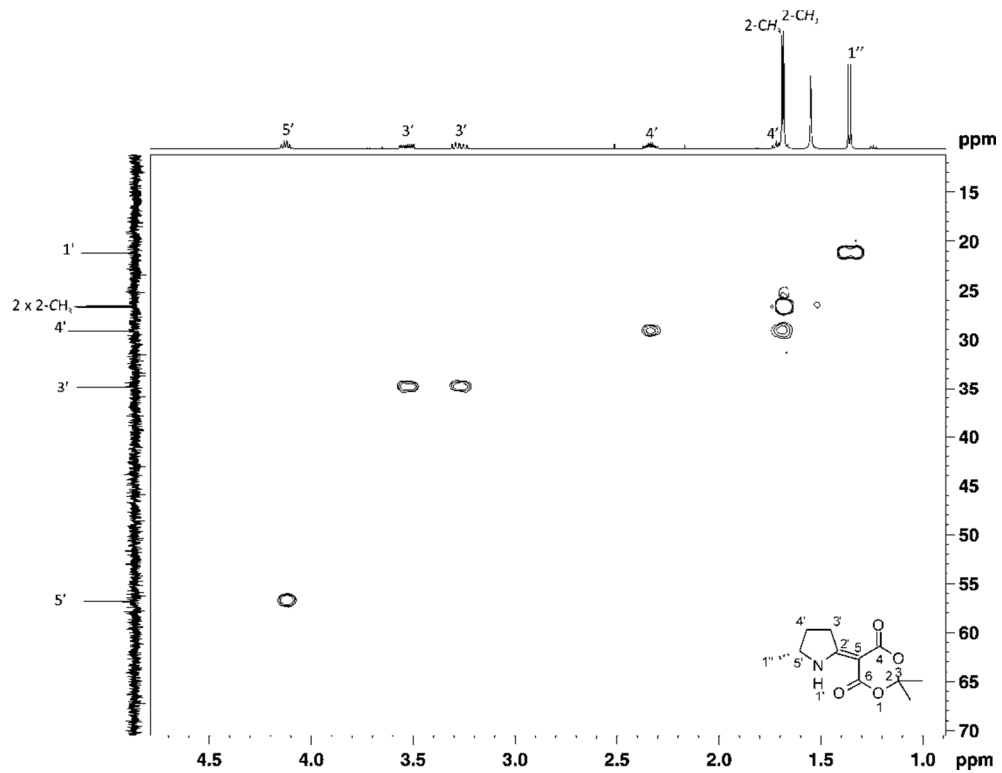


Figure C14: 2D HSQC NMR Spectrum for 2,2-dimethyl-5-[(5R)-5-methyl-2-pyrrolidinylidene]-1,3-dioxane-4,6-dione 136

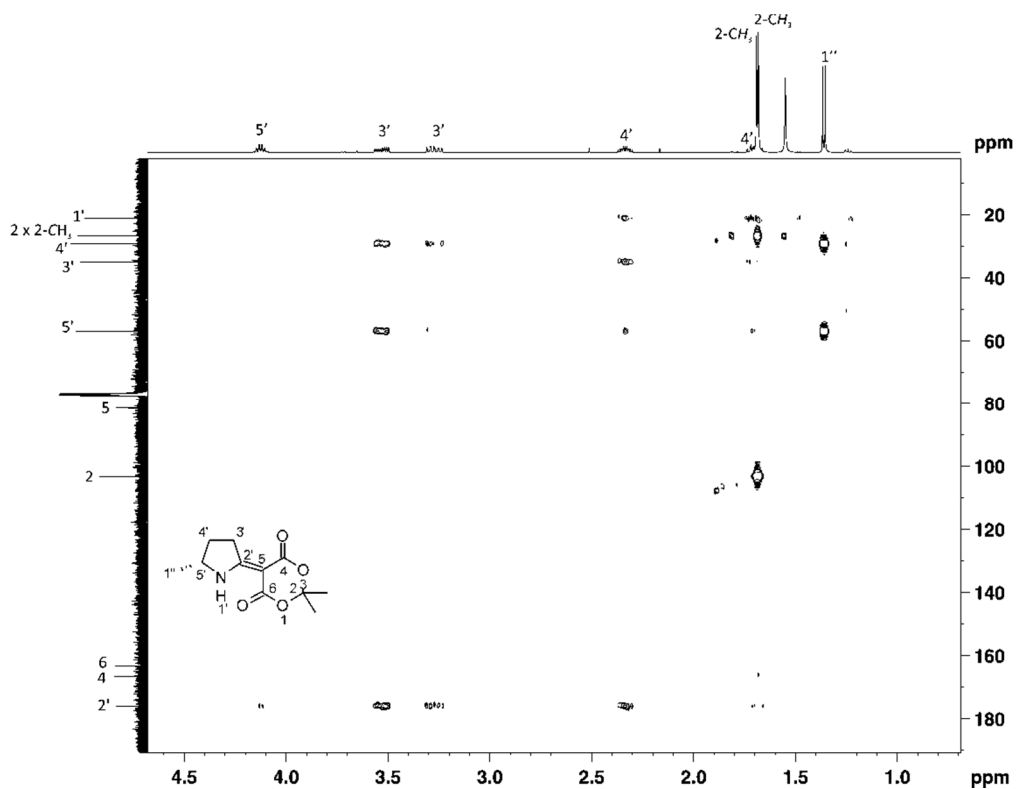


Figure C15: 2D HMBC NMR Spectrum for 2,2-dimethyl-5-[(5R)-5-methyl-2-pyrrolidinylidene]-1,3-dioxane-4,6-dione 136

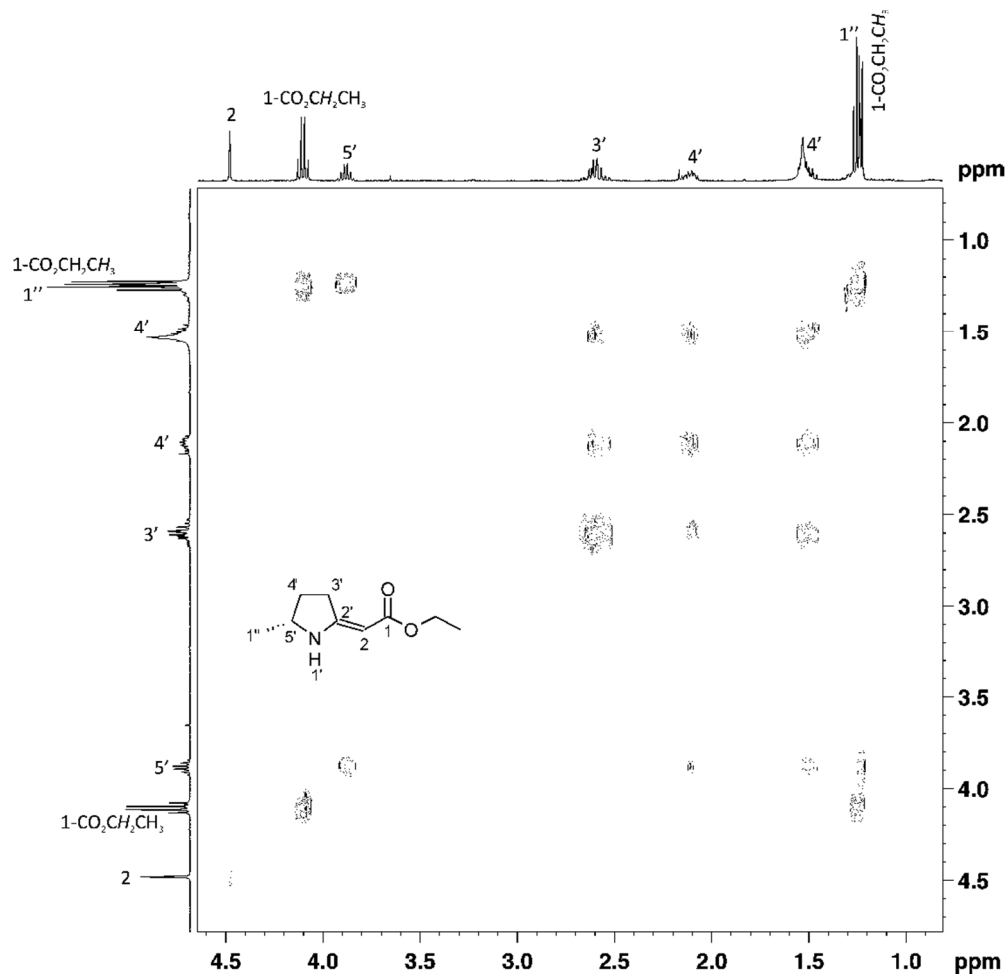


Figure C16: 2D COSY NMR Spectrum for ethyl 2-[(5R)-5-methyltetrahydro-2H-pyrrol-2-ylidene]acetate 127

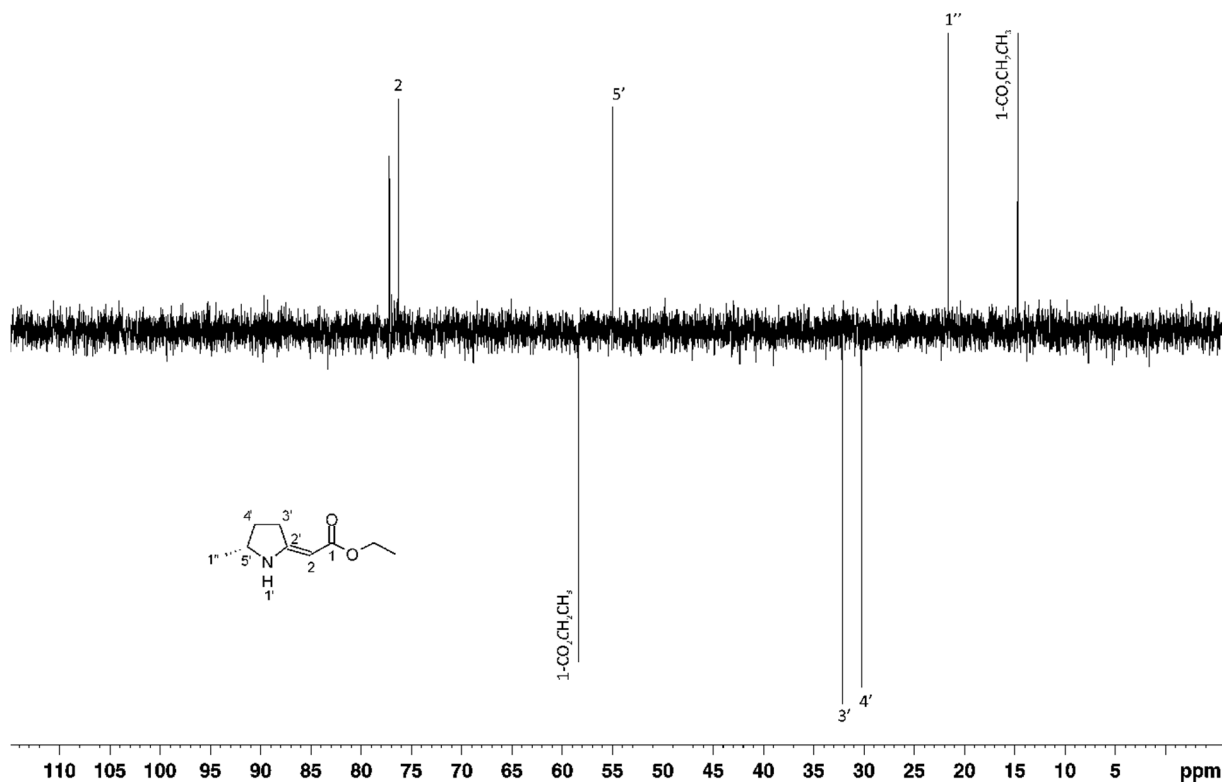


Figure C17: DEPT 135 NMR Spectrum for ethyl 2-[(5R)-5-methyltetrahydro-2H-pyrrol-2-ylidene]acetate 127

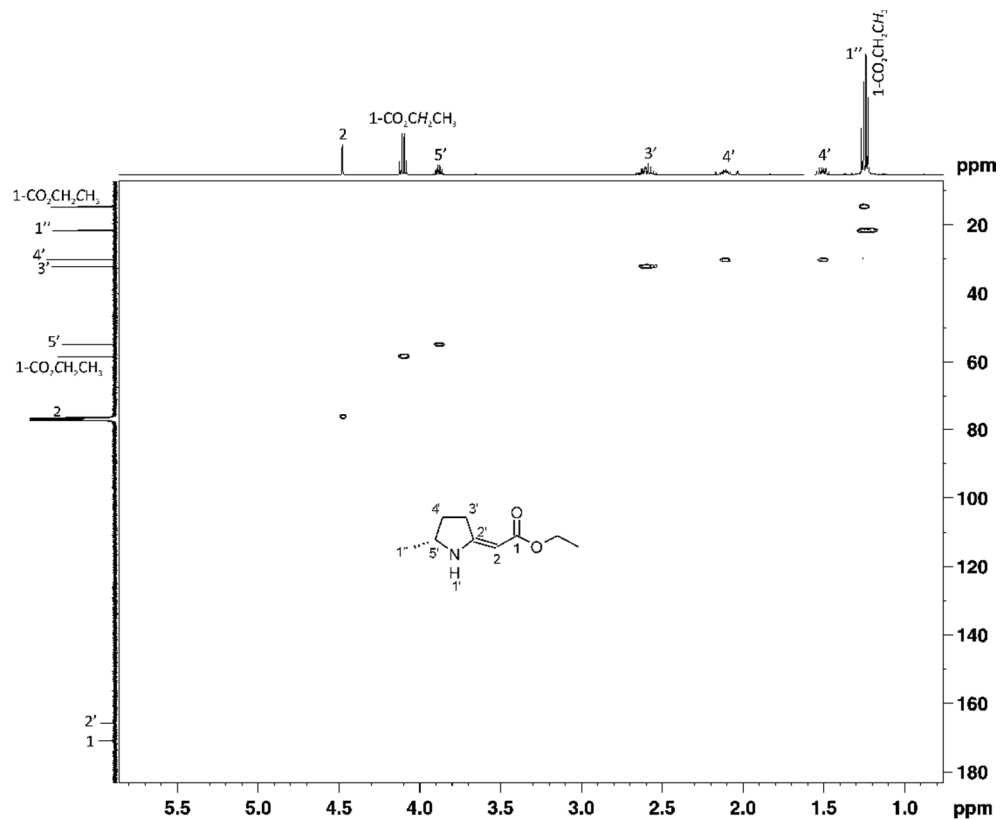


Figure C18: 2D HSQC NMR Spectrum for ethyl 2-[(5R)-5-methyltetrahydro-2H-pyrrol-2-ylidene]acetate 127

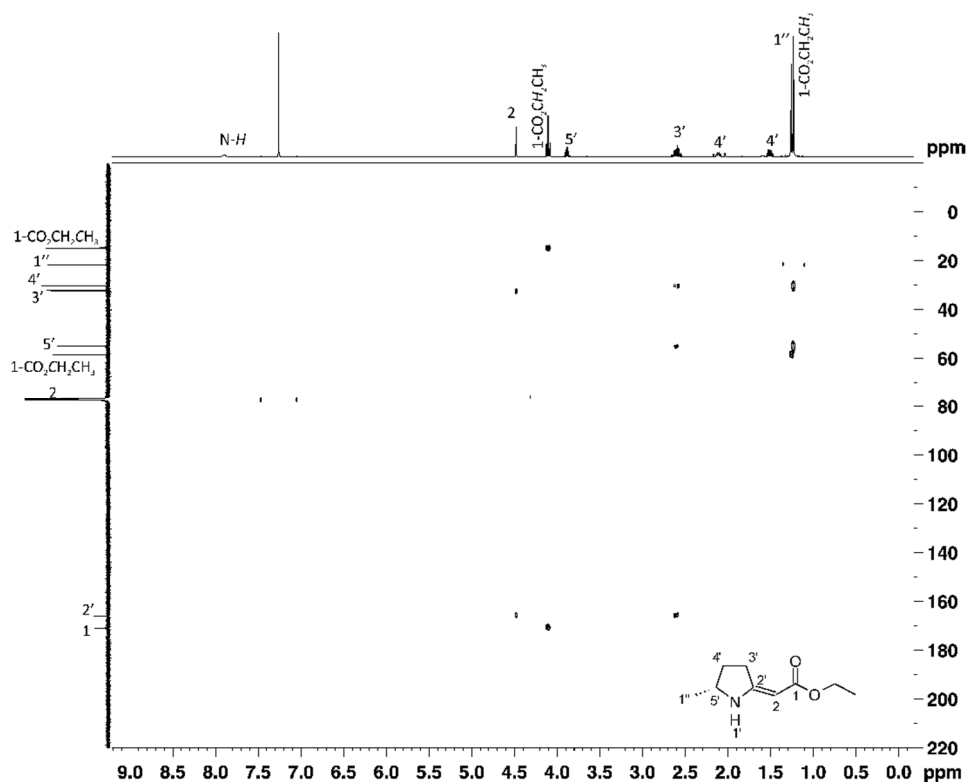


Figure C19: 2D HMBC NMR Spectrum for ethyl 2-[(5R)-5-methyltetrahydro-2H-pyrrol-2-ylidene]acetate 127

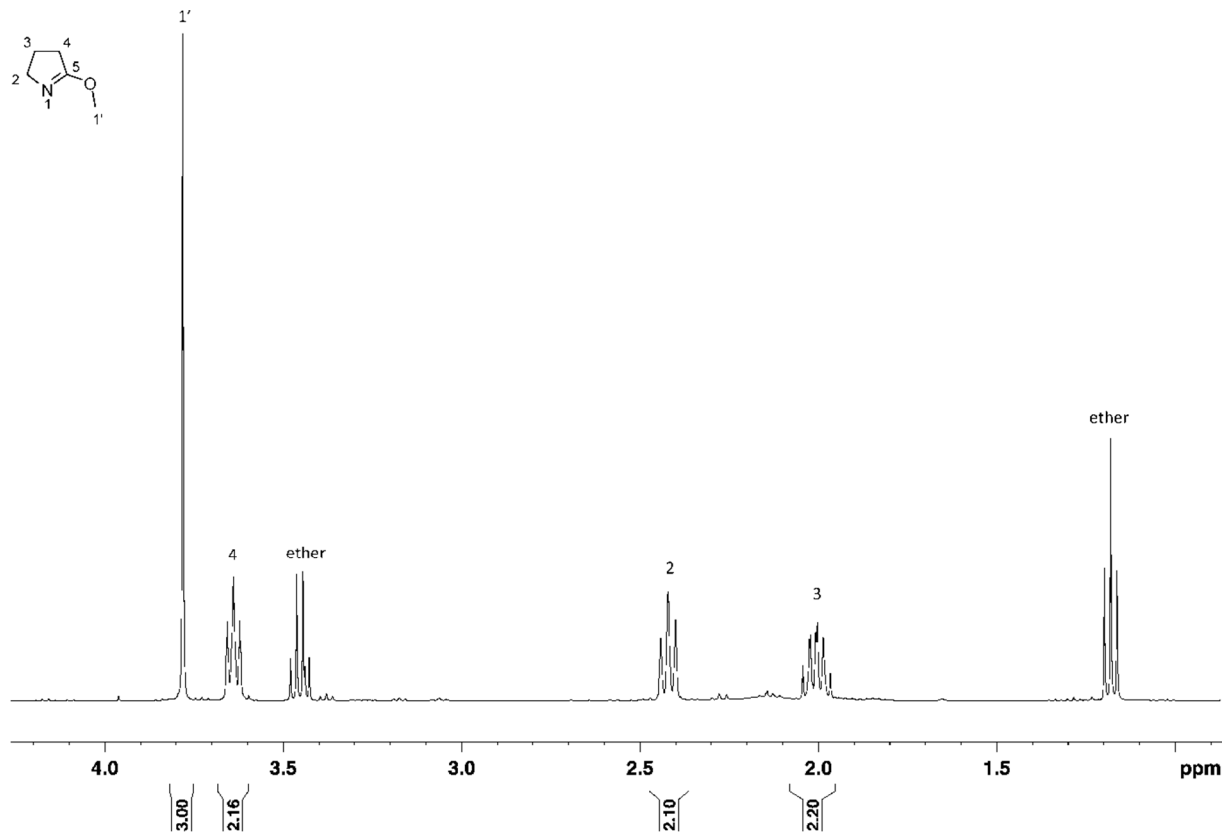


Figure C20: ^1H NMR Spectrum for 3,4-dihydro-5-methoxy-2H-pyrrole 133

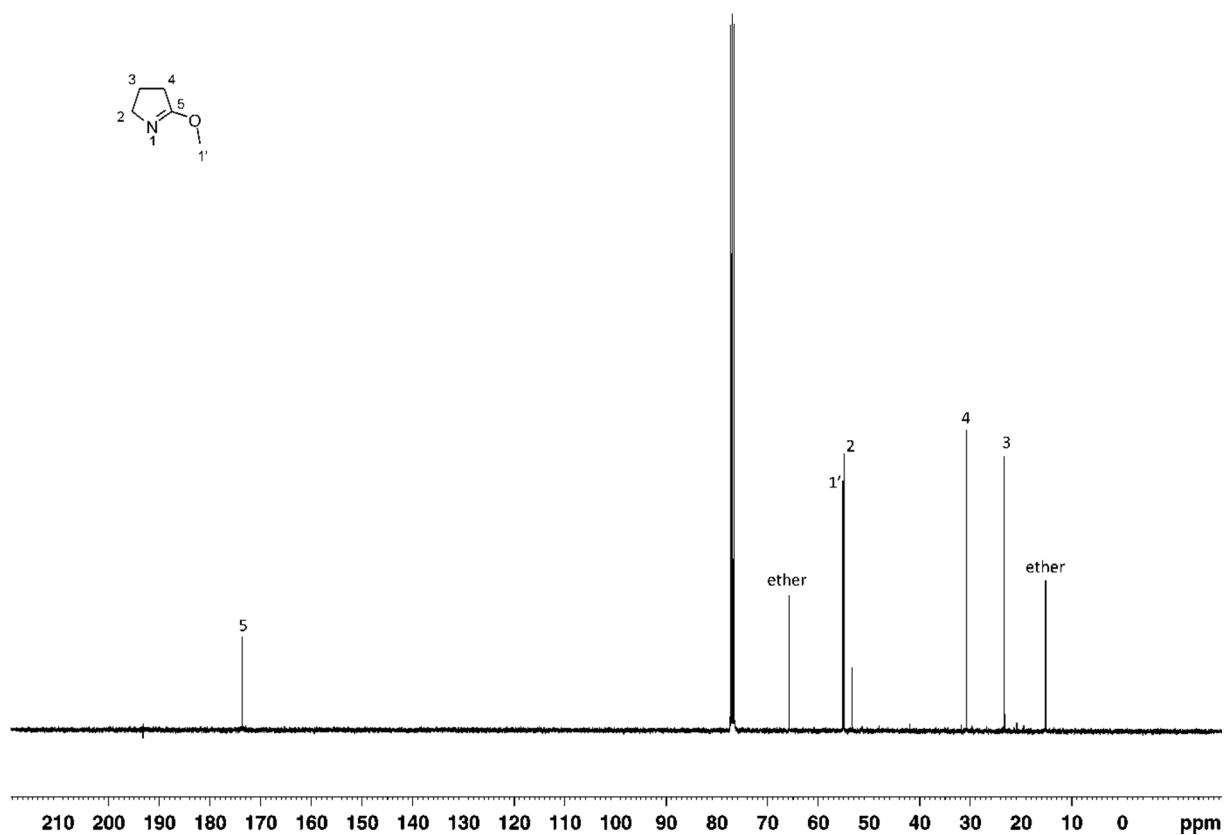


Figure C21: ^{13}C NMR Spectrum for 3,4-dihydro-5-methoxy-2H-pyrrole 133

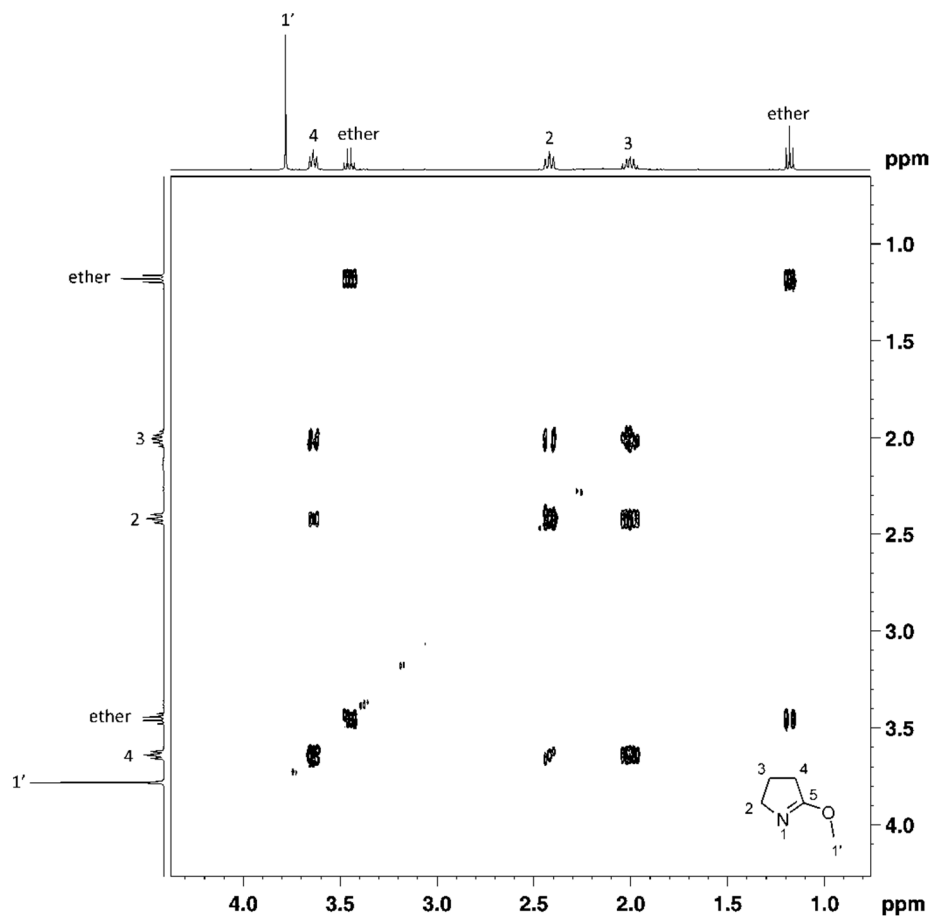


Figure C22: 2D COSY NMR Spectrum for 3,4-dihydro-5-methoxy-2H-pyrrole 133

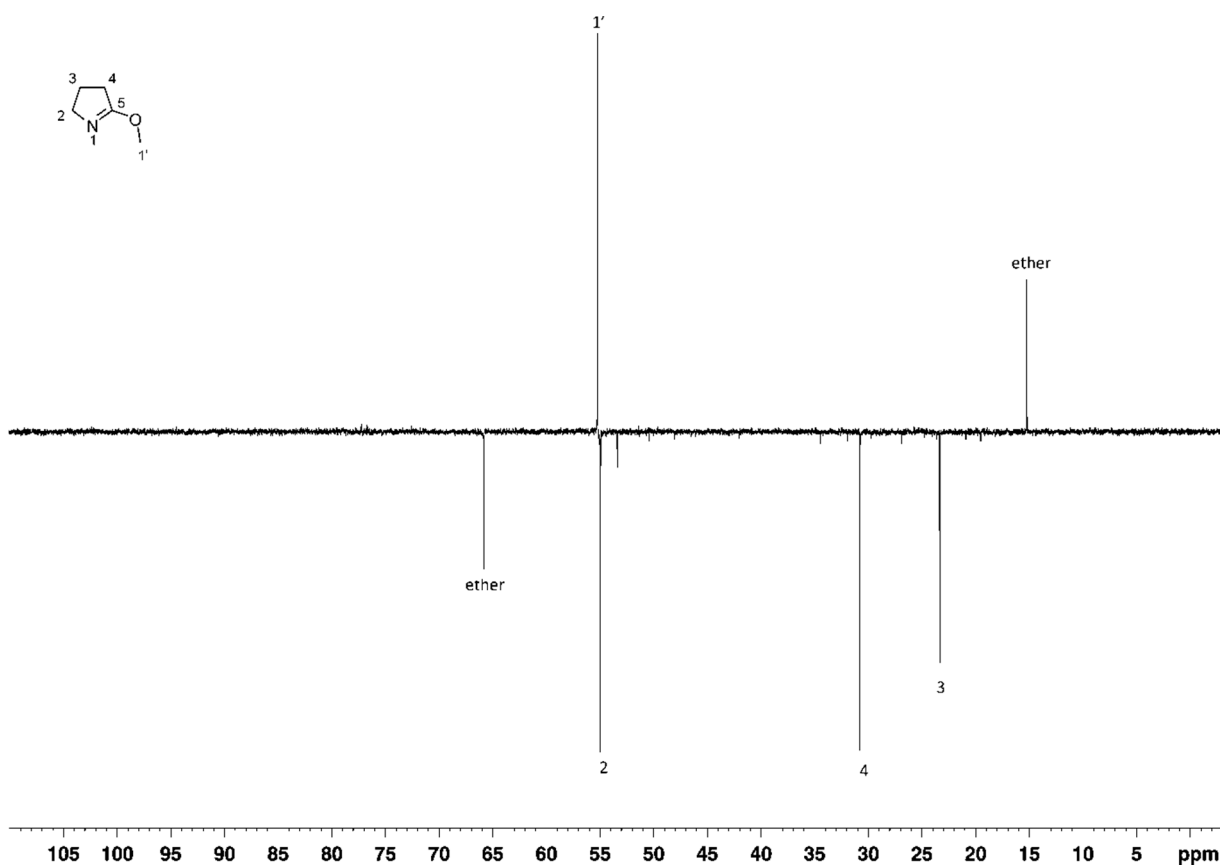


Figure C23: DEPT 135 NMR Spectrum for 3,4-dihydro-5-methoxy-2H-pyrrole 133

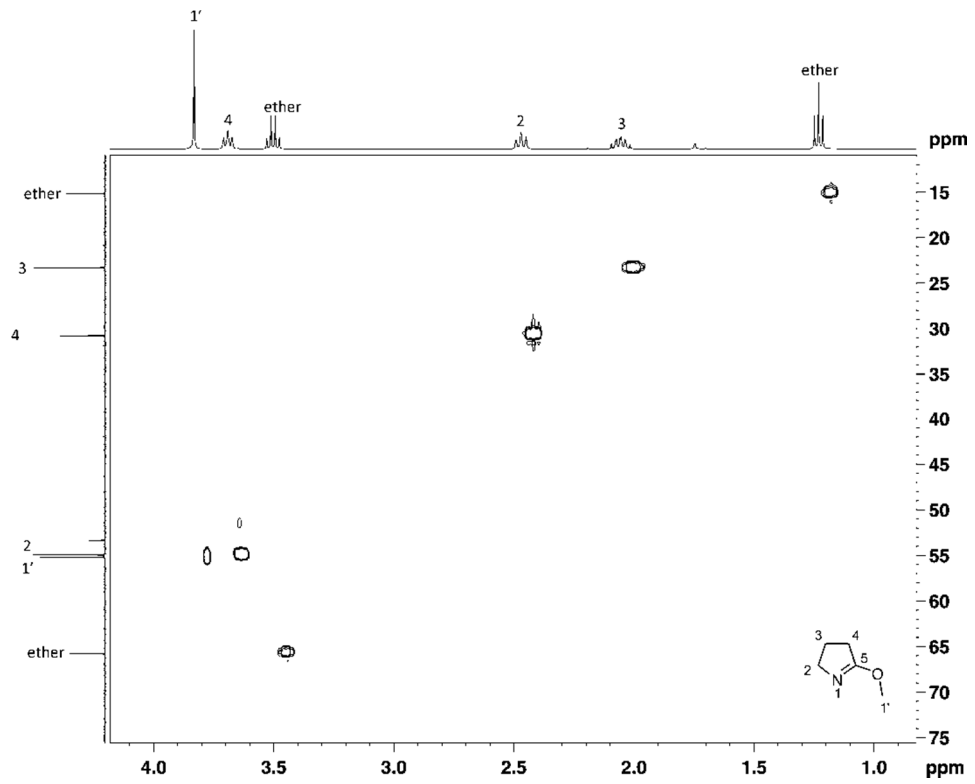


Figure C24: 2D HSQC NMR Spectrum for 3,4-dihydro-5-methoxy-2H-pyrrole 133

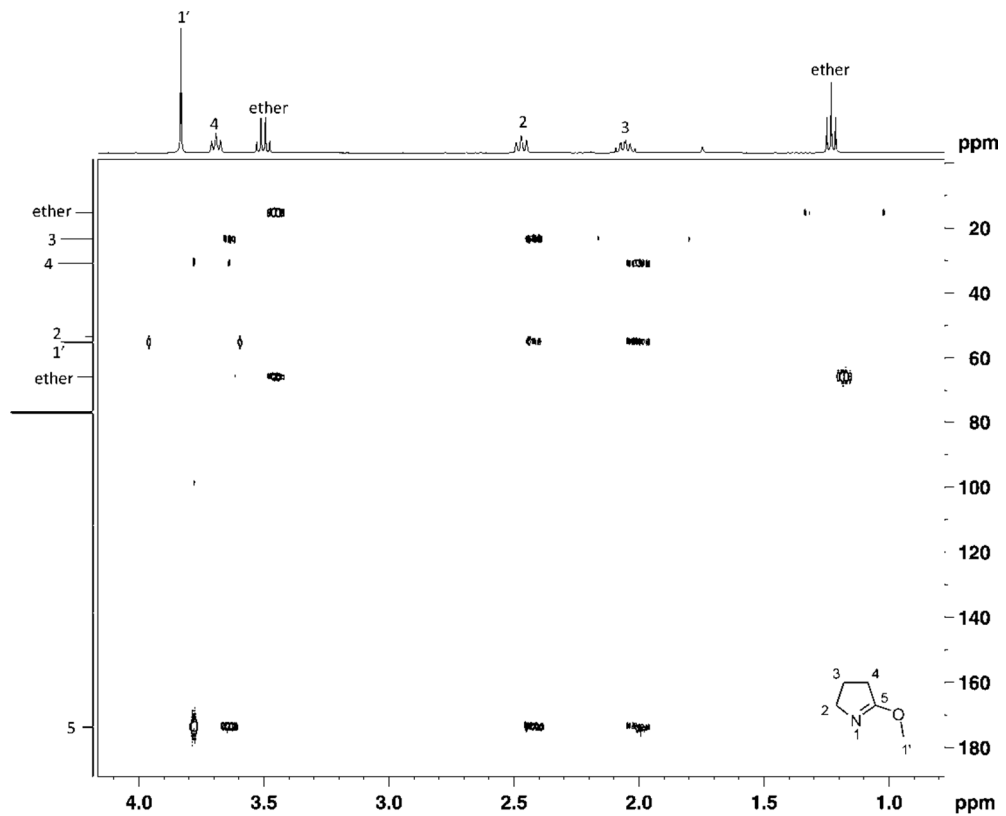


Figure C25: 2D HMBC NMR Spectrum for 3,4-dihydro-5-methoxy-2H-pyrrole 133

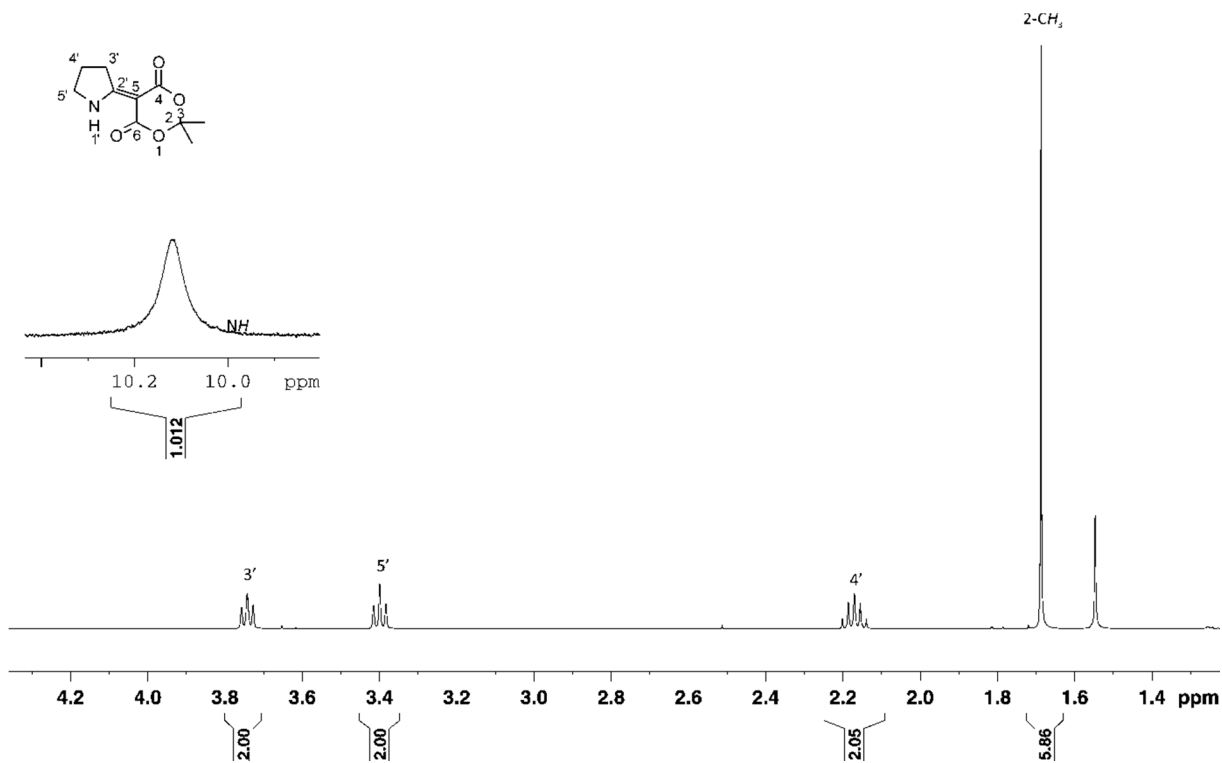


Figure C26: ^1H NMR Spectrum for 2,2-dimethyl-5-(2-pyrrolidinylidene)-1,3-dioxane-4,6-dione 134

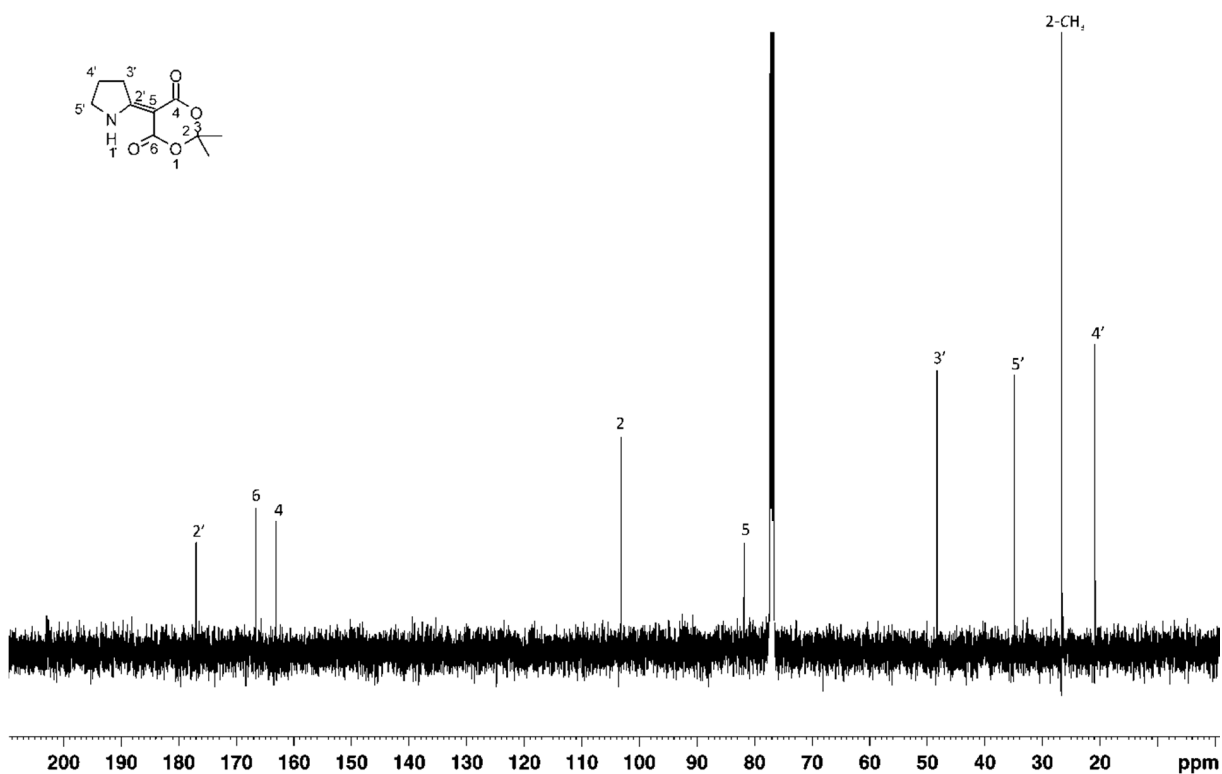


Figure C27: ^{13}C NMR Spectrum for 2,2-dimethyl-5-(2-pyrrolidinylidene)-1,3-dioxane-4,6-dione 134

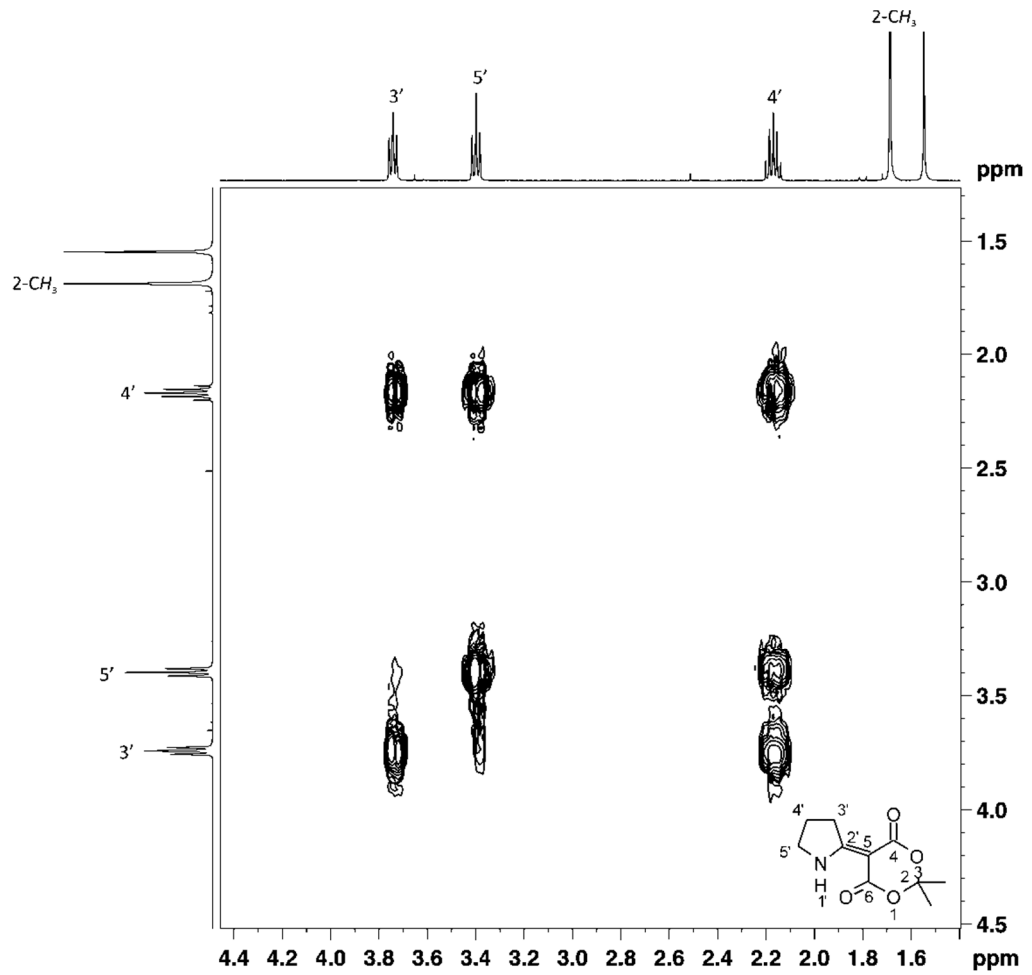


Figure C28: 2D COSY NMR Spectrum for 2,2-dimethyl-5-(2-pyrrolidinylidene)-1-3-dioxane-4,6-dione 134

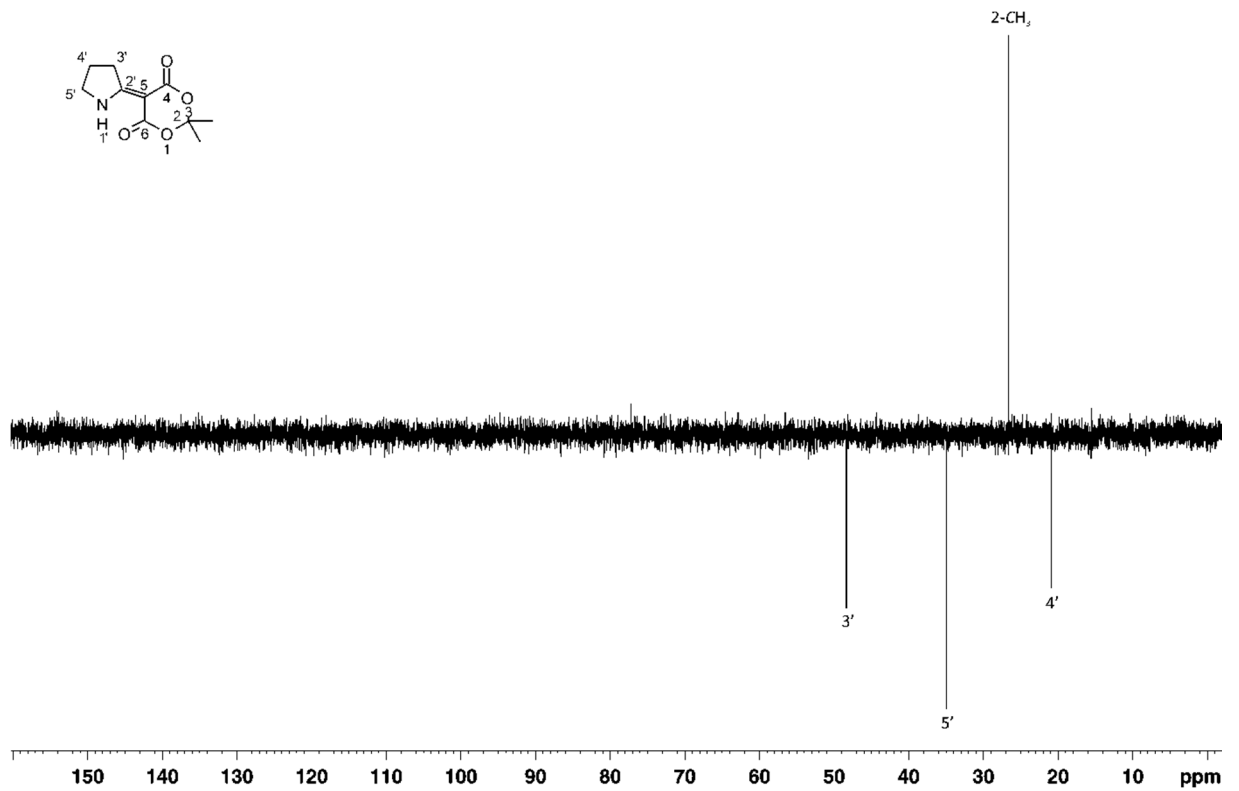


Figure C29: DEPT 135 NMR Spectrum for 2,2-dimethyl-5-(2-pyrrolidinylidene)-1-3-dioxane-4,6-dione 134

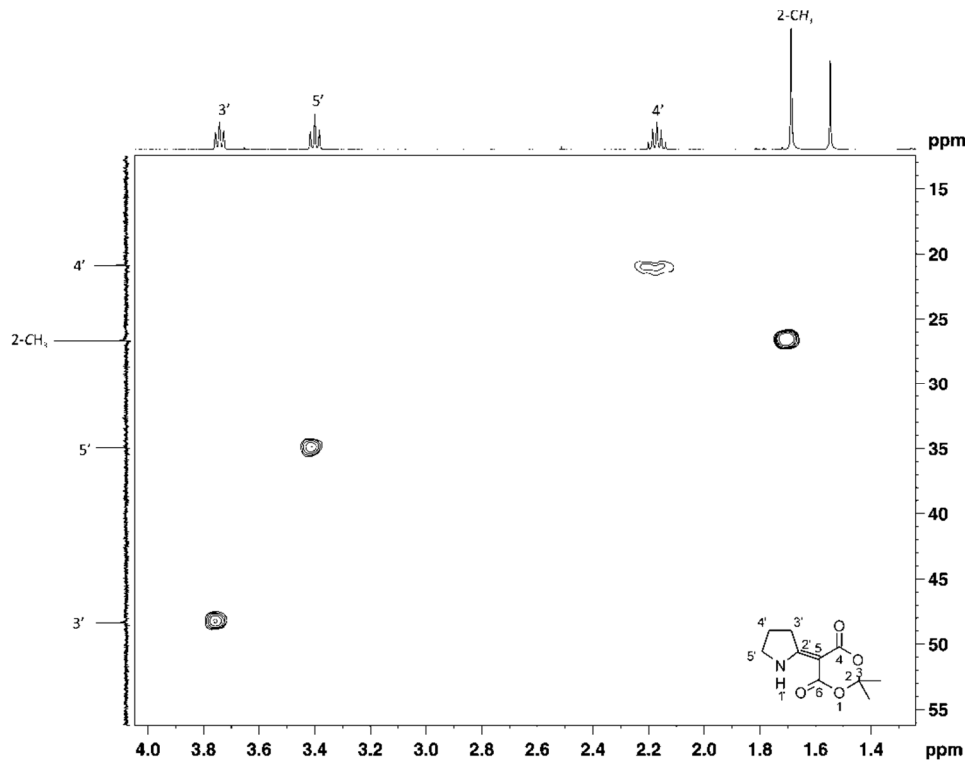


Figure C30: 2D HSQC NMR Spectrum for 2,2-dimethyl-5-(2-pyrrolidinylidene)-1,3-dioxane-4,6-dione 134

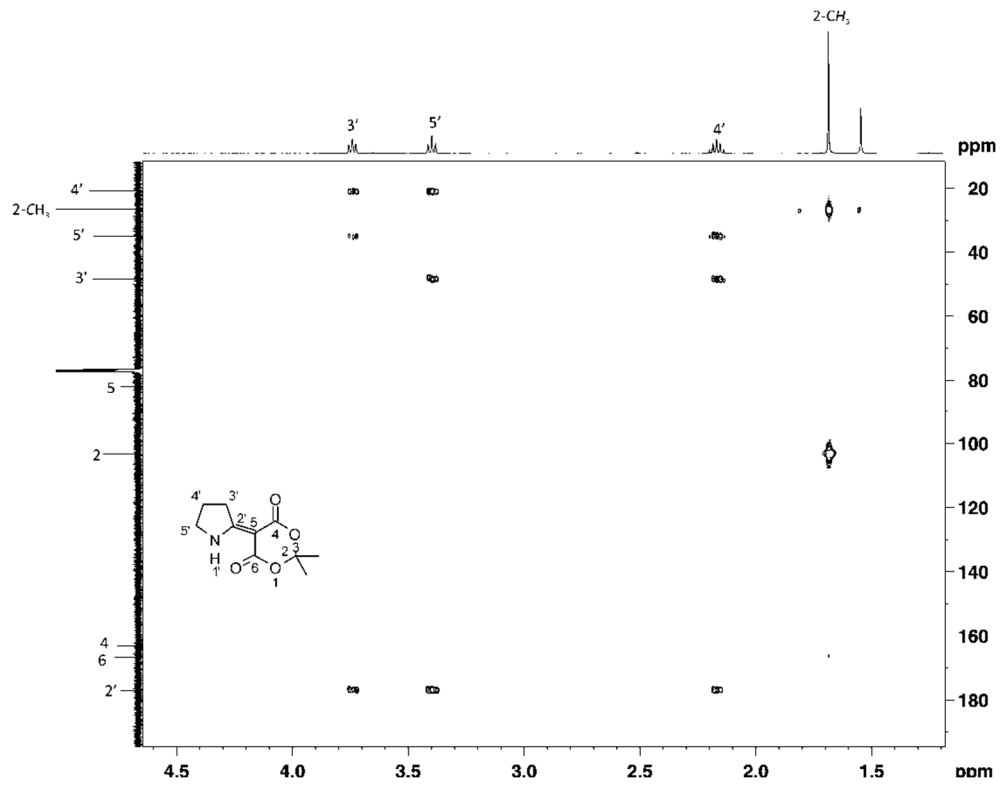


Figure C31: 2D HMBC NMR Spectrum for 2,2-dimethyl-5-(2-pyrrolidinylidene)-1,3-dioxane-4,6-dione 134

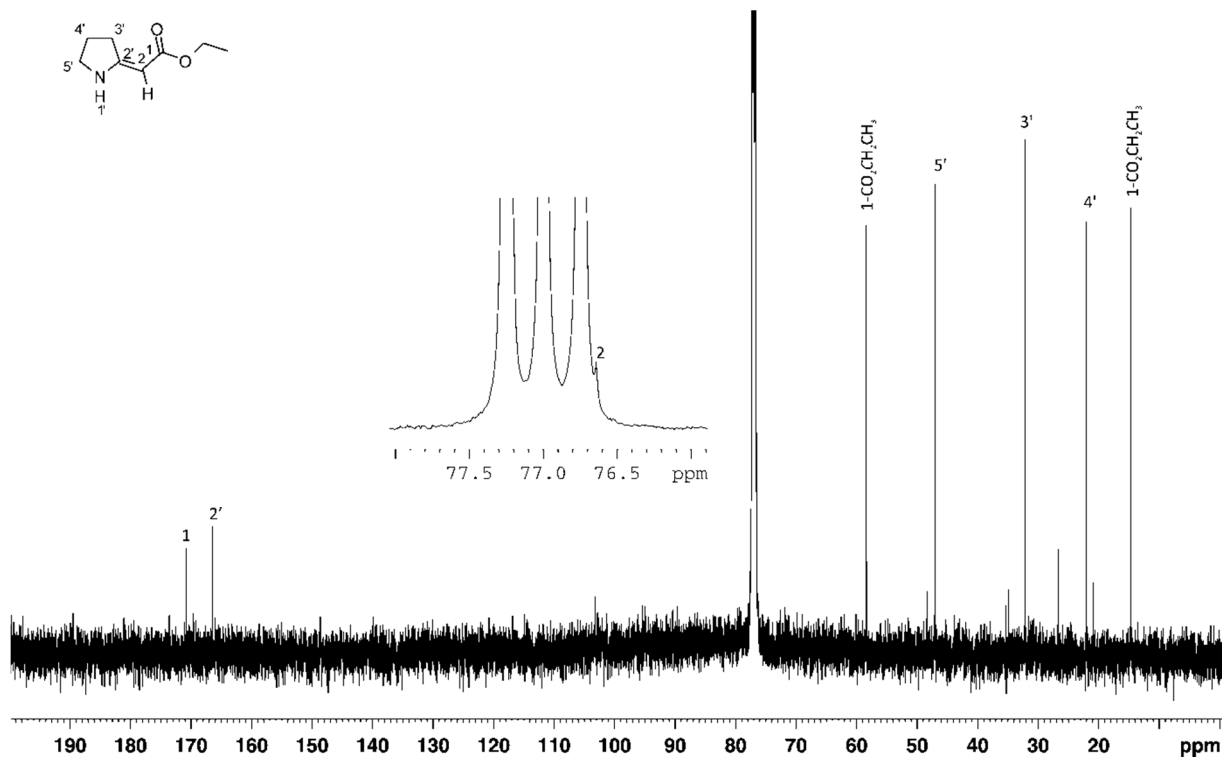


Figure C32: ^{13}C NMR Spectrum for (2Z)-pyrrolidinylidene ethyl ester 111

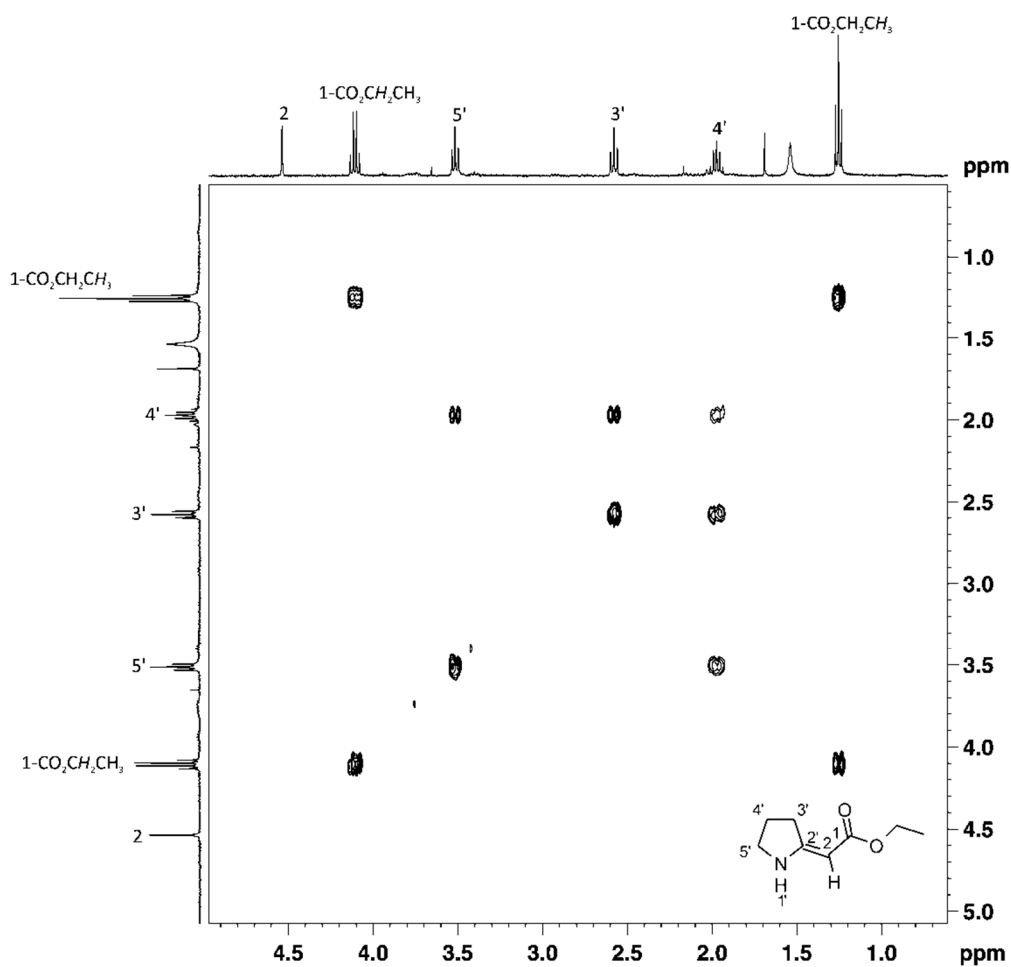


Figure C33: 2D COSY NMR Spectrum for (2Z)-pyrrolidinylidene ethyl ester 111

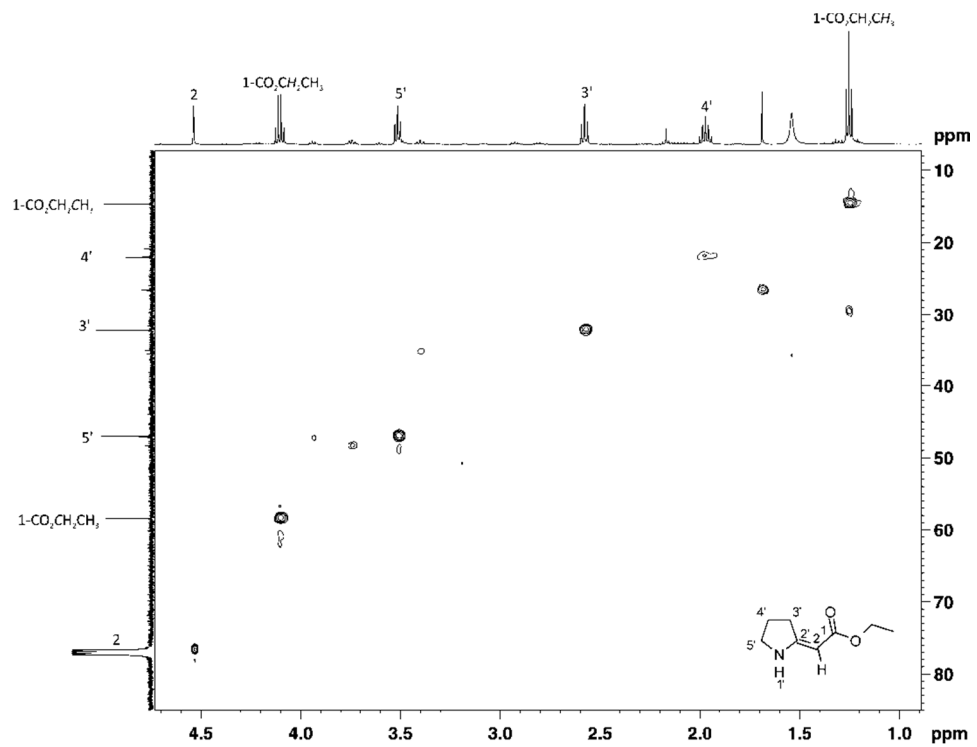


Figure C34: 2D HSQC NMR Spectrum for (Z)-pyrrolidinylidene ethyl ester 111

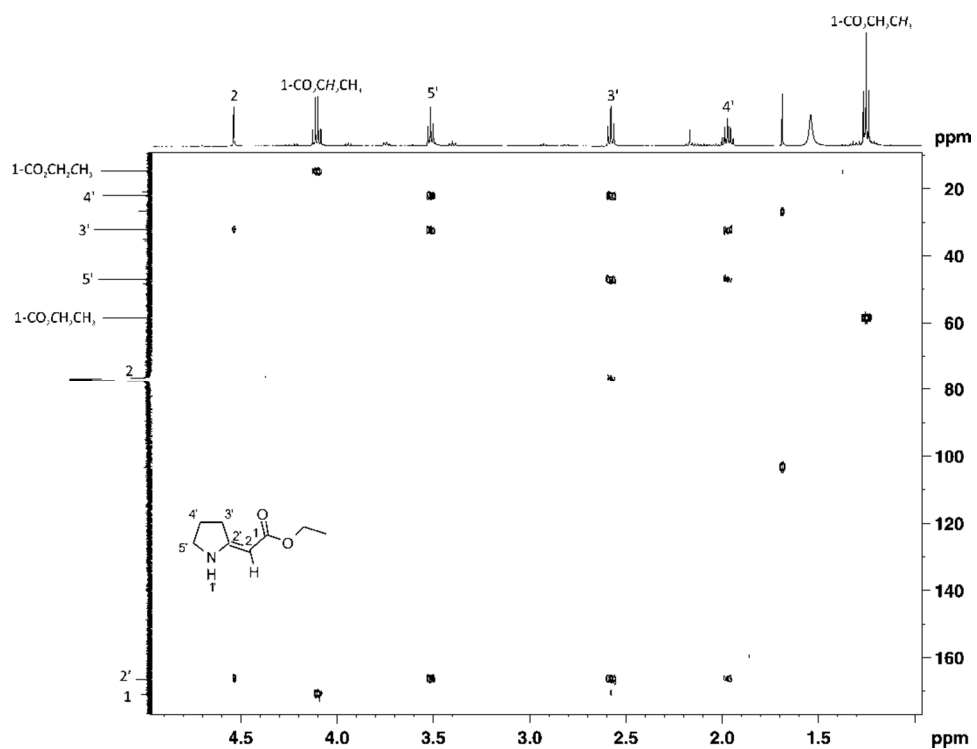


Figure C35: 2D HMBC NMR Spectrum for (Z)-pyrrolidinylidene ethyl ester 111

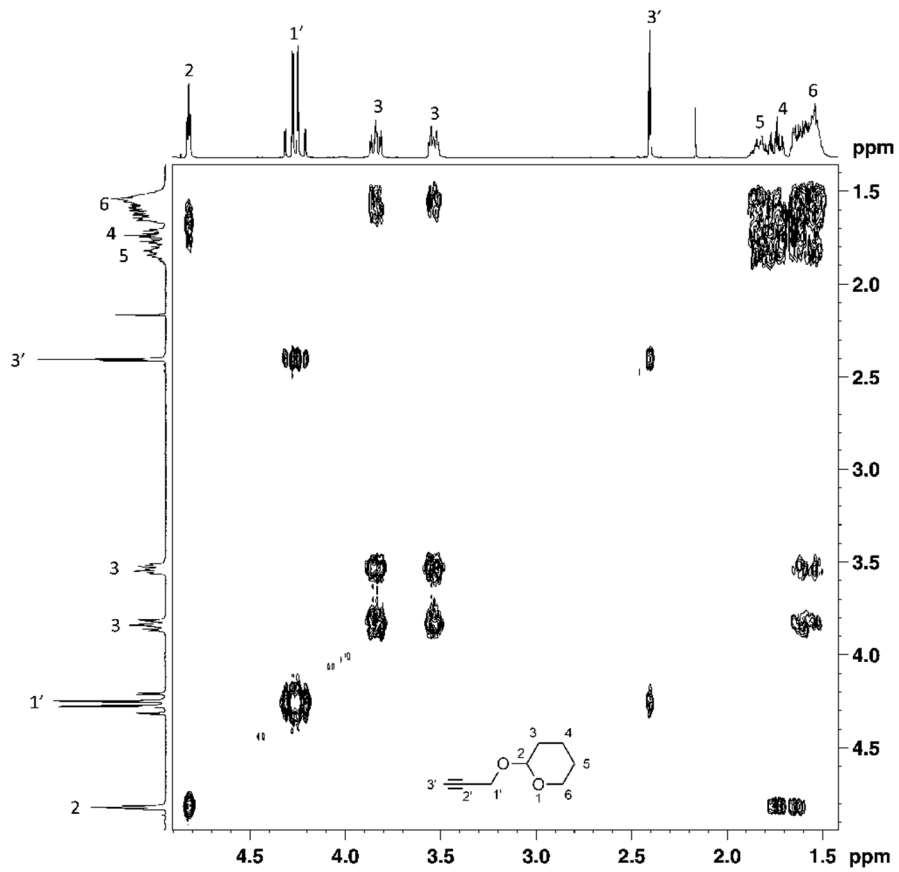


Figure C36: 2D COSY NMR Spectrum for 2-propynyl tetrahydro-2H-pyran-2-yl ether 138

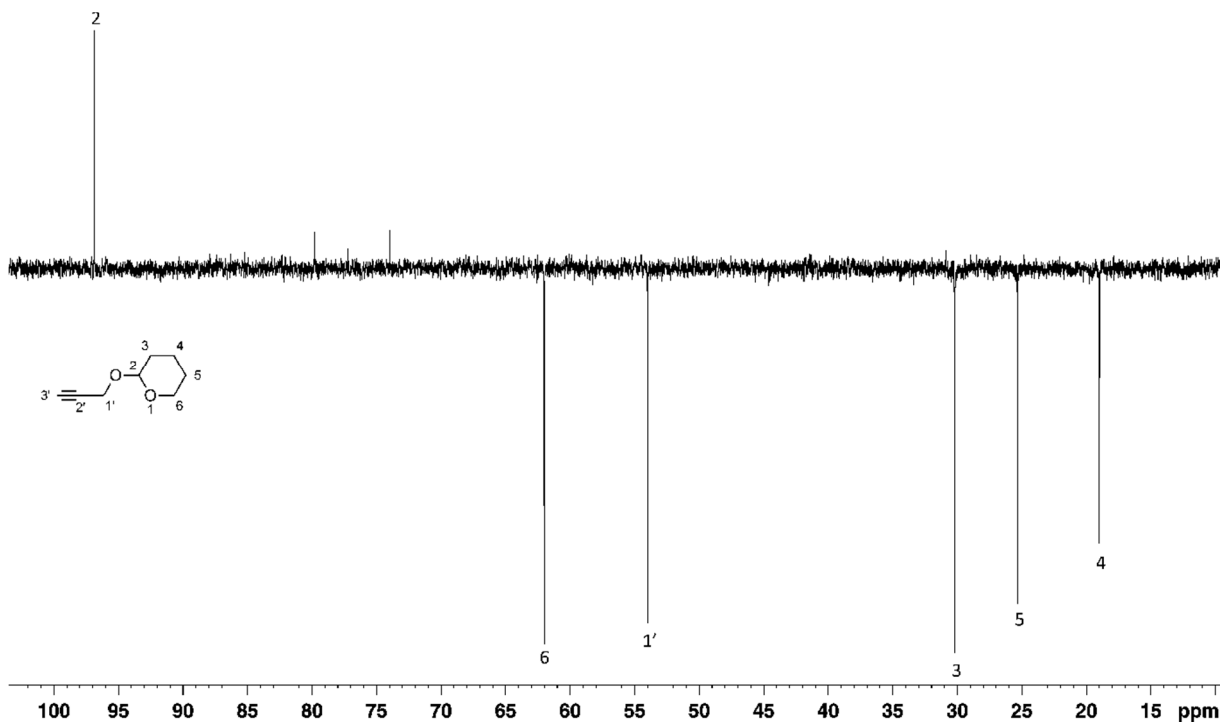


Figure C37: DEPT 135 NMR Spectrum for 2-propynyl tetrahydro-2H-pyran-2-yl ether 138

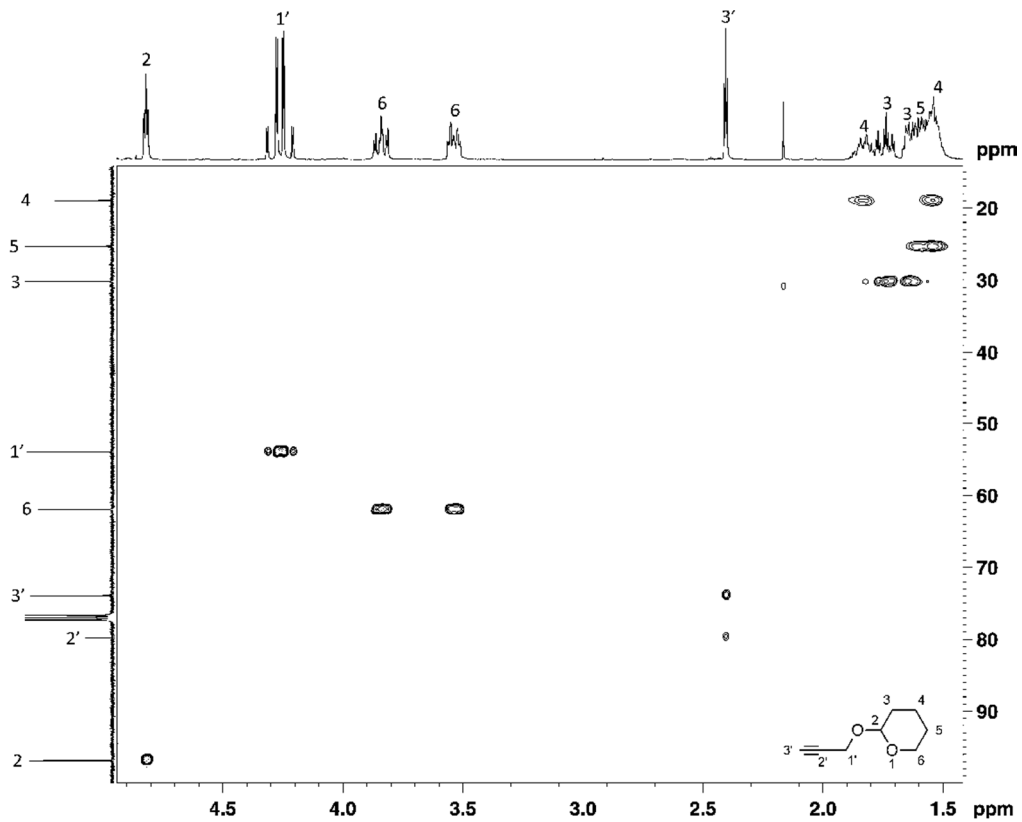


Figure C38: 2D HSQC NMR Spectrum for 2-propynyl tetrahydro-2H-pyran-2-yl ether 138

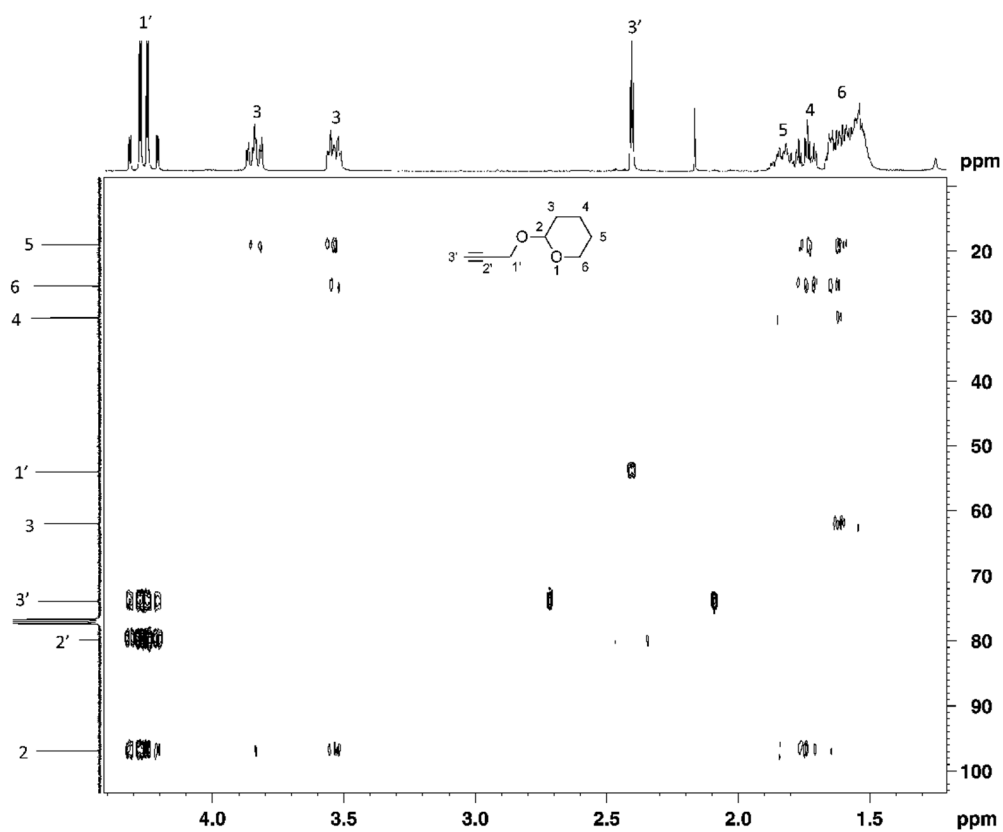


Figure C39: 2D HMBC NMR Spectrum for 2-propynyl tetrahydro-2H-pyran-2-yl ether 138

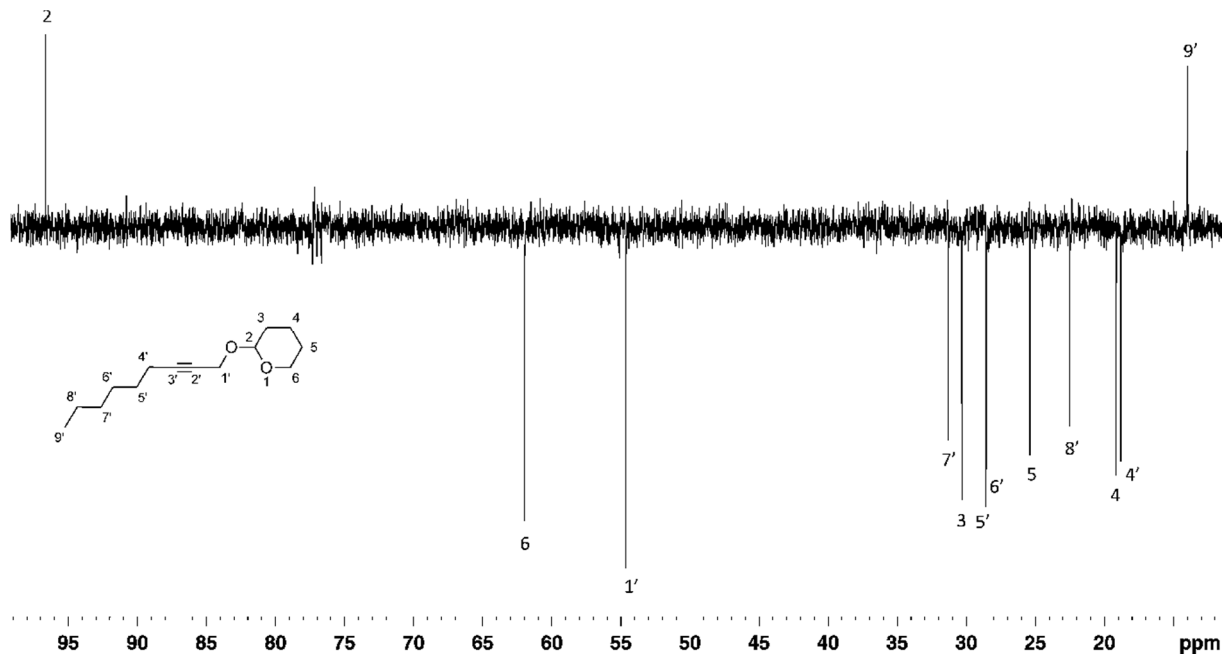


Figure C40: DEPT 135 NMR Spectrum for 2-nonyl tetrahydro-2H-pyran-2-yl ether 139

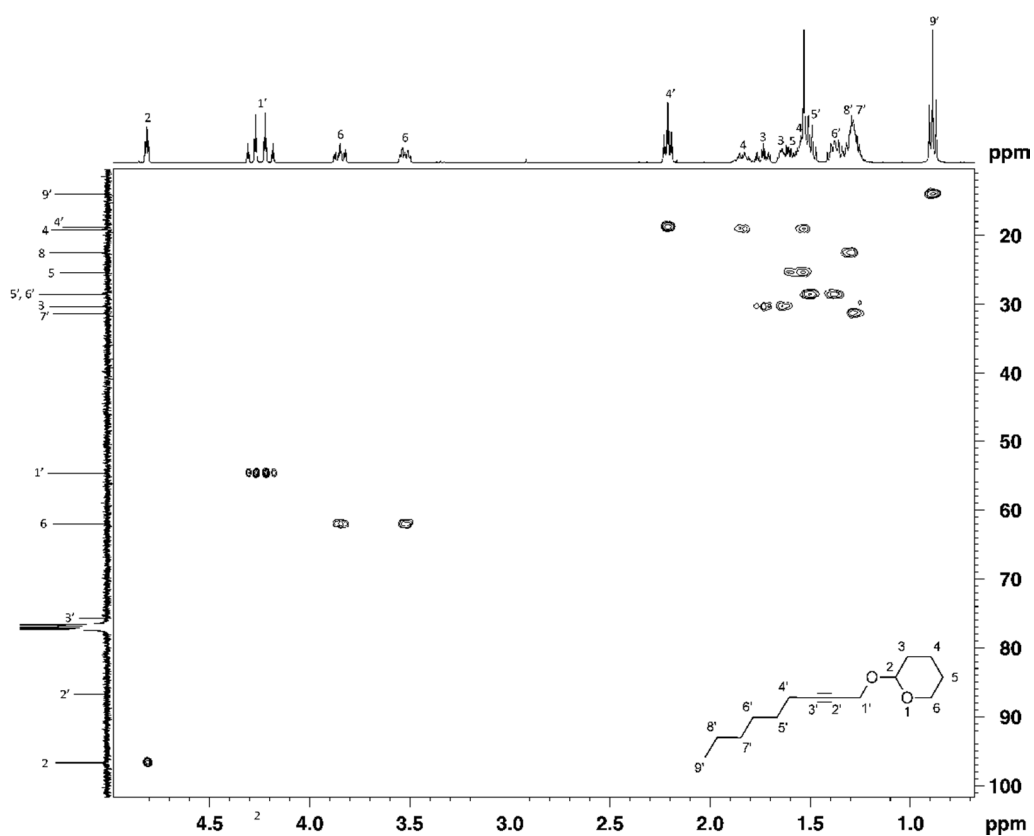


Figure C41: 2D HSQC NMR Spectrum for 2-nonyl tetrahydro-2H-pyran-2-yl ether 139

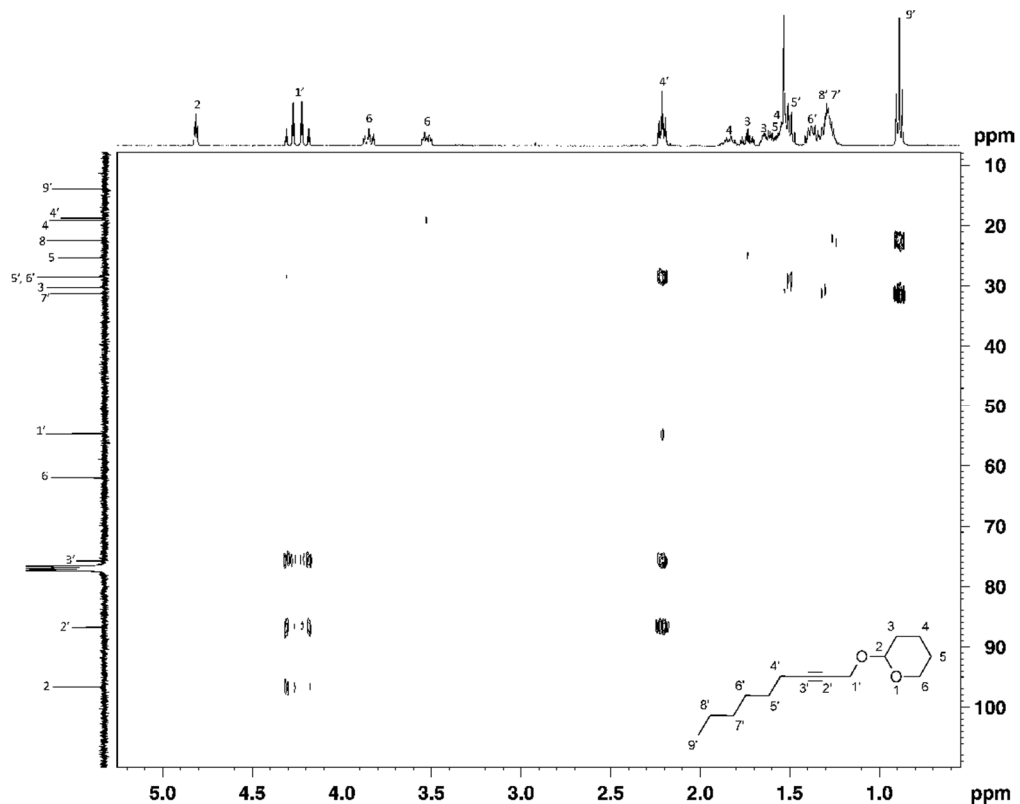


Figure C42: 2D HMBC NMR Spectrum for 2-nonyl tetrahydro-2H-pyran-2-yl ether 139

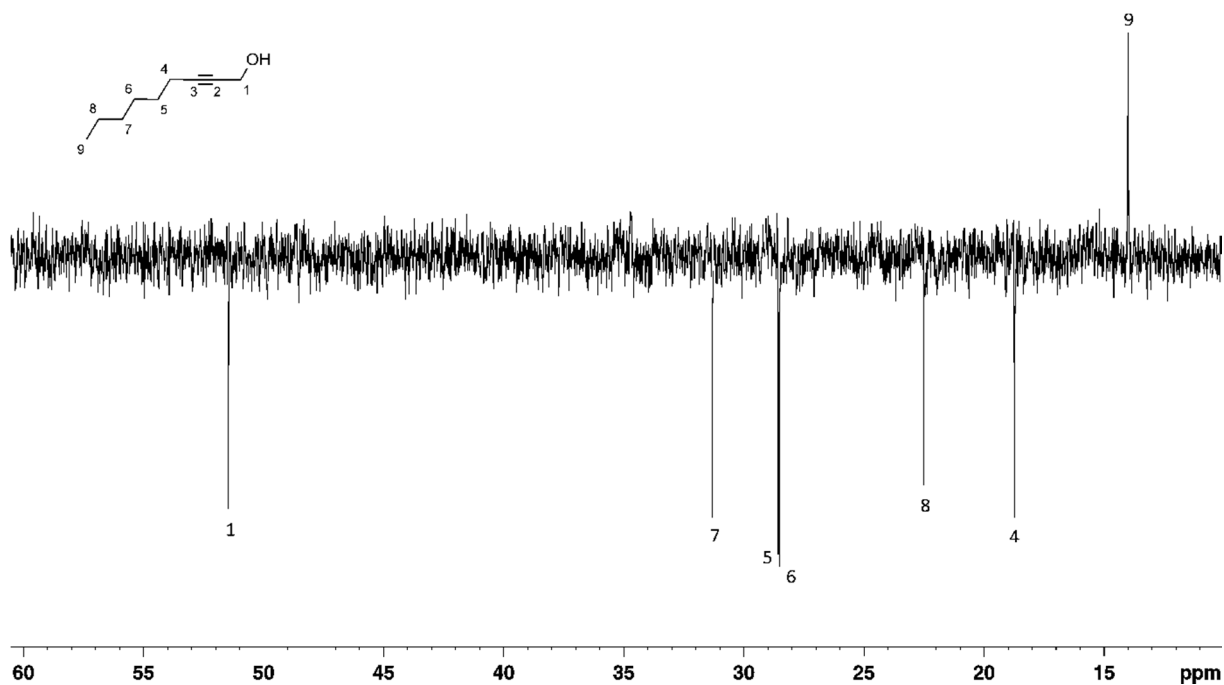


Figure C43: DEPT 135 NMR Spectrum for 2-nonyl-1-ol 142

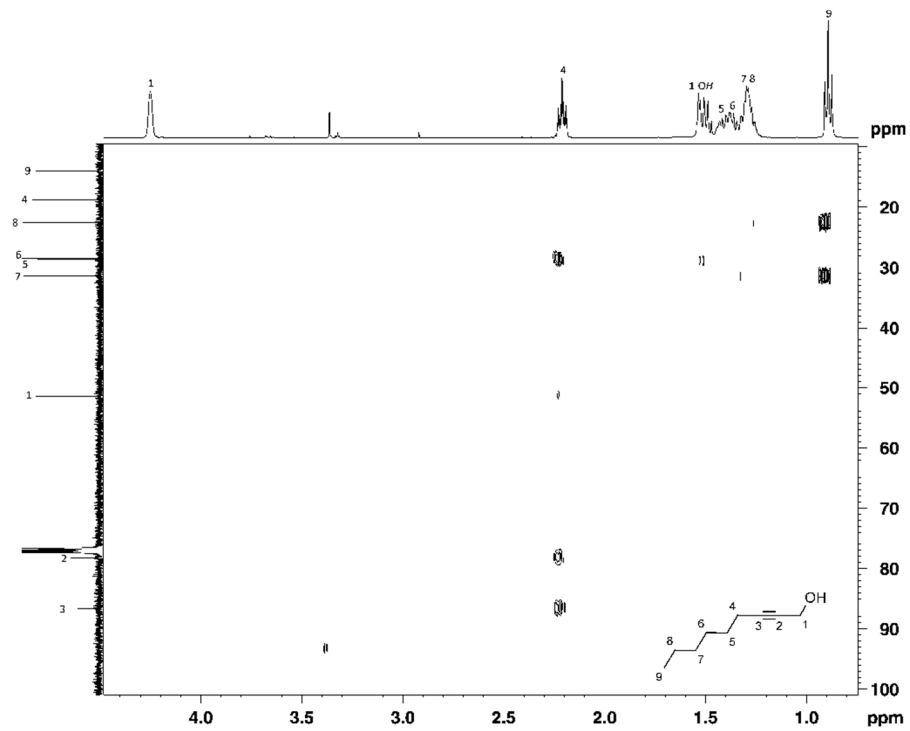


Figure C44: 2D HMBC NMR Spectrum for 2-nonyn-1-ol 142

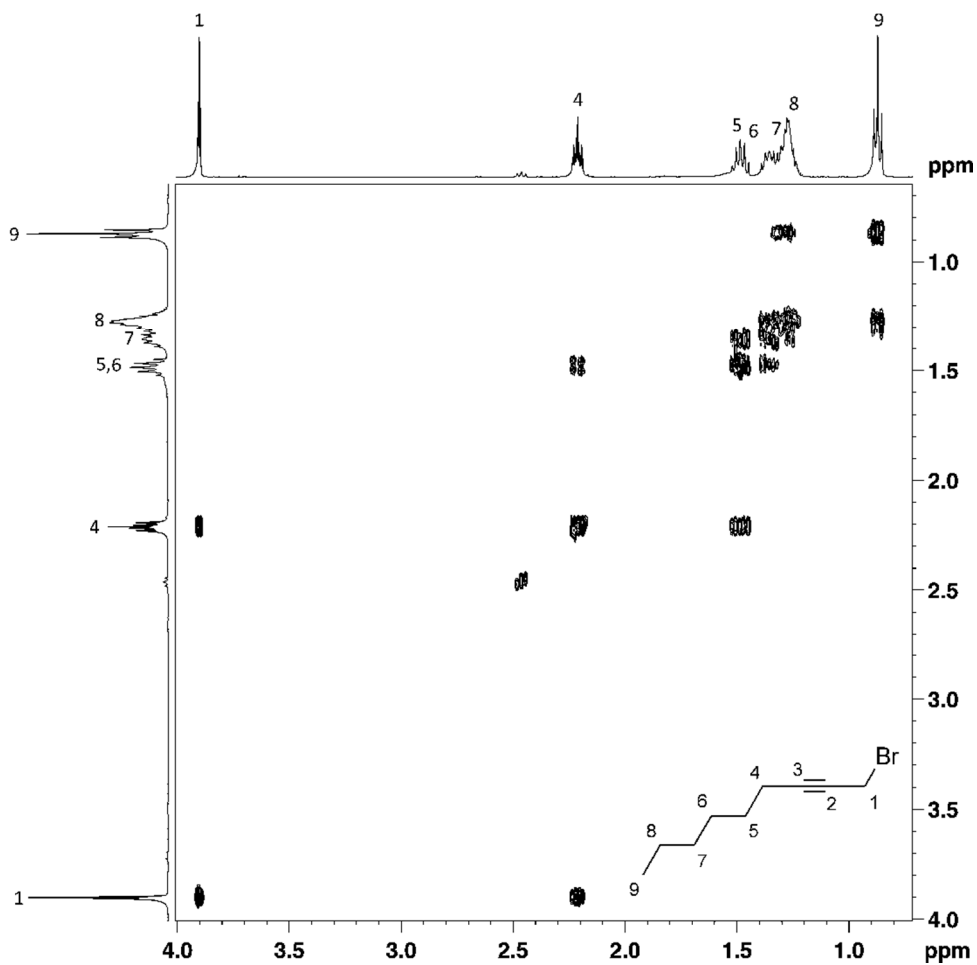


Figure C45: 2D COSY NMR Spectrum for 1-bromo-2-nonyne 131

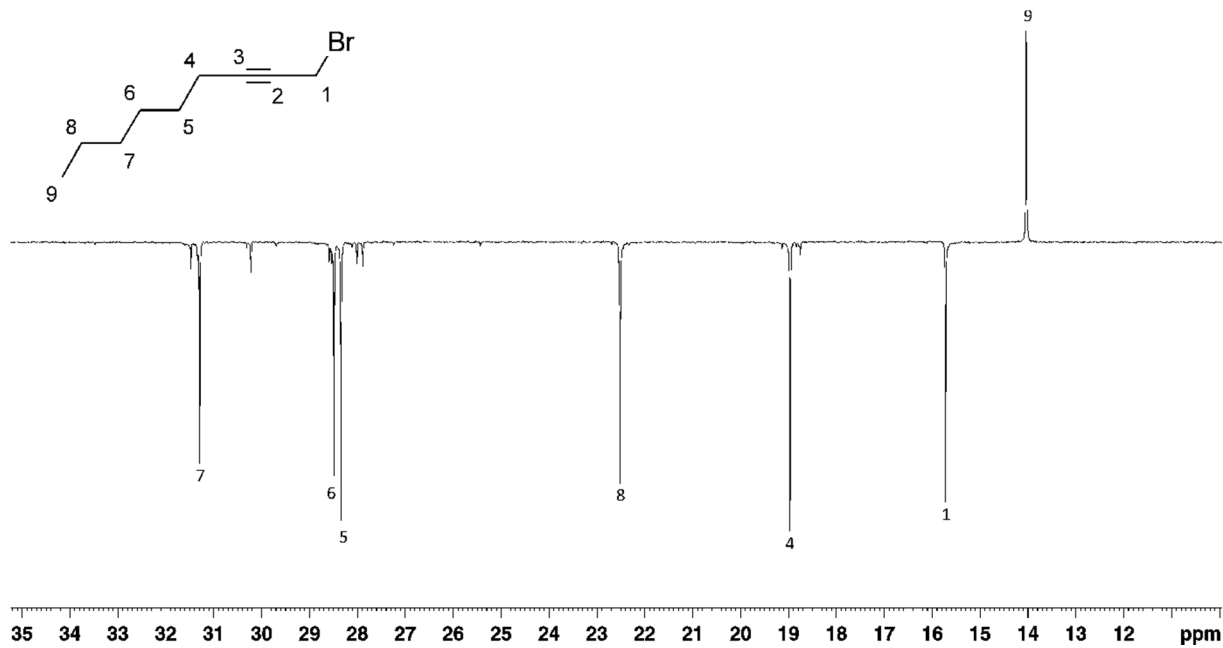


Figure C46: DEPT 135 NMR Spectrum for 1-bromo-2-nonyne 131

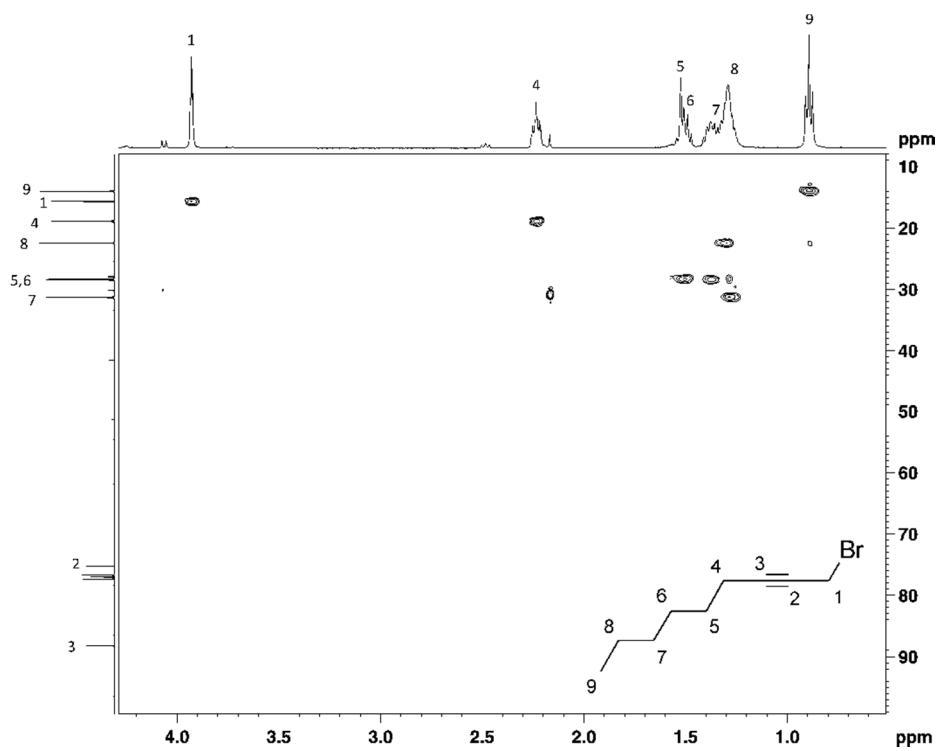
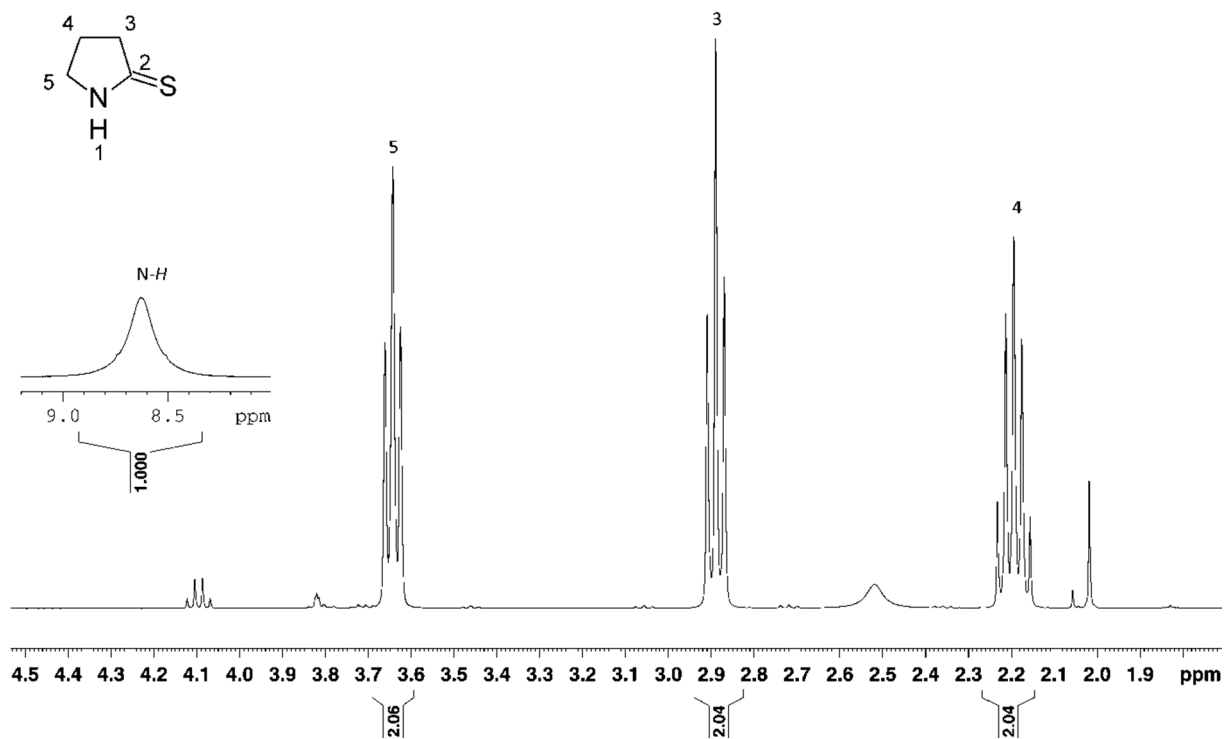
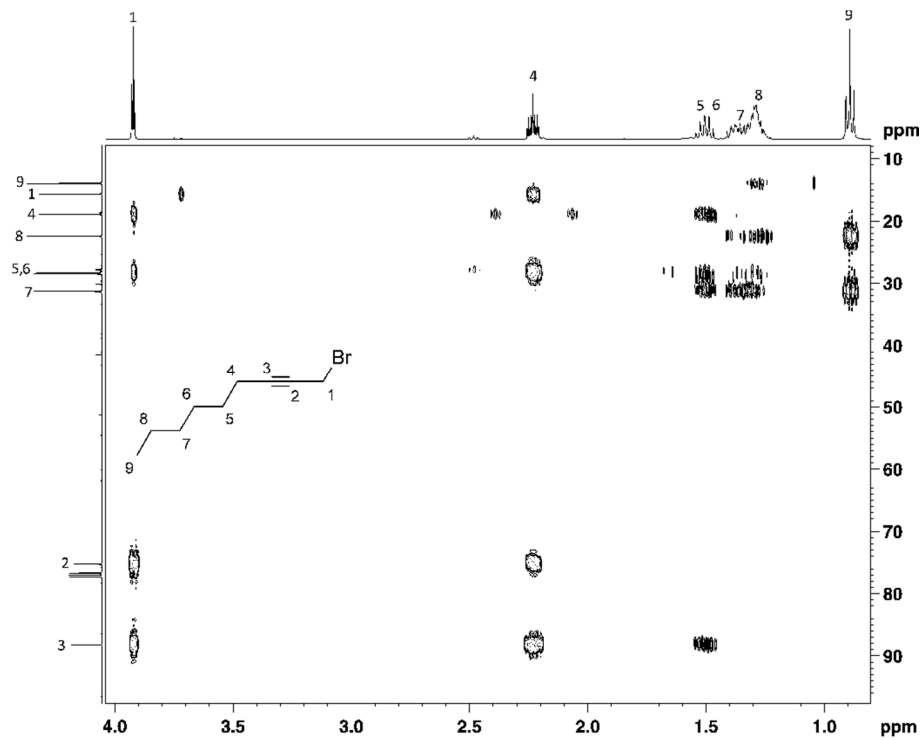


Figure C47: 2D HSQC NMR Spectrum for 1-bromo-2-nonyne 131



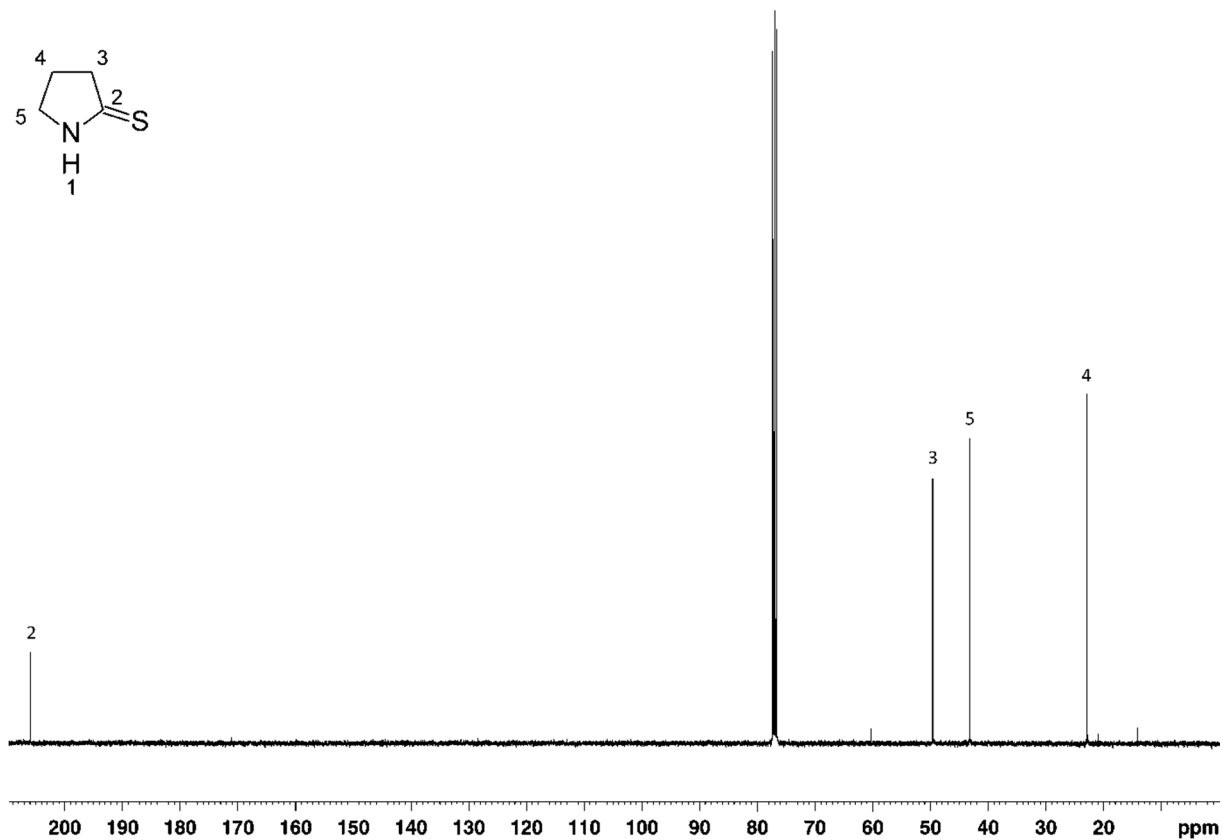


Figure C50: ^{13}C NMR Spectrum for 2-pyrrolidinethione 116

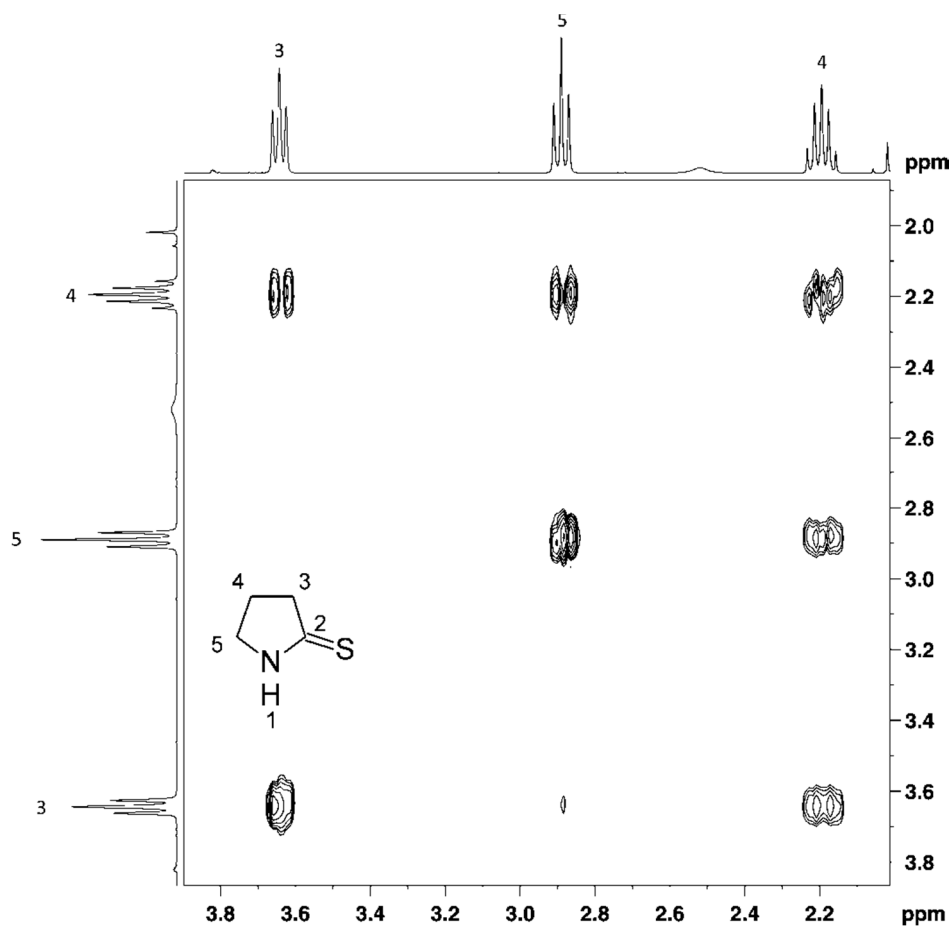


Figure C51: 2D COSY NMR Spectrum for 2-pyrrolidinethione 116

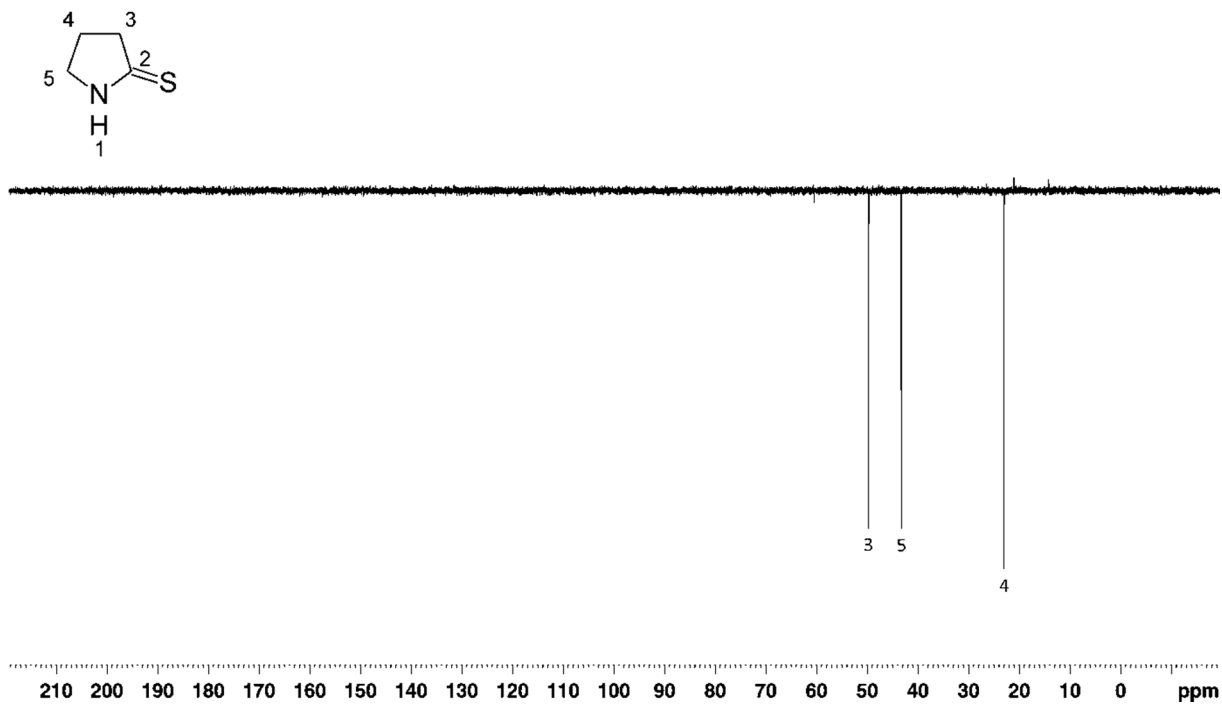


Figure C52: DEPT 135 NMR Spectrum for 2-pyrrolidinethione 116

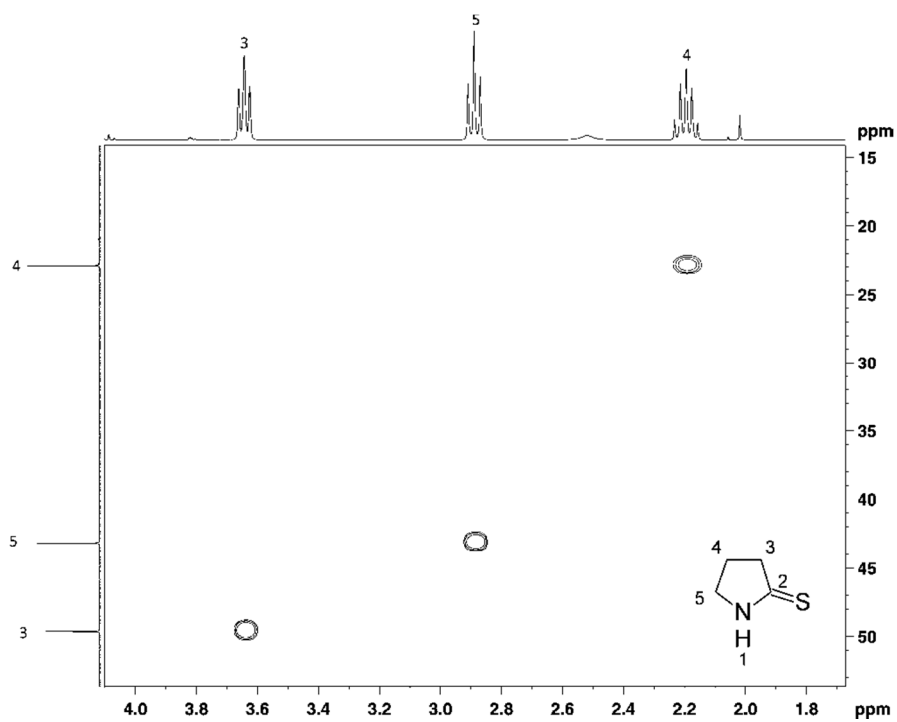


Figure C53: 2D HSQC NMR Spectrum for 2-pyrrolidinethione 116

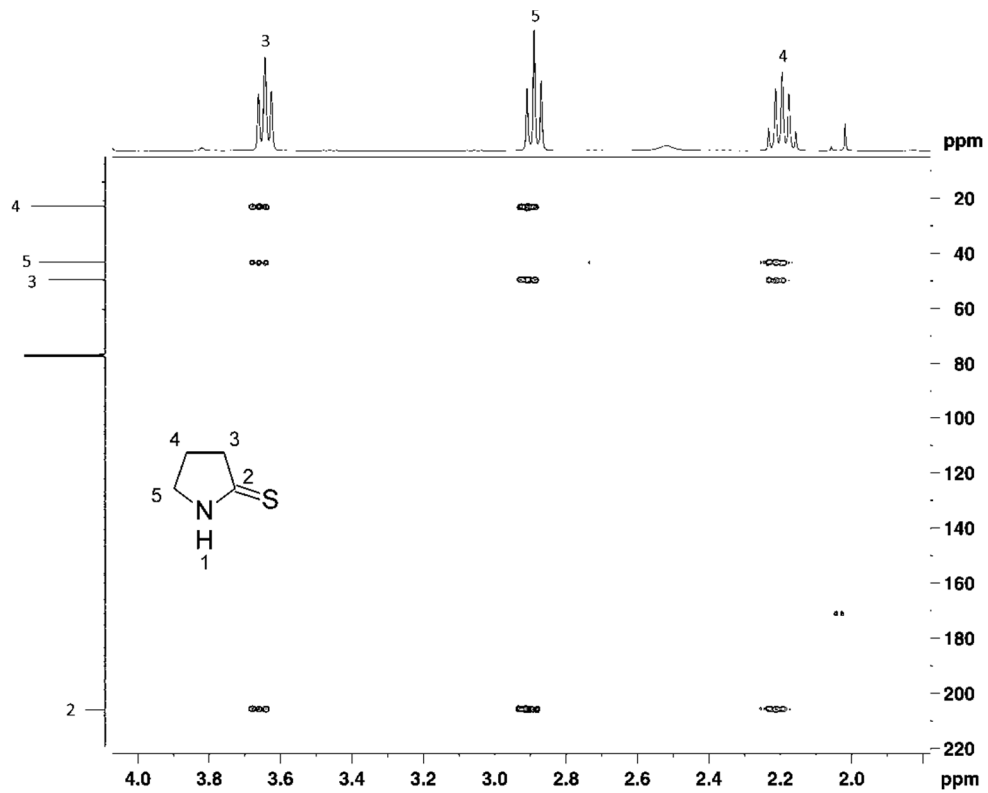


Figure C54: 2D HMBC NMR Spectrum for 2-pyrrolidinethione 116

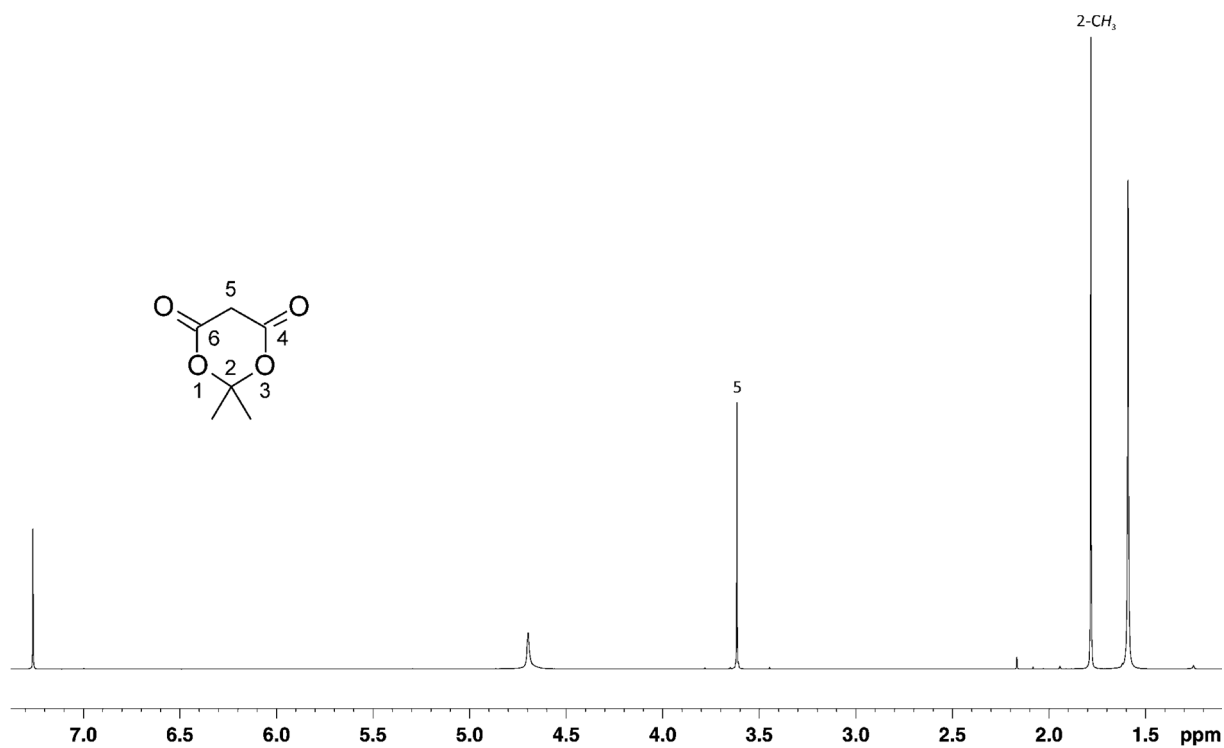


Figure C55: ¹H NMR Spectrum for 2,2-dimethyl-1,3-dioxane-4,6-dione (Meldrum's Acid)

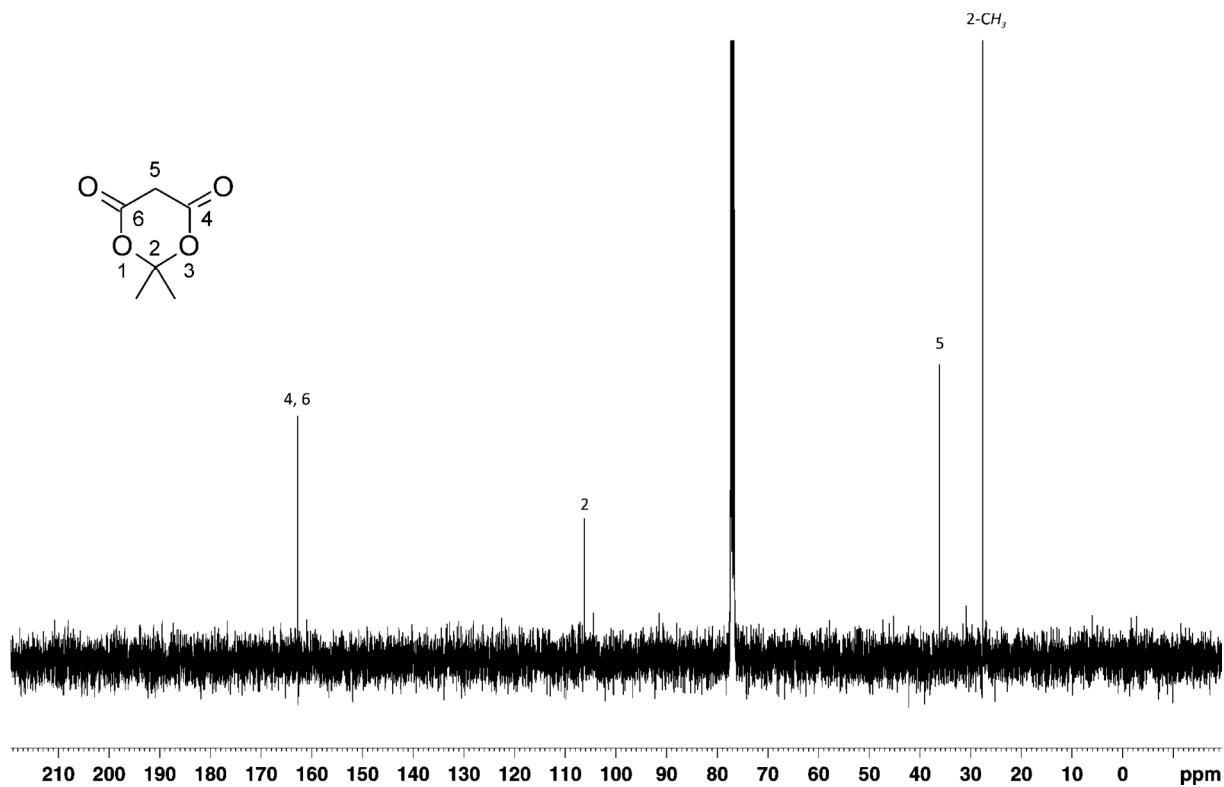


Figure C56: ^{13}C NMR Spectrum for 2,2-dimethyl-1,3-dioxane-4,6-dione (Meldrum's Acid)

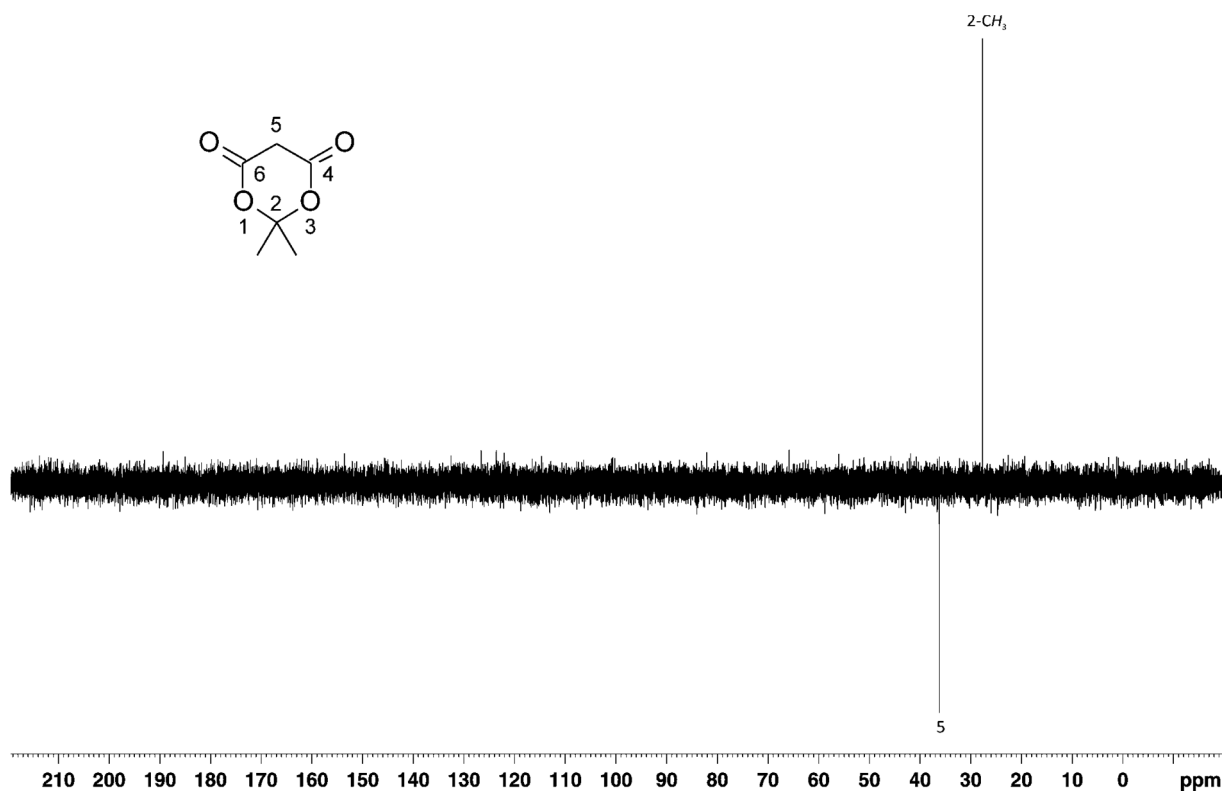
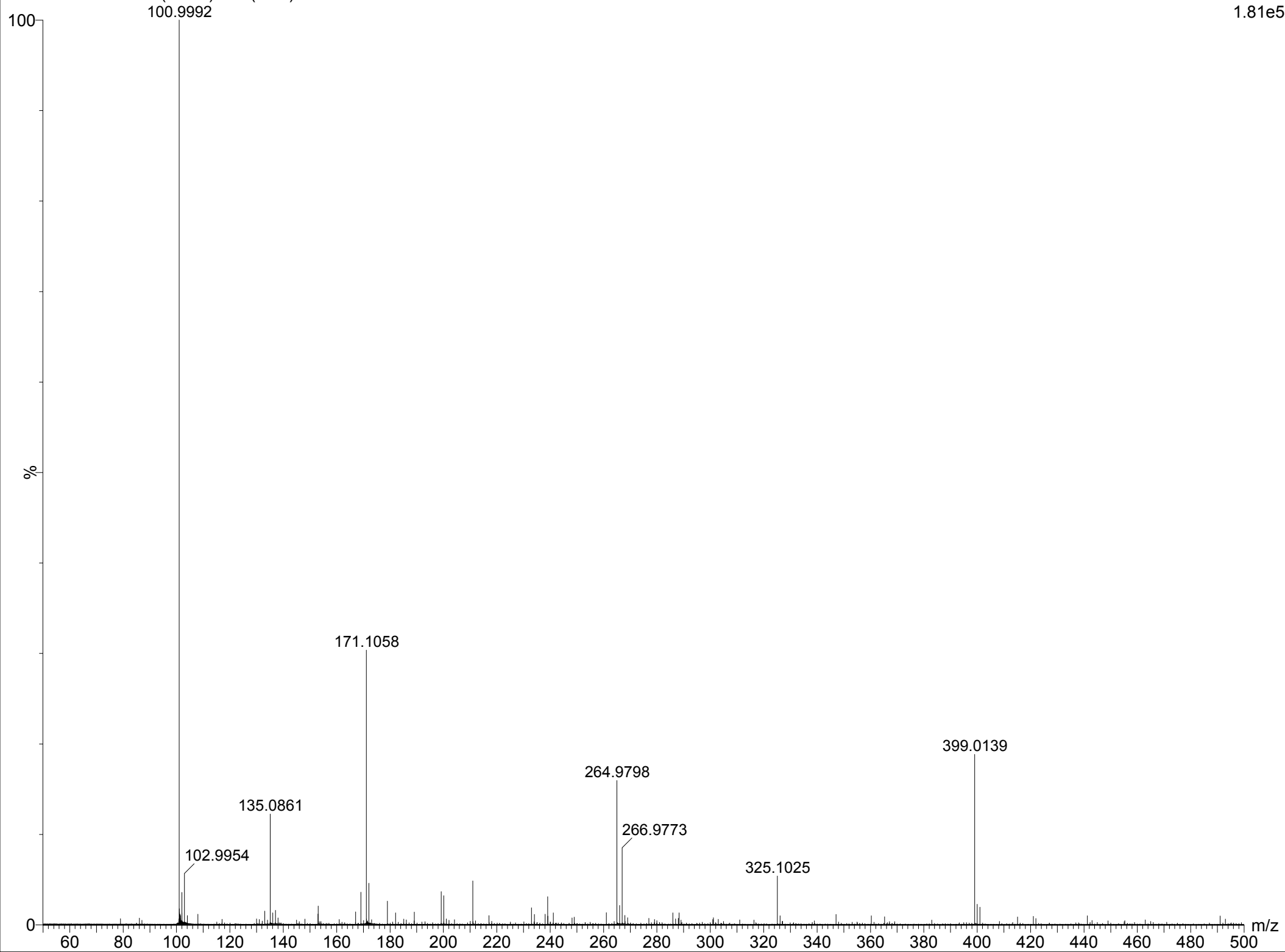


Figure C57: DEPT 135 NMR Spectrum for 2,2-dimethyl-1,3-dioxane-4,6-dione (Meldrum's Acid)



Single Mass Analysis

Tolerance = 5.0 PPM / DBE: min = -1.5, max = 100.0

Element prediction: Off

Number of isotope peaks used for i-FIT = 3

Monoisotopic Mass, Even Electron Ions

65 formula(e) evaluated with 1 results within limits (up to 20 closest results for each mass)

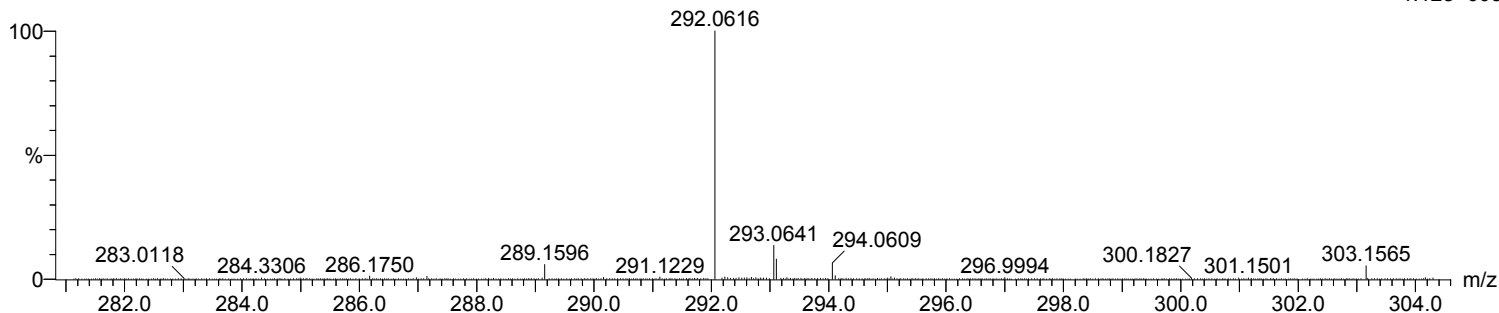
Elements Used:

C: 10-15 H: 15-20 N: 0-5 O: 0-5 Na: 0-1 S: 0-1

id-3-19 54 (1.789) Cm (1:61)

TOF MS ES+

1.12e+005

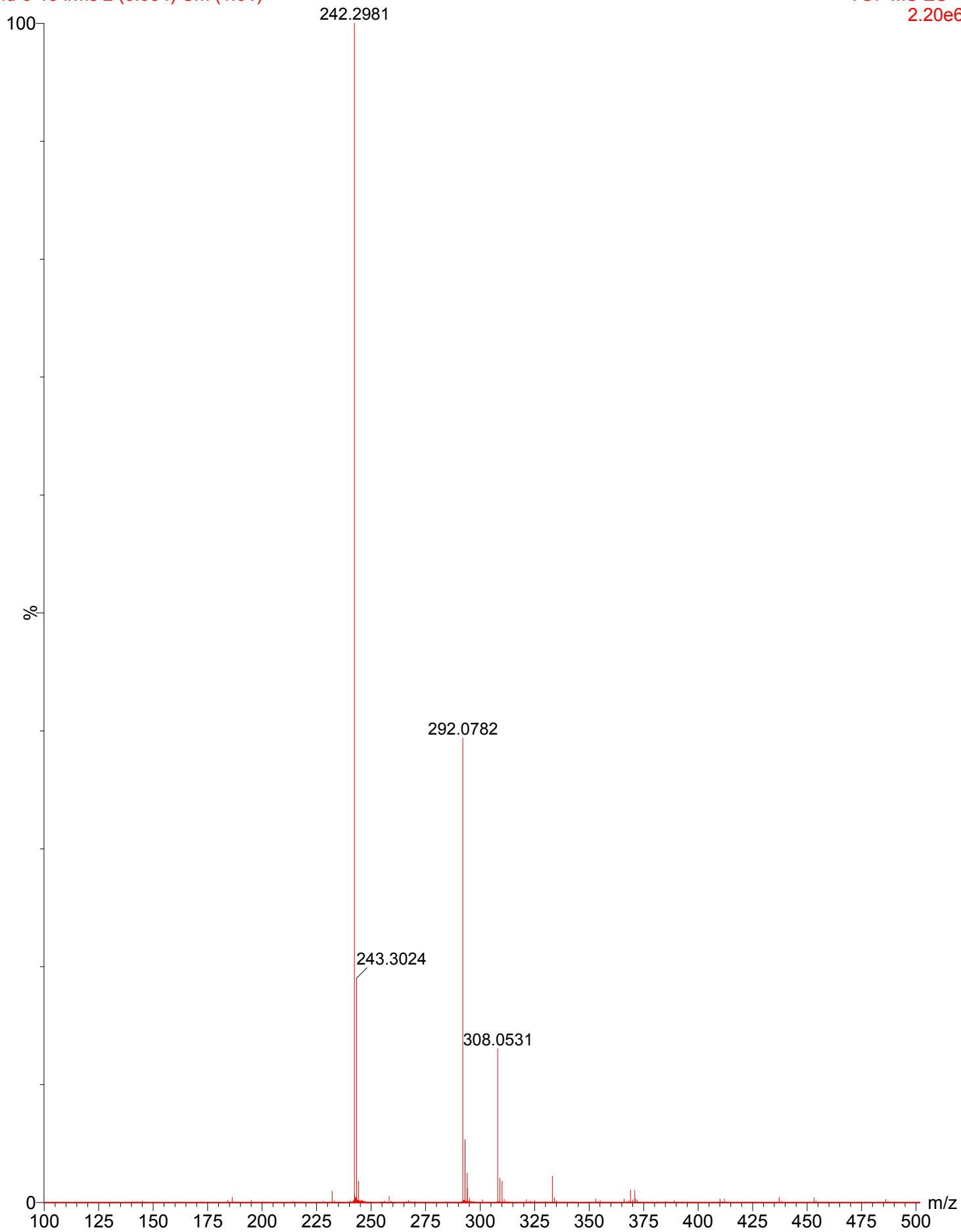


Minimum: -1.5
Maximum: 5.0 5.0 100.0

Mass	Calc. Mass	mDa	PPM	DBE	i-FIT	i-FIT (Norm)	Formula
292.0616	292.0619	-0.3	-1.0	5.5	610.9	0.0	C12 H15 N O4 Na S

id-3-19 I rms 2 (0.034) Cm (1:61)

TOF MS ES+
2.20e6



Single Mass Analysis

Tolerance = 5.0 PPM / DBE: min = -1.5, max = 100.0

Element prediction: Off

Number of isotope peaks used for i-FIT = 3

Monoisotopic Mass, Even Electron Ions

45 formula(e) evaluated with 1 results within limits (up to 20 closest results for each mass)

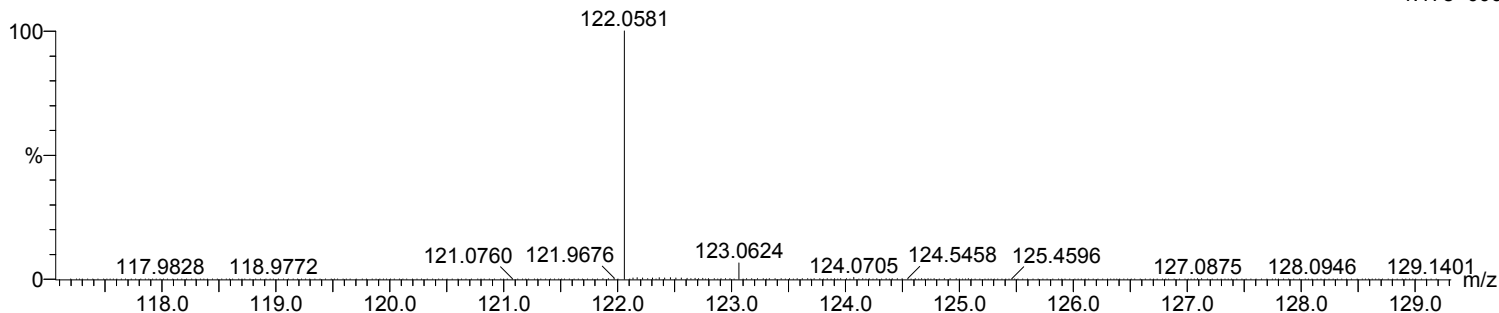
Elements Used:

C: 5-10 H: 5-10 N: 0-5 O: 0-5 Na: 0-1

id-4-19(b) 61 (2.025) Cm (1:61)

TOF MS ES+

1.17e+006



Minimum: -1.5
Maximum: 5.0 5.0 100.0

Mass	Calc. Mass	mDa	PPM	DBE	i-FIT	i-FIT (Norm)	Formula
122.0581	122.0582	-0.1	-0.8	1.5	904.3	0.0	C5 H9 N O Na

Single Mass Analysis

Tolerance = 5.0 PPM / DBE: min = -1.5, max = 100.0

Element prediction: Off

Number of isotope peaks used for i-FIT = 3

Monoisotopic Mass, Odd and Even Electron Ions

1 formula(e) evaluated with 1 results within limits (up to 20 closest results for each mass)

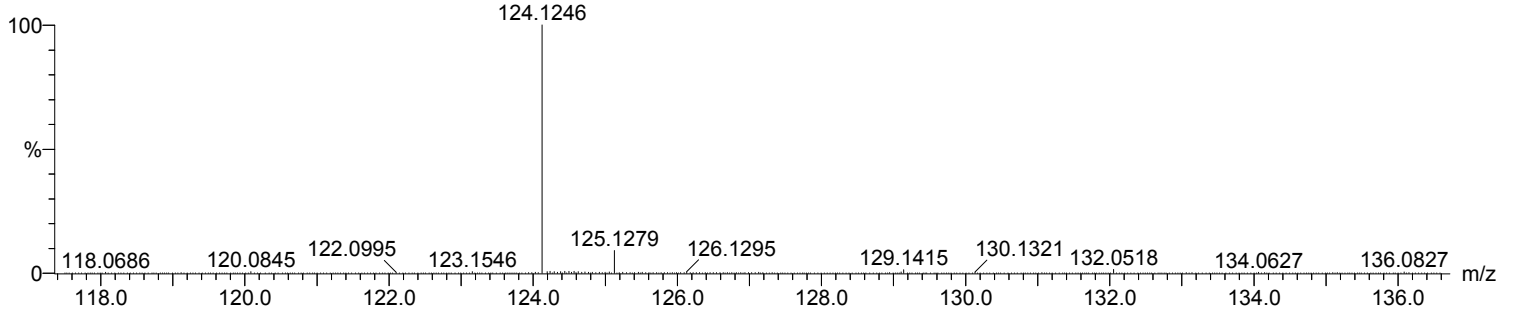
Elements Used:

C: 5-10 H: 15-20

id-16-5 18 (0.574) Cm (1:61)

TOF MS AP+

3.76e+005



Minimum: -1.5
 Maximum: 5.0 5.0 100.0

Mass	Calc. Mass	mDa	PPM	DBE	i-FIT	i-FIT (Norm)	Formula
124.1246	124.1252	-0.6	-4.8	2.0	782.1	0.0	C9 H16

Single Mass Analysis

Tolerance = 5.0 PPM / DBE: min = -1.5, max = 100.0

Element prediction: Off

Number of isotope peaks used for i-FIT = 3

Monoisotopic Mass, Odd and Even Electron Ions

1 formula(e) evaluated with 1 results within limits (up to 20 closest results for each mass)

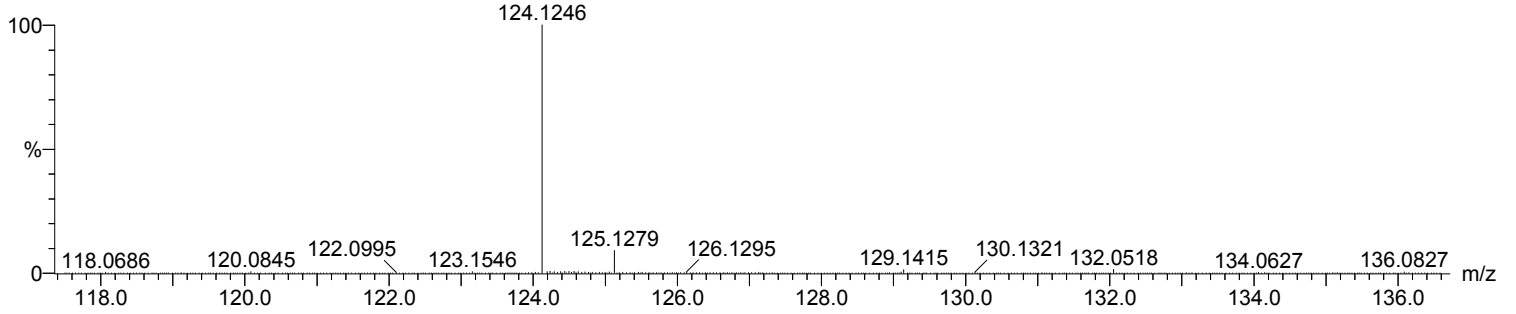
Elements Used:

C: 5-10 H: 15-20

id-16-5 18 (0.574) Cm (1:61)

TOF MS AP+

3.76e+005

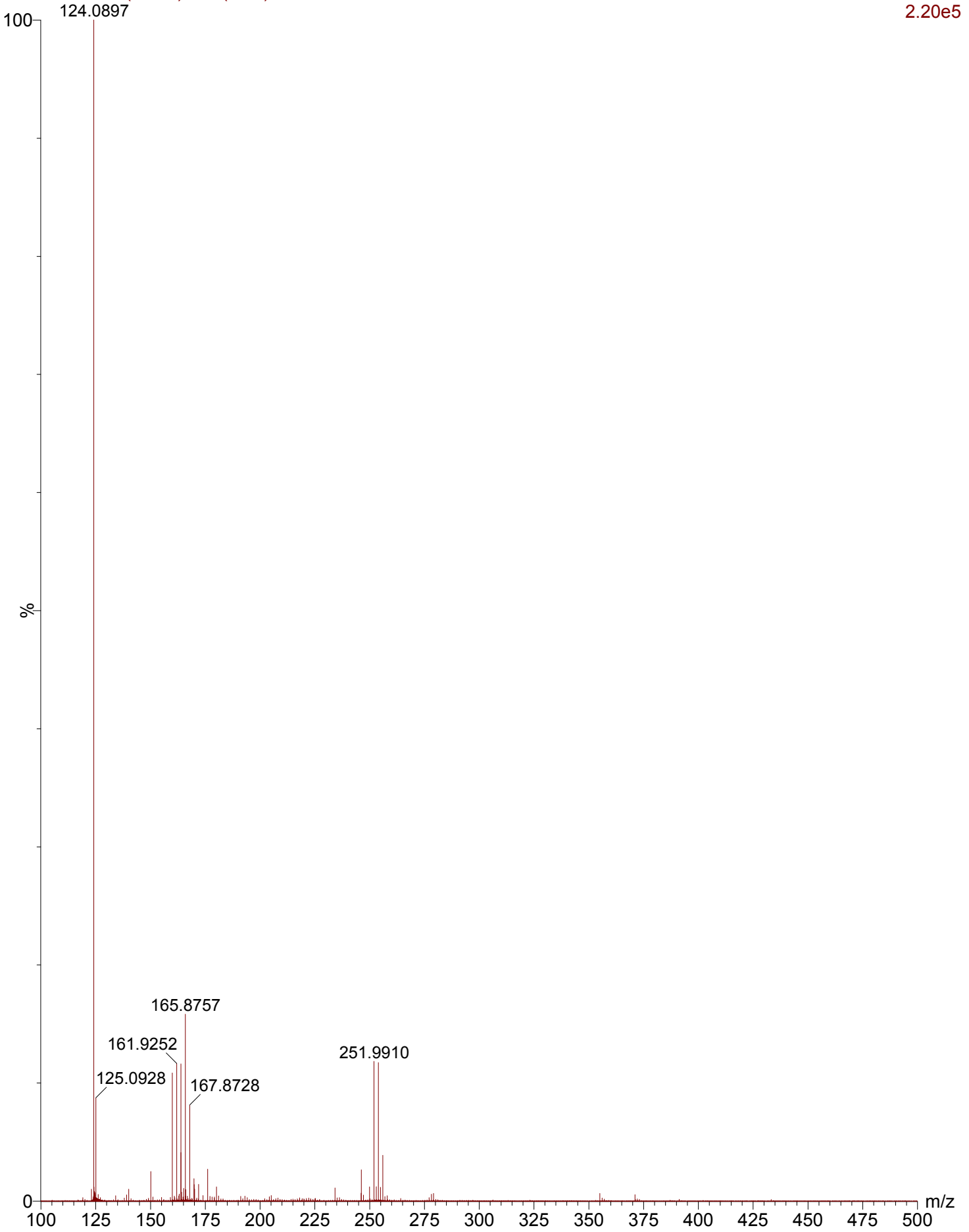


Minimum: -1.5
 Maximum: 5.0 5.0 100.0

Mass	Calc. Mass	mDa	PPM	DBE	i-FIT	i-FIT (Norm)	Formula
124.1246	124.1252	-0.6	-4.8	2.0	782.1	0.0	C9 H16

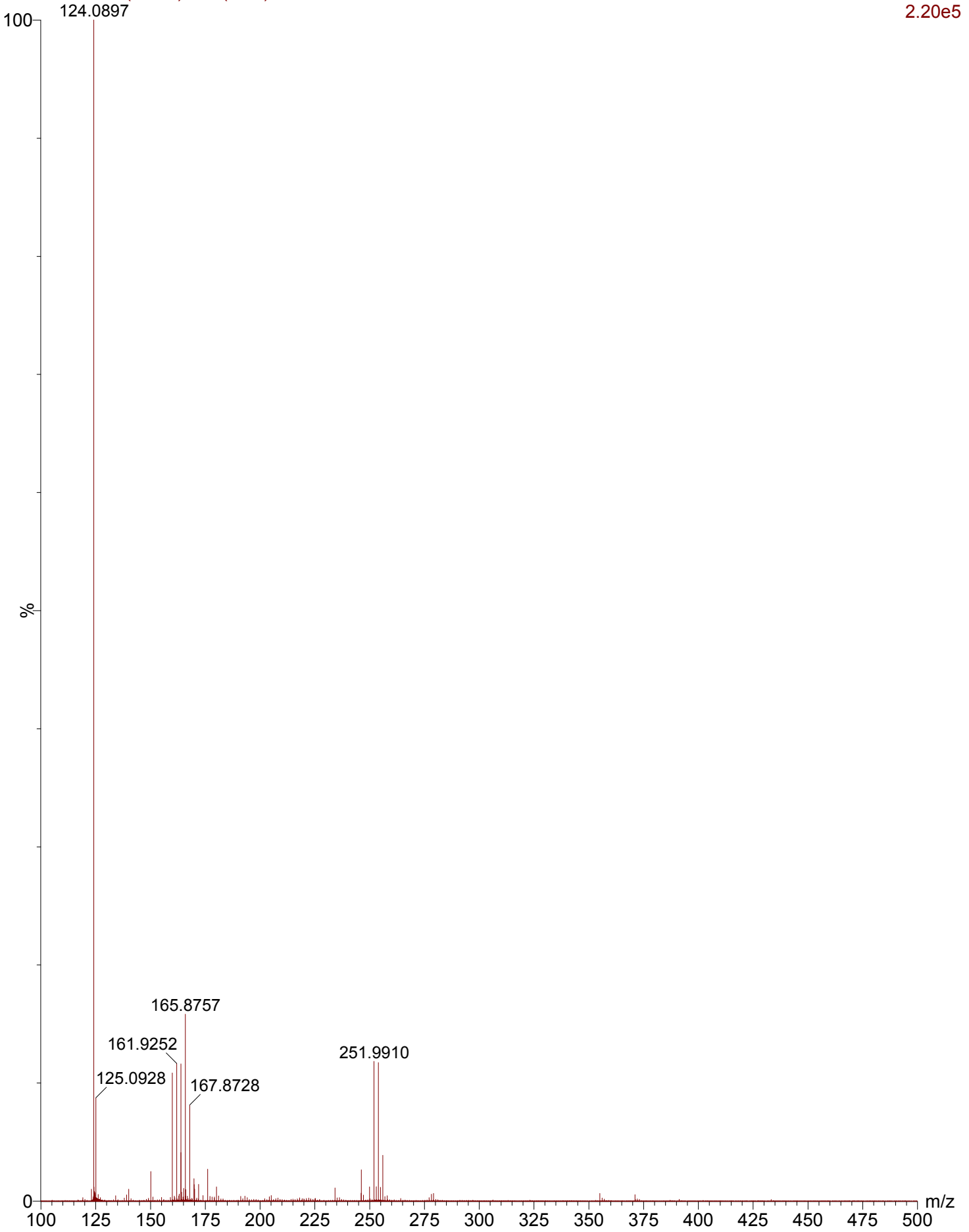
id-16-5 lrms 61 (2.025) Cm (1:61)

TOF MS AP+
2.20e5



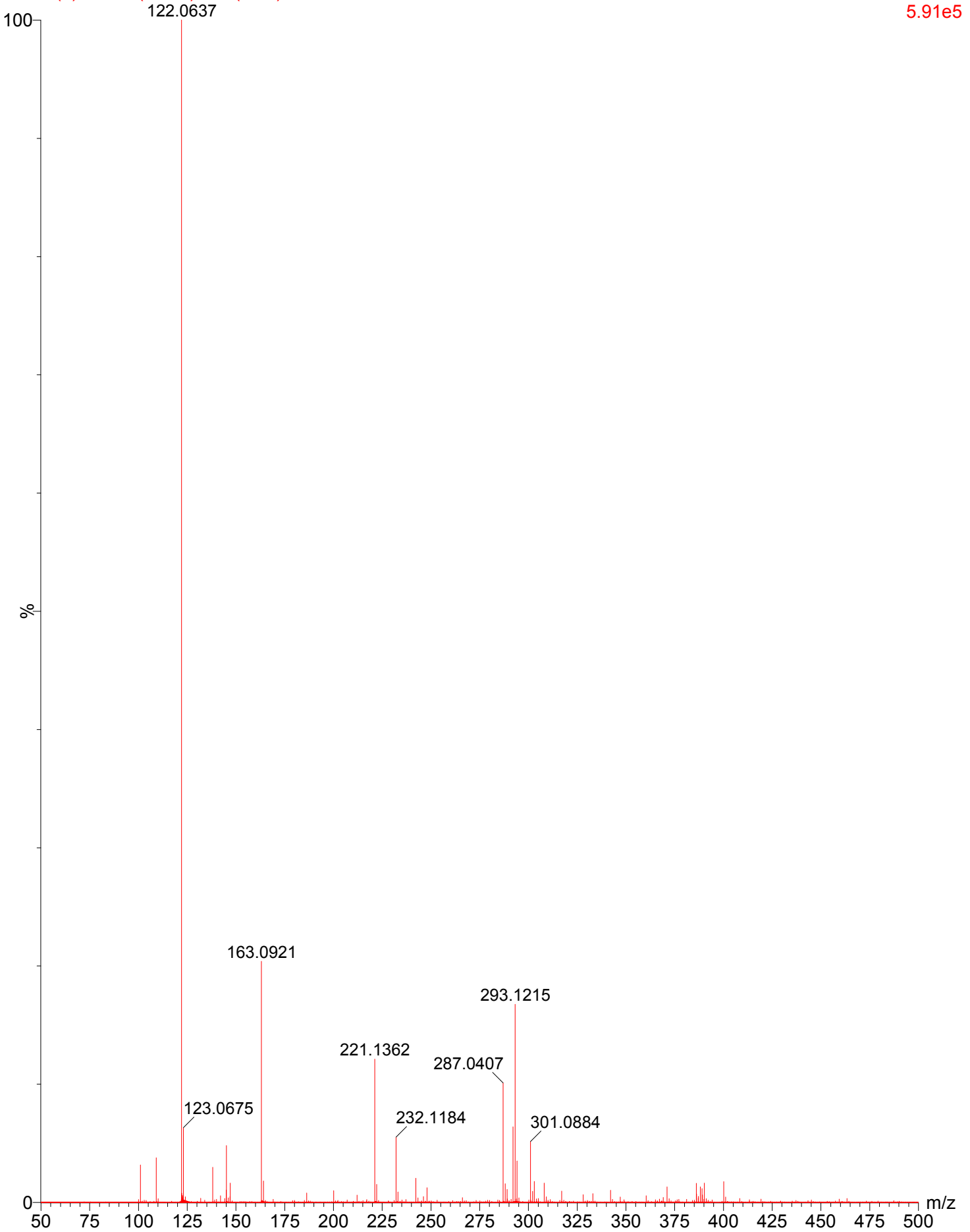
id-16-5 lrms 61 (2.025) Cm (1:61)

TOF MS AP+
2.20e5



id-4-19(b) lrms 9 (0.270) Cm (1:61)

TOF MS ES+
5.91e5



Single Mass Analysis

Tolerance = 50.0 PPM / DBE: min = -1.5, max = 100.0

Element prediction: Off

Number of isotope peaks used for i-FIT = 3

Monoisotopic Mass, Even Electron Ions

21 formula(e) evaluated with 1 results within limits (up to 20 closest results for each mass)

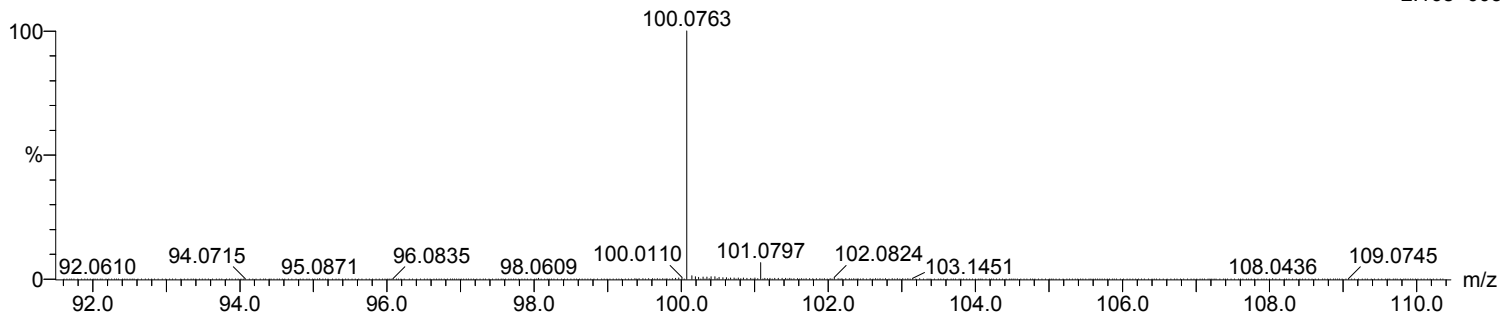
Elements Used:

C: 5-10 H: 10-15 N: 0-5 O: 0-5

lactim ether 2 (0.034) Cm (1:61)

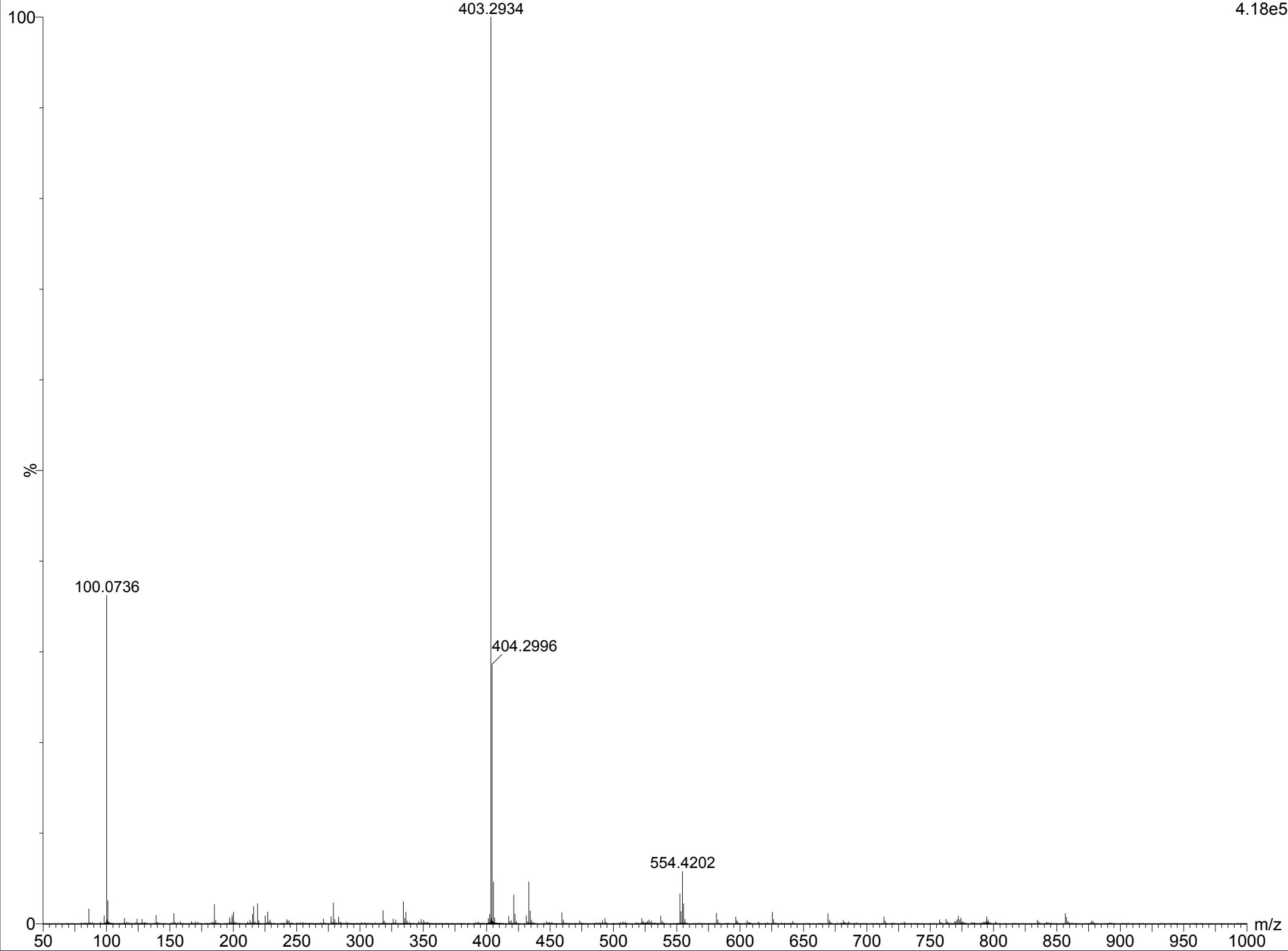
TOF MS ES+

2.16e+005



Minimum: -1.5
 Maximum: 5.0 50.0 100.0

Mass	Calc. Mass	mDa	PPM	DBE	i-FIT	i-FIT (Norm)	Formula
100.0763	100.0762	0.1	1.0	1.5	739.6	0.0	C5 H10 N O



Single Mass Analysis

Tolerance = 50.0 PPM / DBE: min = -1.5, max = 100.0

Element prediction: Off

Number of isotope peaks used for i-FIT = 3

Monoisotopic Mass, Even Electron Ions

23 formula(e) evaluated with 1 results within limits (up to 20 closest results for each mass)

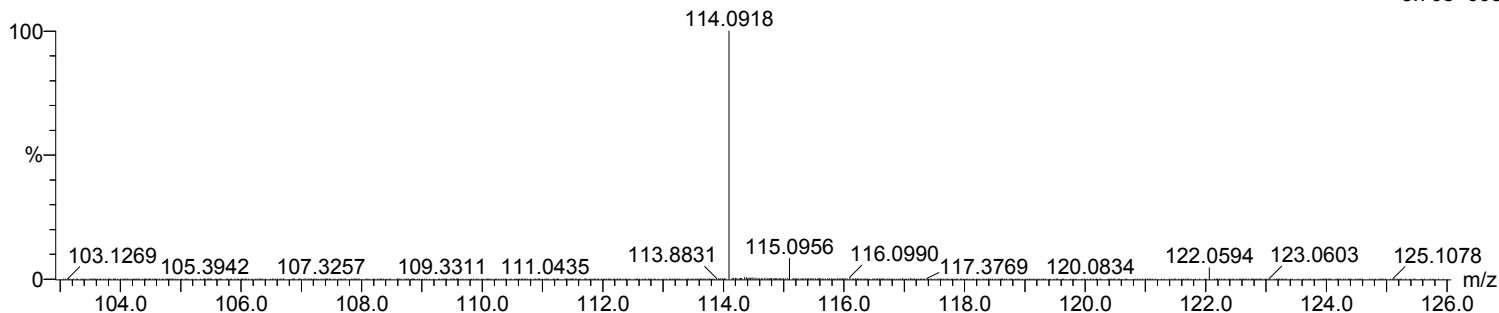
Elements Used:

C: 5-10 H: 10-15 N: 0-5 O: 0-5

methyl lactim ether 17 (0.540)

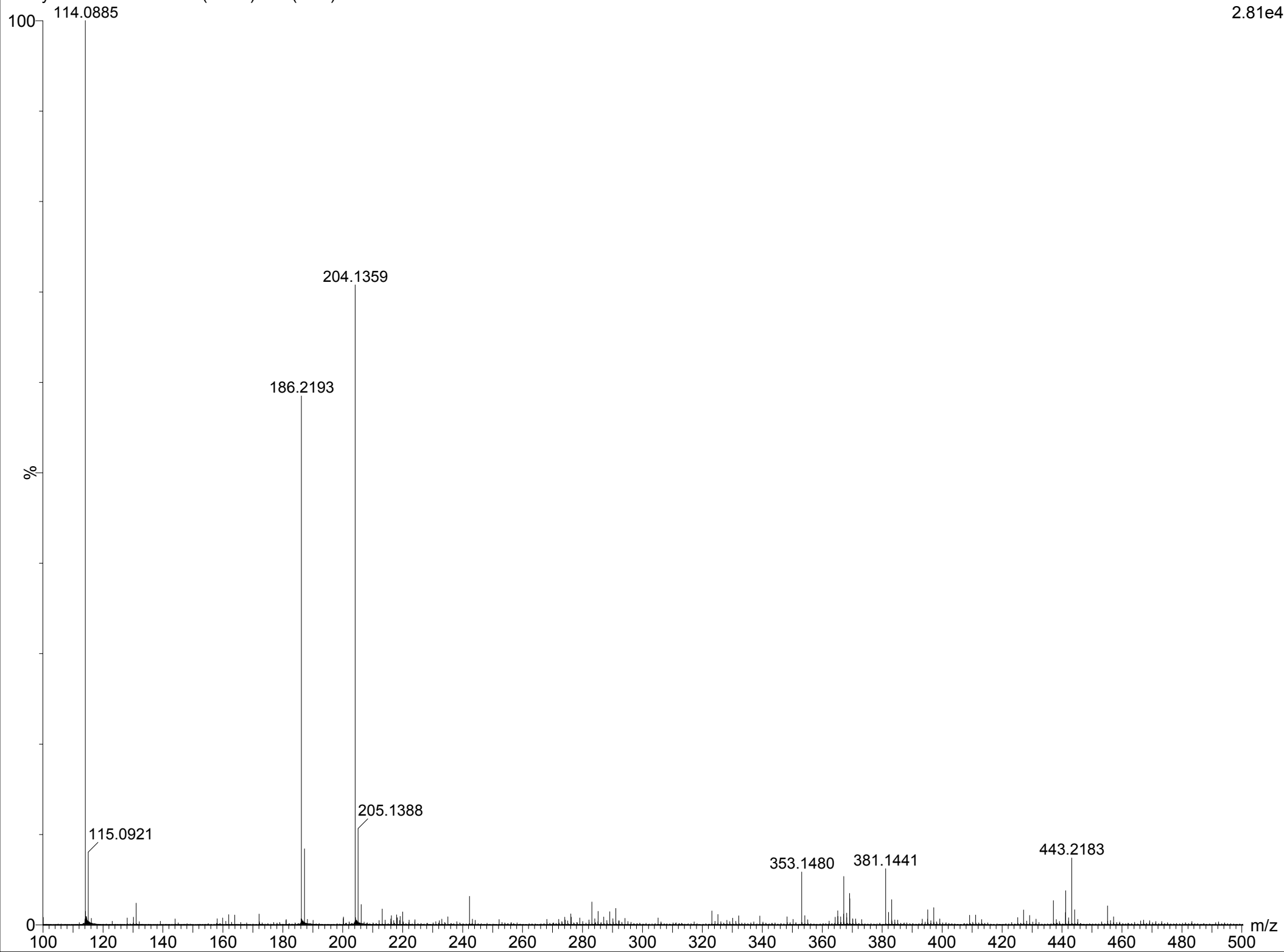
TOF MS ES+

8.70e+003



Minimum: -1.5
 Maximum: 5.0 50.0 100.0

Mass	Calc. Mass	mDa	PPM	DBE	i-FIT	i-FIT (Norm)	Formula
114.0918	114.0919	-0.1	-0.9	1.5	386.4	0.0	C6 H12 N O



Single Mass Analysis

Tolerance = 5.0 PPM / DBE: min = -1.5, max = 100.0

Element prediction: Off

Number of isotope peaks used for i-FIT = 3

Monoisotopic Mass, Even Electron Ions

5 formula(e) evaluated with 1 results within limits (up to 20 closest results for each mass)

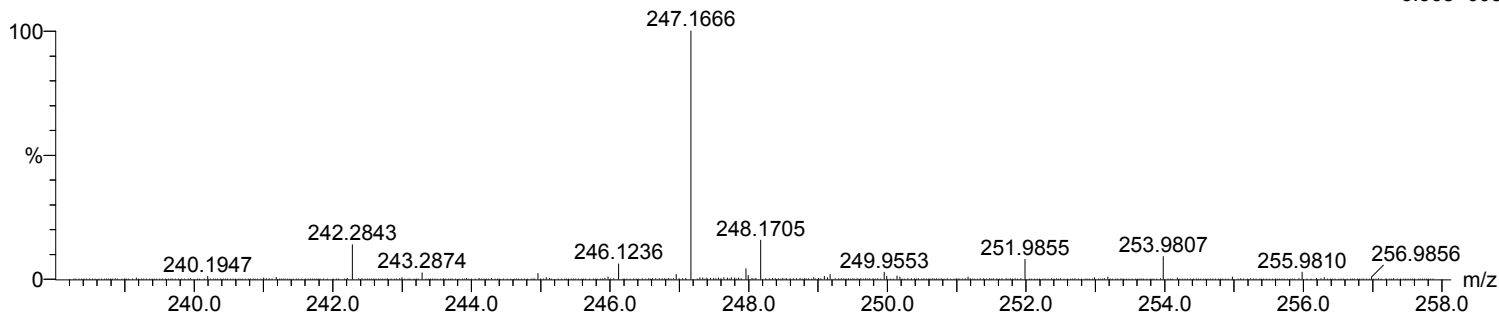
Elements Used:

C: 10-15 H: 20-25 O: 0-5 Na: 0-1

id-14-8 16 (0.506) Cm (1:61)

TOF MS ES+

3.36e+005



Minimum: -1.5
 Maximum: 5.0 5.0 100.0

Mass	Calc. Mass	mDa	PPM	DBE	i-FIT	i-FIT (Norm)	Formula
247.1666	247.1674	-0.8	-3.2	2.5	742.9	0.0	C14 H24 O2 Na

